Université de Montréal

Links between inadequate immune responses to viral infections and disease outcome in humans

Par

Elsa Brunet-Ratnasingham

Département de microbiologie, infectiologie et immunologie

Faculté de médecine

Thèse présentée en vue de l'obtention du grade de Philosophiae Doctor (Ph.D.)

en Virologie et Immunologie

December 2021

Université de Montréal

Faculté des études supérieures et postdoctorales

Département de microbiologie, infectiologie et immunologie, Faculté de médecine

Cette thèse intitulée

Links between inadequate immune responses to viral infections and disease outcome in humans

Présentée par

Elsa Brunet-Ratnasingham

A été évalué(e) par un jury composé des personnes suivantes

Dr. Hugo Soudeyns

Président-rapporteur

Dr. Daniel E. Kaufmann

Directeur de recherche

Dr. Hélène Decaluwe

Membre du jury

Dr. David G. Brooks

Examinateur externe

Dr. George Szatmari

Représentant du doyen

Résumé

Deux pandémies virales touchent aujourd'hui des millions d'individus : la pandémie du *Coronavirus Disease 2019* (COVID-19), causée par le Syndrome respiratoire aigu sévère coronavirus 2 (SRAS-CoV-2) et celle du Syndrome d'Immunodéficience Acquise (SIDA) causée par le Virus de l'Immunodéficience Humaine (VIH). Ces deux maladies diffèrent par leur physiopathologie, dont une meilleure compréhension a permis le développement de traitements efficaces. Pourtant, ces deux pandémies persistent. Une infection par SARS-CoV-2 peut être mortelle en raison d'une réponse immunitaire exacerbée et potentiellement retardée. Le VIH à l'inverse échappe continuellement à la réponse immunitaire, l'affaiblissant au cours des années jusqu'au développement du SIDA, ouvrant la porte à des maladies opportunistes mortelles. L'intérêt global de cette thèse était d'étudier comment la réponse immunitaire échoue pour ces deux infections.

L'objectif de la première étude était de trouver un biomarqueur sanguin robuste et fiable pour prédire le risque de mortalité des patients hospitalisés pour la COVID-19. Nous avons mesuré la quantité d'ARN viral, de cytokines et de marqueurs de dommages tissulaires, ainsi que la réponse humorale contre le virus dans des échantillons de plasma de 279 patients à travers trois cohortes. Nous avons trouvé que l'ARN viral mesuré environ 11 jours après le début des symptômes, et ajusté pour l'âge et le sexe, peut prédire la mortalité dans les 60 jours suivant le début des symptômes. Nous avons également trouvé que des fortes concentrations de cytokines inflammatoires et de marqueurs de dommages tissulaires, ainsi qu'un faible niveau d'anticorps liant le *Region Binding Domain* (RBD) de la protéine *Spike* de SARS-CoV-2, sont aussi associées à la

mortalité. Dans un deuxième projet, nous nous sommes servis d'outils de réduction de dimensionnalités combinant les facteurs associés à la mortalité, permettant une stratification des patients en quatre groupes basés uniquement sur leur profil immuno-virologique plasmatique. Un seul de ces groupes est lié à une plus grande mortalité. Mis ensemble, nos travaux permettent une meilleure compréhension de l'hétérogénéité des patients hospitalisés pour la COVID-19, incluant l'identification des patients à haut risque de mortalité. Ces données pourraient servir à cibler les traitements thérapeutiques selon la réponse immunologique du patient.

Notre troisième étude portait sur l'étude de la dysfonction des lymphocytes T CD4+ spécifiques du VIH. Ceux-ci sont affaiblis par l'infection au VIH et perdent leur capacité à combattre l'infection. Notre objectif était de caractériser la réponse au blocage du point de contrôle immunitaire (BPCI - immunothérapie qui renverse partiellement la dysfonction des lymphocytes T) PD-1 parmi les divers types des lymphocytes T CD4+. Nous avons d'abord comparé l'état de dysfonction des lymphocytes chez deux cohortes de personnes vivant avec le VIH (PVVIH) non-traitées. Pour l'une des deux cohortes, la virémie est contrôlée par le système immunitaire (cohorte dite de « Contrôleurs Élites »), à l'inverse de la seconde cohorte (dite « Virémique »). Les lymphocytes T CD4+ des personnes virémiques perdent leur activité antivirale et ont une forte expression de points de contrôles immunitaires. Au contraire, les contrôleurs élites ont une charge virale indétectable en l'absence de thérapie antirétrovirale (TAR), et des lymphocytes T CD4+ relativement fonctionnels. En réponse au BPCI, les lymphocytes T CD4+ spécifiques du VIH démontrent une plus grande réponse chez les PVVIH virémiques, via l'augmentation du nombre de cellules produisant des cytokines. Chez ces individus, toutes les fonctions

mesurées augmentent, à l'exception des cytokines associées aux cellules T CD4+ folliculaires auxiliaires qui sont impliquées dans l'amorçage des réponses immunologiques des lymphocytes B. Ces données montrent qu'il existe une réponse spécifique des sous-types de lymphocytes T CD4+ aux BPCI. Ce projet démontre l'avantage du blocage du ligand de PD-1 (PD-L1) sur les effets hétérogènes au niveau unicellulaire, soulignant l'importance de considérer les T CD4+ dans les analyses futures des essais cliniques évaluant le bénéfice des BPCI.

Mis ensemble, cette thèse permet une meilleure caractérisation de la réponse immunologique contre un virus à infection aiguë et, dans un second temps, un autre à infection chronique. Ces études permettent une meilleure compréhension de l'hétérogénéité dans la réponse immunologique des personnes infectées qui, si prise en compte dans des essais cliniques, pourrait aider à expliquer la variété de l'efficacité des traitements.

Mots-clés : SRAS-CoV-2, VIH, infections virales humaines, immunologie, cellules T, cytokines, réponse humorale, blocus de point de contrôles immunologiques.

Abstract

Viral infections are a major cause of disease in humans. Pandemics refer to virulent viruses that spread across more than one continent. In the last century, two major such pandemics have occurred with still-current repercussions: the acquired immunodeficiency syndrome (AIDS) pandemic caused by the Human Immunodeficiency Virus (HIV), and the Coronavirus Disease 2019 (COVID-19) pandemic by the severe acute respiratory coronavirus 2 (SARS-CoV-2). The diseases caused by both of these viruses are very different in their pathophysiology. A better elucidation of these diseases has already allowed researchers to develop therapeutic treatments against these infections; however, both pandemics caused by these viruses are ongoing. While SARS-CoV-2 proves to ultimately be fatal by an exacerbated and perhaps delayed immune response against the virus, HIV rather evades the host's immune response, weakening it over time until inducing a severe immunocompromised state, opening the door for fatal opportunistic diseases. The overarching goal of this thesis was to study the failings of the immune response against each virus, and extract information useful to guide therapeutic practices.

The objective of the first study was to find a robust and reproducible predictor of fatal outcome among patients hospitalized for their COVID-19. We profiled the plasma of a total of 279 patients across three independent cohorts to measure SARS-CoV-2 viral RNA, antibody responses against the virus and the quantities of inflammatory cytokines and markers of tissue damage. We found that plasma viral RNA could reproducibly predict fatal outcome on samples collected at 11 days after symptom onset, when adjusted for age and sex. Plasma vRNA's predictive accuracy was maintained at earlier timepoints.

We also found that low SARS-CoV-2-region-binding-domain (RBD)-specific IgG, low SARS-CoV-2-specific antibody-dependent cellular cytotoxicity, and elevated cytokines and injury markers were also strongly associated with mortality. In a second study using dimensionality reduction tools, we were able to separate our cohort in four distinct « patient clusters », based on their immunovirological plasma profile, with one cluster enriched in fatal outcomes. Our findings better characterize the heterogeneity of hospitalized COVID-19 cases, and may be useful in directing targeted therapeutic treatments.

In our third study, our objective was to characterize the response of dysfunctional HIV-specific CD4+ T cells to immune checkpoint blockade (ICB) across multiple subsets. We first sought to compare the functional state of HIV-specific CD4+ T cells among two cohorts of HIV-infected untreated indivduals, based on their ability to spontaneously control viral replication. Elite controllers, who have no detectable viral load in the absence of anti-retroviral therapy (ART), had more functional HIV-specific CD4+ T cells than their viremic counterparts, as well as lower levels of dysfunction-related transcription factors and immune checkpoint expression. We then compared the response of HIV-specific CD4+ T cells to ICB and saw greater increase in functionality in the dysfunctional cells of viremic individuals. All functions assessed were increased except for B-cell helping T follicular-helper-associated functions, underlying subset-specific responses to ICB. This effect was largely lost once ART was initiated, suggesting that the use of ICB would be optimal right before the initiation of ART.

Together, our results contribute to a better understanding of two pandemic-causing viral infections, and reveal key considerations for therapy.

Keywords: SARS-CoV-2, HIV, human viral infections, immunology, T cells, cytokines, humoral response, immune checkpoint blockade.

Résumé de vulgarisation

Les infections virales sont une cause majeure de maladie chez l'homme. Lorsqu'un virus se propage sur plus d'un continent, on parle de pandémie. Deux grandes pandémies sont toujours d'actualité : la pandémie de coronavirus 2019 (COVID-19) causée par le coronavirus respiratoire aigu sévère 2 (SRAS-CoV-2), et la pandémie du syndrome de l'immunodéficience acquise (SIDA) due au virus de l'immunodéficience humaine (VIH). Ces maladies causent la mort par des mécanismes très différents. Alors que le SRAS-CoV-2 s'avère fatal par une réponse immunitaire exacerbée, tandis que le VIH échappe continuellement à la réponse immunitaire de l'hôte, l'affaiblissant au fil du temps jusqu'à un état d'immunodépression grave. La caractérisation des mécanismes de ces maladies a permis le développement des traitements thérapeutiques. L'objectif principal de cette thèse était d'étudier les défaillances de la réponse immunitaire humaine contre chacun de ces virus, et d'en extraire les informations utiles pour guider les pratiques thérapeutiques.

Notre première étude s'est concentrée sur la COVID-19, où nous avons essayé de trouver un biomarqueur facile à mesurer dans le sang qui prédisait les cas fatals. Nous avons mesuré plusieurs protéines ainsi que la quantité de matériel génétique (ARN) du virus dans le sang de 279 patients hospitalisés pour leur COVID-19, prélevés au début de leur maladie. Nous avons constaté que l'ARN du SRAS-CoV-2 prédit fiablement la mortalité, après ajustement en fonction de l'âge et du sexe. Pour mieux comprendre l'évolution de la maladie d'un point de vue immuno-virologique, nous avons utilisé dans notre deuxième étude des outils bio-informatiques nous permettant de simultanément considérer tous les analytes mesurés. Nous avons constaté qu'il existe quatre " types " de réponses

immunitaires, dont l’un est fortement lié à la mortalité. Nos résultats permettent de mieux caractériser l'hétérogénéité des cas de COVID-19 hospitalisés, et peuvent être utiles pour orienter des traitements thérapeutiques ciblés.

Notre troisième étude s'est concentrée sur le VIH, où notre objectif était de caractériser la réponse des cellules T CD4+ dysfonctionnelles reconnaissant spécifiquement le virus, à une immunothérapie appelée blocage du point de contrôle immunitaire (BPCI). Ce traitement peut inverser partiellement le dysfonctionnement des cellules T. Nous avons d'abord comparé l'état des cellules T CD4+ spécifiques du VIH dans deux cohortes de personnes infectées par le VIH et non traitées, en fonction de leur capacité à contrôler spontanément la réplication virale. Les contrôleurs élites, qui contrôlent la charge virale la rendant indétectable en absence de traitement antirétroviral (TAR), avaient plus de cellules T CD4+ fonctionnelles spécifiques du VIH que leurs homologues virémiques, incapable de contrôler le virus. Dans les cellules des individus virémiques, le BPCI augmentaient plus fortement leurs fonctionnalités. Toutes les fonctions évaluées ont été augmentées par BPCI, à l'exception de celles associées aux cellules T folliculaires aidant les cellules B, suggérant que les réponses aux BPCI dépend du sous-type de cellules T CD4+. Cet effet est largement perdu chez les personnes sous TAR, ce qui suggère que l'utilisation du BPCI serait optimale juste avant l'initiation du traitement antirétroviral.

Cette thèse a permis une caractérisation approfondie de la réponse immunitaire humaine contre deux infections virales. Ces résultats permettent de mieux comprendre l'hétérogénéité entre les personnes infectées, et pourraient aider à orienter les thérapies ciblées.

Lay Abstract

Viral infections are a major cause of disease in humans. Pandemics refer to virulent viruses that spread across more than one continent. In the last century, two major such pandemics have occurred with still-current repercussions : the Coronavirus Disease 2019 (COVID-19) pandemic caused by the severe acute respiratory coronavirus 2 (SARS-CoV-2), and the acquired immunodeficiency syndrome (AIDS) pandemic by the Human Immunodeficiency Virus (HIV). These diseases can cause death through very different mechanisms : while SARS-CoV-2 proves to ultimately be fatal by an exacerbated and perhaps delayed immune response against the virus, HIV rather evades the host's immune response, weakening it over time until inducing an severe immunocompromised state. Better elucidation of the mechanisms behind these diseases have already allowed researchers to develop therapeutic treatments against these infections ; however, both pandemics caused by these viruses are ongoing. The overarching goal of this thesis was to study the failings of the immune response against each virus, and extract information useful to guide therapeutic practices.

Our first study focused on COVID-19, where we tried to find a good biomarker of fatal outcome that was easy to measure in plasma. We measured multiple proteins and the amount of the virus' genetic material (RNA) in the plasma of 279 patients hospitalized for their COVID-19 collected early in their disease. By comparing our measurements, we found that SARS-CoV-2 RNA was the best predictor of fatal outcome, when adjusted for age and sex. Next, to better understand how the disease evolved from a immunovirological perspective, we used bio-informatic tools to simulteaneously consider

all our measurements. We found that there are four « types » of patients, and only one type is strongly enriched in fatal outcome. Our findings better characterize the heterogeneity of hospitalized COVID-19 cases, and may be useful in directing targeted therapeutic treatments.

Our second study focused on HIV, where our objective was to characterize the response of dysfunctional CD4+ T cells which specifically recognize the virus, to an immunotherapy called immune checkpoint blockade (ICB) which is known to partially reverse dysfunction of T cells. We first compared the functional state of HIV-specific CD4+ T cells among two cohorts of HIV-infected untreated individuals, based on their ability to spontaneously control viral replication. Elite controllers, who have no detectable viral load in the absence of anti-retroviral therapy (ART), had more functional HIV-specific CD4+ T cells than their viremic counterparts. We then compared the response of HIV-specific CD4+ T cells to ICB and saw greater increase in functionality in the dysfunctional cells of viremic individuals. All functions assessed were increased except for B-cell helping T follicular-helper-associated functions, underlying subset-specific responses to ICB. This effect was largely lost once ART was initiated, suggesting that the use of ICB would be optimal right before the initiation of ART therapy.

This thesis allowed for an in-depth characterisation of the human immune response against two viral infections. These findings allow for a better understanding of the heterogeneity among infected people, and could help direct targeted therapies.

Table of contents

List of Tables

List of Figures

Abbreviations

Acronyme	Long name
ACE2	Angiotensin converting enzyme 2
ADCC	Antibody-dependent cellular cytotoxicity
AIM	Activation-induced marker
APC	Antigen-presenting cells
APOBEC3	Apolipoprotein B editing complex
Arm	Armstrong strain
ART	Antiretroviral therapy
ARV	Antiretroviral
AUC	Area under curve
BALF	Bronchoalveolar lavage fluid
BIC	Bayesion information criterion
CD	Cluster of differentiation
cDC	Classical dendritic cells
Cl13	Clone 13
CP	Chronic progressor
CSR	Class switch recombination
CTL	Cytotoxic T lymphocytes
CTLA-4	Cytotoxic T lymphocyte-associated antigen 4
DAMP	Danger-associated molecular pattern
DSO	Days since symptom onset
EC	Elite controller
FMT	Fecal matter transplant
GALT	Gut-associated lymphoid tissue
GC	Germinal center
HIV	Human immunodeficiency virus
HLA	Human leukocyte antigen
HR	Hazard ratio
IC	Immune checkpoint
ICB	Immune checkpoint blockade
IFN	Interferon
Ig	Immunoglobulin
IL	Interleukin
IN	Integrase
ISG	Interferon-stimulated genes
LCMV	Lymphocytic choriomeningitis virus
MERS	Middle east respiratory syndrome

MHC	Major histocompatibility complex
nAE	non-AIDS event
Nef	[HIV] Negative regulatory factor
NK	Natural killers
nsp	Non-structural protein
OR	Odds ratio
Orf	Open reading frame
PAMP	Pathogen-associated molecular pattern
PD-1	Programmed cell death protein 1
PIC	Pre-integration complex
PRR	Pattern recognition receptor
RBD	Receptor binding domain
Rev	[HIV] Regulator of expression of virion proteins
RM	Rhesus macaques
RNA	Ribonucleic acid
ROC	Receiver-operating curve
RT	Reverse transcriptase *or* reverse transcription
RTC	Replication-transcription complex
S	Spike
SARS-CoV-1	Severe acute respiratory syndrome coronavirus 1
SARS-CoV-2	Severe acute respiratory syndrome coronavirus 2
sgRNA	Subgenomic ribonucleic acid
SHM	Somatic hypermutation
Tat	[HIV] Transactivating protein
TCR	T cell receptor
TFH	T follicular helper
TH	T helper
TIGIT	T cell immunoreceptor with Ig and ITIM domains
TLR	Toll-like receptor
TMPRSS2	Transmembrane protease serine 2
UC	Uninfected control
VI	Viral integrase
Vif	[HIV] Virion infectivity factor
VL	Viral load
vRNA	Viral RNA

To Andréanne Deslippe

Ackowledgements

I would like to thank Dr. Daniel E. Kaufmann for you invaluable mentorship, your patience, and above all for trusting me in trying new things. Your scientific input and clinical perspective have really enriched my education, and I am extremely grateful for all the opportunities you have given me, whether it be conferences or collaborations. The ski escapades were also a lot of fun !

I would also like to thank all the members of the Kaufmann lab. I am very grateful for Dr. Antigoni Morou for taking me under her wing when I first arrived in the lab, teaching me the ropes, her friendship and encouragements, even after she moved to Germany. I'd also like to thank Dr. Amy Baxter, always ready to help out and save me from a crisis or two. A very special thank you to Dr. Julia Niessl, a very good friend/the best immunology-brain-storming person to have sit across from your desk, and my partner in crime Gérémy Sannier, who's compassion and humour have made the last years of my PhD that much more fun. I'd also like to thank Dr. Mathieu Dubé for input on my various projects, our two newest post-docs Drs.Manon Nayrac and Alexandre Nicolas for their energy and scientific input, and Nathalie, Gloria, Mélanie, Roxanne and Rose for lending a (very appreciated!) helpful hand! Thanks to past students Vincent Morin and Marc Khoury for their friendship.

I'd like to thank all the researchers and students at the CRCHUM, that have helped make it an exciting place to work. I'd specially like to thank the flow cytometry platform for their expertise and helpfulness, and the BSL-3 platform for maintaining a comfortable environment to work in. Special thanks to the Finzi and Chomont labs for their help in processing so many samples so efficiently and their scientific input. I'd also like to thank

the students of the 9th floor for the social events critical for maintaining my mental health, as well as all members of the immunopathology axis for their scientific input. A very big thanks to my very close friends Sai Priya Anand, Jérémie Prévost, and Myriam Verly for your support this whole time and all the fun along the way! Beyond the CRCHUM, I'd also like to thank the great collaborators I've had the chance to work with : Alina Dyachenko, Sacha Morin, Gaël Moquin-Beaudry, Olivier Tastet, Sirui Zhou, and Marc Messier-Peet and the whole OAS1 group – it's been a very enjoyable way to learn new fields !

I was lucky to study where I grew up so I was surrounded by great friends. Huge thanks to Laurence Vincent for fresh air, pharmacology talk and helping me with my French, Winona Djougoué for always checking up and distracting me, Andréanne Deslippe for encouraging me to do my best and helping me out, and Frank Feldmann for always being available to unwind. I'd also like to give a great big thank you to Federico Pratesi, who entered my life exactly at the right time, and has been a pillar of support and understanding ever since.

Finally, I'd like to thank my whole family, but most of all brother Marc, and parents Dr. Montse Llinas-Brunet and Giri Ratnasingham, for always believing in and helping me the whole way. It would not have been possible without your encouragements and love.

I had not realized, going into this 6-year endeavour, the amount of hurdles that makes up a PhD. I am so very grateful to all of you for helping me over them. It's been my sincere pleasure to know you.

XXX

Chapter 1 – Introduction

The immune response is an intricate, multi-layered system which affects all parts of the human body. It is implicated, at least to some extent, in most (if not all) human diseases. In the vast majority of pathogen infections, the immune response is effective in defending the host.

The immune response in a physiological context

The immune response is roughly split between 2 overarching categories: the innate immune response and the adaptive immune response. The innate immune response reacts to non-specific stimuli and provides an immediate yet unspecific response. The adaptive response specifically recognizes one molecular motif (epitope). This allows it to target pathogens in a targeted manner, increasing the efficiency of the response. However, the adaptive response is slower to fully develop. It is the adaptive immune response which creates immunological memory, allowing for long-lasting immunity. Both these arms interact extensively and are essential to fight off all kinds of harmful agents, like viral, bacterial or fungi infections, cancerous cells, parasites, etc., with the main goal of preserving the host.

Innate immune response to viral infection

Globally, the innate immune response includes all aspects of the immune response which are not adaptive, meaning that do not require rearrangement of the cell germ-line to function (discussed later) (Chaplin, 2010). This very broad category also includes non-cellular components:

Non-cellular components

Physical barriers, including the epithelial cell layers that make up the skin and the respiratory, gastrointestinal and genitourinary tracts. The layer of secreted mucous, which trap microbes and is constantly refreshed, are also part of this category.

Soluble bioactive small molecules and proteins, which are present in biological fluids and naturally possess antimicrobial and/or signalling activity.

Cytokines are a large group of signalling molecules secreted by (often activated) cell groups and which, by binding cell surface receptors, trigger signalling cascades with diverse downstream results. They are also central in T cell activation (Curtsinger and Mescher, 2010). **Chemokines**, a subgroup of cytokines, recruit cells by creating a gradient that the target cell will follow upstream. **Interleukins** (IL), another type of cytokines, are essential in a number of aspects of the immune response, including maintenance, growth, modulation of the immune response, and differentiation of immune cells (Justiz Vaillant and Qurie, 2021).

Interferons are key signalling molecules, and span three distinct families. Type I IFN include 13 IFN alpha (IFNa) subtypes, one IFN beta (IFNb) and a number of others, and

are the most broadly expressed IFNs. Type II IFN includes IFN gamma (IFNg), mainly produced by activated T and NK cells. Finally, the third family are type III IFNs, made up of 4 IFN lambdas (IFNl). Type III IFN have similar functions to type I IFN, but their action is restricted to epithelial cells, as their receptor is not as common (McNab et al., 2015). Each family of IFN binds to their own set of surface receptors to activate a specific transcription pattern, leading to the expression of interferon-stimulated genes (ISGs) (Platanias, 2005). Some of these are restriction factors (host proteins with direct antiviral activity). Some ISGs also reduce transcription and translation mechanisms, in view to slow down viral replication, while others increase antigen presentation and the abundance of pattern-receptor recognition (PRR) (Altfeld and Gale, 2015), so infected cells are better recognized and cleared. In addition, they enable recruitment and activation of immune cells like dendritic cells, macrophages and NK cells (Altfeld and Gale, 2015). Together, these mechanisms slow viral spread. Finally, ISGs will also play an important role in the recruitment and priming of adaptive immunity cells.

Other small bioactive molecules rather coat a microbe to enhance antiviral activity against it (such as phagocytosis). One such example are the surfactant proteins, pulmonary proteins which bind to target ligands on pathogens and enhance their clearance by immune cells (Nayak et al., 2012).

Another group still are the exquisitely complex **complement proteins**. This group of more than 30 soluble proteins coats the surface of a microbe to enhance phagocytosis or create pores to destroy it. They also elicit proinflammatory mediators (Dunkelberger and Song, 2010).

Pattern-recognition receptors (PRR), expressed on all cell types, bind to pathogen-associated molecular patterns (PAMPs – molecular structures that are common in microbes) and/or danger-associated molecular patterns (DAMPs), molecular structures found in cellular debris, for example following damage caused by the infection. Some PRR are membrane-bound like the toll-like receptors, which bind to a range of microbial by-product like lipopolysaccharide (from the membrane of gram negative bacteria) or double-stranded RNA (during the replication cycle of a virus). Other PRR are rather cytoplasmic proteins, like RIG-1-like receptors which bind to viral nucleic acids. Upon binding their target PAMP, the PRR initiate intracellular signalling cascades which induce type I interferons, cell death or cytokines (Dunkelberger and Song, 2010).

Although these non-specific functions are widespread throughout the body, there are some cell types, activated by the aforementioned mechanisms, which embody the innate immune response.

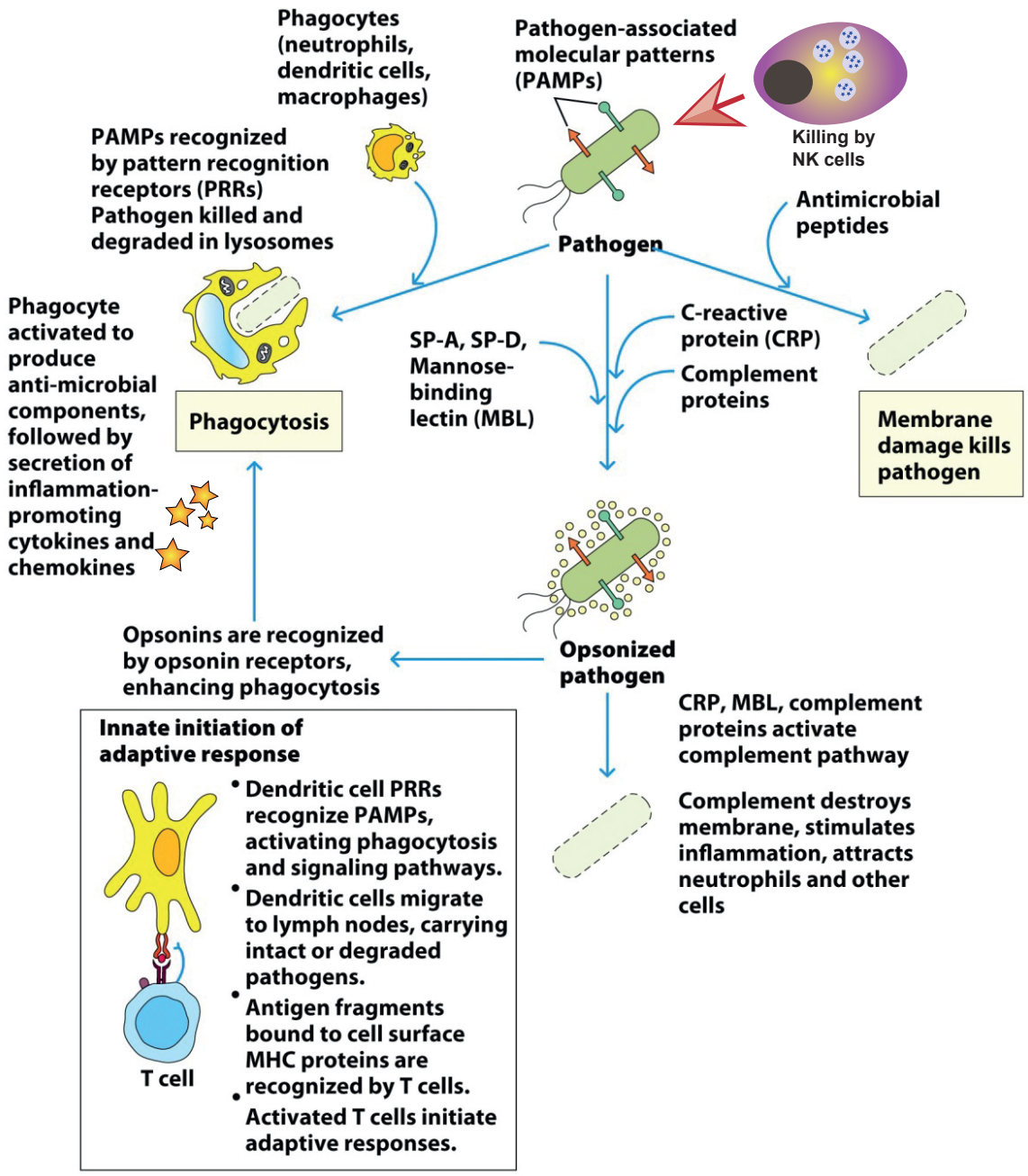

Figure 1.1. Mechanisms of the innate immune response contributing to the elimination of an invading pathogen. Upon recognition, a pathogen can be i) phagocytosed and degraded intracellularly ; killed by NK cells ; destroyed by bioactive small molecules, either directly (for example through the formation of pores by the complement cascade) or through opsonization (pathogen is “tagged” for easier identification by phagocytes). PAMPs also contribute to activation of dendritic cells, thus initiation the antigen-presentation and T cell-priming processes. Included from (Kuby Immunology, seventh edition), in accordance with allowed permissions.

Cellular components

Natural killer (NK) cells are a subpopulation of lymphocytes which target infected, transformed or stressed cells that over express NK activating ligands (NKp46, NKG2D, DNAM1) or under-express certain physiological markers (MHC I) as a consequence of their state (Bjorkstrom et al., 2021). NK cells can also mediate antibody-dependent cellular cytotoxicity through FC receptor FcgRIII (CD16). NK cells kill aberrant cells without priming through the release of cytotoxic granules containing granzymes and perforin. Perforin forms pores in the target cell's membrane, allowing for granzyme to penetrate within the cell and induce its apoptosis. NK cells also produce IFNg (Bjorkstrom et al., 2021), IL-2, IL-15, IL18 and type I IFNs (Bjorkstrom et al., 2021), which activate other immune responses and promote NK survival, proliferation and activation.

Granulocytes, so called because of their many granules, comprise neutrophils and monocytes, among others.

Neutrophils are short-lived circulating cells with multiple functions. They accumulate in large quantities at the site of infection, where they fight off the infecting agent by producing reactive oxygen species. (Kennedy and DeLeo, 2009). They are among the major phagocytic cells, clearing microbes and particles bound by immunoglobulins and complement (Chaplin, 2010). They can also produce a number of inflammatory chemokines such as CXCL9/10/11 and CCL2/3/20, depending on the trigger (Tecchio et al., 2014).

Monocytes circulate through the blood, patrolling the vascular endothelium, from which

they can rapidly be recruited to an infection site. They first produce inflammatory mediators, then differentiate into macrophages, and can replenish the macrophages in tissue at steady state.

Macrophages are long-lived tissue-resident phagocytes and, depending on the environmental cues they received, they can be 1) inflammatory, 2) anti-inflammatory or 3) healing. These cells are very plastic, meaning they can switch from one state to another.

1) The combination of IFNg and TNFa activates macrophages. These so-called "classically activated" macrophages have enhanced microbicidal activity (production of superoxide anions and oxygen or nitrogen radicals) and secrete high levels of pro-infammatory cytokines, including IL-1, IL-6 and IL-23 (Mosser and Edwards, 2008). These macrophages also express chemokines CXCL9, CXCL10, and CXCL11 which, through CXCR3 signalling, attracts NK and T cells (Martinez et al., 2009).
2) The anti-inflammatory population is induced by glucocorticoids and TGFb (produced by macrophages following phagocytosis of apoptotic cells in pro-inflammatory contexts), although they also arise at the later stages of the adaptive immune. This population produces high levels of IL-10, and express high levels of co-stimulatory molecules CD80 and CD86, implying antigen presentation, although less efficiently than DC (Mosser and Edwards, 2008).
3) Wound-healing macrophages occur through IL-4 stimulation, which allows them to produce precursors of key components of the extracellular matrix (Kreider et al., 2007).

Finally, the Dendritic cells (DC) bridge the gap between innate and adaptive immune responses by principally serving as antigen-presenting cells (APCs). There are three major DC populations: 1) conventional or classical DC (cDC)1 and cDC2, 2) plasmacytoid DC (pDC) (Collin and Bigley, 2018), and 3) an additional population derived from

monocytes (mo-DC).

1) cDC are specialized in antigen-presentation: immature cDC have high endocytic activity, which allows internalization of microbes for degradation into epitopes. Upon stimulation by microbial product or inflammatory stimuli, they express major histocompatibility complex (MHC)-peptide complexes and co-stimulatory molecules at their surface, ready to prime CD4+ T cells (Satpathy et al., 2012). While both cDC types can efficiently cross-present and produce IL-12, cDC2 in humans also produces IL-23, TNFa, CXCL8/IL-8 and IL10, while cDC1 can also present necrotic antigens to T cells (Rhodes et al., 2019).
2) Through TLR7 and TLR9 in endomoses, pDC sense viral nucleic acids, upon which they express high levels of type I IFN, TNF, IL-6 and Granzyme B. pDC are rather poor antigen-presentors (Siegal et al., 1999), and express CD4 and multiple chemokine receptors, namely CXCR3, CXCR4, CCR2 and CCR7 (Collin and Bigley, 2018).
3) Mo-DC, also known as “inflammatory DC”, are absent at steady state. They differentiate from monocytes and egress from the bone marrow via CCR2 to go to the site of inflammation. They can secrete IL-1, TNFa, IL-12 and IL-23.

Antigen presentation

APCs mediate antigen presentation to T cells via the major histocompatibility complex (MHC), known has the Human Leukocyte Antigen (HLA) in humans. MHC class I molecules bind peptides for presentation to CD8+ T cells, and are expressed on nearly all somatic cells in physiological context. Cytosol-derived peptides are processed and loaded onto MHC class I, making it ideal to recognize infected cells. MHC class II is used to present peptides to CD4+ T cells. Outside the thymus, MHC class II is expressed on APCs and phagocytes, although it can be up regulated following IFNg stimulation. It is loaded with peptides derived from the processing of intravesicular pathogens or extracellular

pathogens, uptaken through phagocytosis, micropinocytosis or receptor-mediated endocytosis. APCs load their MHC either by phagocyting some infected cells and trafficking to the secondary lymphoid organs densely populated with T cells, or by capturing particulate antigen and pathogens trafficked through the lymphatics into the lymph nodes (Janeway, 2016).

Phagocytic APC can, after phagocyting dead cells, process them and present exogenous peptides on the MHC class I, in what is called cross-presentation. If the DC was activated through PRR ligation or CD4+ T cell help prior to cross-presentation, this results in the productive activation of CD8+ T cells (i.e. cross-priming) (Gutierrez-Martinez et al., 2015).

Adaptive immune response to viral infection

As mentioned previously, immune cells of the adaptive immune response have a single specificity. For this reason, it is slower than the innate, as it requires first the correct matching of an antigen with a specific cell, and then the priming of said cell, which normally happens between 6-10 days in humans. The two main factions are T cells, expressing a T cell receptor (TCR) and B cells, with B cell receptors (BCR).

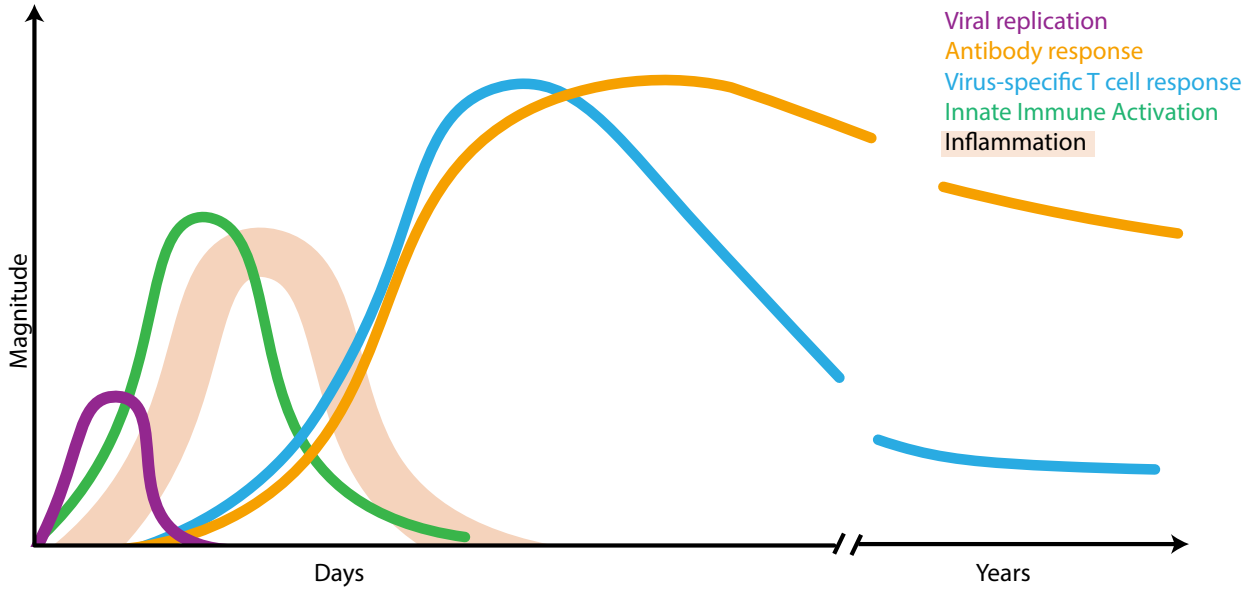

Figure 1.2 Schematic of a perfect immune response with activation of the adaptive immune response in humans. Wiral infection rapidly activates the innate immune response, resulting in inflammation. These processes allow efficient activation of both the cellular response mediated by T cells and the humoral response from B cells. T cells further aid in increasing antibody specificity and in differentiation into plasmablasts, creating a pool of specific antibodies which are replenished over time. Meanwhile, virus-specific T cells contract, with a small population of memory T cells persisting. Figure based on (Sette and Crotty, 2021).

T cells

Based on the chains that compose their TCR, there are two types of T cells: T cells with αβTCR, which make up around 90% of all circulating T cells and generated in the thymus, and those with γδTCR, which are in majority generated in an extrathymic compartment

(McVay and Carding, 1996). Because they are the most common, αβT cells (herein simply referred to as T cells), are the most studied. In the thymus, this population is further distinguished between two subsets, on the basis of their co-receptor: cluster of differentiation (CD)4+ T cells, known as helper T lymphocytes (T_H), and CD8+ T cells, known at cytotoxic T lymphocytes (CTL).

The heterodimeric TCR, made of one alpha and one beta chain, is made up of constant and hypervariable regions. Multiple V, D and J segments make up the *TCRA* and *TCRB* loci. Recombination and gene rearrangement of these segments, the addition of nucleotides between their junctions, and diversity in alpha and beta chain pairing create a highly diverse repertoire of TCRs. These undergo strict selection processes in the thymus, where T cells with non-functional rearrangements or autoreactive (meaning they react too strongly to epitopes present in the host's cells) TCRs are eliminated. Fewer than 5% of T cells survive the selection process, and can enter the circulation as naïve T cells. The result of this is a pool of highly diverse naïve T cells, in terms of capacity to recognize epitopes.

In the advent of a primary viral infection, there are three distinct phases that characterize the T cell response:

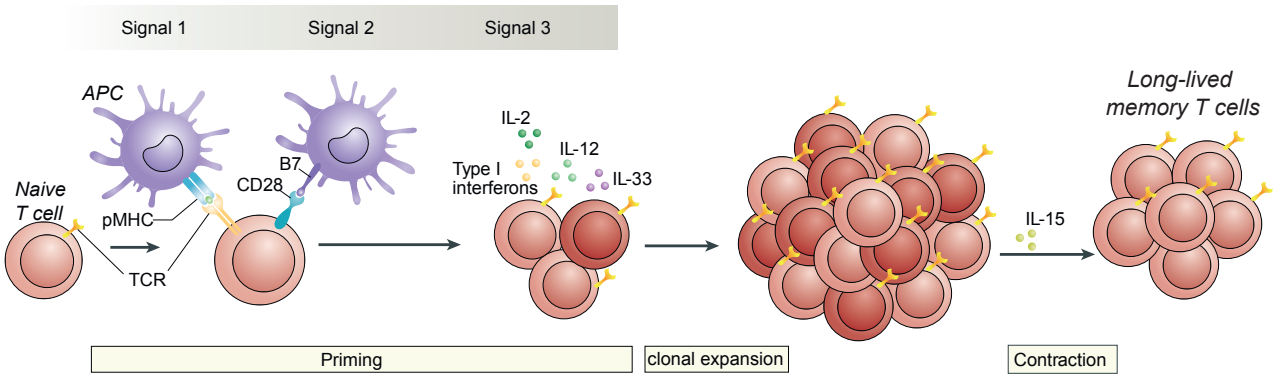

Figure 1.3 Phases of the T cell response. To allow for stimulation, never-exposed naïve T cells' TCR must recognize the peptide-MHC complex expressed on an antigen-presenting cell (APC) – signal 1. The T cell must also receive co-stimulation mediated by CD28-B7 binding (signal 2) and cytokine signalling from the milieu (signal 3). Priming allows for clonal expansion, whereby a single clone (T cell with a given specificity) will multiply and create a large pool of activated T cells with effector functions. Once the infection cleared, most cells undergo apoptosis except for a small, stable pool of long-lived memory cells maintained by IL-15 and IL-7. Figure modified from (Adams et al., 2020).

Upon breaching the barrier, a virus infects a cell and, through activation of the innate immune system, inflammation occurs. Antigen-presenting cells (APCs) load their MHC with viral epitopes. APCs then present their epitopes to T cells, either on MHC class I for CD8+ T cells, or MHC class II for CD4+ T cells, along with critical costimulatory signals (B7/CD80/CD86 interaction with CD28) and cytokines. In response to this, newly activated T cells enter the expansion phase, where they proliferate in mass and differentiate into effector cells, with a distinct epigenetic and transcriptomic profile (Kaech and Cui, 2012; Masopust and Schenkel, 2013). Only T cells activated by the APC proliferate, creating a pool of clones (i.e. T cells with the same TCR, so the same specificity). This transition is characterized by the loss of lymphoid homing molecules CCR7 and CD62L, and gain of CCR5, through which they are directed to sites of inflammation. As a result, the effector cells exit the lymphoid tissues and, through the circulation, migrate to sites of inflammation (Wherry et al., 2004), where they are maintained by IL-2 (Tham et al., 2002). As we will

discuss later, these effector T cells are key in aiding the control of viral infections through diverse mechanisms.

After the clearance of the viral infection and resolution of the inflammation, T cells enter the contraction phase, where 90-95% of the expanded clones are cleared by apoptosis (Prlic and Bevan, 2008). This step is necessary, as sustaining so many effector cells is taxing. In the final maintenance phase, a small subset persists as memory T cells, a quiescent self-renewing population that can be quickly reactivated to perform effector functions upon antigen recognition (Masopust and Schenkel, 2013). IL-7 and IL-15 keeps their numbers constant over time (Gasper et al., 2014). Two populations of memory T cells are found in circulation : T central memory (which home to secondary lympoid organs through the expression of CCR7) and T effector memory (circulate through non-lymphoid tissues and express CCR5) (Sallusto et al., 1999). It is also worth noting that 98% of T cells are not in the blood, but rather in the tissues; some effector T cells which went to the tissues stayed there as persistent tissue-resident memory T cells. They provide the first line of defence against tissue-invading pathogens (Thome and Farber, 2015).

CD4+ T cells

Helper T cells (TH) primarily act to regulate cellular and immune responses. Based on the environmental cues received at the time of activation, they will polarize towards different archetypes, governed by distinct master transcription factors, and with the ability to produce a specific set of cytokines (Becattini et al., 2015). A dominant lineage-specific transcription factor will counteract the others, but CD4+ T cells are plastic and undergo functional reprogramming. As such, CD4+ T cells show a great degree of plasticity in

moving away from one subset and towards another, as well as by having traits of multiple subsets at the same time (Becattini et a*l.*, 2015). The differentiation of the CD4+ T cell subset depends on the pathogen, and an aberrant polarization can result in ineffective pathogen clearance (Pirmez et al., 1993).

Regulatory T (Treg) cells can either be natural, meaning that they developed their regulatory functions in the thymus, or induced, when they are activated in the presence of IL-10. They express the transcription factor FoxP3 and suppress activation through the secretion of IL-10 and TGFb, as well as through inhibitory cell-to-cell contacts (Becattini et al., 2015).

TH1 cells are the prototypical antiviral subset, and are induced by IL-12 co-stimulation. They are characterized the expression of T-bet and/or EOMES and produce IFNg, IL-2, TNF-a and lymphotoxin. A subset of Th1 also have cytolytic functions like perforin and granzyme B secretion. Th1 cells express CXCR3. (Becattini et al., 2015).

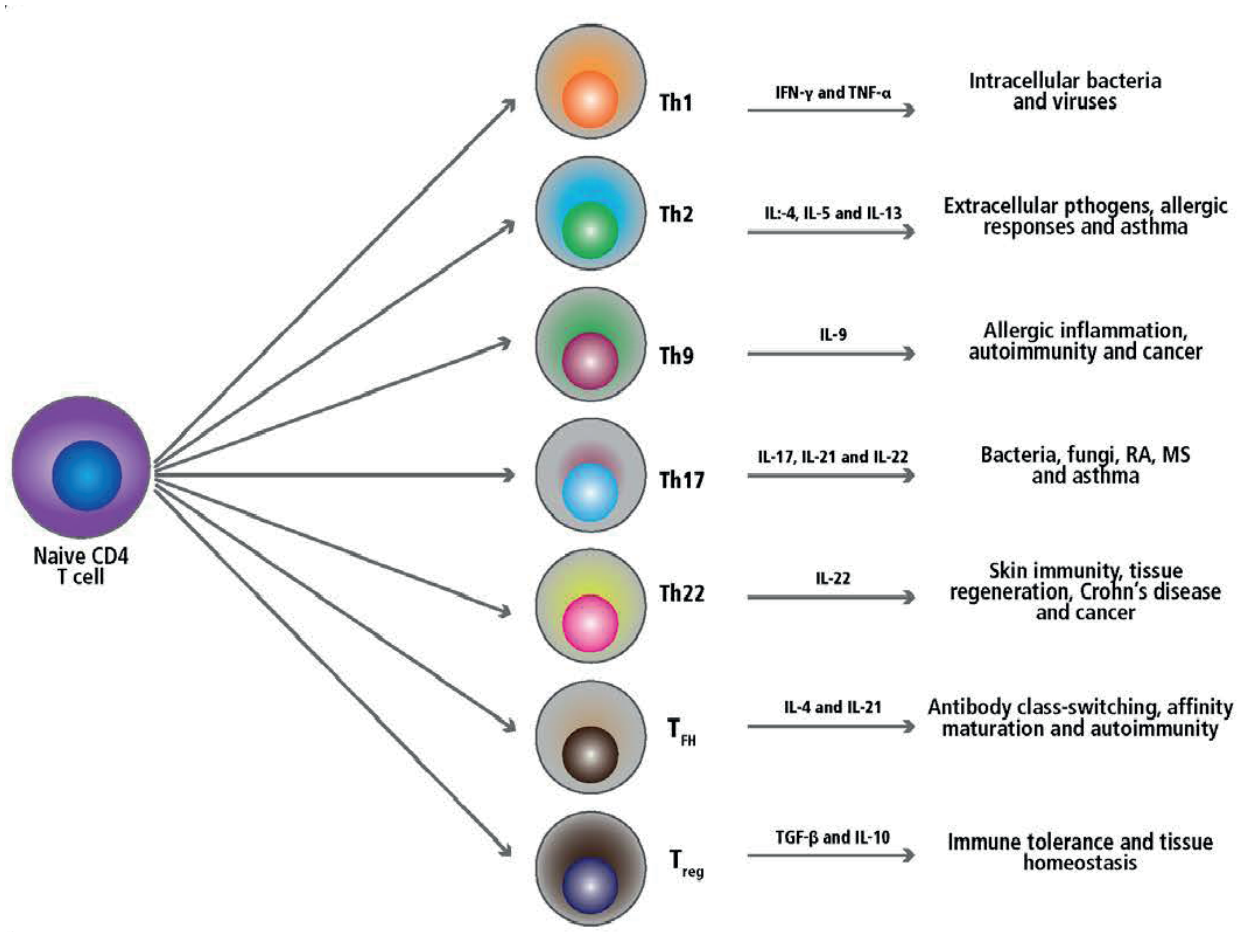

Figure 1.4 Overview of CD4+ T helper cell subsets

TH2 cells are induced by IL-4 and express the transcription factor GATA-3. They produce IL-4, IL-5, IL-9, IL-13 and GM-CSF. These cells are important to fend off extracellular multicellular pathogens, like helminths and nemathods. (Becattini et al., 2015).

TH17 are induced by TGFb and IL-6, and their transcription factor is RORgC. They produce IL-17 and IL-22 (Liang et al., 2006) and express CCR6 and gut-homing integrins. (Becattini et al., 2015).

Th22 also express CCR6, are regulated by AHR and produce IL-22 without IL-17 (Becattini et al., 2015). They play an essential role in repairing the mucosal barrier.

T follicular helper (TFH) provide help to B cells. Their master transcription factor (which is a repressor) is Bcl-6, and they produce IL-21 and CXCL13. Their signature chemokine receptor, CXCR5, allows them to migrate to germinal centres in lymphoid tissues, where they can activate B cells and select high-affinity clones, thus playing a key role in the production of high-affinity antibodies (Sallusto, 2016).

The advent of single-cell RNA seq analyses, in conjunction with increasingly precise tools, has brought into question the validity of this archetype model. Pure populations of TH subsets are rarely observed. Effector CD4+ T cells span a continuum, with a transcriptomic profile principally associated to their cell state (for example, proliferation, response to IFN, resting) (Kiner et al., 2021). Analyses of transcriptome and chromatin availability did not reveal discrete polarizations, supporting the theory of a continuum (Cano-Gamez et al., 2020; Kiner et al., 2021). Only Treg and naïve CD4 T cells are completely distinct from effector cells (Kiner et al., 2021).

Tools to study CD4 T cells

The most specific way to identify virus-specific CD4+ T cells is through the use of MHC-peptide complexes, most often biotin-labeled and bound to streptavidin, which forms a tetravalent complex – tetramer (Nepom, 2012). These tetramers will only bind to specific TCRs and do not require additional manipulation of the cells. The multitude of immunogenic epitopes harbored by a single pathogen, compounded to the extreme diversity of the human MHC II (called HLA class II), make tetramers hard to apply to

heterogeneous cohorts. Conversely, they are particularly useful in contexts of limited genetic diversity (for example, infections in syngeneic mice) (Nepom, 2012).

Alternative assays have depended on cytokine production to detect activated cells. At the population level, the overall cytokine profile can be measured in the supernatant of stimulated cells by ELISA-type assays. To get a sense of the number of virus-specific T cells a sample contains, ELISpot can be used, where cytokine production is captured within a small vicinity of where it was produced, allowing to “count” the number of cytokine-producing cells. Finally, intracellular staining can be used to detect cytokines accumulated within CD4+ T cells stimulated in the presence of a blocker of protein transport. Although more widely applicable than tetramers and high throughput, they rely on the detection of a limited set of cytokines, directing the type of virus-specific CD4+ T cell captured (Schmidt and Sester, 2013; Reiss et al., 2017).

A relatively newer method called the activation induced marker (AIM) assay relies on the upregulation of surface markers following the activation of a cell by peptide stimulation (Reiss et al., 2017). There are multiple combinations of AIM which are employed, based on the time of stimulation and the tissue from where the cells are collected. Although the type of AIM used influences what the TH populatons are detected (Reiss et al., 2017), AIM combinations capture a larger and more diverse pool of virus-specific CD4+ T cells than cytokine-based assays (Niessl et al., 2020b). Stimulation with multiple peptides also means more virus-specific CD4+ T cells captured than with tetramer staining. Preservation of the cell’s transcriptome enables the use of AIM for bulk (Morou et al., 2019) and single-cell RNA Seq assays (Meckiff et al., 2020b).

CD8+ T cells

In secondary lymphoid organs, dendritic cells presenting peptides prime f naïve CD8+ T cells (Zhang and Bevan, 2011). This priming is dependent on CD28 co-stimulation, and further enhanced by inflammatory cytokines including type I IFN and co-stimulatory ligands. The primary activation of CD8+ T cells can be dependent of CD4+ T cell priming of DC (against HSV-1) or independent (as for influenza and LCMV) (Bevan, 2004). However, CD4+ T cells promote memory CTL development (Shedlock and Shen, 2003) and play a central role in CD8 T cell reactivation upon secondary challenge (Janssen et al., 2003). CD4+ T cells also enhances recruitment of CD8+ T cells into infected sites (Nakanishi et al., 2009).

CD8+ T cells' antiviral function is very direct: once they recognize infected cells (which present viral epitopes on their MHC I), they kill the infected cells through secretion of perforin and granzymes, similarly to NK cells, or through Fas-FasL-depdendent apoptosis induction. Finally, CD8+ T cells also produce pro-inflammatory cytokines like IFNg and TNFa. (Zhang and Bevan, 2011)

B cells

After their formation, naïve B cells leave the bone marrow and are activated by interacting with a cognate CD4+ T cell. When these interactions occur outside the germinal centre (GC), the naïve B cells differentiate into antibody secreting cells (plasma cells) which are typically short-lived. These quickly-generated cells provide a rapid burst of antibodies which mediate early antiviral protection, despite not being highly specific for the invading pathogens (MacLennan et al., 2003).

Alternatively, B cells enter lymphoid organs and present processed antigens (taken from

nearby follicular dendritic cells) on their MHC II. They compete for limited TFH help and, if successful in their match, migrate to a distinct site within the GC where they proliferate and undergo somatic hypermutation. This latter process introduces single nucleotide exchanges randomly in the BCR, in an attempt to increase its affinity. B cells will then return for more interactions with TFH, and repeated cycles and selections ultimately leads to highly specific B cells. These B cells can differentiate into long-lived plasma cells or memory B cells and enter the circulation (Crotty, 2011).

In addition to promoting proliferation and activation of B cells, cytokines and co-stimulation from the TFH can lead to class-switch recombination (CSR). CSR happens by rearranging the constant region of the immunoglobulin's heavy chain through DNA excision and ligation, changing the class but not the specificity of the antibody (Vaidyanathan and Chaudhuri, 2015).

These different classes of antibodies vary in both conformation and in function (Schroeder and Cavacini, 2010). **IgM** is the first immunoglobulin expressed during B cell development, and it is present on antigen-inexperienced naïve B cells. When antigenic stimulation occurs, IgM form pentamers, for which their multiple interactions can make up for their typically low affinity (due to little SHM at this point). IgM opsonize antigen, which can block *de novo* infection and activate the complement cascade. Another antibody class found on naïve B cells are **IgD**. Circulating levels of IgD are very low and known to react with specific bacterial proteins and thus activate B cells. **IgG** is the predominant class of antibody, typically making up 75% of all antibody found in the serum, and is a product of CSR. Monomeric IgG can opsonize pathogens, activate the complement cascade, and inhibit viral entry. IgG antibodies also bind to the Fc-receptors expressed on multiple

immune cells, and activate pathogen-clearing processes like antibody-dependent cellular cytotoxicity, antibody-dependent phagocytosis, and release of soluble inhibitors. **IgA,** also a result of CSR, are secreted as monomers or dimers and are predominantly found in mucosal surfaces, where they protect from pathogen binding to the mucosal surface and may facilitate antigen uptake by dendritic cells for downstream presentation. Finally, **IgE** is strongly associated with hypersensitivity and allergic reaction: it binds with very high affinity to a mast-cell receptor, and causes their degranulation. (Schroeder and Cavacini, 2010)

In summary, there is extensive cross-talk between the different components of both the innate and adaptive immune response, which allows for their high efficacy. However, there are instances where the immune response can fail, either by being too strong and causing immunopathology, or by being outrun by an evolutionary machine of a virus. The immune response can be modulated or boosted therapeutically. However, to know what aspects need help, we first need to understand how exactly the immune response failed at its task. In the following sections, we will discuss the human immune responses against two pandemic-causing viruses of acute (SARS-CoV-2) or chronic nature (HIV), and focus on what went wrong, with the perspective of zoning in on therapeutic approaches that would cure or minimize the repercussions of the infections.

Acute viral perturbations : SARS-CoV-2

In December 2019, a new strain of coronavirus was characterized in Wuhan, China, and is thought to have occurred following a zoonotic transmission. Within months, this virus called SARS-CoV-2 had spread worldwide. As of December 18th 2021, there have been 275 million reported cases, with over 5 million deaths, across 222 countries and territories (https://www.worldometers.info/coronavirus/?utm_campaign=homeAdvegas1?). While the advent of protective vaccines has slowed the saturation of hospitals, mutated variants keep this pandemic going. It is crucial to study the mechanisms of how this coronavirus causes such severe symptoms, how to identify quickly the patients at greatest risk of developing critical disease, and how to help them overcome it.

Viral characteristics

SARS-CoV-2 is part of the family of coronaviruses (order Nidovirales, suborder Coronavirineae, family Coronaviridae, subfamily Orthonocoronavirinae, genera betacoronavirus). It is an enveloped positive-sense single-stranded RNA virus with a very large genome (>30kb), exclusively infecting mammalian cells (V'Kovski et al., 2021). Before the pandemic, we predominantly encountered its milder cousins behind the common cold (HCoV-229E, HCoV-OC43, etc.), although other infamous highly-pathogenic coronaviruses have already caused epidemics (SARS-CoV, MERS). SARS-CoV-2 virions include the structural proteins Spike (S – viral entry), envelope (E), membrane (M – E and M incorporate RNA genome into viral particle during assembly) and nucleocapsid (N – encapsulates RNA genome) (V'Kovski *et al.*, 2021)

Replication cycle

SARS-CoV-2's Spike (S) homotrimeric glycoprotein binds angiotensin converting enzyme 2 (ACE2) via it's receptor binding domain (RBD) of the surfaced-exposed S1 part, and mediates entry into the cell (Letko et al., 2020). Transmembrane protease serine 2 (TMPRSS2) facilitates viral entry by cleaving ACE2 (Hoffmann et al., 2020). Once the virus is up taken, it first fuses with the cellular membrane, then is released and uncoated. Two large open reading frames (ORFs) are immediately translated into polyproteins, which are turned into 15 non-structural proteins (nsp), the majority of which form the replication and transcription complex (RTC) (Gorbalenya et al., 2006). The RTC includes a RNA proofreading function which maintains genome integrity (Gorbalenya et al., 2006). Full-length negative-sense genomic copies are produced, which serve as a template to produce viral genome to be packaged, as well as to make more RTC and nsp. The synthesis of negative-strand RNAs also produces subgenomic negative-strand (sgRNAs). They serve as templates for the nested sg positive-strand mRNAs, which go onto produce the structural and accessory proteins (V'Kovski et al., 2021).

The concerted effort of some nsp and host cell factors leads to the formation of viral replication organelles. Once the RTC is anchored in their double-membrane wall (Wolff et al., 2020), they allow for viral genomic RNA to replicate and be transcribed hidden from cellular sensors (Klein et al., 2020; Stertz et al., 2007). Translated structural proteins go to the endoplasmic reticulum-to-Golgi intermediate compartment, where they interact with N-encapsidated genomic RNA, and bud into the lumen of secretory vesicular compartments (Klein et al., 2020). These now complete virions exit the infected cell via lysosomal trafficking pathways (Ghosh et al., 2020).The virus can productively infect lung

epithelial cells, but also intestinal cells and epithelium of other organs (Wang et al., 2020d; Xiao et al., 2020).

Some of SARS-CoV-2 proteins help in immune evasion. The virus has at least 5 accessory proteins (not structural, not part of the RTC, and not necessary for replication in cell culture but often play roles in a natural host) (V'Kovski et al., 2021). One accessory protein, ORF8, binds MHC I to mediate its degradation *in vitro* (Zhang et al., 2021), and ORF3b antagonized IFN (Konno et al., 2020). nsp can also counteract immune responses: nsp1 affects cellular translation in the cytoplasm to favour viral over cellular RNA, effectively blunting expression of IFN types I and III (Thoms et al., 2020).

Variants

The massive worldwide spread of the virus, coupled with massive sequencing efforts of a number of countries, has revealed that the SARS-CoV-2 genome has mutated through single nucleotide changes, insertion/deletions events, and, perhaps, recombination events (Ignatieva et al., 2021). Alinement of 77 801 genome sequences collected globally identified 15 018 mutations, of which 14 824 were single-nucleotide polymorphism (Hu et al., 2021). As of July 4th 2021, there were 1 295 identified variants (using the Pango lineage method(, where variants are a cluster of infections with shared ancestry and epidemiologically relevant – i.e., they did not die out) (https://www.ecdc.europa.eu/en/covid-19/variants-concern) (https://cov-lineages.org/global_report.html). Only a small minority of mutations, however, are expected to change the virus' fitness. Thus, few of these variants are "of concern" meaning that mutations they carry affect the viral fitness, transmissibility and/or antigenicity of the infecting virus, as well as the severity of the infection : B.1.1.7, B.1.351, N.1.617.2, P.1

and the new omicron variant (https://www.ecdc.europa.eu/en/covid-19/variants-concern) (https://cov-lineages.org/global_report.html). The variants of interest sometimes have convergent mutations (appeared separately in two different variants),

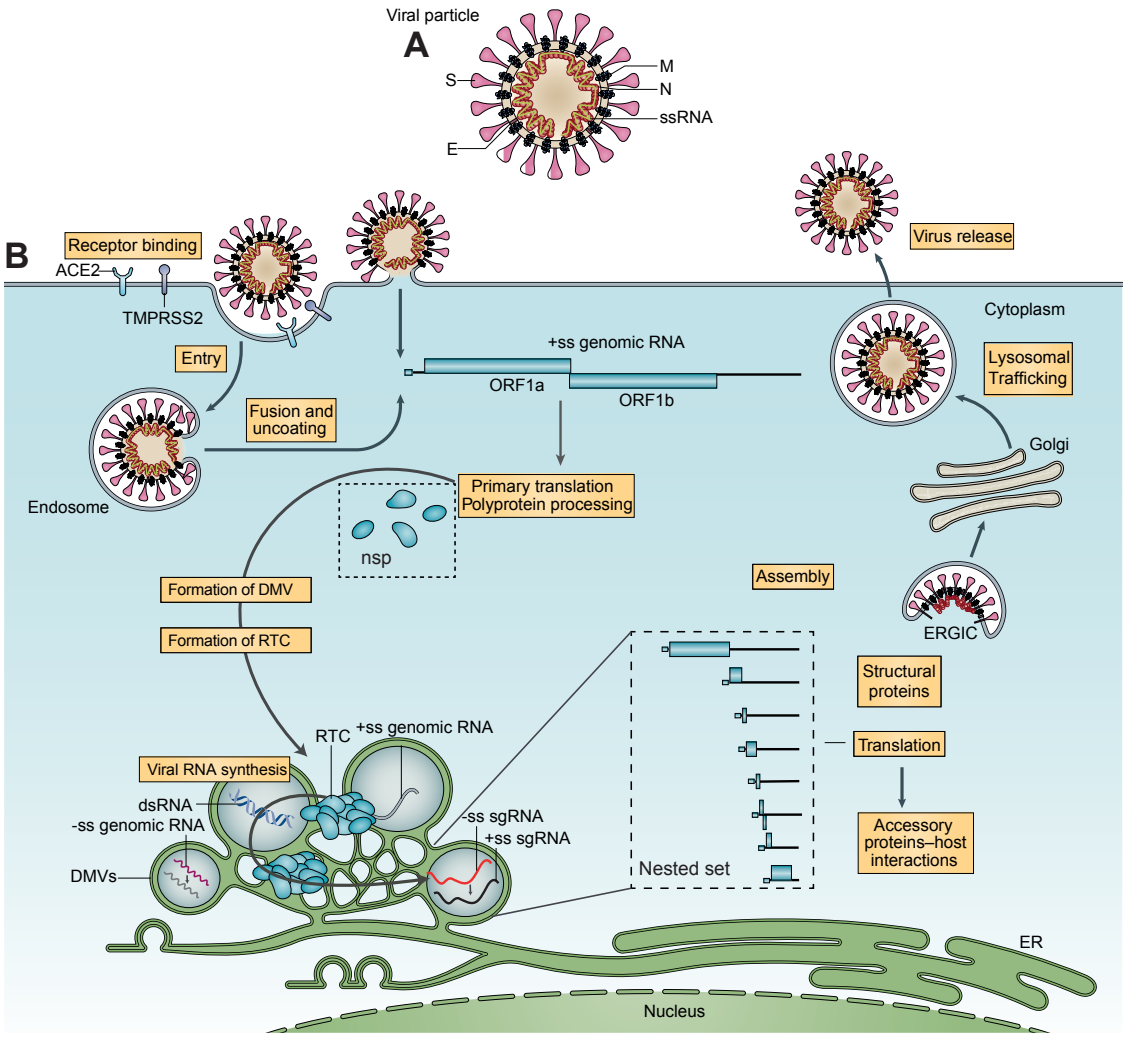

Figure 1.5 SARS-CoV-2 structure and replication cycle. A) Components and structure of a mature SARS-CoV-2 viral particle. Single strand RNA genome is encapsulated by the nucleocapsid proteins (N), and contained within a host-derived membrane punctuated by the viral transmembrane structural proteins membrane (M) and envelope (E), and the protruding trimeric glycoprotein Spike (S). B) Schematic of SARS-CoV-2 replication cycle within an infected human cell. Viral particle binding to the host cell is mediated by the interaction of viral protein S with host's ACE2, and viral uptake and fusion is enabled by host factor TMPRSS2. Viral particle is then uncoated, and viral RNA is translated into two large open reading frames, ORF1a and ORF1b. These are transcribed into the polyproteins, which in turn are processed into non-structural proteins (nsp). These nsp usher the formation of double-membrane vesicules (DMVs) and form the replication and transcription complex (RTC). Viral RNA is replicated and/or transcribed into the nested set of subgenomic (sg) mRNAs, which are translated into the structural or accessory proteins. The structural proteins enter the endoplasmic reticulum (ER) membranes and transit through the ER-to-Golgi intermediate compartments (ERGIC). The ERGIC interact with the new N-encapsidated genomic RNA and buds into the lumen of secretory vesicules. Lastly, it is secreted by exocytosis. Figure modified from (V'Kovski *et al.*, 2021)

suggesting evolutionary advantages. These mutations primarily affect Spike, and resulted in greater infectivity and/or decreased antibody-binding (Harvey et al., 2021). Other viral proteins are also changed in variants: deletions in ORF8 detected in a variant resulted in enhanced *in vitro* replication, although no difference in viral loads in nasopharyngeal samples (Su et al., 2020). Variants of concern are monitored by public health authorities, as they have different susceptibilities to vaccines (Krause et al., 2021) and treatments like monoclonal antibodies, and differ in rates of infectivity (Hu et al., 2021).

Clinical manifestations

The progression of COVID-19 has distinct “phases” : then early infection, pulmonary, and hyperinflammation phases (Figure 1.6) (Siddiqi and Mehra, 2020)**.** The early phase spans inoculation and initial establishment of the infection, characterized by non-specific flu-like symptoms. These include fatigue, fever, dry cough, and loss of smell and/or taste, although other less frequent symptoms comprise headache, hemoptysis (coughing blood), diarrhea, anorexia, sore throat, chest pains, chills, nausea, and vomiting (Hu et al., 2021). Clinically, this stage presents lymphopenia. The range of severity is highly person-dependent, and the high proportion of infected individuals who were asymptomatic or who have mild symptoms likely facilitated interindividual spread.

A proportion of infected people progress onto the pulmonary phase, where they develop viral pneumonia with replication of the virus in the lower respiratory tract. The leading symptom is hypoxemia, or low blood oxygenation (Diagnosis and Treatment Protocol for Novel Coronavirus Pneumonia (Trial Version 7), 2020), although it is sometimes not

accompanied by hypoxia. Tell-tell signs of lung involvement are also apparent with chest imaging, which show bilateral infiltrates or ground glass opacities.

A minority of people progress onto the final stage of hyperinflammation, characterized by extrapulmonary systemic hyperinflammation syndrome. It is at this stage that markers of systemic inflammation as well as markers of tissue damage are highest. It is also characterized by acute respiratory distress syndrome (ARDS), septic shock and/or multi organ failure (Hu et al., 2021).

Severity classification varied between research groups, so for the purpose of this thesis: **critical** patients **are hospitalized individuals requiring mechanical ventilation** (i.e. they reached the third phase); **severe** patients are **hospitalized and require nasal cannula** (reached phase II with hypoxia); **moderate** patients **are hospitalized without requiring additional oxygen** (phase II without hypoxia); **mild** patients are **not hospitalized for their SARS-CoV-2 infection**, and asymptomatic patients present no COVID-19 symptoms (both in phase I). In a report on 72 314 cases among the first in China, 80% were mild-to-severe and 20% were critical, 5% of which had terminal disease (Hu et al., 2021.)

Greater severity of COVID-19 is associated to age, male sex, pre-existing chronic conditions like diabetes, obesity, hypertension, muco-obstructive lung disease, renal failure and heart disease (Brodin, 2021). As apparent with the symptoms, consequences of SARS-CoV-2 infection are not exclusive to lungs. Infection can also lead to longer-term disease grouped under the umbrella-term “long COVID”, symptoms persisting longer than 2 months after initial infection. These include persisting fatigue, myalgia, intestinal disturbances, skin manifestations, and postural orthostatic tachycardia syndrome (Brodin,

2021).

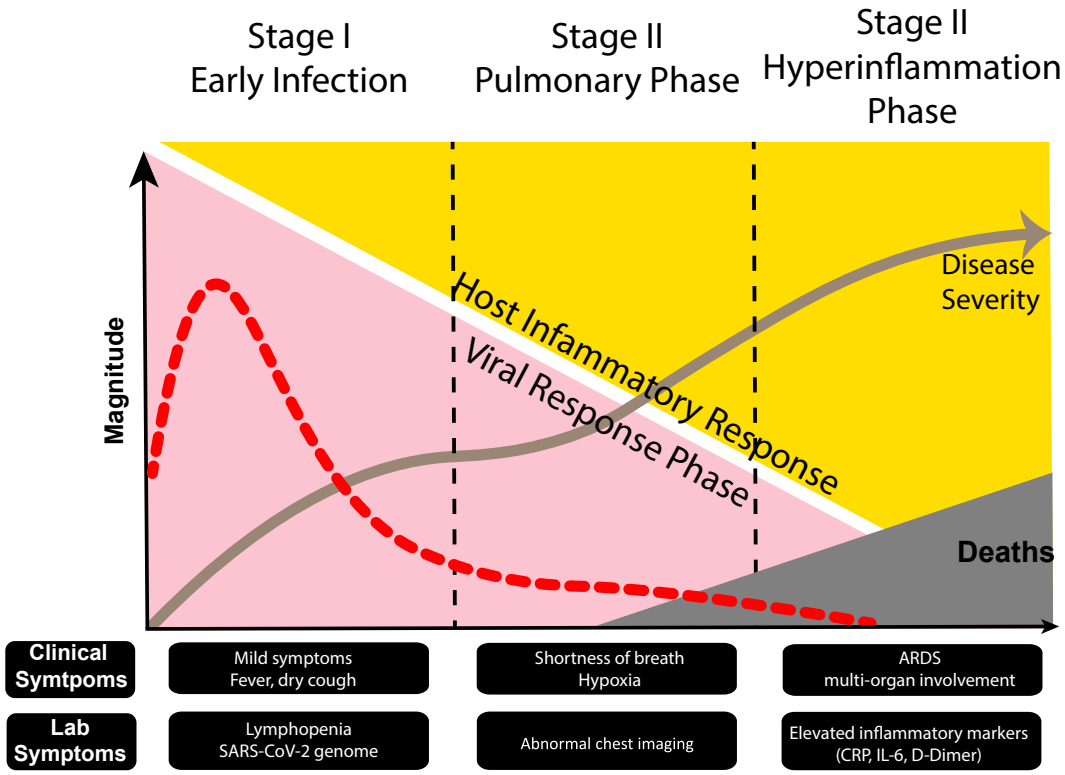

Figure 1.6 Stages of COVID-19 with associated symptoms. The early phase constitutes the establishment of the disease, with viral replication in the upper airways. This phase is characterized by mild non-specific symptoms and lymphopenia. In the second phase, inflammation occurs in the lungs with subsequent loss of respiratory capacity. Patients may start to be hospitalized at this stage, with a few fatalities occurring. The final phase is systemic hyperinflammation, characterized by high plasma levels of inflammatory cytokines. At this stage, critical patients are usually put on mechanical ventilation. Damages can extend to multiple organs, often kidneys and heart. It is during this stage that most COVID-19-related deaths occur. *Modified from* (Siddiqi and Mehra, 2020)

A distinguishing feature of COVID-19-related ARDS is “silent” hypoxamia, where individuals with critically low blood O_2 levels experienced no or minor discomforts normally associated to this state, like shortness of breath or laboured breathing (Dhont et al., 2020; Guan et al., 2020; Siswanto et al., 2020). Most cases had an almost normal lung compliance (i.e. expansion capacity) (Sorbello et al., 2020). However, patients with low compliance and elevated D-dimer (a protein fragment liberated upon dissolution of a blood clot ; high levels of D-dimer in blood are suggestive of hypercoagulability and/or

thrombosis) are at increased risk of death(Grasselli et al., 2020). The central feature of COVID19 pneumonia is low oxygen saturation in the blood (Diagnosis and Treatment Protocol for Novel Coronavirus Pneumonia (Trial Version 7), 2020) due to compromised lung function. This can arise following decreased lung perfusion (disruption of the blood flow to the alveoli) and/or lung ventilation (disruption of air penetrating into the alveoli). The cause may be a number of non-exclusive pathophysiological events initiated by SARS-CoV-2.

Pathogenesis

In the lungs

The first cell type infected by SARS-CoV-2 are the ciliated cells of the epithelium of the nasal cavity (Hou et al., 2020), where ACE2 expression is high. In pre-symptomatic and early symptomatic phases, active viral replication is oberserved in the upper respiratory tract (Wolfel et al., 2020). It peaks around 3-5 days post symptom onset (Pan et al., 2020; Yilmaz et al., 2021), playing an important role in the high transmissibility of the virus.

The virus then makes its way to the lower respiratory tract, where it can infect a number of cells. How the virus gets there is unclear, although micro particles are likely involved (Wilson et al., 2020).

Infection of alveolar pneumocytes (Yao et al., 2020) can disrupt the gas exchange interface. Autopsies revealed disrupted membranes of type II pneumocytes in particular (Carsana et al., 2020). These foamy-type cells secrete pulmonary surfactants which maintain surface tension, preventing alveoli collapse (Fehrenbach, 2001). Such surfactants can also play antibacterial and immunomodulatory roles, like Surfactant

protein D (SP-D) (Sorensen, 2018). Although SP-D can be produced by multiple cell types, detection of SP-D in circulation is often found in acute and chronic lung injury (Gaunsbaek et al., 2013), owing to intravascular leakage following loss of the air-lung barrier integrity (Hastings et al., 1992).

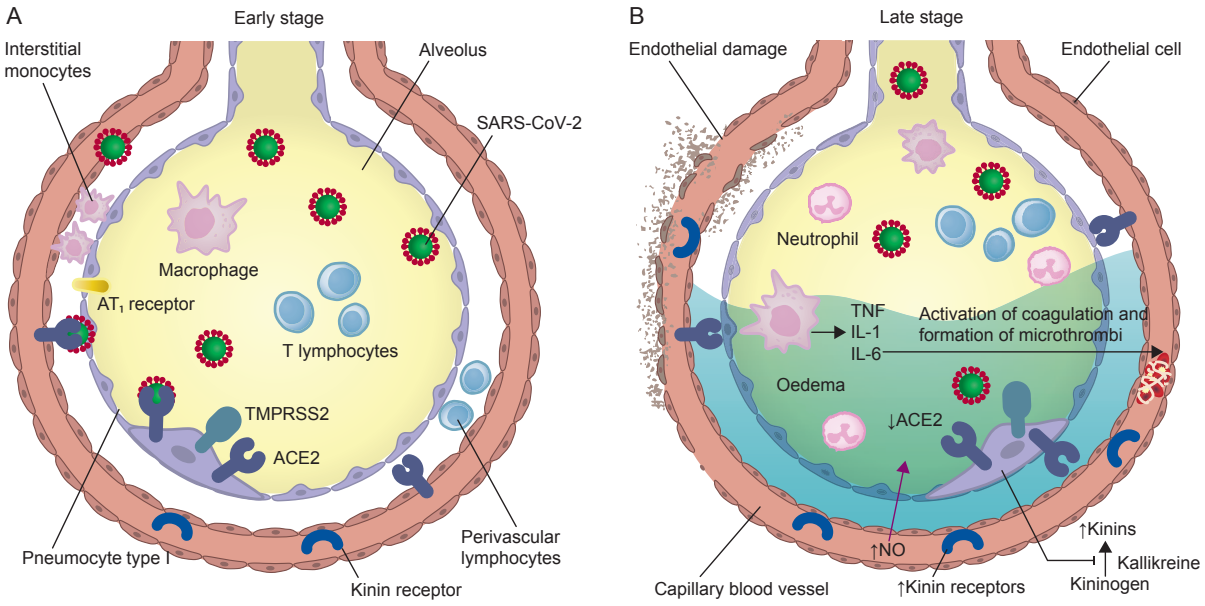

Figure 1.7 Lung pathogenesis during SARS-CoV-2 infection in humans. A) In the early infection (stage I), SARS-CoV-2 infects bronchial epithelial cells, type I and type II alveolar pneumocytes and capillary endothelial cells, allowing their replication and spread. Infected cells release inflammatory signalling molecules, activating innate immune responses and recruiting help. B) As immunopathology of SARS-CoV-2 infection progresses due to direct cytotoxicity from the virus and/or killing from immune cells, kinins produced from the injured tissue cause vascular smooth muscle relaxation, increasing vascular permeability. This leads to angioedema, and can progress to pulmonary edema filling the alveolar space. This also leads to downstream activation of coagulation, further spurred on by the proinflammatory cytokine, and which can cause microthrombi. Figure from (Osuchowski et al., 2021), used within permissions.

Bronchial epithelial cells can also directly be infected by SARS-CoV-2 (Ehre, 2020). Their infection is likely behind the accumulation of mucus and cell debris found in the bronchi, leading to diffuse damage to the respiratory tract (Hellman et al., 2020). Endothelial cells are also infected (Liu et al., 2021; Varga et al., 2020). Within the lungs, this infection and

ensuing inflammation may be the direct cause of microangiopathy (disease affecting small blood vessels) (Varga et al., 2020). Indeed, COVID-19-related alveolar damage is often observed alongside thrombotic microangiopathy (Sadegh Beigee et al., 2020), where a blood clot blocks a small blood vessel, for example those bringing unsaturated blood to get re-oxygenated. These platelet-fibrin microthrombi reduce the alveoli surface area participating in the gas exchange (Carsana et al., 2020), effectively reducing lung perfusion.

As the disease progresses, vasoactive peptides (kinins) cause vascular smooth muscle relaxation, a process normally controlled by ACE2 expressed on pneumocytes (Osuchowski et al., 2021). Without ACE2, vascular permeability and angioedema increase, processes further enhanced by proinflammatory cytokines TNFa, IL-1 and IL-6, as well as nitric oxide release (Osuchowski et al., 2021). Pulmonary oedema fills the alveolar spaces, reducing O_2 transfer from the air into the blood (diffusion capacity). In addition, lung fibrosis also plays a role in lung deterioration. It is primarily driven the TGF-b, secreted from the injured and/or inflamed lung (Wilson and Wynn, 2009), although the excessive amounts found in COVID-19 may also be attributable to CD4+ T cells (Ferreira-Gomes et al., 2021).

Through the combination of these events, fluid and fibrin fill the alveoli (Hellman *et al.*, 2020), which undergo remodeling (Carsana et al., 2020). There Is also neovascularisation, complete with increases in several markers of angiogenesis (Ackermann et al., 2020). The lungs of patients deceased of COVID-19 are heavier, owing to oedema and congestion (Carsana et al., 2020). Lung fibrosis is also frequent in these autopsied lungs (Edler et al., 2020). These mechanisms all contribute to the hypoxeamia

of severe COVID-19+ patients.

Throughout the body

A number of clinical manifestations of COVID-19 are not only found in the respiratory tract (reviewed in (Gupta et al., 2020)). SARS-CoV-2 can infect a range of cells types, including cardiocytes, olfactory sustentacular, bile duct cells (Wang et al., 2020d). Like with intestinal and other epithelia cells, infection can lead to *de novo* virus production (Xiao et al., 2020). Macrophages can also be infected (Wang et al., 2020a).

Inflammation of endothelial cells, with the resulting hypercoagulability, is also observed outside the lungs. Venous thrombosis, seen in 21-69% of critical COVID-19 patients (Klok et al., 2020), was much more prevalent than normally observed in ICU (7.5%) (Obi et al., 2015). In line with the greater incidence of thrombosis, patients with critical COVID-19 have increased fibrinogen (Thachil et al., 2020) and D-dimer levels than moderate (Lippi and Plebani, 2020) or non-COVID-19 pneumonia (Jirak et al., 2021) patients.

RNAemia (presence of viral RNA in blood products) was an important correlate of both disease severity and fatality in COIVD-19 patients (Fajnzylber et al., 2020; Hogan et al., 2020; Prebensen et al., 2020). The quantity of plasma viral RNA did not correlate with that found in nasal swabs (Prebensen et al., 2020), suggesting that factors other than high viral presence at the site of infection influence viremia. Plasma SARS-CoV-2 viral RNA found in acutely-infected COVID-19+ individuals does not seem infectious (Andersson et al., 2020). While autopsies studies have found SARS-CoV-2 across multiple organs, the virus' dissemination seems to be through invasion of endothelia and transport via CD14+ monocytes and macrophages (Yao et al., 2021). It is unclear whether direct infection by SARS-CoV-2 plays a part in these extrapulmonary symptoms, or if it's rather circulating

viral by-products which trigger immunopathology. Nonetheless, plasma vRNA correlates with increased hypertension and respiratory rates, signs of worsening COVID-19 (Gutmann et al., 2021).

Antiviral treatment

The SARS-CoV-2 pandemic has resulted in an enormous use of modelling and artificial intelligence to screen drugs for re-purposing.

Remdesivir, a broad-spectrum antiviral, inhibits the viral RNA-dependent RNA polymerase in SARS-CoV-1 and MERS (Agostini et al., 2018). It demonstrated *in vitro* inhibitory activity against SARS-CoV-2 (Wang et al., 2020c) prior to the start of the Adaptive Covid-19 Treatment Trial (ACTT-1) clinical trial (Beigel et al., 2020). Remdesivir or a saline placebo was administered daily for up to 10 days in 541 and 517 hospitalized patients, respectively. Although remdesivir significantly shortened hospitalization times and diminished COVID-19 severity (most significantly in the 18 – 40-year-old age group and severe cases), there was no significant benefit on survival (Beigel et al., 2020).

Another antiviral tested comes from the HIV field: Lopinavir, an HIV-1 protease inhibitor for which ritonavir increases half-life. Lopinavir has *in vitro* antiviral activity against SARS-CoV-1 (Chen et al., 2004), MERS (Sheahan et al., 2020) and SARS-CoV2 (Choy et al., 2020), and so was tested in a clinical trial by the RECOVERY group (Group, 2020). 1616 recruited patients received Lopinavir-ritonavir every 12h for up to 10 days, or not (control group: n = 3424). There was no association to lower 28-day all-cause mortality, nor to other metrics (hospitalization stay, progression), even if administered early in the course of the disease (< 7 days after symptom onset).

Thus, the antivirals were not effective against SARS-CoV-2 infection. As the cause of death from COVID-19 is thought to be primarily due to immunopathology rather than direct cytopathology caused by the virus itself, the inflammation may be a better target. The three drug categories which improved survival benefit in COVID-19 in clinical trials are either immunotherapies or immunomodulatory drugs: the corticosteroid dexamethasone (Group et al., 2021b; Group et al., 2020; Tomazini et al., 2020), the two IL-6 blockers tocilizumab (Investigators et al., 2021) and sarilumab (Group et al., 2021c), and the Janus kinase (JAK) inhibitor Baricitinib (Marconi et al., 2021). To better understand the effectiveness of these immunomodulatory drugs, we will first discuss the host immune responses against SARS-CoV-2.

Innate immune responses activated upon SARS-CoV-2 infection

Critical cases of COVID-19, in the acute phase of the infection, present a distinct plasmatic profile than uninfected and convalescent donors (Laing et al., 2020), non-critical COVID-19 cases (Lucas et al., 2020) or non-COVID-19+ critical sepsis cases (Gutmann et al., 2021). This “COVID-19 signature” has revealed dysregulation in a number of immune pathways:

A) Aberrantly high activation of the complement cascade

In the blood, multiple components of the complement cascade increased in the plasma of critical COVID-19 individuals in comparison to sepsis cases (Gutmann et al., 2021) or to non-critical COVID-19 (Messner et al., 2020). Proteins of this cascade also bind to SARS-CoV-2 Spike (Gutmann et al., 2021). Furthermore, MBL2 and PTX3 were significantly associated to fatality in critical COVID-19+ cases (Gutmann et al., 2021). MBL2, which binds glycoproteins on the viral surface (Ip et al., 2005), forms complexes with PTX3 and

activates the complement system independently of antigen-antibody complexes (Ma et al., 2011). This mechanism may explain the overreaction of the complement cascade in critical COVID-19, even with a delay in antibody responses targeting the virus. This mechanism can at least partially link the greater severity associated with finding viral products in the blood.

Severe cases of COVID-19 also have greater levels of agents of the complement cascade in the BALF (Carvelli et al., 2020).

B) Delayed acute-phase immune responses

Evidence shows type I IFN being critical in SARS-CoV-2 infections. Patients with severe COVID-19 have an impaired type I IFN response (Hadjadj et al., 2020). In coparison to the slu, it is delayed (Galani et al., 2021), which is at least in part due to the activity of the viral proteins (Lei et al., 2020). Dendritic cells collected in acute COVID-19 infection produced lower levels of type I IFNs as those from healthy controls (Arunachalam et al., 2020; Zhou et al., 2020a). SARS-CoV-2 is highly sensitive to type I IFN, making this delay central in the progression of the infection (Mantlo et al., 2020).

This delay in type I IFN responses can simultaneously allow for greater viral replication of SARS-CoV-2 and delay the priming of the adaptive immune response.

C) Cytokine storm

A cytokine storm is a broad term relating to the hyperactivation of the immune response, characterized by a huge release of interferons, interleukins, chemokines, etc., and is associated to ARDS. The cytokine IL-6, which induces proinflammatory responses, correlates with severity and outcome in COVID-19 (D'Alessandro et al., 2020), although

this may not be exclusive to COVID-19, and rather a sign of acute infection. For example, autopsied lungs of patients with COVID-19 compared to those infected with H1N1 showed similarly high IL-6 mRNA levels, whereas CXCL8 and CXCL13 were uniquely elevated in the COVID-19 lungs (Ackermann et al., 2020). Increased cytokine signals may have indirect consequences of the viral infection : for example, bacterial DNA and LPS, potentially stemming from a breach in the lung integrity following SARS-CoV-2 infection, correlate positively with inflammatory cytokines (Arunachalam et al., 2020).

D) Expansion of innate immune cell populations

Neutrophilia is present in COVID-19 patients (Mathew et al., 2020). The peripheral neutrophils include the highly activated subset, the myeloid-derived suppressor cells (MDSCs), suggestive of emergency hematopoiesis (Metzemaekers et al., 2021), and a high proportion of immature neutrophil granulocytes (Carissimo et al., 2020). The serum of COVID-19 patients features high levels of neutrophil extracellular trap (NET) (Zuo et al., 2020). Autopsied lungs revealed neutrophil infiltration in some patients (Schaefer et al., 2020). These may have been recruited by the high levels of neutrophil-recruiting chemokines CXCL1, CXCL2 and CXCL8 found in the BALF of critical cases (Zhou et al., 2020b) and/or by their exacerbated Th17 responses in lungs (Schaefer *et al.*, 2020).

Monocytes are also increased in COVID-19 (Lucas et al., 2020) and undergo a shift from CD16+ towards the classic CD14+ (Wilk et al., 2020). Monocytes display high levels of IL-1 and IL-6 in critical cases, associated to bystander effect (Liao et al., 2020), and migrate to the lungs in COVID-19 (Liao et al., 2020). Single-cell RNA Seq on monocytes and macrophages collected in the BALF of COVID-19 patients reveal increased signatures of hypoxia, wounding and FCR signalling, concomitant with decreased antigen presentation

(Xu et al., 2020). HLA-DR expression on monocytes is also greater in deceased patients following COVID-19 (Wang et al., 2020b). Dendritic cells, specifically plasmacytoid and myeloid, are reduced in the blood and lungs of COVID-19 patients (Wilk et al., 2020; Liao et al., 2020). Blood pDC have a decreased ability to produce IFNa and TNFa upon sitmulation with TLR ligands (Arunachalam et al., 2020), and myeloid cells in general have a reduction in their machinery for antigen presentation (Arunachalam et al., 2020). Reduction in cytokine profile suggests that the increase in cytokines originates from tissue rather than from PBMCs (Arunachalam et al., 2020). These altered phenotypes impede DC help of T cells, such as proliferation (Zhou et al., 2020a). Paired single-cell RNA sequencing on myeloid cells collected from BALF and blood showed the same defect in interferon production among the myeloid cells in the lungs (Xu et al., 2020). However, they produced massive amounts of chemokines pertinent for the recruitment of T cells (CXCL9, CXCL18).

These aberrations can have repercussions on the adaptive response. Leukocytes infiltrate are observed in autopsied lungs, with perivasuclar T cells and macrophages in the alveolar lumen, and lymphocytes and monocytes in the intestitium (Carsana et al., 2020).

Adaptive immune responses activated upon SARS-CoV-2 infection

T cells

T cells are central in the antiviral response. Circulating CD4+ and CD8+ T cells both present traits of activation, although they are reduced in counts (Mathew *et al.*, 2020). Indeed, the ratio of neutrophil-to-lymphocytes has been proposed as a prognostic marker

for severity (Ma et al., 2020). While decreases are only observed in the naïve and central memory subsets of CD8+ T cells (Mathew et al., 2020), all CD4+ T cell memory populations drop, and correlate negatively with CXCL10 (Laing et al., 2020). In spite of lymphopenia, all T cell populations had increased markers of cycling (Laing et al., 2020). Shared T cell clonotypes between BALF and blood support recruitment from blood into the lungs (Xu et al., 2020). Perivascular T lymphocytes in lung endothelium and epithelium was observed in severe COVID-19 (Ackermann et al., 2020), suggesting they can also be drivers of immunopathology. However, end-stage disease is associated with exacerbated neutrophil, and not lymphocyte, infiltration into the lung (Long et al., 2020).

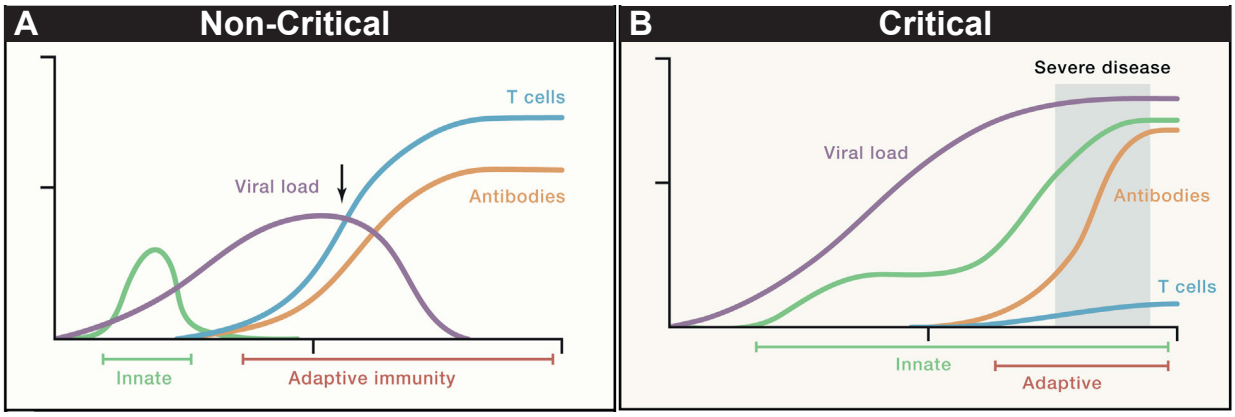

Figure 1.8 Current understanding of the adaptive immune response and viral load kinetics in non-critical vs critical SARS-CoV-2 infection in humans. A) Conceptual schematic of a non-critical, average infection, whereby the innate immune response is slightly delayed upon viral replication, and are of moderate magnitude and short duration. SARS-CoV-2-specific T and B cells arise in response, coinciding with the clearance of the virus, and are maintained over time. B) Conceptual schematic of a critical infection, characterized by a greater delay in innate immune response upon viral replication. Innate immune response in sustained, and SARS-CoV-2-specific T and B cells are delayed, resulting in a longer persistence of the virus in the host. While CD8 responses seem lower in critical than non-critical cases, the same was not observed for CD4+ T cells. Figured modified from (Sette and Crotty, 2021).

SARS-CoV-2-specific CD8+ T cells also develop quickly upon infection (Schulien et al., 2021). They express high levels of IFNg, GZMB, TNFa and CD107a (Rydyznski

Moderbacher et al., 2020; Schulien et al., 2021). Strong SARS-CoV-2-specific CD8+ T cell responses, both in terms of frequency of AIM and in cytokine production, were associated to better outcome (Rydyznski Moderbacher et al., 2020). After recovery, patients which suffered from a milder form of SARS-CoV-2 infection have greater SARS-CoV-2-specific CD8+ T cell responses than those which had a critical infection (Lafon et al., 2021). This was not observed for SARS-CoV-2-specific CD4+ T cell responses, nor for specific IgG amounts.

SARS-CoV-2-specific CD4+ T cells are of greater magnitude and more often detected than their CD8+ counterparts (Grifoni et al., 2020), sometimes as early as 2-4 days post symptom onset (Rydyznski Moderbacher et al., 2020). Strong CD4+ responses show a stronger associated to lessened severity than neutralizing antibodies (Rydyznski Moderbacher et al., 2020). Timing is key : whereas rapid responses of SARS-CoV-2-specific CD4+ T cells were seen in mild disease (Tan et al., 2021), critical cases of COVID-19 show a delay in their SARS-CoV-2-specific T cell responses (Zhou et al., 2020a). Spike is immunodominant, although CD4+ T cells can recognize most of SARS-CoV-2's proteins (Grifoni et al., 2020). SARS-CoV-2-specific CD4+ T cells expressed high amounts of IFNg and IL-2, in line with a prototypical Th1 antiviral population *(Rydyznski Moderbacher et al.,* 2020). Single-cell RNA Seq revealed that SARS-CoV-2-specific CD4+ T cells, compared to specificities to other viral infections, were enriched in a profile of TFH and enhanced cytotoxicity (Meckiff et al., 2020b). SARS-CoV-2-specific cTFH were split among two distinct populations. The first population correlated positively with anti-SARS-CoV-2 antibody responses and is associated with mild disease. The second population, of greater proportion in severe disease, has high expression of GZMB and Prf, and is

rather negatively correlated with antibody response (Meckiff et al., 2020b). This latter population is enriched in the IFN response signature (Meckiff et al., 2020b). SARS-CoV-2-specific CD4+ T cells of some hospitalized individuals were also enriched in clusters of CD4-CTL that underwent large clonal expansion and correlated negatively with SARS-CoV-2-specific Tregs, more present in mild disease (Meckiff et al., 2020b). Both CD4-CTLand the cytotoxic cTFH clusters expressed chemokines CCL3/4/5, all involved in recruitment of myeloid cells (Meckiff et al., 2020a). SARS-CoV-2-specific CD4+ T cells are also CCR6+, so associated with TH17 and TH22. However, IL-17a expression is low in these cells, and although they are able to produce IL-22 (Weiskopf et al., 2020), this was not associated to reduced severity (Rydyznski Moderbacher et al., 2020). In this case, CCR6 expression is likely associated to lung homing, which could have been validated with CXCR6 staining. Th2-associated cytokines, like IL-13, IL-5, IL-9 and IL-4, were not detected by ICS in SARS-CoV-2-specific CD4+ T cells (Rydyznski Moderbacher et al., 2020) nor in culture media of SARS-CoV-2 peptide-stimulated PBMCs (Weiskopf et al., 2020). These observations highlight that Th1, TFH and CTL are likely the key players in the anti-SARS-CoV-2 response.

The frequency of B cells is unchanged in COVID-19 infection (compared to uninfected controls), but there is an increase in the frequency of plasma blasts (Mathew et al., 2020). Both are unchanged in BALF (Liao et al., 2020). Functional SARS-CoV-2-specific B cells likely appear quickly, as almost all patients seroconvert by 2 weeks post symptom onset (Prevost et al., 2020). Anti-spike IgM, IgA and IgG all occur at similar times (Suthar et al., 2020). Lymph nodes from deceased COVID-19+ patients revealed the absence of GC

and accompanying lack of GC B cells, which coincided with a block in TFH differentiation. These absences have been proposed to explain the typically poor durability of the humoral response to coronaviruses (Kaneko et al., 2020). In addition, critical COVID-19 cases with poor clinical outcome were characterized by a plasma blast dominance over early B cell response (Mathew et al., 2020).

The antibody response is thought to play an important role in SARS-CoV-2, as in many viral infections. A lot of attention was initially on neutralizing antibodies, in which the IgM isotype is most active (Gasser et al., 2021). Neutralization by plasma of COVID-19 patients can be detected as soon as 3 days after symptom onset, but is highly variable among individuals (Rydyznski Moderbacher et al., 2020). Neutralization was not differential between patients which survive their infection and those who do not (Zohar et al., 2020), suggesting that the neutralizing capacity of plasma may not be central in controlling viral replication once infected. It is increased in severe disease(Chen et al., 2020), although this may likely be due to increased/sustained antigen load seen in severe disease. For example, patients with mild disease also have lower SARS-CoV-2 antibody responses than critical patients, when compared within a similar timeframe of acute infection (Wang et al., 2020f) or after resolution (Zhou et al., 2020a). Administration of neutralizing monoclonal antibodies in a clinical trial demonstrated a relatively small effect on viral load (Weinreich et al., 2021).

Neutralization capacity may not be key in the setting of an acute SARS-COV-2 infection. Similar to the T cell responses, patients which succumb to COVID-19 present a delay in their IgG antibody response, (Zohar et al., 2020). In a mouse-model of accelerated SARS-CoV-2-mediated immunopatogenesis, a non-neutralizing yet FCR-permitting antibody,

but not a neutralizing with FCR-non-permitting counterpart, was protective against fatality (Ullah et al., 2021).

The presence of antibodies *per se,* either neutralizing or with Fc function, again may not be the main antiviral factor. Patients with primary antibody deficiencies like agammaglobulinaemia (Quinti et al., 2020) or on anti-B cell therapies did not exhibit worse disease course or outcomes (Montero-Escribano et al., 2020). These patients contrast strikingly to those with chronic renal failure, a condition known to delay the generation of antigen-specific T cells and antibody responses after challenge (Litjens et al., 2008). Patients with chronic renal disease are at greater risk of xritical disease (Suleyman et al., 2020). The antibody response correlates with the SARS-CoV-2-specific CD4+ T cell response (Ullah et al., 2021), so the kinetics and magnitude of the antibody response may simply be a reflection of the central CD4+ T cell response. A loss of correlation between features of SARS-CoV-2-specific CD4+ T cells and the humoral response, as is seen in older patients, was associated with greater severity (Rydyznski Moderbacher et al., 2020).

Table 1.1 Reported efficacy of COVID-19 treatments

Group	Drug	First Author	Country	Treated group			Usual care group			95% Confidence Interval				Other observations
				Total	Mortality	% of deceased	Total	Mortality	% of deceased	Rate Ratio*	Min	Max	REF	
Glucocorticoids														
RECOVERY	Dexamethasone	P. W. Horby	UK	2104	482	23%	1110	4321	26%	**0.83**	0.75	0.93	33933206	Dexamethasone lowered disease severity and hospital duration.
CoDEX	Dexamethasone	B. M. Tomazini	Brazil	151	85	56%	148	91	61%	0.97	0.73	1.03	32876695	Dexamethasone lowered disease severity. OR
REMAP-CAP	Hydrocortisone	D. C. Angus	USA	137	41	30%	101	33	33%	0.97	0.53	1.95	32876697	*Hydrocortisone lowered disease severity.
IL-6R blockers														
BACC Bay		J. H. Stone	USA	161	9	6%	82	3	4%	1.51	0.44	5.13	33085857	Only included hospitalized patients not on mechanical ventilation
COVACTA		I. O. Rosas	USA	294	58	20%	144	28	19%	1.02	0.62	1.68	33631066	
EMPACTA		C. Salama	USA, MX, KE, SA, PE, BR	249	26	10%	128	11	9%	1.23	0.6	2.52	33332779	
REMAP-CAP		A. C. Gordon	USA	353	98	28%	402	142	35%	**0.71**	0.52	0.96	33631065	
RECOVERY	Toci/Sari	N/A	UK	2022	621	31%	2094	729	35%	**0.85**	0.76	0.94	33933206	
Meta-analysis by REACT	*Toci/Sari*	M. Shankar-Hari	*Merged cohorts*	6449	1407	22%	4481	1158	28%	0.86	0.79	0.95	34228774	*Combined 27 trials*
	Tocilizumab	*Sub-analysis on Tocilizumab only*		4299	960	22%	3749	1023	27%	0.83	0.74	0.92	34228774	*Combined 19 trials*
	Sarilumab	*Sub-analysis on Sarilumab only*		2073	473	23%	753	139	18%	1.08	0.86	1.36	34228774	*Combined 9 trials*
JAK inhibitor														
COV-BARRIER	Batricinib	V.C. Marconi	12 countries	764	62	8%	761	100	13%	0.57	0.41	0.78	34480861	
Convalescent Plasma														
RECOVERY	High-IgG titer Convalescent Plasma	P. W. Horby	UK	5795	1399	24%	5763	1408	24%	1	0.93	1.07	PMC8121538	
Meta-analysis by RECOVERY		*11 trials*	*Merged cohorts*	6642	1510	23%	6589	1545	23%	0.98	0.91	1.06	PMC8121538	*Did not include CONCOR-1 trial*
CONCOR-1	Convalescent Plasma of varying Ab titer	P. Bégin	Canada	343	75	22%	173	40	23%	0.95	0.67	1.33		
Neutralizing monoclonal antibodies														
ACTIV-3	Bamlanivimab	J.D. Lundgren	USA	163	9	6%	151	5	3%	1.39	0.4	4.83	33356051	*COCHRANE-reported numbers
RECOVERY	Casirivimab+Imbedivimab	P.w. Horby	UK	4839	944	20%	4946	1026.00	21%	0.94	0.86	1.03	*Preprint*	*Irrespective of baseline antibody status
		Sub-analysis on seronegative		1633	396	24%	1520	451.00	30%	0.8	0.7	0.91		
		Sub-analysis on seropositive		2636	411	16%	2636	383.00	15%	1.09	0.78	1.22		

*Reported Ratio Rate is adjusted when available (age, center).

Only included trials with at least 100 participants per group.

Only included trials which measured therapeutic use of drugs in hospitalised COVID-19 patients.

UK = United Kingdom ; USA = United States of America ; MX = Mexico ; KE = Kenya ; SA = South Africa, PE = Peru, BR = Brazil

Therapeutic immune modulation in COVID-19

As previously mentioned, the three drug categories improve survival benefit in COVID-19: the corticosteroid dexamethasone *(Group et al., 2021b; Group et al., 2020; Tomazini et al.*, 2020), the two IL-6 blockers tocilizumab (Investigators et al., 2021) and sarilumab (Group et al., 2021c), and the Janus kinase (JAK) inhibitor Baricitinib (Marconi et al., 2021).

Dexamethasone

Dexamethasone is a glucocorticoid, belonging to the family of corticosteroid drugs (https://pubchem.ncbi.nlm.nih.gov/compound/Dexamethasone). Binding of this steroid to glucocorticoid receptor on cell membrane forms a complex which is translocated to the nucleus and interferes with AP-1 and NFbK-inducible genes like IL-1/2/6/8, TNFa and IFNg (Chikanza, 2002). It also induces IL-10 production through synthesis of glucocorticoid response element. At high doses, dexamethasone attenuates T cell responses by disrupting TCR signalling (Van Laethem et al., 2001) and modulating calcium signalling (Harr et al., 2009). Dexamethasone also reduces lung edema through ameliorated permeability of the pulmonary vasculature (Huang et al., 2014) and up-regulation of alveolar liquid clearance (Folkesson et al., 2000). Finally, dexamethasone' is also anti-fibrotic, by preventing collagen accumulation upon acute lung injury (Wigenstam et al., 2018).

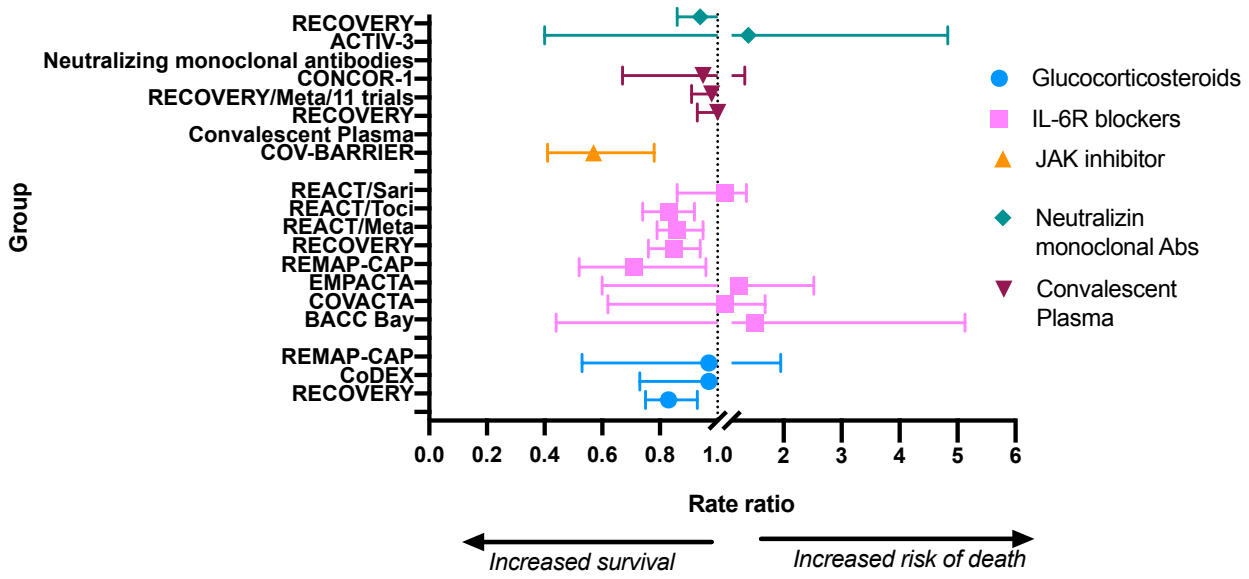

Figure 1.9 Rate ratios on outcome based on immunotherapies in acute COVID-19 among hospitalized patients. Figure up to date as of September 2021.

Given the inflammatory nature of COVID-19's pathology, dexamethasone was quickly considered as a immunomodulatory therapy. Patients were recruited for a large clinical trial in the UK as soon as March 2020 with the results first released in June 2020 (Group et al., 2021b). The randomized trial included 6425 patients, split into a moderate-dose dexamethasone-treatment group (roughly 1/3) and a group which received usual care only. Patients were treated with dexamethasone for up to 10 days or until discharge, and primary outcome was all-cause mortality within 28 days of randomization. The trial showed a significant reduction in mortality in the treated group (23% vs 26%), with the greatest survival benefit observed in the critical patients (29% vs 41%). In contrast, there was no survival benefit in the moderate patients, for which treatment was potentially harmful due to as serious adverse effects (4 cases in total). Treatment was associated to shorter hospital durations and fewer progression in severity. Importantly, the trial showed that survival benefit was only observed if treatment was initiated at or after 7 days after

symptom onset (although these patients tended to be critical). This suggests that the treatment is most effective once edema is already present in the lungs, rather than in the acute viral phase. Dexamethasone was associated with delayed viral clearance in cases of SARS (Lee et al., 2004), MERS (Arabi et al., 2018) and influenza (Lee et al., 2009). Thus, early administration may impede antiviral responses, which in turn may worsen the direct pathology of the virus.

Other smaller clinical trials were also performed with glucocorticoids : in Brazil, an open-label trial with 299 randomized patients also observed lower disease severity when treated with dexamethasone, but no effect on 28-day mortality (Tomazini et al., 2020). However, a significant caveat of this study, aside from the relatively smaller sample size, was that 35% of the untreated group actually received corticosteroids during the study period. These same results were observed in a randomized trial with 403 patients in the USA (Angus et al., 2020). Another trial in France with 149 patients saw no significant associations (Dequin et al., 2020). It is important to note that these studies were underpowered, given the heterogeneity of the hospitalized cases of COVID-19. The latter two trials used hydrocortisone, reported to be less potent and shorter-acting.

The results of these findings contributed to the changes in standard of care guidelines in many countries, which now recommend the use of glucocorticoids in patients hospitalized for COVID-19.

IL-6 antagonists

The inflammatory pleiotropic cytokine IL-6 is produced by multiple cell types (including T and B cells, DCs, endothelial cells, etc.) in response to infection or tissue damage. Through ligation of it’s surface receptors IL-6R, it activates the JAK/STAT3 pathway,

triggering processes like cytokine production and cell activation (Velazquez-Salinas et al., 2019). It is thus central in inflammation, and has been associated with severity and death in almost all studies investigating plasma cytokine levels in the acute phases of severe COVID-19.

In parallel with dexamethasone, the use of IL-6 blockers have been assessed in clinical trials early in the pandemic. The two humanized monoclonal antibodies used were tocilizumab (marketed under Actemera), and sarilumab (Kevzara), both of which target IL-6R. The largest clinical trial completed to date was again by the RECOVERY group. This trial recruited a total of 4116 patients, split equally between treated with IL-6R blockade (one or two doses within a 24h time span) or receiving usual care (Group, 2021b). This trial primarily used tocilizumab, although sometimes employed sarilumab as well. An additional selection criteria was presence of hypoxia and clinical indication of inflammation (determined by high levels of plasma CRP at the time of randomization). This trial again found a significant survival benefit when treated with IL-6R blocker (see figure 1.9), specifically when used concomitantly with dexamethasone. This treatment also reduced duration of hospitalization, as well as the incidence of renal replacement therapy like hemodialysis (indicative of renal failure). The greatest survival benefit was observed in the moderate cases, while no significant benefit was seen in severe and critical cases. The most benefit was also seen when in patients treated within 7 days after symptom onset, but not if administered later, suggesting an important role of IL-6 in early immunopathology.

Eight smaller clinical trials tested IL-6R blockers in COVID-19 patients, but only REMAP-CAP, the second-largest trial, saw a significant reduction in mortality, once again

underscoring that most trials were underpowered.

JAK inhibitor Baricitinib

JAK inhibitors disrupt the protein's phosphorylation of signal transducer and activator of transcription (STAT). These latter proteins mediate cytokine signals (Kaplan, 2013), and preventing their phosphorylation has a strong anticytokinic effect. Baricitinib selectively inhibits JAK1/2, leading to anti-inflammatory profile (Sanchez et al., 2018), and was predicted as a useful treatment for COVID-19 by artificial intelligence algorithms (Stebbing et al., 2020). It reduced multiple cytokines implicated in COVID-19 pathophysiology (IL-1b, IL-6, TNFa), allowed for rapid recovery of lymphopenia, and increased antibody production (Bronte et al., 2020). Batricinib also has a direct antiviral effect on SARS-CoV-2 propagation, through interference with viral endocytosis (Stebbing et al., 2020).

In the large randomized, placebo-controlled double-blind trial (COV-BARRIER) conducted across 12 countries, 764 patients received daily batricinib (up to 14 days or until discharge), while 761 patients received placebo (Marconi et al., 2021). Recruited patients also had at least one elevated plasma marker of inflammation. The study found a significant reduction in 28-day all-cause mortality risk in the overall population. When the cohorts were stratified, a significant benefit was observed in severe patients (they did not include critical patients at enrolment), men, and patients younger than 65 years old. There was a significant benefit whether patients were co-treated with systemic corticosteroids or not. A second smaller trial did not reach significance for survival benefit, but did show significantly shorter hospitalizations, and fewer adverse effects when treated with a combination of baricitinib and remdesivir (Kalil et al., 2021). Baricitinib has since been approved in Japan, and for emergency use in USA.

Convalescent plasma treatment

Quite early in the pandemic, it was apparent that individuals infected with SARS-CoV-2 generated a neutralizing antibody response. This spurred on the rationale of convalescent plasma treatment (CPT), where these antibody-containing plasma from donors with resolved infections could be administered to severe cases of COVID-19. Antibodies can help control viral replication by neutralizing *de novo* cell infection by blocking binding, by activating phagocytosis, the complement cascade, ADCC, and by enhancing antigen presentation. The use of plasma from donors with resolved infections has been used as passive immunity for pneumonia caused by influenza (Hung et al., 2011).

Once again, the RECOVERY ran the biggest trial (Group, 2021a). Hospitalized patients were administered two 275 ml doses of plasma from convalescent donors previously tested for high titers of anti-S IgG. In total, 5794 patients received convalescent plasma, while 5763 patients were controls. The trial showed no survival benefit in the overall cohort, nor in any subsequent stratification (age, sex, respiratory support, use of corticosteroids). There was a small trend increased survival if treatment was received less than 7 days after symptom onset. This treatment was associated with 16 severe allergic reactions, and 13 cases of serious adverse events.

This lack of effect from convalescent plasma was reported in 10 other studies (Group, 2021a), including the Canadian CONCOR-1 trial (Begin et al., 2021). This latter study noted that increases in ADCC and neutralization capacities of the convalescent plasma were independently associated with better outcome. The importance of the quality of the plasma was similarly underlined in a second study (Joyner et al., 2021). However, the survival benefit noted by this study in the group receiving plasma with high antibody levels

may be because they compared it to recipients of plasma with low antibody levels (and not to a proper control group). Thus, whether the benefit observed in high-titer convalescent plasma was due to actual benefit, or rather because receiving low-titer convalescent plasma increased the risk of fatality, could not be determined.

Taken together, these studies support a lack of survival benefit of using convalescent plasma, at least with the patient groups examined. Although the intended benefit of convalescent plasma administration was to passively provide anti-SARS-CoV-2 antibodies, plasma is a complex tissue which can lead to adverse effects. The alternative strategy is administrating purified antibodies.

Monoclonal antibody

As of May 13th 2022, the Antibody Society's COVID-19 Biologics tracker (antibodysociety.org) reported over 200 potein-based COVID-19 interventions in various stages of development and testing. Over 30 anti-SARS-CoV-2 monoclonal antibodies have entered clinical trials, and four treatments, either single or combination of two monoclonal antibodies, have been approved in at least one country.

The Cochrane systemic review updated in September 2nd 2021 (evidence up to date as of June 17th – no updates as of May 13th 2022) reviewed six randomized controlled trials which used neutralizing antibodies (nAbs) to treat COVID-19 (36 ongoing) (Kreuzberger et al., 2021). Only two of these evaluated their efficacy in hospitalized patients. The ACTIV-3 trial recruited 163 patients treated with a single infusion of bamlanivimab (neutralizing monoclonal antibody with high affinity for RBD), and 151 in the placebo group. The study found no significant effect on mortality, time to discharge or disease progression, although there were serious adverse effects (Group et al., 2021a). Recently,

a study showed the emergence of a mutation in five of six hospitalized COVID-19 patients treated with balmanivimab (Peiffer-Smadja et al., 2021), highlighting the risk of escape mutations when using monotherapies. The second clinical trial, conducted by the RECOVERY group, evaluated the efficacy of two non-competing neutralizing antibodies which target RBD : casirivimab and imbedivimab (Group, 2022). A single dose combining both antibodies in equal amounts were administered to 4839 hospitalized patients, while 4946 received the placebo. Overall survival benefit was non-significant ; however, if the analysis was restricted to seronegative patients at the time of randomization, the treatment resulted in a significant survival benefit as well as decreased progression towards severe disease. The authors of the Cochrane study conclude that none of the trials (counting both in hospitalized patients nor the four other trials on COVID-19+ mild and outpatients) provide meaningful conclusions on the usefulness of monoclonal antibodies in treating SARS-CoV-2 (Kreuzberger et al., 2021). This conclusion may be overly conservative, as the RECOVERY group highlights that the benefit is in the subgroup of patients which have not *yet* generated an appropriate antibody response. This latter group are for example immunocomprised individuals, which may not be able to generate an antibody response, and have extended viral shedding.

The rise of new variants always risk to impede the efficacy of these monoclonal antibodies. As of January 2022, the dominant variant is Omicron (subdivided in three main lineages) (Viana et al., 2022), which demonstrates mutations in a number of the regions of the Spike protein, incluing RBD (Bruel et al., 2022). As neutralizing antibodies target the RBD region, these mutations have lead to decreased sensitivity to neutralizing antibodies *in vitro* (Bruel et al., 2022; Ou et al., 2022). Specifically, the RECN-COV-2 cocktail (imdevimab with

casirivimab), which had shown most success against the Alpha, Beta, Delta and Gamma variants, showed no *in vitro* neutralization capacity of omicron strains (Bruel *et al.*, 2022; Tuccori et al., 2022). The Evosheld cocktail (cilgavimab and tixagevimab) showed better neutralization, with high varaibility depending on the omicron strain considered (Bruel *et al.*, 2022; Tuccori *et al.*, 2022). Screening of different monoclonal antibodies, as well as sequencing the virus in host, becomes necessary to efficitently treat the ongoing viral replication (Bruel et al., 2022).

In summary, treatments which target the inflammatory stages of COVID-19 have a proven benefit in survival in large clinical trials. This has only been demonstrated with SARS-CoV-2-specific monoclonal antibodies in seronegative patients. Other types of treatment, such as convalescent plasma therapy and antiviral drugs, have no survival benefit. Namely, remsidivir which, although it significantly reduced hospitalization duration, did not show a significant effect on fatality (Wang et al., 2020e). This is despite the proven antiviral *in vitro* effect (Wang et al., 2020c).

The lack of effect from direct-acting antivirals, and targeted effect from monoclonal antibodies was unexpected, as these strategies are used against other viral infections. For example, the progression of rabies can be blocked by the administration of monoclonal antibodies, and the same strategy was employed in Ebola, while direct-acting antivirals cure chronic HCV infection. However, SARS-CoV-2 distinguishes itself from these viruses by it’s rapidity : the infection is normally resolved in a couple of days. People infected with SARS-CoV-2 receive treatment once hospitalized. In our cohorts, the median time between onset of symptoms and hospitalization was 5 days, with a range from 3 to 12 days. Thus, it is likely that the window of time when antivirals would be useful is too

short for useful administration, with the exception of immunocompromised individuals with enduring infections. Similarly, monoclonal antibodies are only beneficial in people who have not *yet* produced their own SARS-CoV-2-specific antibodies.

In summary, the principal immunological characteristics of severe COVID-19 are a delayed type I IFN response and delayed adaptive immune response, both of which favour greater and perhaps longer viral replication, resulting in greater damage to the lungs. Therapeutic strategies that specifically target the inflammatory response, rather than viral replication, are most effective in increasing survival. Other immunpathological mechanisms are exacerbated neutrophilia and complement cascade activation. Remaining questions were still how the different components are intertwined, and which are decisive for patient survival.

Chronic viral infection : HIV

During the end of the 1970s and early 1980s, young adults were presenting to clinic with rare conditions only observed in cases of severe immunodeficiency. This disease, later named Acquired Immunodeficiency Syndrome (AIDS), is caused by the human immunodeficiency virus (HIV). This pathogen has fuelled decades of research, resulting in a greater understanding of the human immune system and the discovery of effective disease-halting treatments, antiretrovirals (ARVs). However, there are no widely-applicable therapies for cure, nor any protective vaccine. As a consequence, there are still 38 million people worldwide living with the virus (https://www.who.int/data/gho/data/themes/hiv-aids).

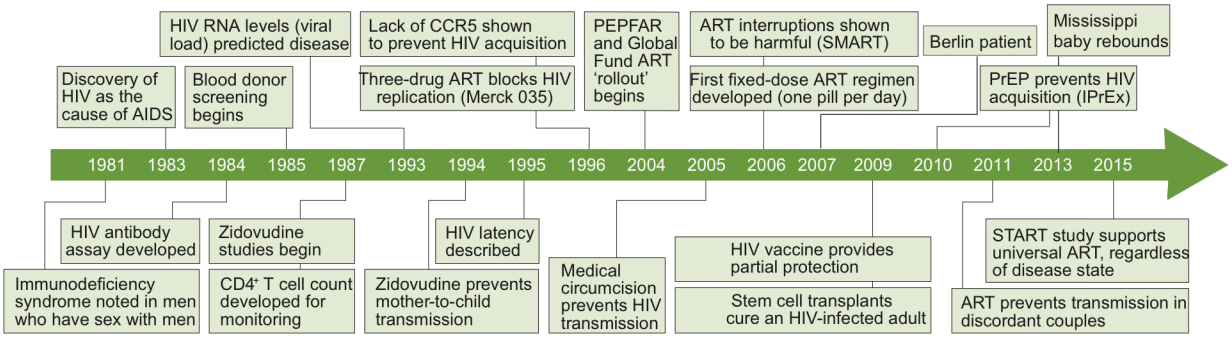

Figure 1.10 Milestones in HIV research. Four decades of research, beginning with the discovery of HIV, have allowed researchers to make this death-sentence a chronic disease. IPrEx: Iniciativa Profilaxis Pre-Exposición study; PrEP, pre-exposure prophylaxis; SMART, Strategies for Management of Antiretroviral Therapy; START, Strategic Timing of AntiRetroviral Treatment. Used with permission from (Deeks et al., 2015).

Viral characteristics

HIV is a lentivirus (Ortervirales order, family of retroviridae, subfamily of orthoretrovirinae and Lentivirus genus). There are two species of HIV: HIV-1 and HIV-2, which likely originated from separate cross-species events (HIV-1 from simian immunodeficiency virus (SIV) in chimpanzees and gorillas, and HIV-2 from SIV in sooty mangabeys). While HIV-2 is less pathogenic and its rates are decreasing worldwide, the more pathogenic HIV-1 is responsible for the majority of the HIV pandemic. HIV-1 is subdivided in four distinct phylogenetic lineages (groups M, N, O and P), with M accounting for the vast majority of cases (Keele et al., 2006). M is further subdivided in 9 subclades with distinct geographical distributions (Bbosa et al., 2019). The subclade C, accounting for 50% of all HIV-1 infections, is the most frequent clade of Southern Africa and Southeast Asia, while in the Americas, Western Europe and Australia, subtype B is dominant (Bbosa et al., 2019). The HIV-1 virion is enveloped by a host-derived double-lipid membrane, punctuated by

multiple trimeric spikes, formed by the surface glycoprotein gp120 and the transmembrane protein gp41 (collectively called the Env trimer). Gp41 links to the matrix, this latter structure, made up of matrix antigen p17, building the inner layer of the virion. Within the matrix, the bullet-shaped capsid, made of 1 500 copies of the p24 protein, holds the two identical single 9.2 kb strands of RNA that makes up the HIV genome (Toccafondi et al., 2021), along with the nucleocapsid proteins that cover the genome. Multiple viral enzymes, such as the reverse transcriptase (RT) and integrase (IN) and accessory proteins, and some host cellular factors are also included within the capsid. The protease is found between the capsid and the matrix (Toccafondi et al., 2021).

Replication cycle

HIV primarily infects CD4+ T cells and, to a lesser extent, macrophages given its tropism. HIV entry is dependent on surface protein expression of CD4 and CCR5 or CXCR4, depending on the tropism of the virion (Kwong et al., 1998). Binding of gp120 with CD4 changes the conformation of the Env trimer, allowing binding with the second co-receptor (Wilen et al., 2012). The hydrophobic fusion protein of gp41 is then exposed and enters into the plasma membrane of the target cells. Gp41 then folds itself (second conformational change), bringing the cell membrane and virion membrane together and allowing their fusion. The capsid fully enters the cytoplasm, protecting the viral genome from cellular sensors (Toccafondi et al., 2021). There is debate as to how long the capsid lasts before its disassembly (Wilen et al., 2012), but is followed by reverse transcription of the genome. This process is done by the viral RT and aided by additional viral proteins which form the reverse transcription process (RTC) (Fassati et al., 2003). The DNA strand is then created based off the RNA template. The lack of proofreading activity of the RT,

as well as cellular enzymes of the apolipoprotein B mRNA editing enzyme catalytic popypeptide-like 3 (APOBEC3) family introduce mutational errors and edit cytidine to uracil. This results in an extremely high mutation rate (Tazi et al., 2010), estimated at one mutation per 1000 – 10 000 nucleotides, which is roughly between 1 and 10 mutations per *de novo* generated genome (Abram et al., 2010). The RTC and HIV DNA make up the pre-integration complex. The PIC traffics along the cytoskeleton network to the nucleus' surface, where it is actively transported into the nucleus thanks to the nuclear localization signals on the PIC's component matrix antigen and viral protein r (Vpr) (Lewis et al., 1992).

Once in the nucleus, the viral integrase (VI) allows for the integration of the viral DNA into the host's genome. The VI assembles with the viral DNA and removes two nucleotides at the 3'-ends of the viral DNA. This creates two reactive hydroxyl groups, which the VI then uses to join phosphates of the cellular DNA (called strand transfer), creating a gap in the cellular DNA. These gaps are closed by the host cell's repair machinery, sealing in the viral genome into that of the cell. This integration is a central reason as to why it is so hard to cure HIV; viral replication can be halted here for long intervals of time, making up the pool of silent reservoirs of virus.

If not halted (or after reactivation of the reservoir), transcription of HIV follows, where its products depend on the stage of the transcription. Initially, only small, multiply-spliced mRNA (<2kb) are produced. Once in the cytoplasm, they are transcribed into the regulatory proteins HIV transactivating protein Tat, the regulator of expression of virion proteins Rev, and the accessory protein negative regulatory factor Nef. Tat returns to the nucleus and, by both modifying the repressing cellular enzymes of the promoter of the HIV genome and recruiting cellular elongation factors to newly-formed HIV RNA, allows

the generation of incompletely spliced and full-length unspliced HIV mRNAs. Rev binds to these longer HIV RNAs and mediates active export (Tazi et al., 2010). Incompletely spliced viral mRNA translates into virion infectivity factor (Vif), Vpr, Vpu (viral protein u) and Env (cleaved into gp120 and gp41), whereas the unspliced mRNA produces the Gag-Pol polyprotein (later cleaved into the matrix antigen), the capsid p24, the nucleocapsid, viral enzyme proteases, the reverse transcriptase, an RNAse, and the integrase (Sundquist and Krausslich, 2012). The full-length mRNA can also be integrated as the viral genome into new particles.

Now that all the virions' components are *de novo* produced, the late phase begins, mainly coordinated by the poly-protein Gag (Sundquist and Krausslich, 2012): 1) It's MA domain allows it to bind to the cell membrane and to locally concentrate Env proteins ; 2) it's NC domains binds the full-length HIV genome ; 3) it's CA domain mediates Gag-Gag interactions that create a lattice of Gag proteins forming the immature virion. The new viral particle is released through cellular factors recruited by Gag's p6 domain (Gottlinger et al., 1991). A final cleavage of the Gag and Gag-Pol poly-protein complexes by the virus' protease produces the structural particles making up the capsid, matrix and nucleocapsid, as well as the other viral enzymes (Sundquist and Krausslich, 2012). Only then is the new viral particle, with its bullet-shaped core, infectious.

During chronic untreated infection, viral replication occurs primarily in GC TFH in lymphoid tissues and TH17 cells in the gut, both cell types being highly permissive to infection (Elhed and Unutmaz, 2010; Kohler et al., 2016; Perreau et al., 2013). However, HIV genome can be found throughout the body (Wong and Yukl, 2016).

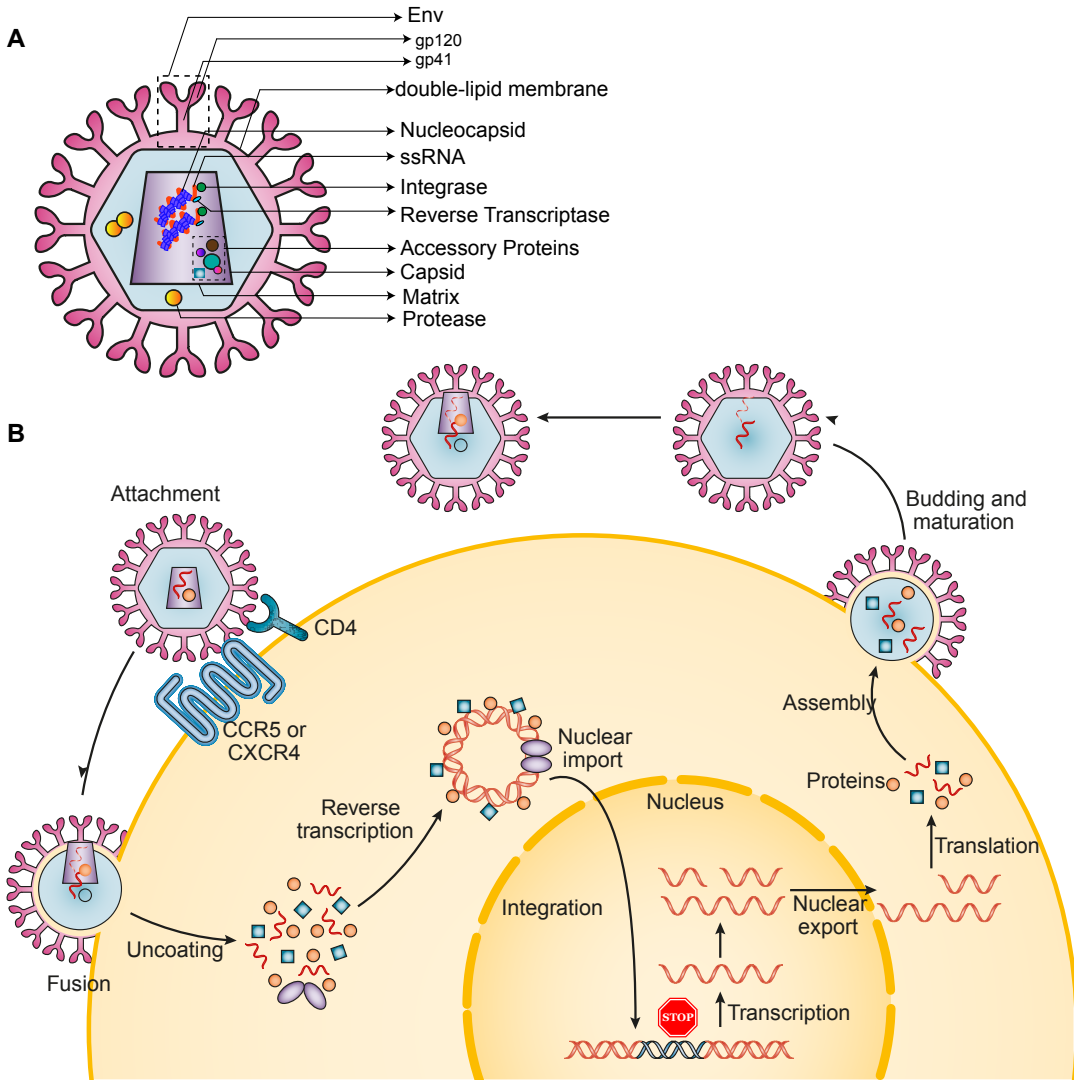

Figure 1.11 HIV structure and replication cycle. A) Components and structure of a mature HIV viral particle. Single strand RNA genome is encapsulated by the nucleocapsid proteins, then by the capsid, which also includes viral proteins like integrase, reverse transcriptase, Vif, Vpr and Nef. This is contained within the matrix and finally encircled by a host-derived membrane punctuated by the viral trimeric Env protein, made of gp120 and gp41. B) Schematic of HIV replication cycle within an infected human cell. Viral particle binding to the host cell is mediated by the interaction of viral protein Env with host's CCR5 or CXCR4 and CD4, enabling fusion with cell membrane. The viral particle is then uncoated, and viral RNA is reverse transcribed. Viral DNA is transported into the nucleus and integrates to the host cell's genome, where it remains transcriptionally silent or proceeds to transcription. Nested viral mRNA is transported into cytoplasm and translated into viral proteins. New viral particles are assembled and bud. Maturation finishes in budded virion and renders them infectious. *Figure modified from (Deeks et al., 2015).*

Anti Retrovirals (ARVs)

The first ARV was approved for FDA in 1987, and as of February 2021, there are 23 such ARVs spanning 8 functional classes (https://hivinfo.nih.gov/understanding-hiv/fact-sheets/fda-approved-hiv-medicines). Because of the extremely high propensity for mutation of the HIV replication cycle, using only 1 ARV rapidly results in viral escape and drug resistance. For this reason, a cocktail of three ARVs from at least two different classes is used to treat HIV-infected individuals. Viral tropism and the presence of quasi species with resistances can affect the potency of a given regiment (Iacob et al., 2017).

As seen previously, the very first step of the viral replication cycle is the attachment of the virion to the cell surface. This is the step targeted by the two most recent classes of ARVs. The first is an attachment Inhibitor, the most recent class of ARV. This class only includes one drug (fostemsavir), approved in 2020, which binds the gp120 protein and prevents interaction with the cell membrane. The second class is a Post-Attachment Inhibitor, also only counts one ARV (ibalizumab), approved in 2018. This drug is a humanized monoclonal antibody which, through binding of CD4, leads to a conformational change of the CD4-gp120 complex, making it unsuitable for viral entry (Iacob et al., 2017).

Beyond attachment, two classes of ARVs are entry inhibitors, with again one drug per class. The Fusion Inhibitor enfuvirtide (T-20) is a peptide which mimics a domain of gp41, competing with the homologous domains of the proteins, effectively disrupting the fusion process (Arts and Hazuda, 2012). The CCR5 Antagonist maraviroc binds to cellular CCR5 and induces a conformational change that make the receptor unable to bind its ligand nor the virus (Iacob et al., 2017). The next step of the replication cycle targeted by ARV is the reverse transcription. For this step, there are two classes of drugs. Nucleoside Reverse

Transcriptase Inhibitors (NRTIs) were the first class of drugs to treat HIV, with zidovudine (AZT), and now count five drugs. During the viral RNA-dependent DNA or DNA-dependent RNA synthesis, the inclusion of these nucleotide analogs prevent the subsequent addition of other nucleotides, resulting in chain termination (Iacob et al., 2017). The Non-Nucleoside Reverse Transcriptase Inhibitors (nNRTIs) rather bind the viral reverse transcriptase (RT) and lead to a conformational change in the substrate-binding site, reducing polymerase activity. This class of drugs also includes 5 compounds (https://hivinfo.nih.gov/understanding-hiv/fact-sheets/fda-approved-hiv-medicines).

The class of Integrase Stand Transfer Inhibitor (INSTIs), comprised of three compounds, bind the integrase-viral DNA complex to inhibit strand transfer. The final group of ARVs are protease Inhibitors, counting six drugs, and block the cleavage of the Gag-Pol poly-protein. This impedes the maturation of the virion, which is blocked in a non-infectious state (Doitsh and Greene, 2016).

These ARVs only target the active replication cycle of HIV and cannot clear the latent viral reservoir. This is why ARVs must be taken for life.

Table 1.2 Summary of antiretrovirals approved for treatment of HIV

Reference : https://hivinfo.nih.gov/understanding-hiv/fact-sheets/fda-approved-hiv-medicines

Drug class	Viral replication stage targeted	Acronyme	Mechanism of action	Example of drugs	Year of FDA approval of first drug in class
Nucleoside Reverse Transcriptase Inhibitors	Reverse transcription	NRTI	Blocks the reverse transcriptase --> HIV cannot replicate its genome	Abacavir, emtricitabine, lamivudine, tenofovir disoproxil fumarate, zidovudine	1987
Non-Nucleoside Reverse Transcriptase Inhibitors (NNRTI)	Reverse transcription	NNRTI	Alters conformation of reverse transcriptase, blocking its action	doravirine, efavirenz, etravirine, nevirapine, rilpivirine	1996
Protease inhibitor	Maturation	PI	Blocks cleavage of Gag-Pol polyprotein, impeding virion maturation	atazanavir, darunavir, fosamprenavir, ritonavir, tipranavir	1996
Fusion Inhibitor	Entry		Disrupts fusion of virion and host membrane	Enfuvirtide	2003
CCR5 antagonists	Entry		Directly blocks CCR5 co-receptor, stoping viral entry into host cell	maraviroc	2007
Integrase Strand Transfer Inhibitor	Integration	INSTI	Inhibition of strand transfer through binding to viral integrase	Cabotegravir, dolutegravir, raltegravir	2007
Attachment Inhibitor	Entry		Prevents interaction of gp120 with cell membrane by binding gp120	Fostemsavir	2020
Post-attachment inhibitors	Entry		Induces conformational change of CD4-gp120 complex, preventing viral entry	ibalizumab-uiyk	2018

Viral Reservoir

Upon integration of the HIV genome into its DNA, a small fraction of infected cells do not continue on to produce virions; the HIV DNA rather enters a transcriptionally silent state, termed latent infection. Since there are no expression of viral, latently infected cells escape the immune response, allowing them to persist for years. This process likely occurs in activated T cells transitioning to a resting state (Van Lint et al., 2013). All latently infected cells are referred to as the HIV's "reservoir", and it is thought to be maintained mainly through homeostatic proliferation of infected cells during ART (Kuo and Lichterfeld, 2018), although perhaps also by sporadic reactivation in tissues with low ART penetrance (Fletcher et al., 2014). This latter phenomenon may also allow some transcriptional activity, and resulting viral by-products may be implicated in the sustained chronic inflammation (Niessl et al., 2020b).

Formation of viral reservois occurs very early upon infection. The "Mississipy-baby",infected at her birth from her mother, was off treatment for only 30 hours, yet this was sufficient to allow for viral rebound when she was taken off ART (albeit with a considerable 27-month delay in rebound) (Ananworanich and Robb, 2014). In the SIVrm model, integrated HIV genome in cells of lymph nodes and gastrointestinal tract were detectable 3 days post-infection, before blood viremia (Whitney et al., 2014).

The size of the reservoir is very stable during ART (Siliciano et al., 2003). Upon ART interruption, viral loads rebounds from reservoir cells within weeks, with plasma VL returning to pre-ART levels (Harrigan et al., 1999). This is thought to occur following activation of cells harbouring latent virus (Zevin et al., 2016) and/or from residual viral replication in tissues hidden from ART (Martinez-Picado and Deeks, 2016).

Disease progression

Viremic patients

HIV is transmitted through biological fluids, primarily through sexual intercourse, but also through blood exchanges, for example by contaminated blood transfusions and pregnancy labour. Although HIV was initially detected mostly in men, new HIV infections are detected in similar scale in both men and women. In most infected individuals, three distinct clinical phases characterize HIV infection.

The acute phase lasts a couple of weeks, and is further subdivided in smaller time lapses. In the first “eclipse” part, a transmitter/founder (TF) virus must pass the mucus layer to come into contact with the resident immune cells of the mucosal epithelium. TF viruses are different from the quasi species found in the serum of HIV-infected individuals. They have increased infectivity and IFN I resistance (Joseph et al., 2015). Furthermore, they are preferentially CCR5-tropic, an advantage given the enrichment of CCR5+ CD4+ T cells in the gastrointestinal mucosa (Poles et al., 2001). In SIV-infected monkeys, foci of infected CD4+ T cells in the female genital tract are observed as soon as 2-4 days after challenge (Stieh et al., 2016). Additional immune cells, including the target CD4+ T cells, are recruited to the site of infection by the inflammation, further increasing the pool of infected cells (Perez-Zsolt et al., 2019). During this phase, lasting 7 to 21 days, there is no viral RNA detectable in the blood, and no clinical symptoms (Cohen et al., 2011). The reservoir is also established at this time (Whitney et al., 2014).

Past the eclipse part, infected CD4+ T cells and HIV-bound DC and myeloid cells transport

HIV into draining lymph nodes, leading to the systemic dissemination of the virus. This phase lasts a few weeks and can be asymptomatic or characterized by acute retroviral syndrome (flu-like symptoms such as headache, nausea, and body aches). Infected individuals experience a rapid depletion of their CD4+ T cells throughout the body, most dramatically in the gut-associated lymphoid tissue (GALT) (Brenchley et al., 2004), while HIV viral load peaks. This initial depletion of CD4+ T cells mainly affects the CCR5+ T_{EM} while sparing CCR5- naïve and central memory CD4+ T cells (Okoye and Picker, 2013). It is thought to arise from direct killing and Fas/Fas ligand-mediated apoptosis (Barber et al., 2006). In the final part of the acute phase, the host's immune response blunts viral replication, resulting in a decline of viremia. Blood CD4+ T cell counts are partially recovered thanks to replenishment by the TCM population (Okoye and Picker, 2013), although the GALT remain highly depleted, particularly within the Th17 population (Brenchley et al., 2004; Elhed and Unutmaz, 2010). This loss increases the susceptibility to bacterial and fungal infections, while decreasing gut integrity. This leads to microbial product translocation from the lumen into the blood stream, establishing a state of chronic immune activation (Brenchley et al., 2006).

The phase that follows is the chronic phase, which lasts anywhere from 3 years (for quick progressors) to 20 years (slow progressors) (Poropatich and Sullivan, 2011). The viral load decreases to a "steady state", at relatively constant amounts of copies/ml of blood. CD4+ T cells maintain a high turnover rate as they continue to be killed off by several mechanisms. An *ex vivo* study has shown that more than 95% of dying cells are abortively infected and cause pyroptosis, a highly-inflammatory form of programmed cell death (Doitsh et al., 2014). CD4+ T cells not carrying the co-receptor necessary for HIV's entry

(CCR5 or CXCR4, depending on the tropism) are spared from this process. Given CXCR4's widespread expression, it may partially explain why early emergence of CXCR4-tropic viruses are associated with pan-CD4+ T cell depletion and quicker progression of the disease (Connor et al., 1997; Harouse et al., 1999). Other mechanisms target the productively infected CD4+ T cells, like apoptosis by viral protease's activation of the caspase-3 pathways (Doitsh et al., 2014). NK and CD8+ T cells kill infected cells and by-stander cells coated by viral products released into circulation (if those cytotoxic by-products themselves do not kill the cells) (Cummins and Badley, 2010). In addition, regulatory pathways, like increased proportions of Treg (Presicce et al., 2011) and greater expression of immune checkpoints (which will be discussed later) may also play a role in the slowing of the replenishment.

During the chronic phase, there is a lot of active viral replication within the susceptible TFH of the GC (Perreau et al., 2013), where the follicular dendritic cells trap a high concentration of HIV particles within immune complexes (Smith-Franklin et al., 2002). As a result, ongoing chronic inflammation leads to extensive scarring of the lymphoid tissue microenvironments (Schacker et al., 2006), disrupting their ability to support T cell homeostasis, for example by IL-7 delivery (Estes, 2013).

The final stage of the infection is AIDS, whereby the infected individual reaches a critically-low CD4+ T cell count, after the disruption of the regenerative capacity of the immune system. AIDS is characterized by the advent of rare diseases only seen in immunocompromised individuals, like Kaposi's sarcoma, cytomegalovirus retinitis, HIV-related encephalopathy, pneumocystis jiroveci pneumonia, etc. These secondary diseases are often what causes the death of infected patients, rather than HIV itself

(Bonnet et al., 2005).

The speed of the disease progression is associated with viral load and CD4+ T cell counts (Deeks et al., 2013). There are two contexts where viral load (and thus disease progression) is blunted: spontaneous or therapeutic control of viral replication.

Elite controllers

The proposed definition of an Elite controller (EC), from the International HIV Controllers Consortium, is an ART-naïve HIV-infected individual with at least three plasma measurements of HIV-RNA below 50 copies/ml for at least one year (Deeks and Walker, 2007). This definition encompasses a rare group of individuals which are heterogeneous in terms of clinical manifestations, genetic background, and immunological factors. Characteristics of the infecting virus has also been linked to EC (Navarrete-Munoz et al., 2020). For example, deletion in Nef in the infecting virus of contaminated blood products allowed for the six recipients to maintain virological suppression for 10 to 14 years (Deacon et al., 1995). However, fully replication-competent HIV, and without deletion, are also found in some EC (Blankson et al., 2007). EC's reservoirs are less frequent than individuals with ART-suppressed HIV (Jiang et al., 2020), although a greater proportion of their reservoir lacked lethal sequence defects. Their reservoir also seems selected towards deep latency, where the virus integrated in reppresive chromatin area (Battivelli et al., 2018), and displayed little mutational escape from CTL, suggesting early seeding (Jiang et al., 2020). Taken together, these evidences suggest that, with the exception of a few unique cases, host factors play a greater role in the elite control of the virus than its sequence, although they are not mutually exclusive.

Among clinical factors, not all EC can maintain normal CD4+ T cell counts (Boufassa et al., 2011; Hunt et al., 2008). Decreased counts are associated to greater systemic inflammation and the advent of non-AIDS-defining events, including cardiovascular disease, atherosclerosis, and cancer (Okulicz et al., 2016; Pereyra et al., 2012). The duration of time an EC can control the infection can vary anywhere between 1 to at least 25 years, after which time there is loss of immunological control and progression of the disease (Navarrete-Munoz et al., 2020).

EC are enriched in certain HLA types, providing the first evidence that genetic background is key. Class I HLA alleles have the strongest independent association with HIV disease outcome, with at least 17 being associated with slower disease progression, and 14 with quicker progression towards AIDS (Goulder and Walker, 2012). HLA-B*27 and HLA-B*57 are overrepresented in EC, with loss of control occurring after viral escape (Kaslow et al., 1996; Miura et al., 2009).

These observations highlight the importance of HIV-specific CD8+ T cells in establishing and maintaining viral control in the absence of ART. This is further supported by the loss of immunological control in EC following a reduction in HIV-specific CD8+ T cell poly functionality and viral suppression capacity (Pernas et al., 2018; Rosas-Umbert et al., 2019).

HIV-specific CD4+ T cells are comparatively understudied, although protective type II HLA, namely HLA-DRB1*15:02 and HLA-DRB1*13:01, have also been associated to slower disease progression (Ranasinghe et al., 2013). Beyond this observation, there are other clear observations that CD4+ T cells contribute to HIV control. High-affinity *in vivo* CD4+ T cell responses against Gag has been associated to HIV control (Benati et al.,

2016). EC also maintain robust HIV-specific Th1 responses and strong proliferative capacities (Ferre, et al., 2010).

To further characterize the HIV-specific CD4+ T cell response of EC, we have sequenced the transcriptome of a sorted pool of these cells from both EC and CP (Morou et al., 2019). We have found that HIV-specific CD4+ T cells of EC have preserved helper differentiation capabilities. Furthermore, our work has shown that EC's HIV-specific CD4+ T cells have a preserved pool of HIV-specific Th17 cells, which correlated negatively with a biomarker of gut dysbiosis (Morou et al., 2019). Finally, not all of the functional traits of HIV-specific CD4+ T cells observed in EC were present in ART. This highlights incomplete restoration on ART which, as we shall see, affects more than the HIV-specific T cell response.

ART-treated patients

Suppression of viral replication by ART reduces ongoing inflammation and significantly restores memory CD4+ T cells in blood and secondary lymphoid tissue, even when initiated during the AIDS phase (Autran et al., 1997). Reconstitution of CD4+ T cells take several years to reach pre-infection levels (Guihot et al., 2011), although initiation during primary infection enhances immune recovery (Le et al., 2013). The amount of CD4+ T cell reconstitution is an important

Among HIV-infected individuals on suppressive ART, serious non-AIDS event (nAEs), such as cardiovascular, liver and renal diseases, are the leading causes of disease and death (Deeks et al., 2013). These are predicted by multiple biomarkers of inflammation and coagulation, highlighting the critical role of chronic inflammation despite ART (Hunt et al., 2016; Kuller et al., 2008; Tenorio et al., 2014). This inflammation is thought to be driven by residual HIV replication (for example in tissues with low ART penetrance),

coinfections, gut mucosal injury with resulting translocation of microbial products, and/or tissue fibrosis (Hsu et al., 2013). Higher CD4+ T cell counts at the time of ART initiation are associated with greater immune reconstitution, lower residual inflammation, and lower prevalence of nAEs (Deeks et al., 2013; Rodger et al., 2013; van Lelyveld et al., 2012). This is also observed eith early treatment initiation. While initiation of ART extremely early (within the first couple of weeks following infection) does normalize coagulation biomarkers to levels seen in uninfected controls, it reduces without normalizing markers of monocyte activation from microbial by-products, inflammation and fibrosis (Sereti et al., 2020).These latter three are associated with death, cardiovascular events and/or disease progression in HIV-infected individuals (Hunt et al., 2014). A marker of enterocyte turnover (I-FABP), representative of intestinal damage, is increased regardless of ART initiation time, and correlate with the amount of integrated HIV detectable in gut tissue (Sereti *et al.*, 2020). Thus, while CD4+ T cell depletion leads to immunodeficiency in chronic infection, persisting inflammation not eradicated by ART leads to increased morbidity and mortality. This remains one of HIV's critical problems.

Animal models

HIV cannot infect species other than humans (unless by using transgenic models). Other animal models of chronic infection have been seminal for the understanding of how a chronic viral infection leads to the deterioration of the immune response.

The animal model closest to HIV is SIV infections in non-human primates (NHP). In natural hosts of SIV (many species of African monkeys, such as the chimpanzees - SIVcp and sooty mangabeys - SIVsm), SIV infection does not develop into a disease. For example, SIV infections in sooty mangabeys and African green monkeys present with high viral

replication and rapid turnover of infected CD4+ T cells in acute infection, but preserved lymph node architectures. They do not have chronic immune activation nor depletion of mucosal and peripheral CD4+ T cells (Chahroudi et al., 2012). Conversely, SIV infections in Asian monkeys, which are not natural hosts, replicates a number of HIV infections in AIDS. The most studied species is the rhesus macaques whom, upon SIV infection (SIVrm), maintain high viral loads, rapid turnover and loss of CD4+ T cells, most importantly in the GALT (Hatziioannou and Evans, 2012). They also display similar clinical syndromes like opportunistic infection (Apetrei et al., 2005). Disease progression in the rhesus macaques is much quicker, reaching AIDS within 1-2 years in the absence of ART (Hatziioannou and Evans, 2012).

NHP being large animals and expensive to maintain, a model of chronic infection in mice is also highly relevant. The workings of an acute viral infection were studied using the Armstrong (Arm) strain of the lymphocytic choriomeningitis virus (LCMV). This acute viral infection, which causes severe inflammation in the meninges, is cleared within 10 days after inoculation. It is characterized by robust antiviral T cell responses. A mutant of this strain (clone 13), was found to generate a chronic infection, cleared 90 days after infection (Ahmed et al., 1984). Both strains only differ by 3 amino acids, none of which being within the T cell epitope. Thus, we can track anti-viral T cell responses of the same specificity between acute and chronic infections. As will be discussed below, much of what we know about cues leading up to exhaustion come from these LCMV models. However, LCMV clone 13 is ultimately cured, in contrast to HIV and other chronic human viral infections, like HCV. Furthermore, major differences between mouse and human immune responses can affect the translationability of results. For example, priming and polarization of CD4 T

cells are not driven by the exact same signals in both species. Chemokines differ substantially between mice and humans. For these reasons, *in vivo* observations made in mice mdels greately benefit from validation using primary cell from humans (Mestas and Hughes, 2004).

Innate immune responses

Antigen-presenting cells are pivotal for T cell priming. During chronic untreated HIV and SIVrm infection, both pDC and mDC are decreased in the blood, the extent of which is associated to increased viral loads (Donaghy et al., 2001). The transcriptome of monocytes and mDCs were distinct between uninfected individuals *versus* chronically-infected untreated individuals. The latter grouped showed increased interferon-response genes, as well as subdued singatures of IL-1 signalling and antigen-processing and presentation (Murray et al., 2020). Although the impact of these changes on T cell responses has been studied in the LCMV model, whose DC compartment present similar traits. Dendritic cells after 21 days of chronic infection presented lower levels of CD80, CD86 and MHC I (machinery for priming and antigen presentation) than those in the acute phase of the infection (Snell et al., 2018). The features of LCMV-specific CD8+ T cells primed by chronic-exposed DC were different from the acute-exposed DC; when primed by the chronic-exposed, their development depended on IL-21 (rather than IL-2), and they had lower immune checkpoint (IC) expression and greater Eomes, TCF-1 and CXCR5 expression. This suggests that decreased signalling strength enforced a memory-like phenotype (Snell et al., 2018). Thus, disruption in T cell priming can also partially explain the suboptimal features of the HIV-specific T cell responses discussed next.

Adaptive immune responses

Beyond targets, HIV-specific T cells are highly implicated in fighting the HIV infection. In all individuals infected with HIV, the T cell response exerts a certain level of viral control, which explains the sharp post-peak decrease of viral load in acute infection. Indeed, depletion of either CD4+ T cells (Ortiz et al., 2011) or CD8+ T cells (Matano et al., 1998) prior to primary SIV infection abrogates the post-peak decline of viral load in NHPs.

In the setting of chronic viral infection, the adaptive immune response is quite different from the prototypical one seen in acute infections. The persistence of antigens stimulates virus-specific cells repetitively, with co-stimulation (in contrast to anergy, where a cell not receiving co-stimulation becomes hyporesponsive (Wherry, 2011)). These changes are seen in a wealth of chronic infections and across species, like LCMV clone 13 infections in mice, SIV infection in primates, and HCV and HBC and HIV in humans (Wherry, 2011).

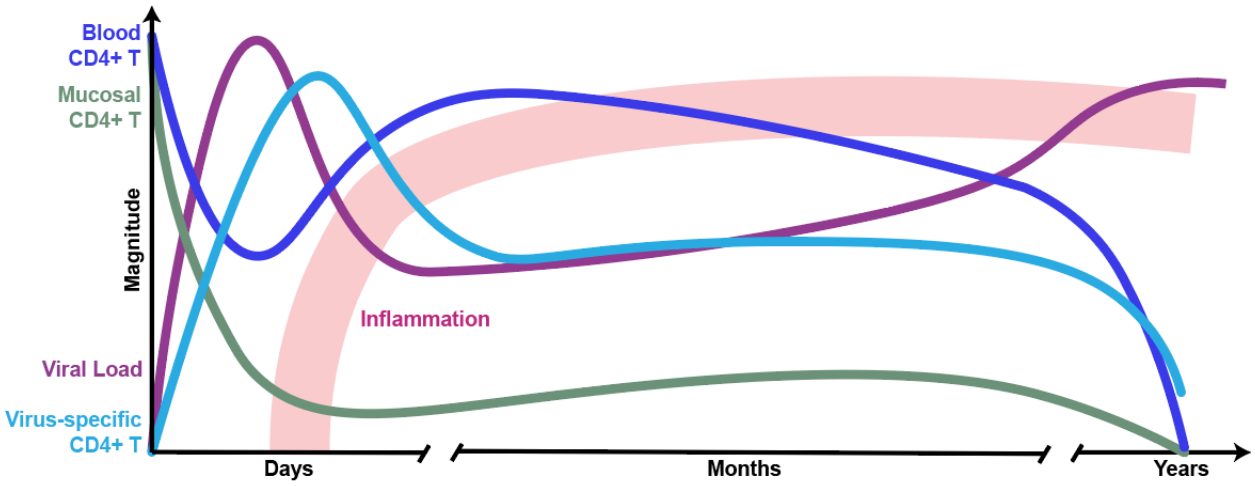

Figure 1.12 Overview of immune response over time in viremic HIV infection.

HIV-specific T cell responses

HIV-specific CD8+ T cells exert a strong effect on the virus itself. Two decades ago, researchers found a temporal association between the advent of HIV-specific CD8+ T cells and the post-peak viral load decrease (Koup, 1994). They recognized that these HIV-specific CD8+ T cells caused the selection of escape variants in HIV-1 (Borrow et al., 1997). CD8 depletion in the SIV model also showed prolonged depletion of CD4+ T cells (Matano et al., 1998). HIV-specific CD8+ T cells in acute HIV infection primarily target Env.

After the immune response fails to clear the primary infection, and we fall into the chronic phase, HIV-specific CD8+ T cells enter a distinct differentiation state referred to as “exhaustion” (Wherry, 2011). Exhausted virus-specific CD8+ T cells follow a hierarchical loss-of-function, preceded by selective elimination of highly-exhausted cells. They are also characterized by high and sustained levels of IC, altered transcription factor profile, and metabolic derangement. Importantly, they are unable to transition into a long-lived quiescent state, rather relying on continuous TCR signalling for maintenance.

Despite their loss-of-function, exhausted CD8+ T cells are not inert. The residual functions they retain drive epitope mutation (Seki and Matano, 2011), and exert some level of viral control, since depleting CD8+ T cells in chronic SIV infection exacerbates viral loads and progression towards AIDS (Schmitz et al., 1999; Jin et al., 1999). When exhausted CD8+ T cells are no longer sustained, containment of viral infection is largely lost (Paley et al., 2012).

Advancement in transcriptomic and epigenetic characterization of exhausted CD8+ T cells have elucidated its development. The central feature seems to be sustained TCR

stimulation (Bucks et al., 2009), resulting in vast epigenetic changes and enhanced chromatin accessibility (Sen et al., 2016). TCR-dependent pathways such as NFAT and SPRY2 are implicated in CD8+ T cell exhaustion (Martinez et al., 2015), and lack of help from CD4+ T cells, whether from depletion (discussed earlier) or skewing (discussed next) also seems to contribute (Matloubian et al., 1994). Other mechanisms likely involved in exhaustion are desensitization of co-stimulatory pathways (Odorizzi and Wherry, 2012), chronic exposure to soluble mediators like type I IFNs (Teijaro et al., 2013; Wilson et al., 2013; Zhen et al., 2017), and destruction of tissue architecture in secondary lymphoid organs (Mueller et al., 2007; Zeng et al., 2011). These changes in chromatin accessibility are reversible only for a short time: LCMV-specific CD8+ T cells transferred from chronically-infected mice to acutely-infected mice could only form memory T cells if transferred early on in the course of the chronic infection (Angelosanto et al., 2012).

Exhausted CD8+ T cells are divided into two subsets, distinguished by their proliferative, self-renew and functional capacities (Im and Ha, 2020). Progenitor exhausted (PE), or stem-cell like CD8+ T cells maintain the pool of virus-specific CD8+ T cells in chronic viral infection (Im et al., 2016; Utzschneider et al., 2016). They are characterized by expression of TCF-1, CCR7, BCL6, EOMES, ICOS, and CD28, and reside in the T-cell zones of lymphoid tissues (Im and Ha, 2020). Despite overlap between these cells and the memory phenotype, TOX is a notable divergence, being highly expressed and maintained in exhausted CD8+ T cells. The expression of this TF is regulated by antigen-induced calcium signalling, and when deleted, results in a defect in PE CD8+ T cells (Alfei et al., 2019). PE can self-renew and = differentiate into a TCF1- terminally differentiated CD8+ T cell subset. This latter subset expressed genes related to effector T cells, like Prdm1,

Tbx21, and their effector molecules Gzma, Gzmb and Prf1 (He et al., 2016).

Immune checkpoints (IC), or inhibitory receptors, are negative regulatory pathways which, in physiological contexts, are key in modulating the strength of the response, limiting immunopathology and autoreactivity (Sharpe et al., 2007). On exhausted CD8+ T cells, they are maintained at very high levels and actively involved in the limiting of their effector functions (Wherry, 2011). The best characterized inhibitory receptor is PD-1/PD-L1-PD-L2 axis.

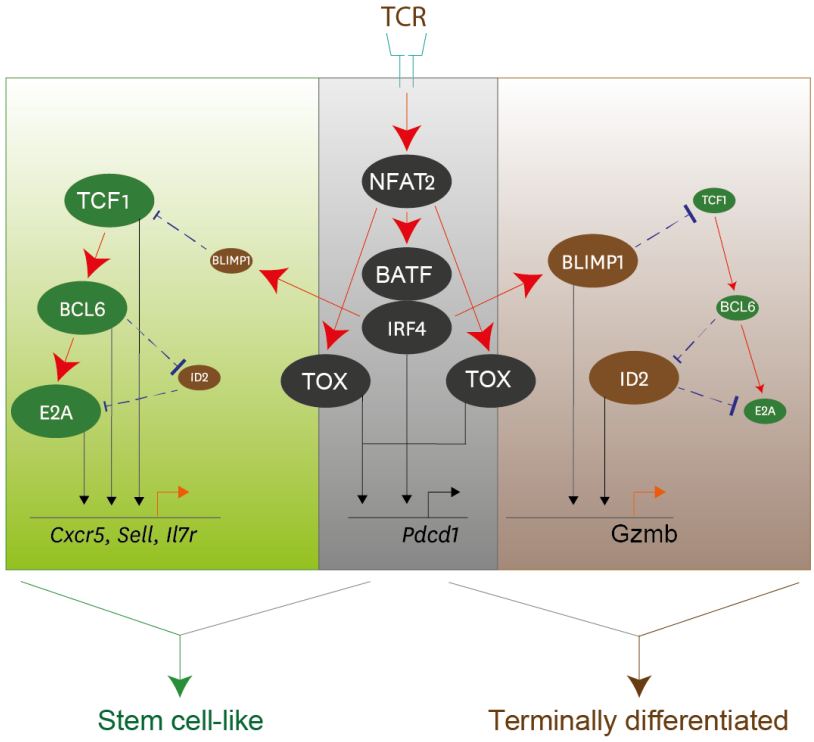

Figure 1.13 Regulation of CD8+ T cell differentiation through transcriptional network in chronic viral infections. Persistent TCR stimulation induces NFAT2, BATF and IRF4 expression, where NFAT2 goes on to activate TOX, and these factors induce PD-1 expression. Stem-cell like subsets highly upregulate TCF1, leading to increased BCL6 and EA2 expression ; this axis induces genes related to stemness. In contrast, IRF4 with BATF up regulate BLIMP1, which in turn represses TCF1. BLIMP1 and ID2 lead to enhanced Gzmb expression and differentiation towards terminally exhausted. Figure from (Im and Ha, 2020), used within permitted use under the terms of the Creative Commons Attribution Non-Commercial License (https://creativecommons.org/licenses/by-nc/4.0/)

HIV-specific CD4+ T cells play a central role in the progression of the HIV infection. Generally, virus-specific CD4+ T cells help with viral control (seen earlier in the NHP model). In the chronic LCMV model, CD4+ T cell depletion prior to infection abrogates the ultimate resolution of the infection (Matloubian et al., 1994). In humans, a robust early HCV-specific CD4+ T cell response is associated to viral clearance, in contrast to patients with low or absent responses who develop a chronic infection (Lindqvist et al., 2012). Finally, elite controllers have robust HIV-specific CD4+ T cells (Emu et al., 2005; Pereyra et al., 2008), although whether those helped with the initial control of the viral infection, or rather their function was preserved in the absence of prolonged viremia, is unclear.

In chronic HIV infection, HIV-specific CD4+ T cells also undergo a separate differentiation state, called “dysfunction”. Like exhaustion, this state is characterized by decreased production of IFNg, TNFa and IL-2, and increase IC expression (Wherry, 2011). However, dysfunctional CD4+ T cells also have a gain of other functions, such as IL-10 and IL-21 production (Brooks et al., 2006; Elsaesser et al., 2009). It is interesting to note that, while antiviral functions typically associated to Th1 are diminished in dysfunctional cells, functions of other polarizations are largely preserved, like B-cell help provided by TFH (Oxenius et al., 1998).

The molecular mechanisms behind the advent of dysfunction of virus-specific CD4+ T cells are incompletely understood. Transcriptome and kinetic analysis of LCMV-specific CD4+ T cells showed functional differences between chronic and acute infection as early as 8 days after infection, namely low TH1-associated functions, high IL-21 mRNA, and a IL-10+ population only found in chronic infection (Crawford et al., 2014). The transcriptional differentiation pattern of dysfunctional CD4+ T cells was distinct compared

to both effector and memory CD4+ T cells. It presented uniquely high IFN-induced genes, and regulation of cell cycling and DNA structure, with reduced signatures of DNA repair, ribosomal function, and antigen receptors/MHC (Crawford et al., 2014). Some of these signatures were commonly enriched in exhausted CD8+ T cells with respect to their memory counterparts, like persistently high IFN-responsive signatures, strongly associated to NFkB complex, NFAT and Eomes (Crawford et al., 2014). Immune checkpoints, increased in both dysfunctional CD4+ T cells and exhausted CD8+ T cells, were in some cases common to both cell types (PD-1), and in others qualitatively different: CTLA-4, CD200 and BTLA were biased towards CD4+ T cells, while CD244, Tim3 and Lag3 were biased to CD8+ T cells (Crawford et al., 2014).

While some transcription factors were similarly regulated in memory and dysfunctional CD4+ T cells in contrast to naïve, dysfunctional CD4+ T cells additionally expressed *Eomes*, *Prdm1* (Blimp-1), *Ikzf2* (Helios – without FoxP3 co-expression), *Nfatc1* and *Maf*. Of note, unlike in exhausted CD8+ T cells where TCF-7 was completely lost, it was preserved in dysfunctional CD4+ T cells (Crawford et al., 2014). Among the heterogeneous pool of dysfunctional CD4+ T cells, the lineage-specific TF was apparent was increased Bcl6, and the clear Th1 enrichment seen in memory CD4+ T cells was missing (Crawford et al., 2014). The LCMV clone 13 model showed that chronic type I IFN stimulation found in chronic viral infections inhibits development of Th1 responses, suggesting that the environment is at least in part responsible to the relative absence of Th1 (Osokine et al., 2014).

To better characterize the function of HIV-specific CD4+ T cells, we analyzed the transcriptome of HIV Gag-specific CD4+ T cells from elite controllers and chronic

progressors (Morou et al., 2019) (see appendix). The HIV-specific CD4+ T cells of EC had increased TH1 and TH17 signatures, with concordant expression of CXCL9/10/11, IL17, and IL22. The robust Th17/TH22 HIV-specific CD4+ T cell response was associated negatively to immune activation and abundance of Proteobacteria in plasma RNA species. EC had up regulation of BCL6 as well as IFN-stimulated genes, in contrast to the LCMV model.

The dysfunctional HIV-specific CD4+ T cells from CP had reduced signatures of T helper differentiation, and an enrichment of *TOX* and TFH signature (including the related genes MAF, ICOS, IL-21, CXCL13, TIGIT, CD200, the latter 5 of which also had greater protein expression). This signature was enriched in both CXCR5+ and CXCR5- subsets, highlighting a skewing towards TFH profile among non-TFH cells. This latter population correlated positively with p24-specific antibody titers in CP, suggesting this skewing affects their functional roles. Indeed, a subset of HIV-specific CD4+ T expressing CXCR5-PD-1+ICOS+ has many features of TFH, like BCL6, Maf and CD84 expression, IL-21 and CXCL13 production, and the ability to provide B cell help (Del Alcazar et al., 2019). This population, present in both LN and blood, was clonally related to TFH and has shared epigenetic landscape (including accessible chromatin for *CXCR5* promoter region), although its transcriptomic profile had greater cellular trafficking signalling (Del Alcazar et al., 2019). As such, HIV infection seems to result in a population with higher TFH-associated characteristics, perhaps as a result of evolutionary advantage. Indeed, in the setting of vaccination prior to challenge in the LCMV model, the strong Th1 response elicited by the vaccines resulted in catastrophic immunopathology (Penaloza-MacMaster et al., 2015). This is not the case in the course of a normal LCMV clone 13 infection, where

most virus-specific CD4+ T cells differentiate towards TFH (Fahey et al., 2011). Furthermore, these LCMV-specific TFH enable the development of late-arising neutralizing antibodies which ultimately allow the mice to control the LCMV infection (Greczmiel et al., 2017). Thus, in the LCMV model at least, the skewing of virus-specific CD4+ T cells away from the prototypical antiviral Th1 phenotype and towards the B-cell helping TFH phenotype provides a clear evolutionary benefit by avoiding immunopathogenesis while diversifying immune strategies (Greczmiel and Oxenius, 2018). The parallels to be drawn between HIV and LCMV clone 13 infections do suggest that similar strategies in both species; however, the addition of HIV's great immune escape capacities makes this strategy insufficient.

Immunotherapy in chronic viral infection : HIV

Although no immunotherapies are currently FDA-approved solely for their anti-HIV action, the use of activating immunotherapies is investigated for two main non-exclusive purposes: stimulating the anti-HIV immune response to confer a functional cure – whereby the immune response alone can contain viral replication to below-detectable levels – and reactivating latent viral reservoirs.

Immune checkpoints in HIV

As mentioned in the introduction, IC are cell-surface inhibitory receptors that, upon binding their ligand, will trigger immunosuppressive signalling pathways. There are many different IC which, through their differential distribution and signalling cascade, affect the immune response differently. Of paramount importance is PD-1, both for its suppressive action on HIV-specific immune responses, as well as its preferential expression on persistently-infected cells in the context on ART (Chomont et al., 2009; Fromentin et al., 2019).

Characteristics of PD-1

PD-1 was first described in apoptotic cell lines in 1992, from where it got its name (Programed-death 1) (Ishida et al., 1992). Murine models uncovered its essential immune halting role, as its deletion led to overt immune activation, namely splenomegaly, B cell proliferation and lupus-like arthritis (Nishimura et al., 1999). In 2003, the first evidence emerged that PD-1 mediated suppression of antiviral response using an adenovirus (Iwai et al., 2003). Only three years later, it was demonstrated that PD-1 expression increased in chronic viral infections, in both the murine LCMV Clone 13 model (Barber *et al.*, 2006) and in human infections like HIV (Day et al., 2006; Trautmann et al., 2006) and HCV (Radziewicz et al., 2007; Urbani et al., 2006). Importantly, all three HIV-related studies showed that blockade of the PD-1 pathway *in vitro* can partially rescue HIV-specific T cell function, and a similar observation was made *in vivo* in the murine model (Barber *et al.*, 2006). These discoveries were seminal in shaping how we now understand PD-1's role in actively inhibiting antiviral responses. These studies developed alongside cancer-focused work, and led to a novel therapeutic concept: immune checkpoint blockade.

PD-1 is a monomeric surface glycoprotein encoded by *PCDC1* gene. In addition to its extracellular and transmembrane portions, PD-1 has an immunoreceptor tyrosine-based inhibitory motif (ITIM) and an immunoreceptor tyrosine-based switch motif (ITSM) on its intracellular motif (Boussiotis et al., 2014). Upon formation of the immunological synapse following MHC-peptide-TCR interaction, it is recruited close to the TCR in a bulls-eye formation (TCR in centre, circled by CD28-ICOS mix, then by PD-1)(Hui et al., 2017). Upon binding to its ligands PD-L1 or PD-L2, SHP1/2 is recruited to the ITSM (Okazaki et al., 2001). Activated SHP-2 is then recruited to the proximally-close intracellular tail of

CD28 and ablates its costimulatory signalling (Hui et al., 2017). This mechanism effectively increases the threshold that TCR signalling must reach to produce an effector function (Andersson et al., 2020), contributing to an overall decrease of effector function, also recently shown *in vivo* (Sandu et al., 2020). PD-1 signalling also induces the expression of inhibitory genes, such as BATF, a negative regulator of AP-1, affecting cytokine production (Quigley et al., 2010). PD-1 signalling promotes lipolysis and fatty acid oxidation over effector-function-preferred glycolysis (Patsoukis et al., 2015). Finally, simultaneous engagement of TCR and PD-1 by naïve CD4+ T cells result in induced Tregs (Francisco et al., 2009), or a regulatory phenotype if on memory CD4+ T cells (Fanelli et al., 2021).

PD-1 expression can be induced on T cells, NK cells, B cells, macrophages and some DC subsets, while the ligands, PD-L1 and PD-L2, are constitutively expressed on DC, macrophages, B cells and mesenchymal stem cells, and induced on DC and macrophages. On T cells, PD-1 is induced following TCR signalling (as early as 24 hours after activation, through calcineurin-activated NFATc1 binding to PD-1's promoter region and by some cytokines, namely IL-6, IL-12 (through STAT binding sites in the promoter region) IL-2, and type I IFNs (through IFN-stimulated response element, concurrent with TCR stimulation) (Cho et al., 2008). PD-1's expression is transient in acute infections, down regulated concomitantly with antigen clearance following the end of TCR signalling and the repressive function of CD8+ memory differentiators T-bet (Kao et al., 2011) and Blimp-1 (Kallies et al., 2009; Bally et al., 2016). Conversely, PD-1's expression is maintained at high levels in the context of ongoing antigen exposure, as is the case with chronic viral infections and cancer. This high expression can be maintained by FoxO1, a

T-bet antagonizer found at high levels in the nucleus during LCMV Cl 13 infections (Staron et al., 2014). High PD-1 expression in LCMV-specific exhausted T cells is maintained even after transfer into naïve hosts (Utzschneider et al., 2013), as well as on HIV-specific T cells after ART-suppression of viral load (Niessl et al., 2020b). This reflects the stable epigenetic profile which is established in exhausted T cells, characterized by the unmethylated DNA in sites of PCDC1 regulatory regions (Youngblood et al., 2011). This demethylation likely follows an activating mechanism, and can be influenced by the cytokine profile (Austin et al., 2014; Bally *et al.*, 2016).

Immune checkpoints blockade

Much of what we know of the *in vivo* effect of blocking the PD-1 pathway comes, of course, from animal models.

Similar to viral infections, cancers must employ immune evasion strategies to avoid detection and continue to develop. A number of these mechanisms utilize immune checkpoints, for example by creating a microenvironment which favours Treg development (Li et al., 2020) or overexpressing their ligands, as is the case for PD-L1/2 (Pauken et al., 2016; Iwai et al., 2002). Immune checkpoint blockade (ICB) has been approved for cancer treatment, where it has been revolutionary. FDA has approved a total of seven monoclonal antibodies which antagonize IC for use against various types of cancer, targeting the CTLA-4 (one) or PD-1 pathway (three targeting PD-1, and three targeting PD-L1).

CTLA-4 blockade in cancer

Although not the focus of this thesis, it is interesting to observe the differences between CTLA-4 *versus* PD-1-targeted ICB, as it helps elucidate their respective mechanisms. CTLA-4 is strongly induced by antigen activation and, through its structural similarity to CD28competes for binding with CD28's ligands CD80 and CD86 (Linsley et al., 1994; Pentcheva-Hoang et al., 2004). As it has a greater affinity for the ligands, this competition disrupts T cell activation of the cell expressing CTLA-4. Through the absence of CD28 signalling and a CTLA-4-mediated reduction in effector-related transcription factors, CTLA-4 promotes anergy (Greenwald et al., 2001). CTLA-4 also hampers the activation of neighbouring cells, as CTLA-4-CD80/CD86 interaction results in the internalization of the latter ligands on the APCs expressing them (Greenwald et al., 2001; Krummel and Allison, 1995; Qureshi et al., 2011). Finally, CTLA-4 is constitutively expressed on Tregs, and is necessary for the release of anti-inflammatory cytokines (Senejani et al., 2012) as well as interfere with CD80/CD86 expression on APCs (Hou et al., 2015; Qureshi et al., 2011).

A monoclonal IgG1k antibody antagonizing CTLA-4 was the first ICB to be FDA approved in 2011 (Hodi et al., 2003), and has resulted in greater survival in difference types of melanoma (Schadendorf et al., 2015). Although the exact mechanisms by which CTLA-4 ICB operate are not fully understood, it is T cell mediated, as ICB in T cell-depleted animals has no tumoricidal effect (Baksh and Weber, 2015). Interfering with the CTLA-4 pathway also results in greater T cell responses against neoantigens (antigens not normally found in host tissue, but which form following mutations) (Snyder et al., 2014; van Rooij et al., 2013). An additional way the IgG1k monoclonal antibody is thought to

work is by inducing antibody-dependent cellular cytotoxicity on the Tregs it binds to (Sharma et al., 2019), although this has not yet been proven in humans. In summary, CTLA-4 blocking antibody tilts the effector/Treg ratio in the tumour microenvironment, which allows for recognition and killing of the tumour cells.

CTLA-4 is thought to act primarily in lymphoid organs, while PD-1 tends to act locally in peripheral tissues (Fife and Bluestone, 2008). CLTA-4 also acts earlier in the course of T cell activation than PD-1. Both these traits are reflected by the respective comorbidities seen in knock-out mice models: knocking out CTLA-4 results in a T cell-mediated lymphoproliferative autoimmune disease (Waterhouse et al., 1995), while knocking out PD-1 results in heterogeneous and later autoimmune phenotypes. This was further enforced by the observation that T cells responding to CTLA-4 blockade were not the same as those responding to PD-1 blockade in a mouse tumour model (Wei et al., 2017). PD-1 blockade has demonstrated broader clinical utility (Waldman et al., 2020) and has outcompeted CTLA-4 blockade in a head-to-head study (Robert et al., 2015; Schachter et al., 2017), which led to its approval by the FDA in 2011. PD-1 blockade also demonstrates less toxicity than CTLA-4 blockade (Michot et al., 2016), although they are generally better tolerated than toxicities associated with traditional chemotherapeutics (Hargadon et al., 2018; Nishijima et al., 2017).

PD-1 blockade in cancer

As mentioned previously, tumours can over express PD-1's ligand, thus inhibiting the function of responding T cells (Blank et al., 2004). In addition, established tumours can induce a dysfunctional state very similar to T cell exhaustion, also by the fact that tumour-specific T cells are stimulated repeatedly.

It was quickly apparent that response to PD-1 blockade varied between patients, even within a cohort of patients afflicted by the same cancer. Thus, researchers sought to explore biomarkers associated with responsiveness to ICB. Markers associated with greater response have been expression of PD-L1 on target tumour (Garon et al., 2015) as well as PD-1-expressing T cells in or close to the tumour prior to treatment initiation (Tumeh et al., 2014), higher mutational burden (Goodman et al., 2017), IFNg-related mRNA profile within the tumour (Ayers et al., 2017), preferential expansion of high avidity T cells recognizing neoantigens following ICB (Simon et al., 2017), proliferation of PD-1+ CD8+ T cells following ICB (Kamphorst et al., 2017a), etc. Even the microbiome was found to impact responsiveness to blockade (Routy et al., 2018). However, contradictory reports on most of these biomarkers are frequent, so that predicticting which patients will benefit from ICB difficult (Ding and Chen, 2019; Prasad et al., 2018).

In CD8+ T cells, response to PD-1 blockade is dependent on CD28 co-expression, as PD-1-SHP-2 complex will directly dephosphorylate CD28 and, only at very high PD-L1 levels, components of the TCR signalling cascade (Hui et al., 2017). Dependence on CD28 was further shown indirectly in patients with lung cancer (proliferating CD8+ T cells after PD-1 blockade were CD28+) (Kamphorst et al., 2017b) and directly with the LCMV clone 13 model (Im et al., 2016; Kamphorst et al., 2017b).

PD-1 blockade in chronic viral infection

Most research surrounding the effect of immune checkpoint blockade on CD4+ T cells in the context of HIV has focused on its potential as a latency reversing agent (LRA). Latent reservoir is enriched in IC-expressing cells, namely LAG-3, TIGIT, and PD-1 (Fromentin et al., 2016). As T cell activation reverses latency, and PD-1 blunts T cell activation, the

potential of PD-1 as an LRA was very clear. A recent study saw that PD-1 engagement inhibited HIV viral transcription, preventing TCR-induced viral reactivation *ex vivo* from primary cells of ART-treated infected individuals (Fromentin et al., 2019). The same study further showed that inhibiting PD-1's signalling, through the addition of a PD-1 blocking antibody, increased viral reactivation in the presence of another LRA or TCR stimulation (Fromentin et al., 2019). *In vivo,* administration of ICB in PLWH treated in the context of cancer often resulted in viral reactivation (meaning spikes in viral load despite continuous ART), but no consistent decrease in the sizes of the reservoirs (Guihot et al., 2018; Scully et al., 2018). It is possible that a decrease in reservoir may be observed in tissues, as was observed following in the lymph nodes of SIV-infected RM following CTLA-4 blockade (Hryniewicz et al., 2006).

ICB also affected the function of virus-specific cells in chronic viral infections, both *in vitro* and *in vivo*. The first demonstration was in the mouse LCMV clone 13 model, showing that PD-L1 blockade can enhance the exhausted virus-specific CD8 T cell response (in terms of proliferation; TNFa and IFNg secretion), leading to decreased viral titers *in vivo* (Barber et al., 2006). This model has allowed to study multiple facets of ICB in viral infections. Mechanistically, responsiveness to PD-1 blockade has been shown to be dependent of CD28 co-expression *in vivo*, by knocking out CD28 in LCMV-specific CD8+ T cells (Kamphorst et al., 2017b). Responsiveness of exhausted virus-specific CD8+ T cells was most pronounced when CD4+ T cells were present, at least in part due to IL-2 production by these latter cells (West et al., 2013; Aubert et al., 2011).

One year after the Barber study, increased function in HIV-specific CD8+ T cells following PD-1 blockade was described *in vitro* (Day et al., 2006). As seen in cancer, increased

functionality upon blockade was primarily observed in HIV-specific CD8+ T cells with intermediate amounts of PD-1. Among HIV-specific CD4+ T cells, increases in function upon blockade were noted among populations of different PD-1 levels (Porichis et al., 2011). *In vitro,* Porichis et al. thus demonstrate that the benefit of aPD-L1 on an increased transcription of IL-2 and IFNg in HIV-specific CD4+ T cells peak at 12 and 24hrs, respectively (Porichis et al., 2011). Protein levels (in supernatants of peptide-stimulated cell cultures) at 48hrs showed a median 2,9 and 2,2-fold median increase of IFNg and IL-2 secretion respectively, with the blockade. Interestingly, they also show that IFNg secretion from proliferating antigen-specific cells only bear weight after 96hrs. As such, PD-L1 has an effect on IFNg and IL-2 secretion on both proliferating and non-proliferating cells. Finally, functions beyond the classically antiviral associated cytokines, namely IL-21 (Porichis et al., 2011) were also observed as increased following blockade, indicating that a multitude of CD4+ T cell functions could be affected by ICB.

In vivo, administration of PD-1 blockade in PLWH resulted in an increase in HIV-specific CD8+ T cells in blood in two of six participants, and showed not toxicity (Gay et al., 2017). In untreated SIV-infected RM, administration of a PD-1-antagonising antibody resulted in expansion and improved functionality of virus-specific CD8+ T cells (Velu et al., 2009). These monkeys also demonstrated longer survival, a reduction in viral load (Velu et al., 2009), reduced interferon signalling and improved gut integrity (Dyavar Shetty et al., 2012). This was not seen in ART-treated macaques (Mylvaganam et al., 2018). While none of these studies looked at the function of SIV-specific CD4+ T cells in response to ICB, they did observe replenished TH17 in gut tissue of viremic RM.

Given the functional heterogeneity of CD4+ T cells, understanding how they respond to

ICB has been lagging behind CD8+ T cells. However, many of the aforementioned evidences suggested they too could be affected. An elegant paper has sought to assess which CD4+ subsets responded to PD-L1 blockade. They transferred transgenic LCMV-specific CD4+ T cells into naive hosts, infected them with LCMV clone 13, administered PD-L1 blocking antibody, and then retrieved them for single RNA Seq and CyTOF (Snell et al., 2021). ICB favoured a terminally-differentiated profile which expressed TH1-associated proteins, rather than the TCF-1+ population, with high Bcl6 and CXCR5 expression (i.e. TFH). ICB also resulted in increased CTL signatures, with accompanying high killing capacity from these cells. Importantly, this report highlighted differential response to ICB based on the polarization of the CD4+ T cells in mice.

In summary, the HIV infection creates a chronic infection that decimates the CD4+ T cell population, resulting in immunodeficiency with associated persisting inflammation. The chronic nature of the viral infection causes dysfunction of the HIV-specific T cell response, which could otherwise control the viral infection. Even if CD4+ T cell depletion is halted by ART, other aspects of the infection remain: disrupted gut integrity, with the resulting inflammation increasing the risks of morbidity and mortality ; dysfunctional T cell response ; lingering reservoirs, as a consequence dependence on life-long antiretrovirals. Strategies which can boost the anti-viral immune response and/or resolve the chronic inflammation are still critically lacking in HIV research. One such strategy is the immune checkpoint blockade, with promising results in animal models, yet for which multiple questions still surround how immune checkpoint blockade affects virus-specific CD4+ T cells in humans. In our lab, we specifically sought to understand how immune checkpoint blockade may affect their different polarisations in humans.

Throughout this introduction, we have seen how a physiological immune response functions. We have also overviewed two viral infections which, through differing mechanisms, can result in catastrophic immunopathology, sometimes leading to death. However, a reccuring theme is heterogeneity : why are only a minority of SARS-CoV-2 infections fatal ? Why are some individuals able to control the HIV infection in the absence of treatment ? What do these differences mean for immunomodulating therapies ? In this thesis, I study inter-individual differences in immune responses to SARS-CoV-2 and to HIV, and what they mean for outcome, and for therapeutic interventions.

Chapter 2 – Hypotheses and objectives

The immunopathology of both pandemic-causing viruses involve the immune system. The immune response, and consequently the immunopathology, can be extremely heterogeneous, mirroring the diversity of the people infected. My overarching hypothesis for this thesis was that *the perturbations on the immune response can explain the heterogeneity of infected peoples' response to viral infection.*

Despite advances in COVID-19 management, there is no consensus on easily measurable early metrics to recognize patients at high risk of evolving towards death. The explosive increase in correlates of COVID-19 severity further complicates biomarker prioritization. Furthermore, while treatment of COVID-19 has markedly improved thanks to vaccination and therapeutic options, there is still a need to know which type of patient would benefit from which type of treatment. Our two first studies consider infection by SARS-CoV-2. **We hypothesized that** 1) metrics of a dysfunctional immune response can be used to predict whom, among acute COVID-19 patients, would succumb to their disease, and 2) can be used to describe the diversity in immunopathology.

Our first objective was to find the best feature, or combination of, captured early in blood and analyzable using clinically-applicable tools, to predict fatal outcome within 2 months of disease onset among hospitalized COVID-19+ patients. The aims were to i) characterize, within our cohort of moderate-to-critical patients, the prevalence and quantities of variables associated with high-fatality – specifically, SARS-CoV-2 viral RNA, inflammation-associated cytokines ; ii) measure their association to fatal outcome among all hospitalized COVID-19 patients or critical patients only ; iii) combine variables

associated to fatal outcome within a single multivariable model, with the goal of achieving the greatest sensitivity and specificity possible ; iv) validate the robustness of our model in 2 independent additional cohorts.

Our second objective was to understand the heterogeneity in the progression of COVID-19, and how it associated to different outcomes. The aims were to i) use data dimensionality methods to identify subsets of homogeneous immune responses ; ii) study the association of outcome with those immune responses, iii) study the differences in the kinetics of the immune responses, and iv) compare the transcriptomic profiles among these subsets to understand the molecular mechanisms driving these different responses.

While keeping with the theme of diversity in response to viral infection, our third study is on HIV infection. CD4+ T helper (TH) cells play a central role in orchestrating the immune response. In chronic diseases such as HIV, sustained antigenic exposure and the inflammatory milieu leads to dysfunction of both CD4+ and CD8+ T cells. Immune checkpoint blockade (ICB) can partially reverse CD8+ T cell dysfunction, and has been pursued to restore the HIV-specific response. CD8+ T responses to ICB require TH. However, TH function varies depending on their lineage, and how ICB affects these different lineages remains unknown. **We hypothesized that** 1) dysfunctional CD4+ T cells would have different sensitivities to blockade of the PD-1 signalling pathway, and ii) these differences stem from the characteristics of the patient, as well as those of the lineages of HIV-specific CD4+ T cells.

For the third project, our objective was to measure which functions of HIV-specific CD4+

T cells from viremic individuals are increased following PD-L1 blockade. The aims were to i) compare the functional profile of dysfunctional HIV-specific CD4+ T cells from viremic patients to the relatively-functional counterparts from spontaneous controllers ; ii) characterize their phenotype, in terms of IC and exhaustion-related TF expression, across multiple lineages of CD4+ T cells ; iii) measure each lineage's response to PD-L1 blockade by measuring the increase of cytokine production in HIV-specific CD4+ T cells following PD-L1 blockade.

Chapter 3 – MANUSCRIPT 1 : Integrated immunovirological profiling validated plasma SARS-CoV-2 RNA as an early predictor of COVID-19 mortality

Status: This research article was published in Science Advances on November 26th, 2021.

Authors contributions:

Conceptualization : EBR, DEK, NC, AF

Data Curation : EBR, NB, CO, MMP, CL, DEK, RMR, GBL, DM, TN, SZ

Formal analysis : EBR, SPA, PG, GMB, AD, GBB, AP, RG, JR, DEK

Funding acquisition : DEK, AF, NC, NA, AP, CL, JBR, MT, MD

Investigation/experiments : SPA, PG, EBR, GBB, AP, MB, FP, RG, AL, JR, JP, GG, JN, MN, GS, HM, CB, JDD, MB, GGL

Biostatistical methodology : AD, GMB

Patient recruitment and cohort administration : NB, DM, MMP, LL, AP, MD, JBR, MC, DEK

Visualization: EBR, GMB, AD

Supervision : MC, MT, NC, AF, DEK

Writing – original draft : EBR, DEK

Writing – review and editing : all authors

Title : Integrated immunovirological profiling validates plasma SARS-CoV-2 RNA as an early predictor of COVID-19 mortality

Short title : Plasma SARS-CoV-2 RNA predicts COVID-19 mortality

Authors : Elsa Brunet-Ratnasingham1,2†, Sai Priya Anand1,3†, Pierre Gantner1,2†, Alina Dyachenko1†, Gaël Moquin-Beaudry1,10, Nathalie Brassard1, Guillaume Beaudoin-Bussières1,2, Amélie Pagliuzza1, Romain Gasser1, Mehdi Benlarbi1, Floriane Point1, Jérémie Prévost1,2, Annemarie Laumaea1, Julia Niessl1,2,, Manon Nayrac1, Gérémy Sannier1,2, Catherine Orban1,4, Marc Messier-Peet1,4, Guillaume Butler-Laporte5,6, David R. Morrison5, Sirui Zhou5,6, Tomoko Nakanishi5,7,8,9, Marianne Boutin1,2, Jade Descôteux-Dinelle1,2, Gabrielle Gendron-Lepage1, Guillaume Goyette1, Catherine Bourassa1, Halima Medjahed1, Laetitia Laurent5, Rose-Marie Rébillard1,10, Jonathan Richard1, Mathieu Dubé1, Rémi Fromentin1, Nathalie Arbour1,10, Alexandre Prat1,10, Catherine Larochelle1,10, Madeleine Durand1,4, J. Brent Richards5,6,7,11, Michaël Chassé1,4, Martine Tétreault1,10, Nicolas Chomont1,2*, Andrés Finzi1,2* and Daniel E. Kaufmann1,2,4,12*

Affiliations :

1Research Centre of the Centre Hospitalier de l'Université de Montréal (CRCHUM), Montréal, QC, Canada.
2Département de Microbiologie, Infectiologie et Immunologie, Université de Montréal, Montréal, QC, Canada.

3Department of Microbiology and Immunology, McGill University, Montréal, Quebec, Canada
4Centre hospitalier de l'Université de Montréal (CHUM), Montréal, QC, Canada
5Lady Davis Institute, Jewish General Hospital, McGill University, Montreal, QC, Canada
6Department of Epidemiology, Biostatistics and Occupational Health, McGill University, Montreal, QC, Canada
7Department of Human Genetics, McGill University, Montreal, QC, Canada
8Kyoto-McGill International Collaborative School in Genomic Medicine, Gaduate School of Medicine, Kyoto University, Kyoto, Japan
9Research Fellow, Japan Society for the Promotion of Science.
10Department of Neuroscience, Université de Montréal, Montréal, QC, Canada
11Department of Twin Research, King's College London, London, UK
12Center for HIV/AIDS Vaccine Immunology and Immunogen Discovery, La Jolla, CA, USA.

†Contributed equally

*Co-corresponding authors. Email : Nicolas Chomont nicolas.chomont@umontreal.ca; Andrés Finzi andres.finzi@umontreal.ca; Daniel E Kaufmann daniel.kaufmann@umontreal.ca

Abstract

Despite advances in COVID-19 management, identifying patients evolving towards death remains challenging. To identify early predictors of mortality within 60 days of symptom onset, we performed immunovirological assessments (SARS-CoV-2 viral RNA, 26 cytokines and tissue injury markers, 6 anti-SARS-CoV-2 antibody responses) on plasma from 279 individuals. On samples collected 11 days after symptom onset in a discovery cohort, high SARS-CoV-2 vRNA, low RBD-specific IgG, low SARS-CoV-2-specific antibody-dependent cellular cytotoxicity, and elevated cytokines and injury markers were strongly associated with mortality, including in patients on mechanical ventilation. Model selection revealed that a three-variable model of vRNA, with predefined adjustment by age and sex, robustly identified patients with fatal outcome (AUC=0.87, adjusted HR for log-transformed vRNA=3.5; 95% CI: 2.0-6.2). This model remained robust in independent validation and confirmation cohorts. Plasma vRNA's predictive accuracy was maintained at earlier timepoints. Plasma SARS-CoV-2 RNA quantitation can help understand disease heterogeneity and identify patients who may benefit from new therapies.

One Sentence Summary (teaser): Statistical models of plasma immunovirological features validate SARS-CoV-2 vRNA as an early predictor of COVID-19 mortality.

Context of research

High amounts of cytokines, tissue damage markers and SARS-CoV-2 viral RNA, as well as low antibody responses against SARS-CoV-2 have all been found as significantly associated to fatal outcome. However, no study has compared these various and often highly correlated biomarkers.

Using multivariate statistical models, we compared, within the same patients and same sampling modalities, the predictive values of these biomarkers. While able to reproduce the predictive values of many of the biomarkers, we found that plasma viral RNA was a superior predictor, which we then validated in two independent cohorts, either from a separate hospital or from a diffence wave of infection. Finally, we found that plasma viral RNA remained a robust predictor when measured at multiple early timepoints.

Taken together, these results highlight SARS-CoV-2 viral RNA measured in plasma as a superior predictor of fatality among patients hospitalized for COVID-19. This biomarker to may be integrated into clinical practice to delineate high-risk patients, or for stratification purposes in clinical trials.

Introduction

Since the beginning of the pandemic, intense efforts have been deployed to define correlates of disease severity and to develop therapies targeting the virus or the pathogenesis of COVID-19. However, to date, only dexamethasone (1-3) and IL-6 blockers (tocilizumab (4), sarilumab (5)) have convincingly shown to provide a survival benefit in randomized controlled trials. While other immune interventions may benefit some subgroups (6), there is currently no consensus on how to predict which critical cases are likely to resolve their infection and which are at a greater risk of fatality, in part due to the high heterogeneity of patients and the very dynamic changes in biological features (2).

Recent reports have identified features linked to severe COVID-19. One is high amounts of viral RNA (vRNA) in plasma, which has been associated with greater severity and worst outcome for other respiratory pathogens, such as SARS-CoV-1 (7, 8), RSV (9), MERS (10), and pandemic-causing strain of influenza A H5N1 (11). Plasma SARS-CoV-2 vRNA has also been linked with increased risk of severe COVID-19 and mortality (12-17).

Dysregulated immune responses are at least in part responsible for the exacerbated pathogenesis occurring in a minority of individuals with SARS-CoV-2 infection. Elevated cytokine levels were among the first reported markers associated to severe COVID-19 disease (17), although inconsistent sampling times sometimes led to weak associations with mortality (18). Narrowing the window of sampling early after symptom clarifies plasma cytokine patterns (19), reminiscent of the Cytokine Release Syndrome (20). Plasma profile around 10 days after symptom onset was highly differential for plasma cytokine profiles of critical versus moderate COVID-19 disease (20) and a

number of cytokines have been associated with increased mortality (21).

Multiple studies support a central role for antibody responses in protective anti-SARS-CoV-2 immunity. The main viral target of antibody immunity is the trimeric Spike glycoprotein, which facilitates SAR-CoV-2 entry into host cells via interaction of its receptor-binding domain (RBD) with angiotensin-converting enzyme-2 (ACE-2) (22, 23). While most infected patients develop anti-Spike and anti-RBD antibodies (24, 25), delayed anti-S IgG antibodies and decreased Fc-effector capacity are associated with increased mortality(26). These reports highlight the complexity of the host's immune response to SARS-CoV-2.

Despite the remarkable speed with which effective SARS-CoV-2 vaccines have been developed and deployed, partial population coverage and, potentially, emergence of resistant variants will lead to ongoing occurrence of infections. From a clinical perspective, it is therefore essential to identify a minimal set of early blood parameters that can be easily and rapidly measured to identify patients at high risk of mortality, while prioritizing parameters that may hint at specific categories of therapeutic interventions. However, the list of blood correlates of COVID-19 severity has tremendously expanded, making such prioritizing a major challenge. Given strong co-upregulation between a number of plasma analytes (for example plasma cytokines and chemokines (20)), there is a need for streamlined analytical models with few virological and/or immunological parameters that provide complementary, rather than redundant, information to better stratify individual patient risk.

In this study, we simultaneously examined multiple parameters in plasma spanning three key aspects of COVID-19 pathogenesis early in disease course (11 ± 4 days post

symptom onset, henceforth described as DSO11): SARS-CoV-2 vRNA, 26 cytokines and tissue injury markers, and 6 measures of SARS-CoV-2-specific antibody responses. We performed uni- and multivariable analysis to identify independent predictors of death. A minimal model combining vRNA, age and sex was particularly robust, and very reproducible in two additional cohorts, and remained predictive even when the samples were collected earlier in disease course.

Results

Study design and patient characteristics

We investigated prospectively enrolled hospitalized COVID-19 individuals (n=279) with symptomatic infection, a positive SARS-CoV-2 nasopharyngeal swab PCR and sampled longitudinally after enrollment. To allow for cross-sectional analysis of early plasma markers, we investigated patients for whom research blood samples were available at 11 (± 4) days after symptom onset (DSO11) (n=217). Our study population was split into a discovery cohort (n=61) in a first hospital, a fully independent validation cohort (n=87) in a second hospital (both of which were infected during the first wave), and a third confirmation cohort (n=69) also collected in the first hospital, but mostly during the second and third waves (see Study Design, Figure S1A). Based on disease severity at DSO11, patients were grouped as critical (requiring mechanical ventilation) versus non-critical (see participant characteristics, Table 1). The discovery cohort included 29 critical and 32 non-critical patients. Plasma profiles were compared to 50 asymptomatic uninfected donors as a control group (uninfected controls – UC) of non-diseased state.

We clinically followed participants for at least 60 days after symptom onset (DSO60). The primary outcome, death by DSO60, occurred in 13 patients, with close to half fatalities occurring between DSO30 and DSO60 (Figure S1B) and mostly in the critical group (Figure S1C).

We performed a slightly reduced immunovirological assessment in the validation cohort, where 19 cases were critical, and 12 deaths occurred before DSO60, and a focused assessment of the confirmation cohort (with 27 critical cases and 11 fatalities)

(Table 1). Because of hospital referral coordination, the validation cohort was of older age than the discovery one, but with less severe respiratory compromise (Table 1). Other basic demographics and prevalent risk factors were consistent with published studies (27) and overall showed minor differences between all cohorts. These features did not statistically significantly differ between the critical vs non-critical groups except for higher rates of admission to ICU and intubation, and duration of hospital stay in critical patients (Table 1), in line with group definition. Finally, for sensitivity longitudinal measurements of the selected statisticial models through different DSO points, we complemented these three cohorts with 62 patients who were sampled very early in disease course (before the DSO11± 4 days time bracket).

Plasma viral load in early disease is strongly associated with COVID-19 mortality

As SARS-CoV-2 vRNA in plasma has been previously linked to mortality, we quantified it in the discovery cohort. We designed an ultrasensitive quantitative real time PCR (qRT-PCR) targeting the N sequence of its genome with a detection limit of 13 copies/mL. The assay was highly specific, with no vRNA detected in UC (Figure 1A). At DSO11, we detected plasma SARS-CoV-2 vRNA in a significantly greater fraction of critical than non-critical patients (Figure 1A). These results suggest that systemic SARS-CoV-2 viremia is a signature of infection severity and/or itself plays a role in disease complications.

We next hypothesized that the amount of viral products, rather than their mere presence, was associated with severe pathogenesis. SARS-CoV2 vRNA levels were higher in critical than non-critical cases (Figure 1B). This difference held when comparing

samples with detectable levels only (p=0.002 - Mann-Whitney test). Most patients who died had high vRNA compared to survivors (Figure 1C), even when the analysis was restricted to critical cases (Figure 1D). In univariate Cox regression analysis (Table 2) we found that an increase of 1 unit of log-transformed plasma vRNA led to a 3-fold increase in mortality risk [Hazard Ratio (HR)= 3.1 (95% Confidence Interval CI: 1.9-5.1), $p < 0.0001$ for all COVID-19 (Figure 1E), and 2.5 (95% CI: 1.4 – 4.7, p=0.004) for critical (Table 2)]. The estimated survival proportions for undetectable (<13 copies/ml), low, or high plasma vRNA were extracted from Cox models (see methods for details) (28). High plasma vRNA was associated with a greater risk of death, whereas there was substantial overlap between the subgroups with low or undetectable plasma vRNA (Figure 1F). A similar trend was observed in the critical group (Figure 1G). Therefore, plasma SARS-CoV-2 vRNA load is not only a correlate of contemporaneous respiratory compromise early in disease course, but is also associated with mortality, including in the critical group.

Markers of immune hyperactivation and tissue damage discriminate disease trajectories

As early elevation of a number of cytokines and chemokines was also associated with adverse COVID-19 outcome (19, 20, 29), we used multiplexed beads arrays to determine plasma levels of 26 proteins associated with adaptive and/or innate immune responses, chemotaxis, or tissue insult related to severe acute respiratory distress syndrome (ARDS, See Table S1 for analyte list). Principal component analysis revealed that the plasma profile largely delineates UC from COVID-19 patients, and highlighted higher cytokine levels and greater heterogeneity in the critical group compared to the non-

critical group (Figure 2A). The outlier critical case at the upper left corner of the PCA was on extracorporeal membrane oxygenation (ECMO) at the time of sampling, a procedure known to affect plasma profile(30). Unsupervised hierarchical clustering solely based on the 26 measured plasma proteins parsed apart 3 patient clusters: I) mostly critical; II) mixed; III) mostly non-critical cases (Figure 2B).

We next compared the levels of each analyte between groups (Figure S2A-D). Several followed a stepwise increase, where non-critical cases had greater cytokine concentrations than UC, and critical cases had the greatest amounts (Figure S2A). These included pro-inflammatory cytokines and chemokines IL-6, GM-CSF, TNF□, CCL2, and CXCL8. Some of the markers of tissue insult (RAGE, Angiopoietin-2)(31) also increased with disease severity, likely reflecting the extent of lung and vascular damage. CXCL9, CD40L, IFN□ and surfactant pulmonary protein D (SP-D) were significantly greater only in the critical cases of COVID-19 compared to UC (Figure S2B), while a few markers did not differ between all three groups (Figure S2C). Some analytes were significantly elevated in COVID-19 groups but did not differ between the critical and non-critical groups, such as CXCL10 (IP10), CXCL13, and D-dimer (Figure S2D). Taken together, the plasma profile reveals overall higher quantities of cytokines in the plasma of COVID-19 patients compared to UC, and select analytes are specifically associated with greater disease severity.

We reasoned these 26 analytes may be differentially linked to the amount of vRNA in plasma. We examined the correlations between individual plasma analytes (Figure S2E), as well as their association with vRNA (Figure 2C). Many analytes were co-upregulated, and several of them also positively correlated with vRNA levels. These latter

correlations were particularly robust for cytokines implicated in innate immune responses such as IL-6 (Figure S2F) and GM-CSF, the marker of lung damage RAGE (Figure S2G), and inflammatory chemokines CXCL8, CXCL10, and CCL2, suggesting a shared trigger or overlap in pathways.

To capture by a single parameter the overall magnitude of the difference in cytokine titers between COVID-19 patients and UC, we created a “CytoScore” from the linear combination of all 26 analytes (See methods for details). It followed a gradual difference, where the non-critical group had lower CytoScores than critical, and UC had the lowest scores (Figure 2D). The CytoScore correlated positively with vRNA (Figure 2E) and can have value in reducing dimensionality of plasma analyte profiling.

As patients who died within DSO60 showed a greater CytoScore than survivors (Figure 2F), even when restricted to critical cases (Figure 2G), we applied Cox regressing analyses to examine the association between the cytokines and mortality over time. We focused on analytes whose concentrations are in the range of robust quantitation by the assay (19/26, see methods for details). For each, we calculated the HR associated with a 1-unit increase of log-transformed concentration (Figure 2H). In addition to the CytoScore, several individual analytes were significantly associated with increased fatality risk, with Angiopoientin-2, RAGE and CXCL13 showing the highest significance ($p < 0.001$). Furthermore, patients with high CytoScore at DSO11 showed a significantly lower rate of predicted survival at DSO60 than the low CytoScore population, both in the entire cohort (Figure 2I) and in the critical group (Figure 2J). Therefore, overall cytokine levels as well as individual cytokines and markers of tissue damage measured at DSO11 are 1) in majority correlated with plasma vRNA and 2) associated with increased risk of mortality

among COVID-19 patients.

Low SARS-CoV-2-specific IgG and limited ADCC associated with COVID-19 mortality

As SARS-CoV-2 antibody responses likely play a critical role in protective immunity against SARS-CoV-2 (26, 32), we measured plasma SARS-CoV-2-specific antibody responses at DSO11. ELISA-based quantification using the SARS-CoV-2 RBD protein and isotype-specific secondary antibodies (24, 33) revealed a broad range in relative quantities of RBD-specific IgM, IgA or IgG in the non-critical and critical groups at DSO11. They did not differ between groups, and were not detected in UC (Figure 3A). These observations were corroborated by a flow cytometry-based assay measuring plasma binding to full-length Spike protein (Spike Ig) on cell surface (Figure 3B), which similarly showed no significant difference between the two COVID-19 groups.

We next assessed the SARS-CoV-2 Spike-specific antibody response for two key antiviral functions: neutralization (Figure 3C) and antibody-dependent cellular cytotoxicity (ADCC, Figure 3D). Here again, the data showed high variability, and no significant differences between the critical and non-critical groups for both readouts. All serology measurements were interrelated (Figure 3E). In contrast, the serology measurements were inversely correlated with plasma vRNA and most cytokines (Figure 3F).

To assess potential consequences of defective antibody responses at this early time point, we compared SARS-CoV-2-specific antibody responses between survivors and non-survivors. For RBD-specific isotypes (Figure 3G), only IgG amounts were significantly increased in survivors, although there was a similar trend for IgA as well. Spike Ig levels were also higher in survivors (Figure 3H). We observed contrasting

patterns with regard to functional humoral responses: while neutralization capacity was similar for both outcomes (Figure 3I), ADCC capacity was superior in survivors (Figure 3J). HR reflected the same observations, where higher ADCC, RBD-specific IgG and Spike Ig were associated with increased survival (Figure 3K). We further modeled this by comparing the survival curves at DSO60 of patients with low or high RBD-specific IgG amounts (Figure 3L), Spike Ig (Figure 3M) or ADCC (Figure 3N) at DSO11, and saw that participants with low responses for these three measurements showed an increased fatality risk. These observations were maintained when the analysis was restricted to the critical group (Figure S3A-C). Taken together, these results highlight that impairment of some SARS-CoV-2-specific antibody responses may contribute to mortality.

Multivariate Cox reveal plasma vRNA as pivotally associated with COVID-19 mortality

As all categories of immunovirological parameters showed some perturbations that predicted fatality, we examined whether these alterations provided redundant information in terms of mortality risk, or if their combined analysis would improve associations with fatal outcome. Within immunovirological categories, we retained only variables significant in univariate Cox analysis ($p < 0.05$; see Table 2), and among those, a global multivariate model was used to select top variables (See methods for details). To evaluate predictive accuracy of the resulting variables in multivariate models, time-dependent receiver operator characteristic (ROC) curves were calculated at DSO60 (principles illustrated in Figure S4A). The area under the curve (AUC), a measure of prediction accuracy, was examined at all distinct event times by plotting the AUC curve over time (principles illustrated in Figure S5A, see methods for details). All final time-dependent Cox models

were reassessed in the validation cohort to validate the accuracy of our findings.

As large studies have shown associations of older age and male sex with severe COVID-19(34), we pre-defined adjustement by age and sex in the models. In the discovery cohort, time-dependent ROC for plasma vRNA showed a strong predictive capacity at DSO60 (AUC=0.84, 95%CI: 0.72-0.96), and a slight benefit when adjusting for age and sex (AUC=0.87, 95%CI:0.76-0.99 (Figure 4A). When applied to the validation cohort at DSO60, vRNA again had a good predictive capacity (AUC=0.75; 95%CI:0.59-0.92), and a benefit when adjusting for age and sex (AUC=0.85; 95%CI: 0.65-1.00) (Figure S4B). Therefore, vRNA is a strong predictor of fatality, and adjusting for age and sex improves its predictive power.

Next, we compared the time-dependent ROC curves for inflammatory and tissue damage markers of the discovery cohort (Figure 4C). Multivariate model selection retained only 1 analyte: Angiopoientin-2. To compare predictive accuracies at DSO60, we selected 3 additional analytes highly significant ($p < 0.001$) in univariate Cox (Figure 2G): CytoScore, CXCL13 and RAGE (Figure 4B). Although no individual inflammatory cytokine was selected, the CytoScore had a high AUC (0.83, 95%CI: 0.71-0.95). Of the two markers of tissue insult, only Angiopoietin-2 (AUC=0.86; 95%CI: 0.55-1.00) remained significant (RAGE: AUC=0.80; 95%CI: 0.33-1.00). The chemokine CXCL13 (AUC=0.82, 95%CI: 0.70-0.94) also had good predictive accuracy. All AUC values stayed quite stable over time (Figure S5D). In the validation cohort, only CXCL13's AUC remained high (AUC=0.84, 95%CI: 0.66-0.98) and significantly discriminatory of mortality ($p<0.05$) (Figures S4C) over time (Figure S5D). These observations confirm that certain markers of tissue insult and chemokine, as well as the overall cytokine levels, were associated with

mortality risk.

For antibody measurements, we observed, within the discovery cohort, overlap of the time-dependent ROC of all three measurements significant in univariate Cox (ADCC: AUC=0.74, 95%CI: 0.44-1.00; Spike Ig: AUC=0.71, 95%CI: 0.25-1.00; RBD-specific IgG: AUC=0.71, 95%CI:0.44-0.97) at DSO60 (Figure 4C). However, the predictive value of all 3 measurements began to drop around DSO30 (Figure S5E). We then applied the analysis to the validation cohort. As the cell-based ADCC assay requires significant infrastructure and technical expertise that may not be available in all clinical settings, we removed ADCC from the validation list of variables, and substituted it by the technically simple RBD-specific IgG, in line with their strong correlation (Figure 3C). The time-dependent ROC curves in the validation cohort for Spike Ig (AUC=0.60; 95%CI: 0.15-1.00) and RBD-specific IgG titers (AUC=0.59, 95%CI: 0.06-1.00) were non-significant, and lower than in the discovery cohort. RBD-specific IgG titers displayed best predictive accuracy of mortality at DSO30 when adjusted for age and sex (RBD-specific IgG: 0.81, 95%CI: 0.50-1.00) (Figure S5G, Table S2). Taken together, these data reveal that the anti-SARS-CoV-2 antibody response is highly associated with mortality within 30 days of symptom onset, but less so afterwards.

After examining each variable in the setting of their category, we sought to identify which single parameter, or combination thereof, is the most robust. All variables selected by multivariate model within each category were considered for a global multivariate model, and age and sex covariates were forced regardless of their significance. In the discovery cohort, the variables selected in the global multivariate model (at DSO60 : AUC=0.91, 95%CI: 0.60-1.00) were vRNA (HR = 2.47, 95%CI:1.30-4.68) and

Angiopoietin-2 (HR = 4.22, 95%CI: 0.66-26.78), alongside the forced variables age (HR = 1.06, 95%CI: 0.99-1.10) and sex (HR= 0.94, 95%CI: 0.24,3.70) (Figure 4D). Only vRNA (p=0.006) remained independently associated with a higher risk of all-cause mortality within DSO60 in the global multivariate model. Of note, this global multivariate model was only slightly better than the three-variable model of vRNA, age and sex at DSO60 (AUC: 0.87, 95%CI: 0.76-0.99) (Figure 4DE). In the validation cohort, the predictive accuracy of the model combining vRNA, Angiopoietin-2, age, and sex did not reach statistical significance (at DSO60 : AUC:0.86, 95%CI: 0.29-1.00) (Figures 4D). However, the exclusion of Angiopoietin-2 improved the model's discrimination in the validation cohort: the three-variable model combining vRNA, age and sex was then significant (AUC=0.85; 95%CI: 0.66-1.00). In both discovery and validations cohorts, the predictive accuracy of this model remained stable over time (Figures 4E,S5G, Table S2). We confirmed the predictive accuracy of plasma vRNA in a third cohort, and again saw a significant association of the three-variable model with fatality (AUC:0.90, 95%CI: 0.84-0.96) (Table S2, Figure 4D).

A number of clinical scores and lab measurements have been developed for risk stratification of acutely ill patients. We therefore compared the predictive capacity of plasma vRNA with that of other measures taken in the clinical setting, namely two metrics of organ failure: the quick sequential organ failure assessment score (qSOFA)(35) and the ratio of partial arterial oxygen pressure and fraction of inspired oxygen (P/F ratio)(36), as well as plasma concentrations of C reactive protein (CRP)(19). All three variables were significantly associated to fatality in univariate analysis and when corrected for age and sex, but inferior to plasma vRNA (Table S2, Figure S4FG). When combined in a

multivariate with this latter parameter, qSOFA, P/F and CRP were no longer significant (Table S2).

Finally, we assessed the predictive accuracy of plasma vRNA when measured outside of the DSO11 timeframe. We observed that as early as DSO5, plasma vRNA was already predictive of fatality, and remained so at least until DSO13 (Table S4, Figure 4F). This observation highlights the flexibility of using plasma vRNA for risk stratification, including at very early time points.

Taken together, these data indicate that, at DSO11, measuring plasma SARS-CoV-2 vRNA in hospitalised COVID-19 patients can be a powerful tool to predict mortality.

Discussion

In the perspective of clinical translation, it is essential to rigorously select among the multitude of markers linked to COVID-19-related mortality. In patients with a spectrum of disease severity, we studied perturbations within three categories of plasma molecules: circulating SARS-CoV-2 vRNA (14), immune and tissue injury markers (29) and SARS-CoV-2-specific antibody responses (26), all of which can be probed by quick and technically robust assays. Strong associations of early parameters with the primary outcome, fatality within 60 days of symptom onset, were observed, and largely maintained when the analyses were restricted to the critical group of patients on mechanical ventilation. Multivariate analyses demonstrated that, because of collinearity between several variables, a limited number of biological features was sufficient to build robust models predicting mortality. SARS-CoV-2 vRNA stood out as an early feature strongly associated with higher mortality risk. The predictive accuracy of plasma vRNA was superior to that observed with the clinical qSOFA and P/F ratio and the clinical CRP quantitation. Combined analysis of SARS-CoV-2 vRNA, Angiopoietin-2, age and sex had greatest predictive accuracy in a discovery cohort, although a simpler model with vRNA, age and sex was almost as robust. This three-parameter model maintained significant and very consistent predictive accuracy in a validation cohort and a confirmation cohort. Plasma vRNA remained predictive of fatality when sampled as early as DSO5 or late as DSO13, indicating that it is an accurate predictor of fatality throughout the typical time of COVID-19-associated hospitalization (DSO7) and ICU admission (DSO10) (17, 37).

The strength of the association between plasma vRNA levels and mortality risk was stronger than previously reported for nasopharyngeal swabs (NSW) (38). In contrast to

plasma, quantification of vRNA in NSW is hard to normalize, varies between types of tests, and depends on sample quality. Cox models showed a 3-fold increase of fatal outcome for every 1-unit increase in log-transformed plasma vRNA quantity. While this association is reminiscent of the remarkable predictive value of plasma viral load for disease progression in untreated HIV-1 infection (39), no study has thus far convincingly demonstrated that therapeutic reduction of SARS-CoV-2 viral loads decreased mortality risk. For example, the antiviral remdesivir reduced viral loads in NSW, duration of symptoms, and hospitalization, but had no significant impact on survival (40, 41). Similarly, although monoclonal anti-Spike antibodies can reduce viral load (42, 43), trials have not yet shown benefit in hospitalized patients. Given disease heterogeneity, it will be important to determine if such interventions specifically benefit the subgroup of patients with high plasma vRNA.

The source and precise nature of the plasma vRNA remains to be better determined. Viral nucleic acids in the plasma do not prove the presence of replication-competent viral particles, as they could be viral debris translocated from damaged lung tissue. This is supported by the correlation we saw between vRNA and RAGE : as RAGE mRNA was not expressed in the PBMCs of severe COVID-19 (29), plasma RAGE likely originates from damaged tissue (31). Besides the cytopathic effects of SARS-CoV-2 on lung epithelium, immunopathological mechanisms likely play key roles in severe COVID-19 pathogenesis (44). Systemic vRNA may trigger pathogen-recognition receptors such as TLRs, in line with strong co-upregulation of interferon-stimulated genes (ISGs) and other inflammatory pathways in vRNA-containing cells (45). This could contribute to the strong correlation observed between the amount of vRNA and IL-6, a pathogen-

associated molecular pattern (PAMP)-triggered inflammatory cytokine (46).

Consistent with previous studies (19, 20), we found significant associations between levels of several immune and tissue damage markers with both disease severity and mortality. Despite strongly significant HR for fatality risk for some analytes, the small sample size of our study resulted in sizeable overlaps between confidence intervals and variable rankings of HR values between the discovery and validation cohorts. An integrated CytoScore partially compensated for individual marker variability by giving an overall assessment of the magnitude of the cytokine storm. Notable individual markers were associated with fatal outcome, including Angiopoietin-2, CXCL13 and RAGE. While Angiopoietin-2 was less strongly correlated with vRNA than RAGE, it appears of significant interest in severe COVID-19 (47). This angiogenic factor has pro-inflammatory effects on the vascular endothelium, can disrupt vascular integrity and has been associated with ARDS (48) and might be a potential druggable target. We also observed a strong correlation of these markers of lung and vascular damage with plasma vRNA levels, which complement other reports showing a similarly strong association with biomarkers of heart and kidney damage (49).

Antibody responses likely contribute to viral control in acute SARS-CoV-2 infection (16, 26), supported by the negative associations we observed between plasma vRNA and SARS-CoV-2-specific antibody responses. Whereas the antibody levels between the critical and non-critical groups were similar, mortality was overrepresented among patients who, at DSO11, had low RBD-specific IgG and low total Spike-binding Ig, although not in those with low RBD-specific IgM response. Low IgG isoform among RBD-specific antibodies of deceased patients may indicate a disruption in B cell functions

requiring T-cell help, like class-switching to IgG, possibly linked to inadequate T follicular helper (TFH) and/or germinal centers (GC) disruption (50). CXCL13 is a key chemokine for recruitment to the GC of TFH and B cells (51), and plasma CXCL13 is a marker of GC activity (52). The positive associations of CXCL13 levels with vRNA loads and fatality risk and the inverse correlation of CXCL13 levels with antibody responses may seem paradoxical, but high amounts of circulating CXCL13 might disrupt the dynamics of B cell recruitment to GCs. In addition, heightened systemic inflammation can impair development of adaptive immunity (53, 54). These mechanisms may converge to reduce RBD-specific IgG responses in patients who succumb to their infection.

Defective early ADCC responses were also significantly associated with fatality, whereas we found only a non-significant trend for neutralization capacity. These observations support that Fc-mediated functions could be important in controlling SARS-CoV-2, in line with recent reports showing that compromised Fc receptor binding strongly correlated with COVID-19 mortality(26), and Spike-specific humoral responses, including higher Fc-effector functions, were enriched among survivors (55). Furthermore, antibodies with intact Fc-effector functions were required for optimal protection against infection and correlated with decreased viral loads in animal models (56, 57).

A limitation of our study is that we focused on inpatients who were usually hospitalized following worsening of their clinical condition, this occurring typically a few days after symptom onset. At this stage, some critical pathogenesis events have likely already occurred, which may narrow the window for some targeted interventions. This also excluded patients who were discharged early in their hospitalisation. Complementary

outpatient studies at very early time points will help identify factors that predict this initial worsening, and determine their overlap with the features detailed here.

The significant interactions we observed between a number of the features measured are compatible with different, non-mutually exclusive mechanisms. Poor development of protective antibody responses may allow persistently high levels of viral replication, which in turn will lead to a cytokine storm. Conversely, high cytokine levels, perhaps driven by systemic vRNA, may disrupt adaptive immune responses. Although our observational study does not allow addressing the question of causation between the immunovirological alterations observed, these measurements can be useful tools to understand heterogeneity in disease trajectories and response to therapy, particularly in the context of large, well-controlled randomized controlled trials. High viral loads and low levels of SARS-CoV-2-specific IgG may be mitigated through antivirals, monoclonal antibodies or convalescent plasma therapy with high IgG content. People with high levels of selected cytokines may benefit the most from targeted immunotherapies. While recent trials have already resulted in improvement in clinical patient care, the predictive accuracy of plasma vRNA we observed and validated in patients hospitalized during the first COVID-19 wave was confirmed in patients recruited during the second and third waves. Still, it will be important to assess how new therapeutic strategies, affect the potential of such immunovirological monitoring not only to predict outcome, but potentially to individualize patient management.

Material and methods

Participants and samples

SARS-CoV-2 positive patients admitted to the Centre Hospitalier de l'Université de Montréal (CHUM) or the Jewish General Hospital (JGH) were recruited into the Biobanque Québécoise de la COVID-19 (BQC19) (58). Samples from CHUM made up the discovery and confirmation cohort, and samples from JGH were the validation cohort. Blood draws were performed at baseline and when possible, at Day 2 (± 3 days) and Day 7 (± 3 days) after enrollment. The study was approved by the respective IRBs and written, informed consent obtained from all participants or, when incapacitated, their legal guardian before enrollment and sample collection. Blood draws were also performed on 50 asymptomatic, NSW PCR negative uninfected controls (UC).

COVID-19 hospitalized patients were stratified based on severity of respiratory support at the DSO11 timepoint: critical patients required mechanical ventilation (endotracheal, non-invasive ventilation, extracorporeal membrane oxygenation - ECMO), and non-critical patients, encompassing patients with moderate disease required no supplemental oxygen and patients with severe disease required nasal cannula for oxygen. Mortality was followed up to 60 days. Medical charts were reviewed by two physicians for data collection on demographics, co-morbidities, risk factors, severity state, time of infection, etc (see Table 1). Median age and range for UC cohort was 37 (32-46), and 30 individuals were males (60%).

Quantification of SARS-CoV2 RNA

Absolute copy numbers of SARS-CoV-2 RNA (N region) in plasma samples were measured by real time PCR. Total RNA was extracted from 230 µL of plasma collected on ACD using the QIAamp Viral RNA Mini Kit (Qiagen Cat. No. 52906). Two master reaction mixes with specific primers and probes were prepared for quantification of N gene from SARS-CoV-2 and 18S (as a control for efficient extraction and amplification). Absolute copy numbers N region in were measured by real time PCR. A positive and no-template controls were included in all experiments. Purified RNA N transcripts (1328 bp) were quantified by Nanodrop and the RNA copy numbers were calculated using the ENDMEMO online tool (see STAR methods for details).

Measurements of plasma analytes by beads array

Duplicates of SARS-CoV-2-inactivated plasma samples were analyzed using a customized Human Magnetix Luminex Assay (LXSAHM-26, R&D, see Table S1 for analyte list).

Some cytokines and tissue damage markers were at very low concentrations, and the quantification platform we used was not sensitive enough to reliably them in most samples. As such, analytes with extrapolated values >90% and negative values>15% were identified by □ in Figures 2, 3 and S2.

CytoScore

For k analytes (n=26), the CytoScore for each sample was calculated as follows

$$\left(\sum_{n=1}^{k}\left(c_{n}-\mu_{n}^{UC}\right)/\left(\sigma_{n}^{UC}\right)\right)/k$$

where

cn is the concentration for analyte n,

μ_n^{UC} is the mean concentration of uninfected control samples for analyte n

σ_n^{UC} is the standard deviation of uninfected control samples for analyte n

Serology measurements

Plasma from uninfected donors were used as negative controls and used to calculate the seropositivity threshold in our ELISA and flow cytometry assays. The monoclonal antibody CR3022(59) was used as a positive control.

RBD-specific ELISA

The SARS-CoV-2 RBD ELISA assay used was recently described (24). The seropositivity threshold was established using the following formula: mean of all COVID-19 negative plasma + (3 standard deviation of the mean of all COVID-19 negative plasma) (see supplemental material for details).

Flow cytometry analysis of cell-surface staining

As recently described(24), plasma from SARS-CoV-2-infected or uninfected individuals (1/250 dilution) were added onto 239T cells expressing Spike and GFP. Alexa Fluor-647-

conjugated goat anti-human IgG (H+L) Abs (Invitrogen) were used as secondary antibodies. The seropositivity threshold was established using the following formula: mean of all COVID-19 negative plasma + (3 standard deviation of the mean of all COVID-19 negative plasma + inter-assay coefficient of variability) (see supplemental material for details).

Virus neutralization assay

As recently described(24), 293T-ACE2 target cells were infected with single-round luciferase-expressing pseudoparticles bearing the SARS-CoV-2 Spike in presence of patient plasma at different dilutions. The neutralization half-maximal inhibitory dilution (ID50) represents the plasma dilution to inhibit 50% of the infection of target cells (see supplemental material for details).

ADCC assay with SARS-CoV-2 Spike expressing cells

As previously described(60), patient plasma was tested for antibody-dependent cellular cytotoxity (ADCC) activity against SARS-CoV-2 pseudo-infected cells. Target cells (1:1 ratio of stained CEM.NKr CCR5+ and CEM.NKr. Spike+) and effector cells (stained PBMCs) were mixed at a ratio of 1:10. Plasma from COVID-19 (1/500 dilution) were added and co-cultures were incubated for 6 hrs. ADCC was calculated by gating on Spike-expressing live target cells and using the formula:

%ADCC= (〖%GFP〗_(targets+effectors)-〖%GFP〗_(targets+effectors+plasma))/〖%GFP〗_targets x 100

%ADCC obtained with plasma was further normalized to positive control. The specificity threshold was established using the following formula: mean of all COVID-19 negative plasma + 3 standard deviation of the mean of all COVID-19 negative plasma.

Clinical scores. The qSOFA and P/F ratios were calculated based on data clinically collected into the patients' medical record of the hospital stay. The qSOFA score (quick Sepsis Related Organ Failure Assessment) was calculated as previously described (35). It uses three criteria, assigning one point for low blood pressure (SBP≤100 mmHg), high respiratory rate (≥22 breaths per min), or altered mentation. The ratio of partial arterial oxygen pressure and fraction of inspired oxygen (P/F ratio) was approximated based on the oxygen saturation measured by pulse oximetry and the fraction of inspired oxygen by nonlinear imputation, as described(36).

CRP quantitation. The measurement of C-reactive protein (CRP) in plasma was performed by the clinical biochemistry laboratories of the respective hospitals where patients were recruited (CHUM and JGH).

Statistical analyses and multivariate models

Methods for univariate models. The association between of measured variables and time to death was analyzed by Cox Proportional Survival Hazard. The dependent variable in all survival analyses was time to death during the follow-up, measured in days. Subjects were censored upon reaching 60 days of follow-up (no patients withdrew within this

timeframe). The time 0 was defined as a day of symptoms onset. Univariate Cox Proportional Hazard regression was used to determine the association plasma analytes and all-cause mortality at DSO60 for all COVID-19+ patients, as well as critical patients' subgroup only. Analytes were log-transformed when they naturally followed exponential distribution, for example vRNA and cytokines. Next, the estimated survival proportions at any given point in time for a undetectable (when applicable), low lower interquartile range level of detectable) or high (upper interquartile range of detectable) were extracted from Cox models(28) and presented in the graphical form(28).

Part 1. Multivariate Cox model. Potential risk factors were grouped in 3 categories: i) vRNA, ii) 26 cytokine variables and iii) 6 antibody variables. Model building was performed in three steps. In the first step, univariate models for risk factor of death by DSO60 were developed, one for each of the covariates in the category; only risk factors p value <0.05 were retained. For the second category of 26 cytokines, an additional criterion of variable selection was applied to ensure the quality of the measurements: the cytokines with extrapolated values >90% and negative values>15% were excluded for future investigation. These exclusion criteria were added as the quantification platform we used was not sensitive enough to reliably quantify some low-concentration analytes, and we wanted to rely on analytes which are well quantified for our multivariate model. 19 cytokines out of 26 were satisfied these criteria. In the second step, categories for which more than one variable had been retained in the first step were focused on; then the stepwise Cox model selection based on the Bayesian Information Criterion (BIC) was used to obtain the most-parsimonious model (lowest value) for each of these categories. This penalized likelihood criterion selects the best variable at predicting data, then adds

one additional variable at a time while accounting for potential overfitting, in the end only selecting the multivariate model with the lowest BIC value, i.e. the most parsimonious. In addition, to keep the risk of overfitting low, no more than six predictor parameters were entered in the multivariate model for our sample of 61 patients(61, 62).

In the third step, all variables retained in the second step were considered; then the BIC was used to obtain a global parsimonious model. Based on the literature (63), age and sex are associated with the mortality for COVID-19 patients, however in the small homogeneous sample in might be hard to detect these relations. Thus, in each model Age and Sex covariates were forced in the multivariate model regardless their significance. Potential interactions between each covariate with age and sex were tested to verify if the effect is consistent across different age and between sex. Potential presence of multicollinearity was assessed by calculating the variance inflation factor (VIF) for each variable. This allowed us to identify and treat in separate models subsets of covariates which were highly correlated.

Part 2. Time dependent ROC curve. To evaluate predictive accuracy of survival models the time-dependent receiver operator characteristic (ROC) curves for right-censored data (64) were calculated, compared across different Cox models and presented in the graphical form. The inverse probability of censoring weighting technique (IPCW) was used for estimating time-dependent ROC curves (65). The area under the curve (AUC) was examined at 60 days as well at all distinct event times by plotting the AUC curve and the 95% confidence limits over time. The day 48 corresponds the last event (fatality) day in the discovery cohort.

Part 3. Independent cohorts validation. All final multivariate Cox models were reassessed

in the validation and confirmation cohorts by executing independently the multivariate models with the same list of variables obtained, in the discovery cohort, in steps 2 and 3. Then, using the same approach described above, the time dependent ROC curves were evaluated in validation dataset to validate our finding.

Sensitivity analysis. Two additional sensitivity analyses were performed. Firstly, to compare predictive capacity of the final selected model vs models with easily available clinical measures (qSOFA, P/F and CRP), the univariate and multivariate Cox regressions were presented. Discovery cohort was used for qSOFA and P/F. Three study cohorts were combined for the analysis with CRP due to partially available data in each cohort.

Secondary, to see how the final results were affected by earlier time point measurements and shorter time windows, three new data sets were extracted from longitudinal measurements of the combined cohorts at DSO[3-7], DSO[8-11] and DSO[12-15] timeframe. The final Cox regressions models were repeated for each dataset.

Declaration of interest, funding, acknowledgements

Acknowledgements

For sample collection and processing, and clinical data retrieva at the CHUM, we thank Dounia Boumahni, Fatna Benettaib, Ali Ghamraoui, Boaz Lahav, Pascale Arlotto, Nakome Nguissant, Kip Brown, Johann Plantin, Stéphanie Matte, Martine Lebrasseur, Gloria Ortega-Delgado, Mélanie Laporte, Caroline Dufour, Isabelle Turcotte, Syllah Mohammed and Natalia Zamorano. We thank Dr. Stefan Pöhlmann (Georg-August University, Germany) for the plasmid coding for SARS-CoV-2 S glycoproteins and Dr. M. Gordon Joyce (U.S. MHRP) for the monoclonal antibody CR3022. For sample collection and processing at JGH, we thank Meriem Bouab, Danielle Henry, Zaman Afrasiabi, Hershlee Vernet, Branka Vulesevic, Nardin Rezk, Nofar Kimchi, Chris Tselios, Charlotte Guzman, Louis Petitjean, Xiaoqing Xue, Maureen Oliveira and Bluma Brenner. For chart review at JGH, we thank Yara Moussa, Olumide Adeleye, Noor Mamlouk, Tala Abdullah, Michael Palayew and Biswarup Ghosh. For administration at JGH, we thank Vincenzo Forgetta, Darin Adra, Jonathan Afilalo and Marc Afilalo. We also thank the flow cytometry and NC3 platforms at the CRCHUM.

Funding

American Foundation for AIDS Research (amfAR) grant 110068-68-RGCV (DEK, NC, AF)

Canada's COVID-19 Immunity Task Force (CITF), in collaboration with the Canadian Institutes of Health Research (CIHR) grant VR2-173203 (DEK, AF)

CIHR grants 365825 and 409511 (JBR)

Canada Foundation for Innovation (CFI): Exceptional Fund COVID-19 grant #41027 to AF, DEK, NC; CFI leader to JBR

Ministère de l'Économie et de l'Innovation du Québec, Programme de soutien aux organismes de recherche et d'innovation (AF)

CRCHUM Foundation

Fonds de recherche Québec-Santé (FRQS) (BQC-19, JBR)

Génome Québec (BQC-19, JBR)

Public Health Agency of Canada (BQC-19,JBR)

FRQS Merit Research Scholar Award (DEK)

FRQS Salary Award (NC, MD, MC, JBR, CL, MT)

FRQS Clinical Research Scholarship (JBR)

Canada Research Chair (AF, AP)

COVID-19 excellence scholarship from the Université de Montréal (EBR)

CIHR fellowships (SPA, PG)

Lady Davis Institute of the Jewish General Hospital (JBR)

NIH Foundation (JBR)

Cancer Research UK (JBR)

Competing interests

JBR has served as an advisor to GlaxoSmithKline and Deerfield Capital. These agencies had no role in the design, implementation or interpretation of this study. Authors declare that they have no other competing interests.

Data and materials availability

All data are available in the main text or the supplementary materials.

References

1. W. H. O. R. E. A. f. C.-T. W. Group et al., Association Between Administration of Systemic Corticosteroids and Mortality Among Critically Ill Patients With COVID-19: A Meta-analysis. JAMA 324, 1330-1341 (2020).
2. B. M. Tomazini et al., Effect of Dexamethasone on Days Alive and Ventilator-Free in Patients With Moderate or Severe Acute Respiratory Distress Syndrome and COVID-19: The CoDEX Randomized Clinical Trial. JAMA 324, 1307-1316 (2020).
3. R. C. Group et al., Dexamethasone in Hospitalized Patients with Covid-19 - Preliminary Report. N Engl J Med, (2020).
4. A. C. Gordon et al., Interleukin-6 Receptor Antagonists in Critically Ill Patients with Covid-19 – Preliminary report. medRxiv, 2021.2001.2007.21249390 (2021).
5. P. W. Horby et al., Tocilizumab in patients admitted to hospital with COVID-19 (RECOVERY): preliminary results of a randomised, controlled, open-label, platform trial. medRxiv, 2021.2002.2011.21249258 (2021).
6. R. Libster et al., Early High-Titer Plasma Therapy to Prevent Severe Covid-19 in Older Adults. N Engl J Med, (2021).
7. I. F. Hung et al., Viral loads in clinical specimens and SARS manifestations. Emerg Infect Dis 10, 1550-1557 (2004).
8. P. R. Grant et al., Detection of SARS coronavirus in plasma by real-time RT-PCR. N Engl J Med 349, 2468-2469 (2003).
9. A. Waghmare et al., Respiratory syncytial virus lower respiratory disease in hematopoietic cell transplant recipients: viral RNA detection in blood, antiviral treatment, and clinical outcomes. Clin Infect Dis 57, 1731-1741 (2013).
10. S. Y. Kim et al., Viral RNA in Blood as Indicator of Severe Outcome in Middle East Respiratory Syndrome Coronavirus Infection. Emerg Infect Dis 22, 1813-1816 (2016).
11. M. D. de Jong et al., Fatal outcome of human influenza A (H5N1) is associated with high viral load and hypercytokinemia. Nat Med 12, 1203-1207 (2006).
12. C. Prebensen et al., SARS-CoV-2 RNA in plasma is associated with ICU admission and mortality in patients hospitalized with COVID-19. Clin Infect Dis, (2020).
13. C. A. Hogan et al., High Frequency of SARS-CoV-2 RNAemia and Association With Severe Disease. Clin Infect Dis, (2020).
14. J. Fajnzylber et al., SARS-CoV-2 viral load is associated with increased disease severity and mortality. Nat Commun 11, 5493 (2020).
15. E. Pujadas et al., SARS-CoV-2 viral load predicts COVID-19 mortality. Lancet Respir Med 8, e70 (2020).
16. C. Gutmann et al., SARS-CoV-2 RNAemia and proteomic trajectories inform prognostication in COVID-19 patients admitted to intensive care. Nat Commun 12, 3406 (2021).
17. C. Huang et al., Clinical features of patients infected with 2019 novel coronavirus in Wuhan, China. Lancet 395, 497-506 (2020).
18. M. Mandel, G. Harari, M. Gurevich, A. Achiron, Cytokine prediction of mortality in COVID19 patients. Cytokine 134, 155190 (2020).
19. A. G. Laing et al., A dynamic COVID-19 immune signature includes associations with poor

prognosis. Nat Med 26, 1623-1635 (2020).
20. C. Lucas et al., Longitudinal analyses reveal immunological misfiring in severe COVID-19. Nature 584, 463-469 (2020).
21. D. M. Del Valle et al., An inflammatory cytokine signature predicts COVID-19 severity and survival. Nat Med 26, 1636-1643 (2020).
22. A. C. Walls et al., Structure, Function, and Antigenicity of the SARS-CoV-2 Spike Glycoprotein. Cell 181, 281-292 e286 (2020).
23. M. Hoffmann et al., SARS-CoV-2 Cell Entry Depends on ACE2 and TMPRSS2 and Is Blocked by a Clinically Proven Protease Inhibitor. Cell 181, 271-280 e278 (2020).
24. J. Prevost et al., Cross-Sectional Evaluation of Humoral Responses against SARS-CoV-2 Spike. Cell Rep Med 1, 100126 (2020).
25. Q. X. Long et al., Antibody responses to SARS-CoV-2 in patients with COVID-19. Nat Med 26, 845-848 (2020).
26. T. Zohar et al., Compromised Humoral Functional Evolution Tracks with SARS-CoV-2 Mortality. Cell 183, 1508-1519 e1512 (2020).
27. E. J. Williamson et al., Factors associated with COVID-19-related death using OpenSAFELY. Nature 584, 430-436 (2020).
28. M. J. Bradburn, T. G. Clark, S. B. Love, D. G. Altman, Survival Analysis Part II: Multivariate data analysis – an introduction to concepts and methods. British Journal of Cancer 89, 431-436 (2003).
29. P. S. Arunachalam et al., Systems biological assessment of immunity to mild versus severe COVID-19 infection in humans. Science 369, 1210-1220 (2020).
30. M. Kowalewski et al., COVID-19 and ECMO: the interplay between coagulation and inflammation-a narrative review. Crit Care 24, 205 (2020).
31. S. Spadaro et al., Biomarkers for Acute Respiratory Distress syndrome and prospects for personalised medicine. J Inflamm (Lond) 16, 1 (2019).
32. W. F. Garcia-Beltran et al., COVID-19-neutralizing antibodies predict disease severity and survival. Cell, (2020).
33. G. Beaudoin-Bussieres et al., Decline of Humoral Responses against SARS-CoV-2 Spike in Convalescent Individuals. mBio 11, (2020).
34. D. A. Berlin, R. M. Gulick, F. J. Martinez, Severe Covid-19. N Engl J Med 383, 2451-2460 (2020).
35. C. W. Seymour et al., Assessment of Clinical Criteria for Sepsis: For the Third International Consensus Definitions for Sepsis and Septic Shock (Sepsis-3). JAMA 315, 762-774 (2016).
36. S. M. Brown et al., Nonlinear Imputation of PaO2/FIO2 From SpO2/FIO2 Among Mechanically Ventilated Patients in the ICU: A Prospective, Observational Study. Crit Care Med 45, 1317-1324 (2017).
37. D. Wang et al., Clinical Characteristics of 138 Hospitalized Patients With 2019 Novel Coronavirus-Infected Pneumonia in Wuhan, China. JAMA 323, 1061-1069 (2020).
38. P. Le Borgne et al., SARS-CoV-2 viral load in nasopharyngeal swabs in the emergency department does not predict COVID-19 severity and mortality. Acad Emerg Med, (2021).
39. W. A. O'Brien et al., Changes in plasma HIV-1 RNA and CD4+ lymphocyte counts and the risk of progression to AIDS. Veterans Affairs Cooperative Study Group on AIDS. N Engl J Med

334, 426-431 (1996).
40. J. H. Beigel et al., Remdesivir for the Treatment of Covid-19 - Final Report. N Engl J Med 383, 1813-1826 (2020).
41. W. H. O. S. T. Consortium et al., Repurposed Antiviral Drugs for Covid-19 - Interim WHO Solidarity Trial Results. N Engl J Med 384, 497-511 (2021).
42. P. Chen et al., SARS-CoV-2 Neutralizing Antibody LY-CoV555 in Outpatients with Covid-19. N Engl J Med 384, 229-237 (2021).
43. D. M. Weinreich et al., REGN-COV2, a Neutralizing Antibody Cocktail, in Outpatients with Covid-19. N Engl J Med 384, 238-251 (2021).
44. D. A. Dorward et al., Tissue-Specific Immunopathology in Fatal COVID-19. Am J Respir Crit Care Med 203, 192-201 (2021).
45. X. Ren et al., COVID-19 immune features revealed by a large-scale single-cell transcriptome atlas. Cell, (2021).
46. L. Velazquez-Salinas, A. Verdugo-Rodriguez, L. L. Rodriguez, M. V. Borca, The Role of Interleukin 6 During Viral Infections. Front Microbiol 10, 1057 (2019).
47. E. Villa et al., Dynamic angiopoietin-2 assessment predicts survival and chronic course in hospitalized patients with COVID-19. Blood Adv 5, 662-673 (2021).
48. C. S. Calfee et al., Plasma angiopoietin-2 in clinical acute lung injury: prognostic and pathogenetic significance. Crit Care Med 40, 1731-1737 (2012).
49. D. Xu et al., Relationship Between Serum Severe Acute Respiratory Syndrome Coronavirus 2 Nucleic Acid and Organ Damage in Coronavirus 2019 Patients: A Cohort Study. Clin Infect Dis 73, 68-75 (2021).
50. N. Kaneko et al., Loss of Bcl-6-Expressing T Follicular Helper Cells and Germinal Centers in COVID-19. Cell 183, 143-157 e113 (2020).
51. S. Crotty, Follicular helper CD4 T cells (TFH). Annu Rev Immunol 29, 621-663 (2011).
52. C. Havenar-Daughton et al., CXCL13 is a plasma biomarker of germinal center activity. Proc Natl Acad Sci U S A 113, 2702-2707 (2016).
53. R. S. Hotchkiss, I. E. Karl, The pathophysiology and treatment of sepsis. N Engl J Med 348, 138-150 (2003).
54. F. V. Sjaastad et al., Polymicrobial Sepsis Chronic Immunoparalysis Is Defined by Diminished Ag-Specific T Cell-Dependent B Cell Responses. Front Immunol 9, 2532 (2018).
55. C. Atyeo et al., Distinct Early Serological Signatures Track with SARS-CoV-2 Survival. Immunity 53, 524-532 e524 (2020).
56. E. S. Winkler et al., Human neutralizing antibodies against SARS-CoV-2 require intact Fc effector functions and monocytes for optimal therapeutic protection. bioRxiv, (2020).
57. A. Schafer et al., Antibody potency, effector function, and combinations in protection and therapy for SARS-CoV-2 infection in vivo. J Exp Med 218, (2021).
58. K. Tremblay et al., The Biobanque quebecoise de la COVID-19 (BQC19)-A cohort to prospectively study the clinical and biological determinants of COVID-19 clinical trajectories. PLoS One 16, e0245031 (2021).
59. M. Yuan et al., A highly conserved cryptic epitope in the receptor binding domains of SARS-CoV-2 and SARS-CoV. Science 368, 630-633 (2020).
60. S. P. Anand et al., Longitudinal analysis of humoral immunity against SARS-CoV-2 Spike in convalescent individuals up to 8 months post-symptom onset. bioRxiv, (2021).

61. F. E. Harrell, Jr., K. L. Lee, R. M. Califf, D. B. Pryor, R. A. Rosati, Regression modelling strategies for improved prognostic prediction. Stat Med 3, 143-152 (1984).
62. E. Vittinghoff, C. E. McCulloch, Relaxing the rule of ten events per variable in logistic and Cox regression. Am J Epidemiol 165, 710-718 (2007).
63. J. Sha et al., Sex Differences on Clinical Characteristics, Severity, and Mortality in Adult Patients With COVID-19: A Multicentre Retrospective Study. Front Med (Lausanne) 8, 607059 (2021).
64. L. A. Blanche P., Viallon V., in Lecture Notes in Statistics, G. M. Lee ML., Pfeiffer R., Satten G., Cai T., Gandy A., Ed. (Springer, New York, 2013), vol. 215.
65. H. Uno, T. Cai, L. Tian, L. J. Wei, Evaluating Prediction Rules for t-Year Survivors with Censored Regression Models. Journal of the American Statistical Association 102, 527-537 (2007).

Figures

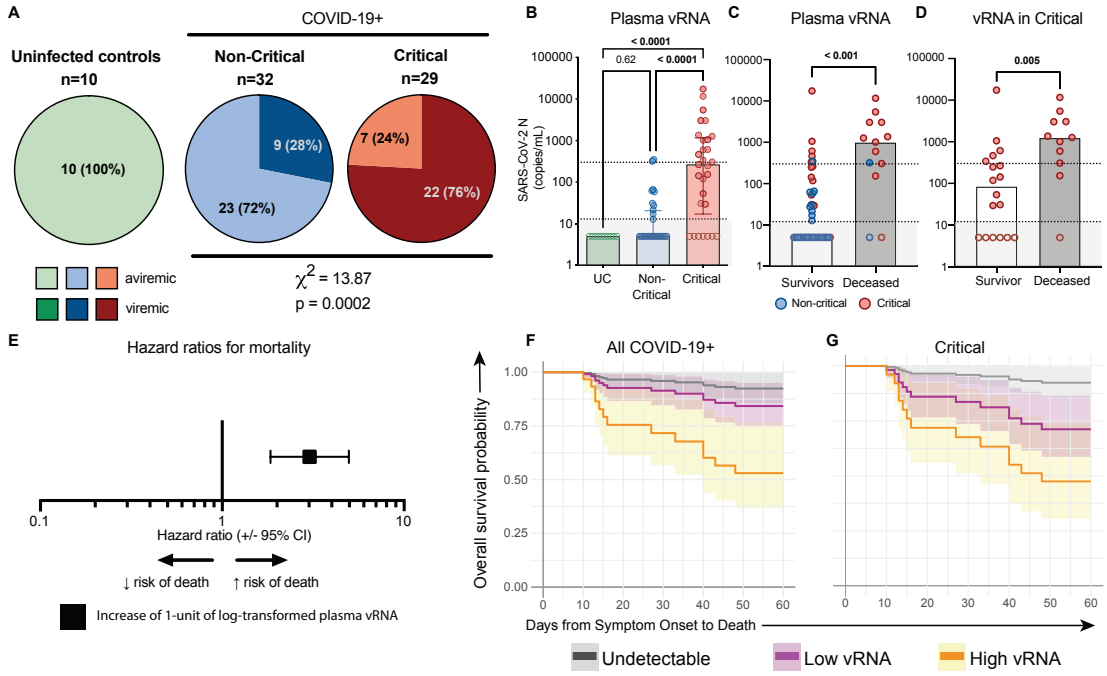

F1

Figure 3.1 High quantity of SARS-CoV-2 RNA in plasma at DSO11 is associated with increased risk of mortality. A) Pie charts representing the fractions of assessed samples which had undetectable (aviremic, light shades, <13 copies/mL) or detectable SARS-CoV-2 vRNA (≥13 copies/mL, dark shades). Numbers in parts refer to the number (and percentages) of patients within each cohort. Non-critical and critical subgroups compared by Chi Square test. B) Quantities of N copies of SARS-CoV-2 RNA detected per mL of plasma in each cohort. Dotted line is the limit of detection (13 copies/mL). Empty shapes have undetectable vRNA (arbitrarily set at 5 copies/mL for representation). CD) Amounts of N copies of SARS-CoV-2 RNA detected per mL of plasma in patients which survived (white column) or died (grey column) by DSO60 for C) total cohort or D) critical subgroup only. Red circles represent critical patients, and blue are non-critical. E) HR with 95%CI calculated using Cox regression for an increase of 1 unit of log10-transformed vRNA (copies/mL). FG) Modelization of the hazard ratio of patients with high (orange, upper IQR), low (purple, lower IQR) or undetectable (grey) plasma vRNA in F) all COVID-19 patients or G) Critical cases only. B) Kruskall-Wallis with Dunn's multiple comparisons test. C) Mann-Whitney test. n = 61 COVID-19 subjects (13 mortalities) or 29 Critical COVID-19 cases (11 mortalities) and 10 UC. IQR = interquartile range, calculated among detectable vRNA quantities only.

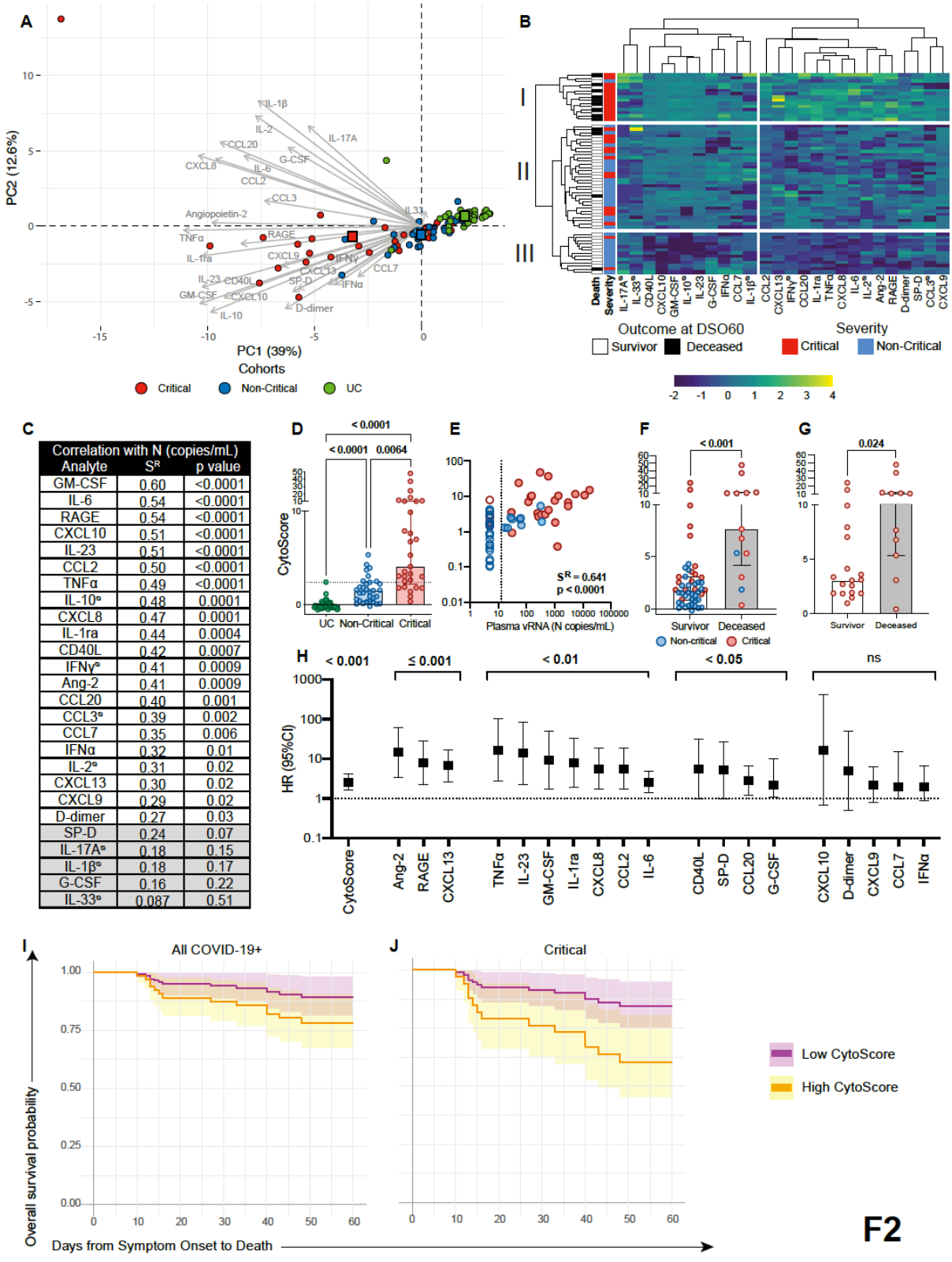
A
PC2 (12.6%)
PC1 (39%)
Cohorts
Critical
Non-Critical
UC
IL-1β
IL-2
IL-17A
CCL20
G-CSF
CXCL8
IL-6
CCL2
CCL3
Angiopoietin-2
IL33
RAGE
TNFα
IL-1ra
CXCL9
IFNγ
CCL7
IL-23
CD40L
CCL13
SP-D
IFNα
GM-CSF
CXCL10
D-dimer
IL-10
B
I
II
III
Death
Severity
Outcome at DSO60
Survivor
Deceased
Severity
Critical
Non-Critical
C
Correlation with N (copies/mL)
Analyte
S^R
p value
GM-CSF 0.60 <0.0001
IL-6 0.54 <0.0001
RAGE 0.54 <0.0001
CXCL10 0.51 <0.0001
IL-23 0.51 <0.0001
CCL2 0.50 <0.0001
TNFα 0.49 <0.0001
IL-10* 0.48 0.0001
CXCL8 0.47 0.0001
IL-1ra 0.44 0.0004
CD40L 0.42 0.0007
IFNγ* 0.41 0.0009
Ang-2 0.41 0.0009
CCL20 0.40 0.001
CCL3* 0.39 0.002
CCL7 0.35 0.006
IFNα 0.32 0.01
IL-2* 0.31 0.02
CXCL13 0.30 0.02
CXCL9 0.29 0.02
D-dimer 0.27 0.03
SP-D 0.24 0.07
IL-17A* 0.18 0.15
IL-1β* 0.18 0.17
G-CSF 0.16 0.22
IL-33* 0.087 0.51
D
CytoScore
UC Non-Critical Critical
< 0.0001
< 0.0001 0.0064
E
Plasma vRNA (N copies/mL)
S^R = 0.641
p < 0.0001
F
< 0.001
Survivor Deceased
Non-critical Critical
G
0.024
Survivor Deceased
H
HR (95%CI)
< 0.001
≤ 0.001
< 0.01
< 0.05
ns
CytoScore Ang-2 RAGE CXCL13 TNFα IL-23 GM-CSF IL-1ra CXCL8 CCL2 IL-6 CD40L SP-D CCL20 G-CSF CXCL10 D-dimer CXCL9 CCL7 IFNα
I
All COVID-19+
Overall survival probability
Days from Symptom Onset to Death
J
Critical
Low CytoScore
High CytoScore
F2

Figure 3.2 High cytokine titers in plasma at DSO11 discriminates critical disease and is associated with increased risk of mortality. A) Principal component analysis (PCA) representation of critical and non-critical patients (at DSO11), and UC (at baseline), on the basis of the 26 plasma analytes. Color-coded squares represent the mean PC coordinates for each group. Length of arrow indicates contribution of analytes to PCs. Numbers in parentheses along axes are the percentage of variance that PC accounts for. **B)** Heatmap analysis of log-transformed concentrations of all 26 plasma analytes (yellow = high relative expression; blue = low relative expression), with unsupervised hierarchical clustering of the analytes (top dendrogram) or of patients (left dendrogram). Left-most column represents outcome at DS60 (white = survival, black = deceased). Following column is the severity of the patient at DSO11. **C**) Table showing the Spearman R values and corresponding p values of correlation of each plasma analyte with plasma vRNA. Values shaded in grey are non-significant. **D)** Comparison of CytoScore of each cohort (see methods for details on CytoScore). **E)** Correlation between plasma vRNA and CytoScore. Empty shapes are aviremics (<13 copies SARS-CoV-2/mL of plasma). **FG)** CytoScore of patients whom survived (white column) or deceased (grey column) by DSO60 for **F)** all COVID-19 patients or **G)** critical subgroup only. **H**) HR with 95%CI calculated using Cox regression for a 1-unit increase of the $\log_{10}$-transformed concentration of each plasma analyte with robust detection (see methods for details) and CytoScore. **IJ)** Modelization of the hazard ratio of patients with high (orange, upper IQR) or low (purple, lower IQR) CytoScore in **I)** all COVID-19 patients or **J)** critical subgroup only. CE) Spearman correlations. D) Kruskall-Wallis with Dunn's multiple comparisons test. F) Mann-Whitney test. For A-B, D-F, color-coded dots represent severity of the patient at DSO11 (red = critical, blue = non-critical), or UC cohort (green). BD) Cytokines with titles annotated by ∅ are poorly detected (See methods for details). n = 61 COVID-19 subjects (13 mortalities) or 29 Critical COVID-19 cases (11 mortalities) and 43 UC. IQR = interquartile range, calculated within the CytoScores of the COVID-19 discovery cohort.

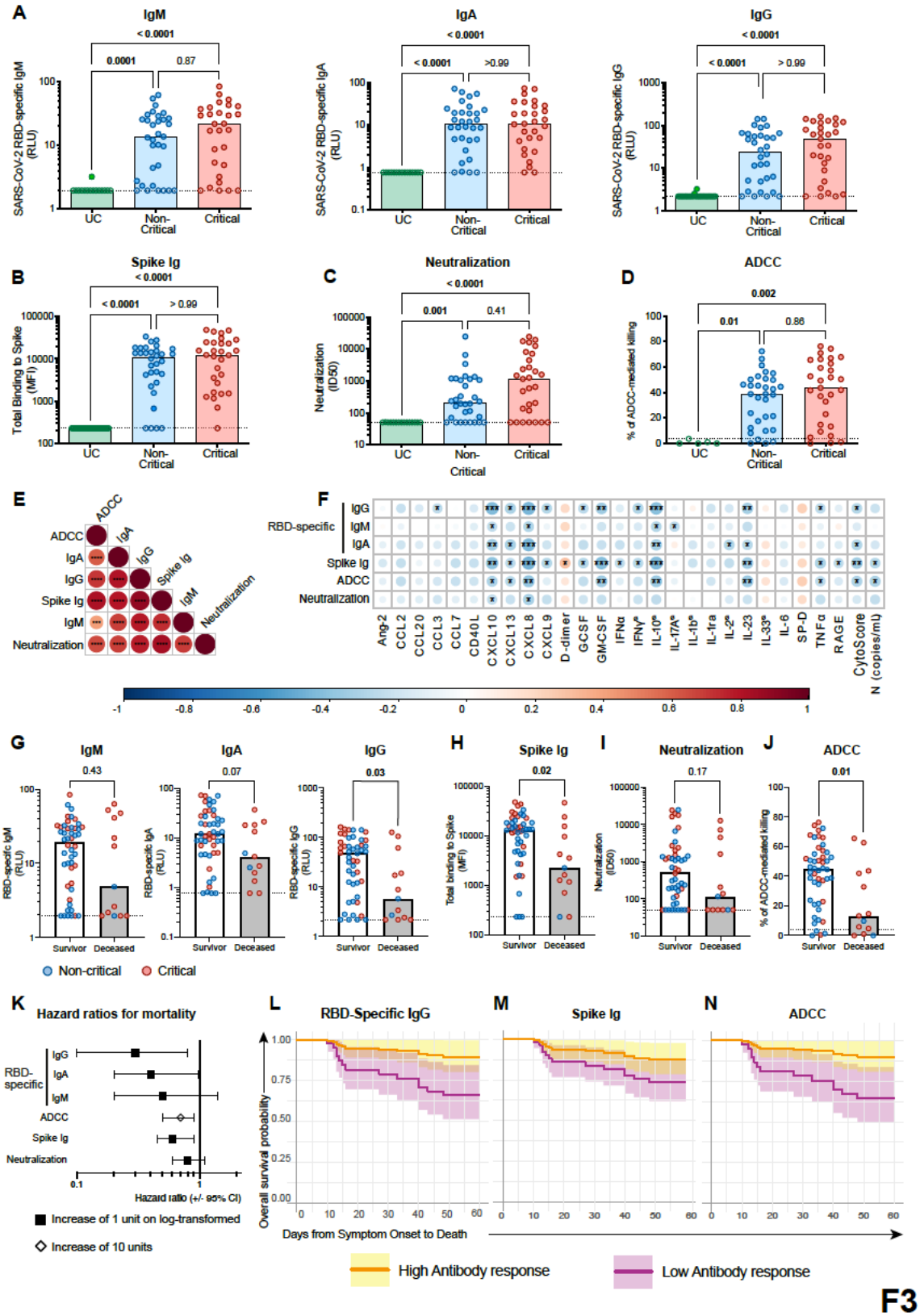
A
IgM
IgA
IgG
SARS-CoV-2 RBD-specific IgM (RLU)
SARS-CoV-2 RBD-specific IgA (RLU)
SARS-CoV-2 RBD-specific IgG (RLU)
< 0.0001
0.0001
0.87
>0.99
> 0.99
UC
Non-Critical
Critical
B
Spike Ig
Total Binding to Spike (MFI)
C
Neutralization
Neutralization (ID50)
0.001
0.41
D
ADCC
% of ADCC-mediated killing
0.002
0.01
0.86
E
ADCC
IgA
IgG
Spike Ig
IgM
Neutralization
F
RBD-specific
IgG
IgM
IgA
Spike Ig
ADCC
Neutralization
Ang-2
CCL2
CCL20
CCL3
CCL7
CD40L
CXCL10
CXCL13
CXCL8
CXCL9
D-dimer
GCSF
GMCSF
IFNα
IFNγ
IL-10
IL-17A
IL-1b
IL-1ra
IL-2
IL-23
IL-33
IL-6
SP-D
TNFα
RAGE
CytoScore
N (copies/ml)
-1
-0.8
-0.6
-0.4
-0.2
0
0.2
0.4
0.6
0.8
1
G
IgM
IgA
IgG
0.43
0.07
0.03
RBD-specific IgM (RLU)
RBD-specific IgA (RLU)
RBD-specific IgG (RLU)
Survivor
Deceased
H
Spike Ig
0.02
Total binding to Spike (MFI)
I
Neutralization
0.17
Neutralization (ID50)
J
ADCC
0.01
% of ADCC-mediated killing
Non-critical
Critical
K
Hazard ratios for mortality
RBD-specific
IgG
IgA
IgM
ADCC
Spike Ig
Neutralization
0.1
1
Hazard ratio (+/- 95% CI)
Increase of 1 unit on log-transformed
Increase of 10 units
L
RBD-Specific IgG
M
Spike Ig
N
ADCC
Overall survival probability
1.00
0.75
0.50
0.25
0.00
0
10
20
30
40
50
60
Days from Symptom Onset to Death
High Antibody response
Low Antibody response

F3

Figure 3.3 Limited IgG responses against SARS-CoV-2 Spike at DSO11 is associated with mortality. A) ELISA-based relative quantification of SARS-CoV-2 RBD-specific antibodies' isotypes IgM (left), IgA (center) or IgG (right) in Relative light units (RLU) normalized to an internal control (CR3022). **B-D)** Comparison of functional properties of the plasma of all three groups, namely **B**) plasma capacity to recognize the SARS-CoV-2 full Spike (Spike Ig) using a flow cytometry-based assay (Median Fluorescence Intensity - MFI); **C**) plasma neutralization activity (unit = half of maximal inhibitory plasma dilution – ID50); **D**) plasma ADCC activity (unit = % of ADCC-mediated killing). **EF)** Correlation matrixes with colors representing the Spearman R value (blue = negative association -1; red = positive association 1), and p values indicated as * in the circles, **E)** between all serology measurements or **F)** of serology measurements *versus* plasma vRNA and plasma analytes. **G-J)** Comparison of serology measurements in patients who survived (white column) or deceased (grey column) by DSO60, for **G)** RBD-specific IgM (left), IgA (center) or IgG (right) or **H)** Full Spike binding, **I**) Neutralization or **J**) ADCC. **K**) Hazard ratio with 95%CI calculated using Cox regression for an increase of 1 unit of $\log_{10}$-transformed (square) or 10 units (diamond) of serology measurements. **L-N**) Modelization of the hazard ratio over time of patients with high (orange, upper IQR) or low (purple, lower IQR) **L**) RBD-specific IgG, **M**) Spike Ig or **N**) ADCC activity in all COVID-19 patients. A-D) Kruskall-Wallis with Dunn's multiple comparison test. EF) Spearman R correlation. F) Cytokines with titles annotated by ∅ are poorly detected. G-J) Mann-Whitney test. For G-J, color-coded dots represent severity of the patient at DSO11 (red = critical, blue = non-critical) and dotted line represents the limit of detection. EFL) $p < 0.05$ = * ; $p < 0.01$ = ***; $p < 0.001$ = ***. n = 61 COVID-19 subjects (13 mortalities) or 29 Critical COVID-19 cases (11 mortalities) and 43 UC. IQR = interquartile range, calculated within the COVID-19 discovery cohort.

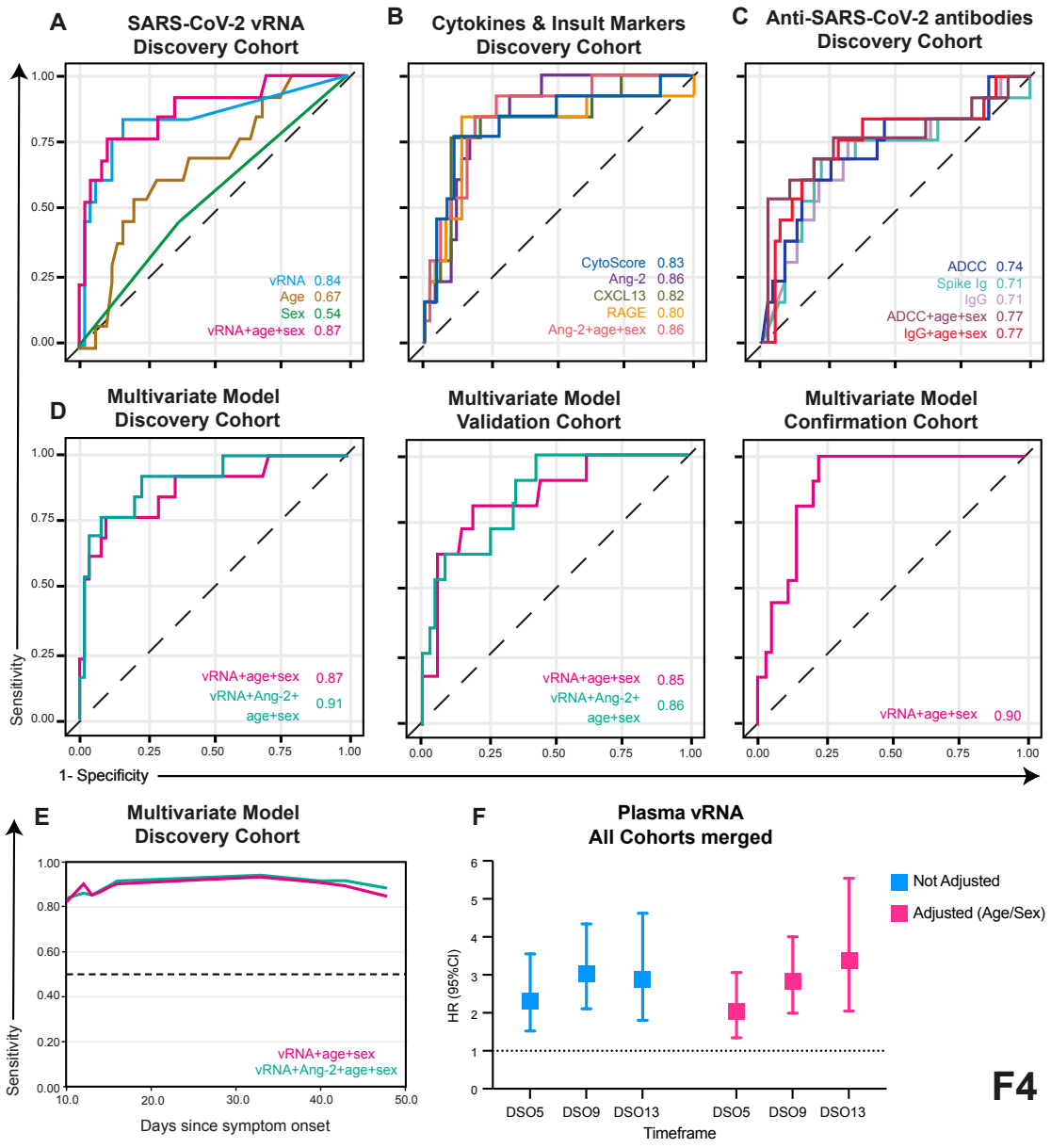

Figure 3.4 Time-dependent ROC curves reveal plasma vRNA as reproducibly associated with mortality in both the discovery and validation cohorts. A-C) Time-dependent ROC curves measured within the discovery cohort for **A)** plasma vRNA, age and sex; **B)** Cytokines and tissue insult markers or **C)** anti-SARS-CoV-2 antibody responses. **D)** Time-dependent ROC curves of top multivariate models selected by BIC stepwise selection in the Discovery (left), Validation (center) and Confirmation cohorts (right). **E**) Time-dependent AUC of multivariate models over time in the Discovery cohort. **F**) Hazard ratio of plasma vRNA when sampled at DSO5, DSO9 or DSO13. HR adjusted for age and sex or not. Discovery : n= 61 ; Validation : n=87 ; Confirmation : n = 69.

Tables

Table 3.1 Baseline characteristics of the participants and respiratory support at time of immunovirological profiling. †

	Discovery cohort (n=61)			Validation cohort (n=87)			Confirmation cohort (n=69)		
Variable	Non-Critical (n=32)	Critical (n=29)	Entire cohort (n=61)	Non-Critical (n=68)	Critical (n=19)	Entire cohort (n=87)	Non-Critical (n=42 or 24)**	Critical (n=27 or 13)**	Entire cohort (n=69 or 37)**
Age	63 (49-80)	62 (51-68)	62 (49-73)	75 (57-88)	70 (55-73)	71 (56-84)	56 (49-71)	70 (57-79)	63 (51-75)
Sex									
Male	17 (53%)	20 (69%)	37 (61%)	33 (49%)	11 (58%)	44 (51%)	29 (69%)	16 (59%)	45 (65%)
Female	15 (47%)	9 (31%)	24 (39%)	35 (51%)	8 (42%)	43 (49%)	13 (31%)	11 (41%)	24 (34%)
Days since symptom onset	10 (8.5-13)	11 (10-12)	11 (9-12)	10 (8-12)	11 (9-12)	10 (9-12)	11 (10-12)	11 (10-13)	11 (10-13)
Days since hospital admission	5.5 (3-7)	5 (3-7)	5 (3-7)	4 (2-8)	5 (3-8)	5 (2-8)	5.5 (3-8.5)	5 (0-5)	5 (3-7)
Respiratory support									
no O2	20 (62%)	0 (0%)	20 (33%)	48 (71%)	0 (0%)	48 (55%)	23 (55%)	0 (0%)	23 (33%)
NC	12 (38%)	0 (0%)	12 (20%)	20 (29%)	0 (0%)	20 (23%)	19 (45%)	0 (0%)	19 (28%)
NIV	0 (0%)	7 (24%)	7 (12%)	0 (0%)	5 (26%)	5 (6%)	0 (0%)	15 (56%)	15 (22%)
ETI	0 (0%)	20 (69%)	20 (33%)	0 (0%)	14 (74%)	14 (16%)	0 (0%)	12 (44%)	12 (17%)
ECMO	0 (0%)	2 (7%)	2 (3%)	0 (0%)	0 (0%)	0 (0%)	0 (0%)	0 (0%)	0 (0%)
Total metabolic risk factors (0-4)	2 (1-3)	2 (1-3)	2 (1-3)						
none	3 (9%)	6 (21%)	9 (15%)						
one or more	29 (91%)	23 (79%)	52 (85%)						

Overweight, yes*	17 (53%)	21 (72%)	38 (62%)						
Hypertension, yes	20 (63%)	15 (52%)	35 (57%)	42 (62%)	13 (69%)	55 (63%)	9 (38%)	9 (69%)	18 (49%)
Dyslipidemia, yes	13 (41%)	11 (38%)	24 (39%)	11 (16%)	3 (16%)	14 (16%)	7 (29%)	11 (85%)	18 (49%)
Diabetes, yes	9 (28%)	10 (35%)	19 (31%)	20 (29%)	9 (47%)	29 (33%)	8 (33%)	11 (85%)	19 (51%)
Total chronic diseases (0-8)	0 (0-1)	0 (0-1)	0 (0-1)						
non	22 (69%)	17 (59%)	39 (64%)						
one or more	10 (31%)	12 (41%)	22 (36%)						
Chronic renal failure, yes	4 (13%)	6 (21%)	10 (16%)	9 (13%)	2 (11%)	11 (13%)	3 (13%)	3 (23%)	6 (16%)
Chronic heart failure, yes	2 (6%)	2 (7%)	4 (7%)	12 (18%)	2 (11%)	14 (16%)	2 (8%)	0 (0%)	2 (5%)
Chronic Respiratory failure, yes	3 (9%)	5 (17%)	8 (13%)	6 (9%)	5 (26%)	11 (13%)	5 (21%)	0 (0%)	5 (14%)
Chronic Liver failure, yes	0 (0%)	0 (0%)	0 (0%)	2 (3%)	0 (0%)	2 (2%)	0 (0%)	0 (0%)	0 (0%)
Organ transplant, yes	2 (6%)	2 (7%)	4 (7%)				n/a	n/a	n/a
Immunosuppression, yes	5 (16%)	4 (14%)	9 (15%)	2 (3%)	2 (11%)	4 (5%)	0 (0%)	3 (25%)	3 (8%)
Active cancer, yes	1 (3%)	3 (10%)	4 (7%)	9 (13%)	4 (21%)	13 (15%)	3 (13%)	0 (0%)	3 (8%)
HIV, yes	1 (3%)	1 (3%)	2 (3%)	1 (2%)	0 (0%)	1 (1%)	n/a	n/a	n/a
Total risk factors (Metabolic/organ, 0-12)	2 (1-3)	3 (1-4)	2 (1-4)						
non	2 (6%)	6 (21%)	8 (13%)						
one or more	30 (94%)	23 (79%)	53 (87%)						
ICU admission, yes	3 (9%)	27 (93%)	30 (49%)	7 (10%)	17 (90%)	24 (28%)	2 (8%)	12 (80%)	14 (35%)
Intubation, yes	2 (6%)	22 (76%)	24 (39%)	7 (10%)	17 (90%)	24 (28%)	1 (4%)	9 (75%)	10 (29%)
Duration of intubation (days)	0 (0-0)	20 (4-27)	0 (0-18)				n/a	n/a	n/a
Duration of hospital stay (or in-hospital death)	10.5 (6-16)	26 (14-44)	16 (9-30)	14 (8-26.5)	23 (19-48)	18.5 (10-28)	10.5 (7.5-14.5)	21 (13-34)	12 (8-27)
Outcome									

Death up to 60 days									
alive	30 (94%)	18 (62%)	48 (79%)	61 (90%)	14 (74%)	75 (86%)	42 (100%)	16 (59%)	58 (84%)
dead	2 (6%)	11 (38%)	13 (21%)	7 (10%)	5 (26%)	12 (14%)	0 (0%)	11 (41%)	11 (16%)

Note: *N_missing=8 patients for Discovery cohort

**Only Age, sex and Days since symptom onset variables have complete data in Confirmation cohort, otherwise the partial data is available for Confirmation cohort

† Values displayed are medians, with IQR: interquartile range in parentheses for continuous variables, or percentages for categorical variables. Percentages are rounded to the nearest unit.

‡ "Non critical illness" includes hospitalized patients with no oxygen support (no O_2) (moderate disease) and oxygen support on nasal cannula (NC) only (severe, but non-critical disease)."Critical illness" includes hospitalized patients on mechanical ventilation, either : positive pressure non-invasive ventilation (NIV), endotracheal intubation (ETI), extracorporeal membrane oxygenation (ECMO).

¶ Only ICU admission and intubation are different between Non-critical and critical, due to selection bias (at $p < 0.05$) in any of the patient characteristic.

For continuous variables, statistical test: Mann-Whitney U test, unpaired t test. For categorical variables, Chi Square test.

Values highlighted in yellow are statistically different between critical and non-critical groups. Values highlighted in blue are statistically different between discovery and validation cohorts.

Values highlighted in green are statistically different between discovery and confirmation cohorts.

Table 3.2 Univariate Cox proportional hazard regression of single variables measured in COVID-19 patient plasma at DSO11.

Variable	Discovery cohort			
	All COVID-19+ at DSO11 (n=61)		Critical COVID-19+ subset at DSO11 (n=29)	
	HR(95%CI) 1 unit	p value	HR(95%CI) 1 unit	p value
Viral Load				
vRNA (copies/mL of plasma)*	**3.1 (1.9, 5.1)**	**<0.001**	**2.5 (1.4, 4.7)**	**0.004**
Serology				
RBD-specific IgG (RLU)*	**0.3 (0.1, 0.8)**	**0.011**	**0.3 (0.1, 0.7)**	**0.005**
RBD-specific IgM (RLU)*	0.5 (0.2, 1.4)	0.186	0.4 (0.1, 1.3)	0.144
RBD-specific IgA (RLU)*	**0.4 (0.2, 0.98)**	**0.045**	**0.3 (0.1, 0.8)**	**0.014**
Spike Ig (MFI)*	**0.6 (0.5, 0.9)**	**0.006**	**0.5 (0.3, 0.8)**	**0.002**
Neutralization (ID50)*	0.8 (0.6, 1.1)	0.172	**0.7 (0.5, 0.9)**	**0.020**
ADCC (%) ♦	**0.7 (0.5, 0.9)**	**0.006**	**0.1 (0.5, 0.9)**	**0.004**
Cytokines				
Angiopoietin-2*	**14.5 (3.4, 62.1)**	**0.001**	**6.7 (1.4, 33.0)**	**0.018**
CCL2/JE/MCP-1*	**5.6 (1.7, 18.4)**	**0.005**	2.8 (0.8, 10.2)	0.115
CCL20/MIP-3 alpha*	**2.9 (1.2, 6.8)**	**0.016**	1.4 (0.5, 4.0)	0.578
CCL7/MCP-3/MARC*	4.0 (1.0, 15.6)	0.050	5.2 (0.9, 30.7)	0.068
CD40 Ligand/TNFSF5*	**5.6 (1.0, 30.8)**	**0.049**	6.7 (0.8, 55.7)	0.080

CXCL10/IP-10/CRG-2*	16.7 (0.7, 423.5)	0.088	5.5 (0.2, 161.2)	0.323
CXCL13/BLC/BCA-1*	**6.7 (2.6, 17.2)**	**<0.001**	**4.3 (1.6, 11.7)**	**0.005**
IL-8/CXCL8*	**5.6 (1.7, 18.6)**	**0.005**	**3.8 (1.0, 14.3)**	**0.048**
CXCL9/MIG*	2.2 (0.8, 6.4)	0.133	1.2 (0.5, 2.9)	0.621
D-dimer*	5.0 (0.5, 49.9)	0.174	0.4 (0.02, 8.5)	0.548
G-CSF*	**3.3 (1.1, 10.2)**	**0.034**	**3.5 (1.1, 10.8)**	**0.032**
GM-CSF*	**9.4 (1.7, 50.7)**	**0.009**	**7.3 (1.02, 51.4)**	**0.047**
IFNα*	2.4 (0.9, 6.5)	0.087	2.4 (0.8, 7.0)	0.114
IL-1ra/IL-1F3*	**8.0 (1.9, 33.7)**	**0.004**	2.8 (0.6, 14.4)	0.214
IL-23*	**13.7 (2.2, 85.6)**	**0.005**	**7.2 (1.1, 46.3)**	**0.038**
IL-6*	**2.6 (1.4, 5.0)**	**0.003**	1.5 (0.7, 3.3)	0.315
SP-D*	**5.2 (1.0, 26.3)**	**0.047**	2.2 (0.3, 15.7)	0.433
TNFα*	**16.5 (2.7, 102.5)**	**0.003**	6.6 (0.9, 50.9)	0.069
RAGE/AGER*	**7.9 (2.3, 27.9)**	**0.001**	**4.4 (1.01, 18.9)**	**0.049**
CytoScore**	**2.6 (1.6, 4.2)**	**<0.001**	**1.9 (1.1, 3.4)**	**0.0335**

*Variables are $\log_{10}$ transformed. HR shown are for an increase of 1 unit of $\log_{10}$-transformed variable.

**Refer to Material and Methods for details.

♦HR for increase of 10 units.

RLU = Relative Light Units, normalized to internal control (CR3022) (see methods for details). ADCC = antibody-dependent cellular cytotoxicity

Supplemental Data

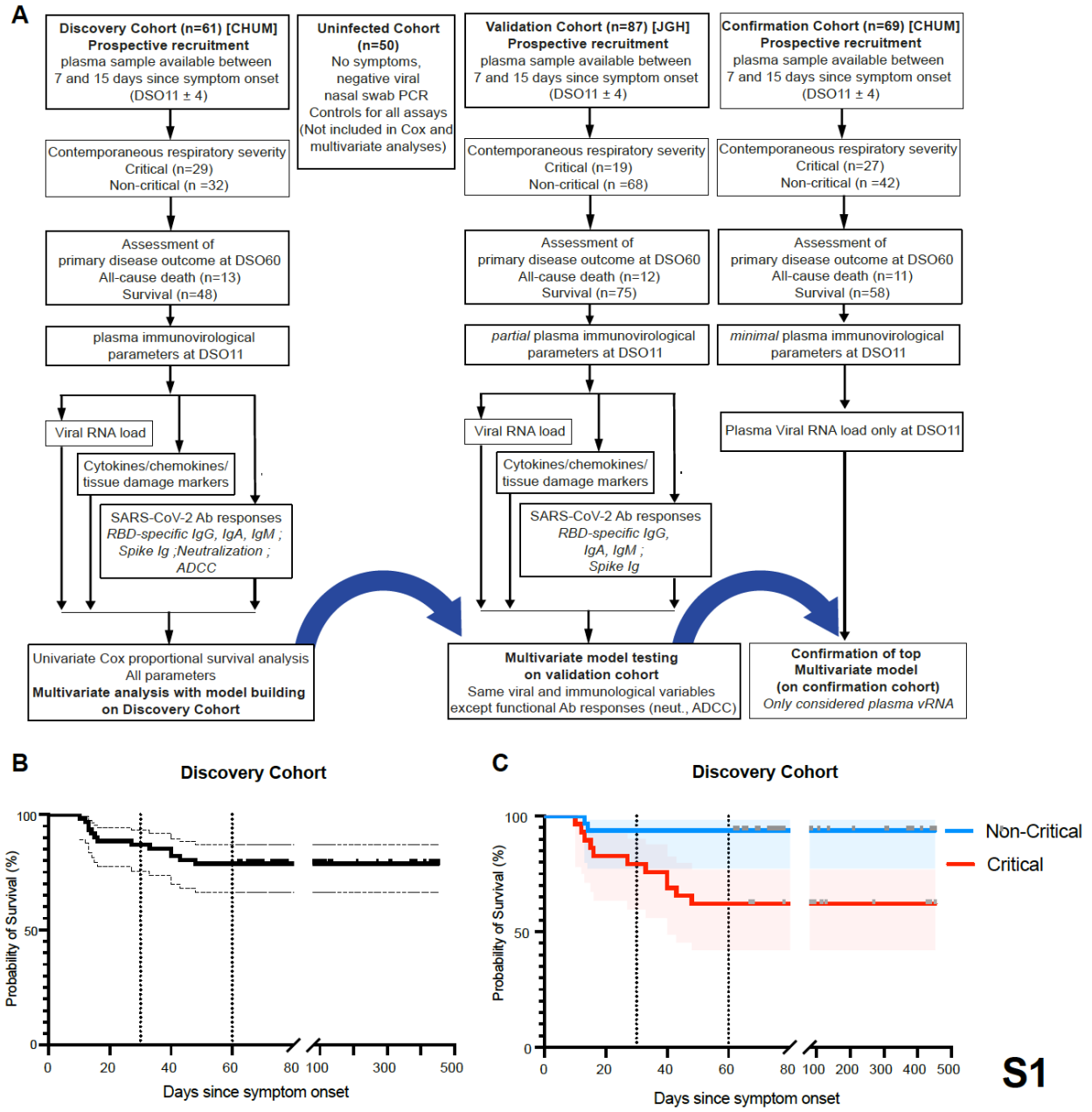

Fig. S3.1 **Study design** (A) Study Design and analyses performed on the three COVID-19 cohorts (discovery, n=61; validation, n=87; and confirmation, n=69) and the uninfected cohort. In addition, 62 patients who were sampled at very early time points (before DSO7) were included for longitudinal testing of selected models. (B) Survival curve in the discovery cohort based on days since symptom onset. (C) Within the discovery cohort, Kaplan-Meier analysis of survival in Non-critical (blue) compared to Critical (red) subgroups, whose disease severity was assessed at DSO11. Curves compared using Log-rank (Mantel-Cox) test. n = 61 COVID-19 patients (13 fatalities).

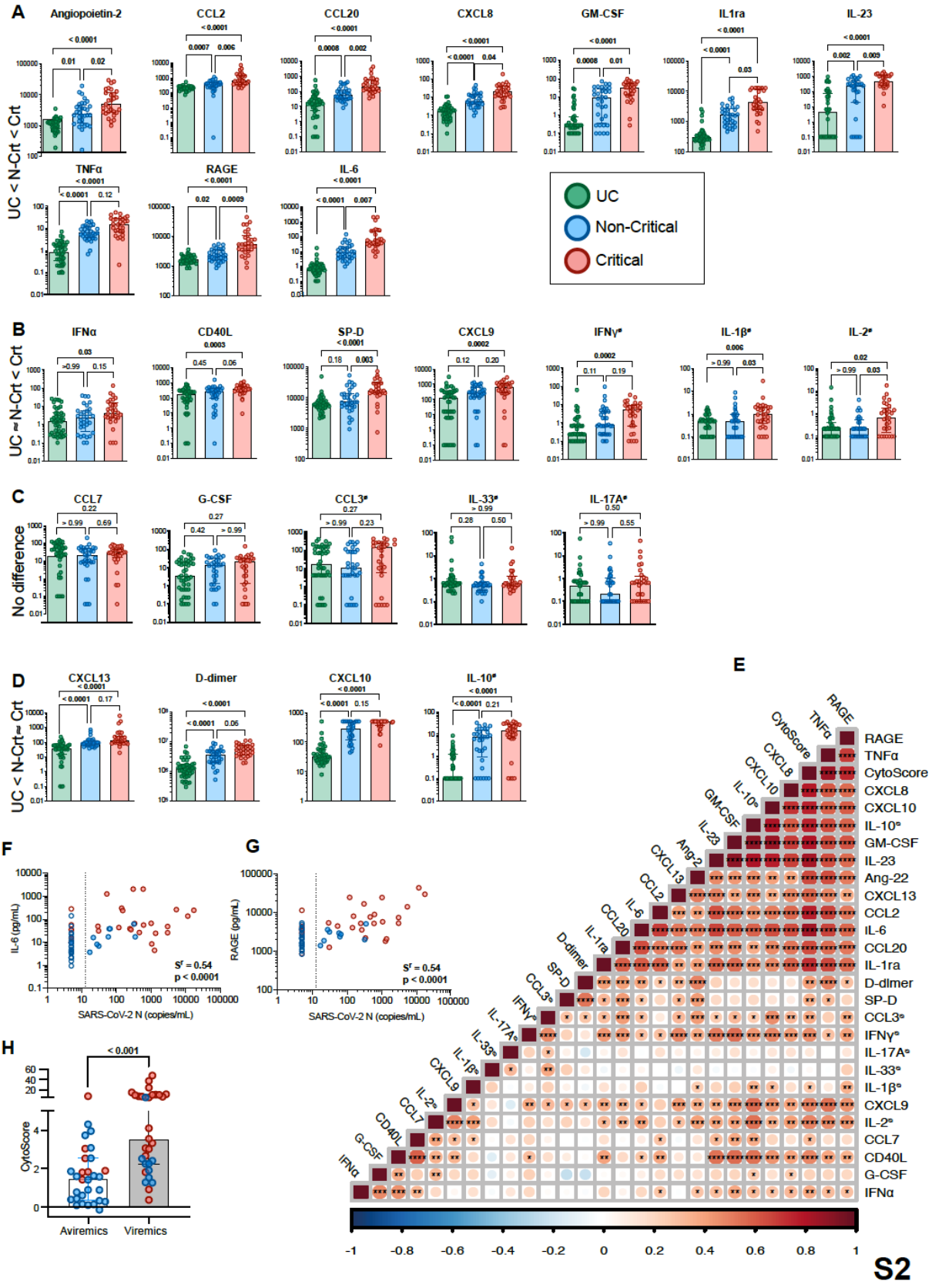
A
Angiopoietin-2
CCL2
CCL20
CXCL8
GM-CSF
IL1ra
IL-23
TNFα
RAGE
IL-6
UC < N-Crt < Crt
UC
Non-Critical
Critical
B
IFNα
CD40L
SP-D
CXCL9
IFNγ*
IL-1β*
IL-2*
UC ≈ N-Crt < Crt
C
CCL7
G-CSF
CCL3*
IL-33*
IL-17A*
No difference
D
CXCL13
D-dimer
CXCL10
IL-10*
UC < N-Crt ≈ Crt
E
RAGE
TNFα
CytoScore
CXCL8
CXCL10
IL-10*
GM-CSF
IL-23
Ang-22
CXCL13
CCL2
IL-6
CCL20
IL-1ra
D-dimer
SP-D
CCL3*
IFNγ*
IL-17A*
IL-33*
IL-1β*
CXCL9
IL-2*
CCL7
CD40L
G-CSF
IFNα
-1
-0.8
-0.6
-0.4
-0.2
0
0.2
0.4
0.6
0.8
1
F
IL-6 (pg/mL)
SARS-CoV-2 N (copies/mL)
S² = 0.54
p < 0.0001
G
RAGE (pg/mL)
SARS-CoV-2 N (copies/mL)
S² = 0.54
p < 0.0001
H
CytoScore
Aviremics
Viremics
< 0.001
S2

Fig. S3.2 Inflammatory cytokines, chemokines and markers of tissue damage are increased in critical cases of COVID-19. (A-D) Comparison of cytokine concentrations between critical COVID-19, non-critical COVID-19 and UC. Cytokines and markers of tissue damage grouped according to differential detection: (**A)** Greatest in critical (Crt), but also higher in non-critical (N-Crt) compared to UC; (**B)** Similar between UC and non-critical, but greater in critical COVID-19; (**C)** No differences between all three groups; (**D)** Greater in COVID-19 compared to UC, but similar between non-critical and critical. (**E)** Correlation matrix of all 26 plasma analytes and CytoScore (see methods for details on CytoScore). Color of circle represents Spearman R value (red = 1, blue = -1) and respective p values are represented by * within circles ($p < 0.05$ = *; $p < 0.01$ =** ; $p<0.001$=*** ; $p<0.0001$=****). (**FG)** Correlation of plasma vRNA and plasma concentration of (**F)** IL-6 or (**G)** RAGE (pg/mL). (**H)** Comparison of CytoScore between aviremics (<13 vRNA copies/mL) and viremics ($\geq$ 13 copies/mL). Mann-Whitney test. A-D) Kruskall-Wallis with Dunn's multiple comparisons test. For A-D, F-H, color-coded dots represent severity of the patient at DSO11 (red = critical, blue = non-critical, green=UC). For A-E, cytokines with titles annotated by $\varnothing$ are poorly detected (see methods for details). n = 61 COVID-19 subjects (13 mortalities) and 43 UC.

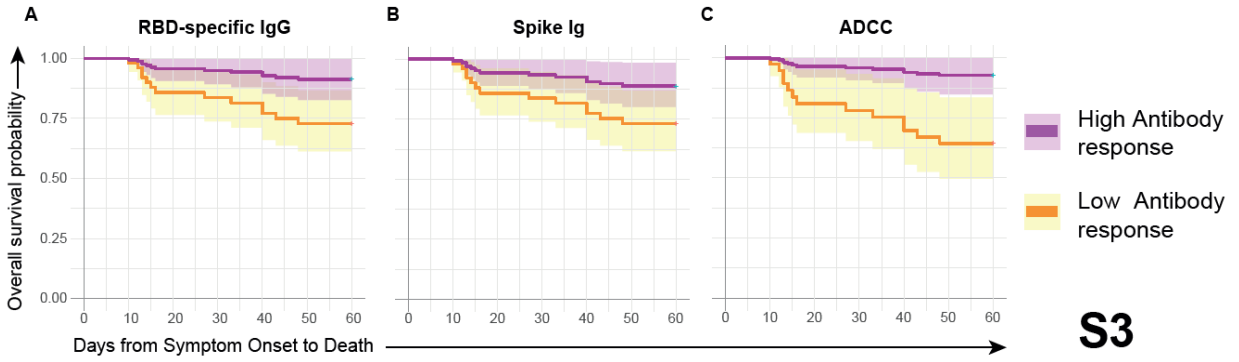

Fig. S3.3 Association of poor outcome with low RBD-specific IgG titers is maintained in the critical COVID-19 group. (A-C) Modelisation of the predicted survival curves of patients with high (orange) or low (purple) (**A)** RBD-specific IgG, (**B)** Spike-specific Ig or (**C)** ADCC activity in critical COVID-19 patients. n = 29 Critical COVID-19 cases (11 mortalities). The predicted values were calculated from the respective Cox regression models.

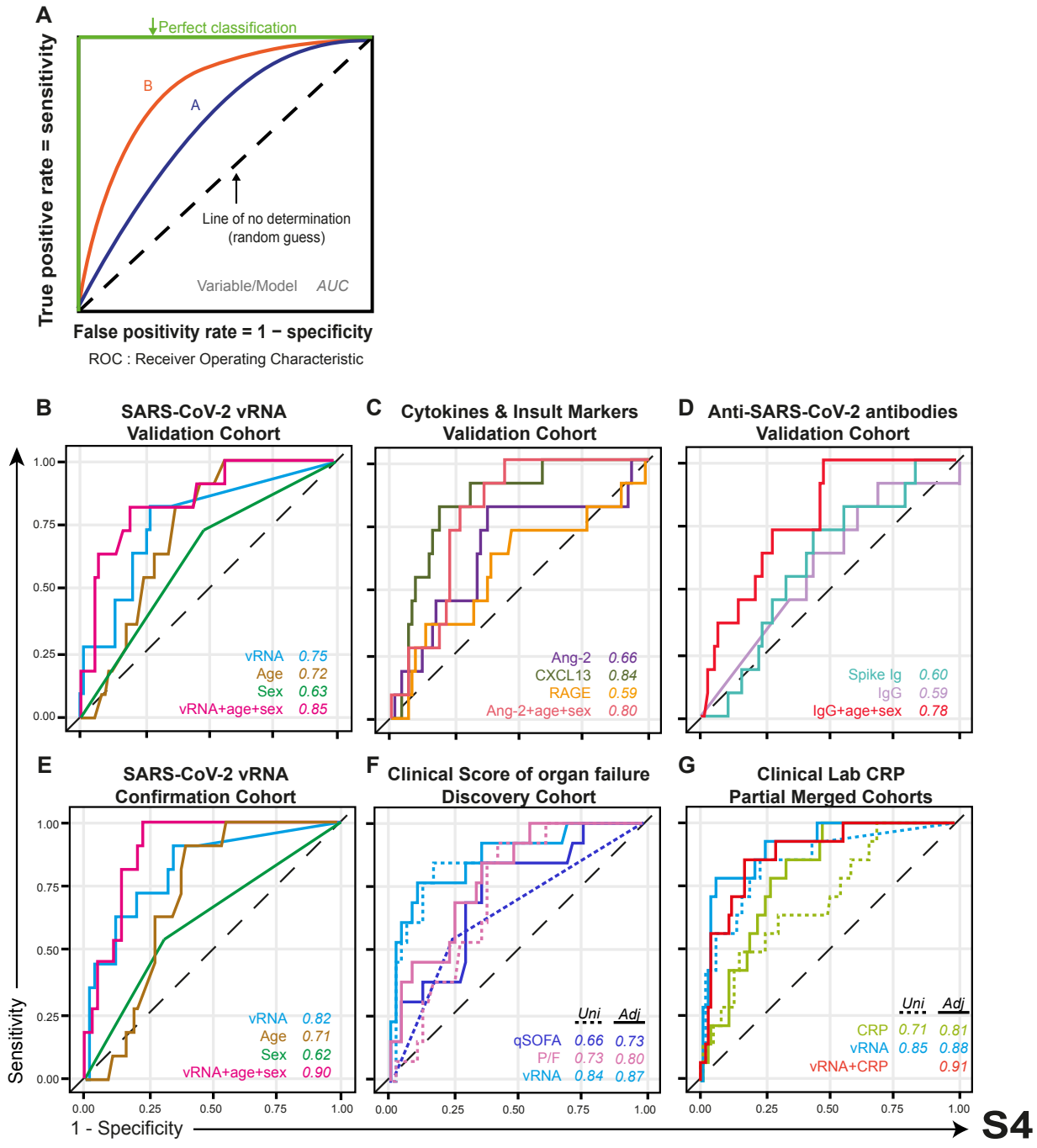

Fig. S3.4 Reproducibility of predictive accuracy for mortality in the validation and confirmation cohorts. **A**) Concept of time-dependent ROC curves. A ROC is defined by the false-positive rate and true-positive rate, which depicts relative trade-offs resulting from changing the test threshold. The best possible prediction model (100% sensitivity and 100% specificity) would yield a “square curve”, reaching the upper left corner (green line). A completely random guess (chance) would give a point along the diagonal dotted black line (line of no determination). In the present study, the ROC curves were used compare the predictive accuracy of different immunovirological parameters measured in plasma at DSO11. These ROC curves were time-dependent, meaning they vary depending on the time between symptom onset and death considered. Here, model B is superior to A. ROC curves are further characterized by AUC, a measure of

test accuracy (1.0= best possible test; 0.5=no discrimination). **(B-G)** Time-dependent ROC curves measured (**B-D**) within the validation cohort for (**B)** plasma vRNA, age and sex, (**C)** Cytokines and tissue insult markers or (**D)** anti-SARS-CoV-2 antibody responses; (**E**) within the confirmation cohort for plasma vRNA, age and sex; (**F)** within the discovery cohort for quick SOFA (qSOFA) and P/F ratio; **(G)** within a combination of samples across cohorts (those for whom CRP clinical lab quantitation was available within the DSO11 time point) for CRP clinical lab measurements and vRNA in the same subset of patients. (B-G) Legends with color-coded variables are on the bottom left of panels, and values in italic are the AUC at 60 days after symptom onset associated to the variable or model. For (FG), ROC curves of adjusted values (age+sex) are in continuous lines, whereas models for univariate analyses are in dashed lines. AUC values are given at 30 days or 60 days after symptom onset. (B-D): n = 87; (E) n = 69; (F) n = 61; (G) n = 113. See Supplemental Table 2 for details.

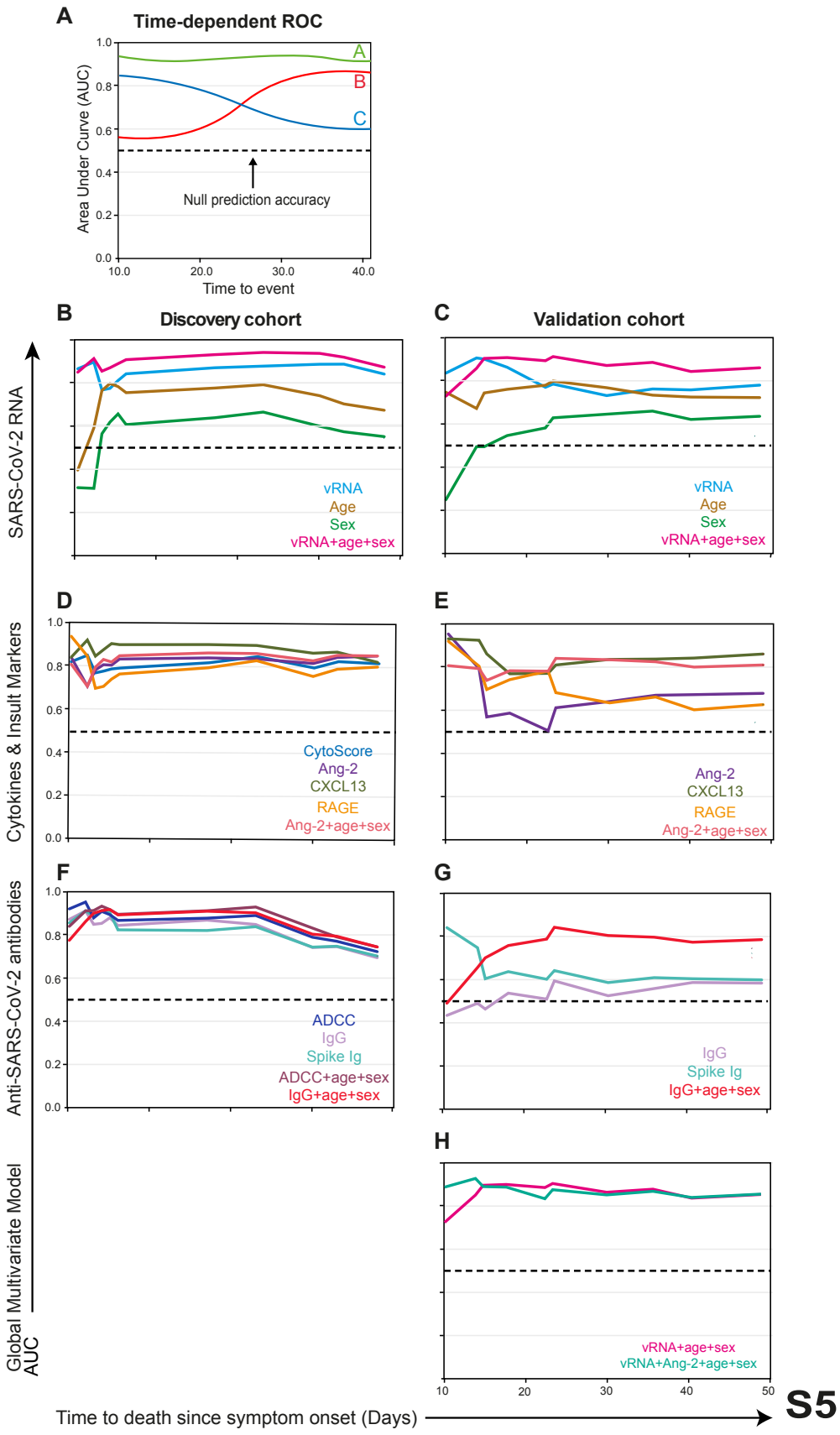
A
Time-dependent ROC
Area Under Curve (AUC)
Time to event
Null prediction accuracy
A
B
C
B
Discovery cohort
C
Validation cohort
SARS-CoV-2 RNA
vRNA
Age
Sex
vRNA+age+sex
D
E
Cytokines & Insult Markers
CytoScore
Ang-2
CXCL13
RAGE
Ang-2+age+sex
F
G
Anti-SARS-CoV-2 antibodies
ADCC
IgG
Spike Ig
ADCC+age+sex
IgG+age+sex
H
Global Multivariate Model AUC
vRNA+Ang-2+age+sex
Time to death since symptom onset (Days)
S5

Fig. S3.5 Predictive accuracy of immunovirological markers over time, in the discovery and validation cohorts. **A**) Concept of time-dependent AUC changes. To observe changing accuracy overtime, AUCs for a given measurement were plotted against time to death. AUC values closer to 1 (top) have better predictive accuracy; AUC values close to 0.5 have poor prediction accuracy. In this example, measurement A maintained the greatest prediction accuracy throughout time, whereas C > B before DSO30, then B > C after DSO30. (**B)** Time-dependent AUC of plasma vRNA, age and sex for validation cohort; (**CD)** Time-dependent AUC of plasma cytokines and tissue damage markers for (**C**) discovery cohort or (**D**) validation cohort; (**EF)** Time-dependent AUC of SARS-CoV-2 antibody responses for (**E**) discovery cohort or (**F**) validation cohort. (**GH**) Time-dependent AUC for top measurements captured by multivariate model analysis in the (**G**) discovery cohort or (**H**) validation cohort. n = 61 for discovery cohort; 87 for validation cohort. Legends with color-coded variables are on the bottom left of panels, and values in italic are the AUC values associated to the variable.

Table S3.1. Full list of analytes measured in plasma by beads arrays

Analyte	Bead Region
Angiopoietin-2	26
CCL3/MIP-1 alpha	35
CCL20/MIP-3 alpha	33
CXCL9/MIG	52
CXCL13/BCA-1	28
G-CSF	54
IFNα	63
IL-1β/IL-1F2	57
IL-2	27
IL-8/CXCL8	18
IL-17/IL-17A	43
IL-33	14
SP-D	62
CCL2/JE/MCP-1	25
CCL7/MCP-3/MARC	37
CD40 Ligand/TNFSF5	74
CXCL10/IP-10/CGR-2	21
D-dimer	43
GM-CSF	46
IFN-γ	29
IL-1ra/IL-1F3	30
IL-6	13
IL-10	22
IL-23	76
RAGE/AGER	45
TNFα	12

Human Magnetic Luminex ® Assays, from R&D Systems (Biotechne)
Premixed Multiplex
Kit Catalog Numbers : LXSAHM-26
Kit Lot Number : L134818

Table S3.2 Time-dependent AUC for representative variables per category in all three cohorts.

Cohort	Model[a]		DSO30[b]	DSO60[b]	Overall: IAUC[c]	Maximum AUC[d]	Time Max AUC[e]
Discovery n=61	vRNA	Not-adjusted	**0.87 (0.76, 0.98)**	**0.84 (0.72, 0.96)**	0.84	**0.90 (0.83, 0.96)**	12
		Adjusted	**0.93 (0.82, 1.00)**	**0.87 (0.76, 0.99)**	0.90	**0.94 (0.84, 1.00)**	33
	Ang-2	Not-adjusted	**0.85 (0.53, 1.00)**	**0.86 (0.55, 1.00)**	0.82	**0.86 (0.55, 1.00)**	48
		Adjusted	**0.87 (0.54, 1.00)**	**0.86 (0.54, 1.00)**	0.83	**0.87 (0.54, 1.00)**	27
	IgG	Not-adjusted	**0.88 (0.60, 1.00)**	0.71 (0.44, 0.97)	0.84	**0.92 (0.63, 1.00)**	12
		Adjusted	**0.93 (0.71, 1.00)**	**0.76 (0.58, 0.95)**	0.88	**0.94 (0.71, 1.00)**	15
	vRNA +Ang2	Not-adjusted	**0.91 (0.58, 1.00)**	**0.91 (0.60, 1.00)**	0.88	**0.93 (0.60, 1.00)**	43
		Adjusted	**0.95 (0.64, 1.00)**	**0.91 (0.62, 1.00)**	0.91	**0.96 (0.65, 1.00)**	33
Validation n=87	vRNA	Not-adjusted	**0.73 (0.55, 0.91)**	**0.75 (0.59, 0.92)**	0.82	**0.92 (0.82, 1.00)**	12
		Adjusted	**0.89 (0.67, 1.00)**	**0.85 (0.65, 1.00)**	0.89	**0.93 (0.70, 1.00)**	22
	Ang-2	Not-adjusted	0.63 (0.13, 1.00)	0.66 (0.14, 1.00)	0.65	0.95 (0.19, 1.00)	8
		Adjusted	0.83 (0.28, 1.00)	0.80 (0.26, 1.00)	0.79	0.84 (0.29, 1.00)	22
	IgG	Not-adjusted	0.52 (0.04, 1.00)	0.59 (0.06, 1.00)	0.53	0.59 (0.08, 1.00)	22
		Adjusted	0.81 (0.50, 1.00)	0.78 (0.48, 1.00)	0.75	**0.85 (0.52, 1.00)**	22
	vRNA +Ang2	Not-adjusted	0.74 (0.24, 1.00)	0.77 (0.25, 1.00)	0.81	0.96 (0.30, 1.00)	12
		Adjusted	0.87 (0.30, 1.00)	0.86 (0.29, 1.00)	0.90	0.95 (0.32, 1.00)	12
Confirmation n=69	vRNA	Not-adjusted	**0.77 (0.53, 1.00)**	**0.82 (0.68, 0.97)**	0.83	**0.98 (0.95, 1.00)**	19
		Adjusted	**0.90 (0.81, 1.00)**	**0.90 (0.84, 0.96)**	0.91	**0.95 (0.85, 1.00)**	19

Values are AUC (95%CI), and AUC at $p<0.05$ are in bold.
[a] AUC values given either not adjusted (only variable(s) listed) or adjusted (age and sex).
[b] AUC values are given at 30 days or 60 days after symptom onset
[c] Integrated AUC (IAUC) is the average of all AUC from DSO10-60.
[d] Maximum AUC is the best prediction accuracy of the variable (measured at DSO11)
[e] Date since symptom onset at which that maximum AUC was achieved

Table S3.3 Comparison between time-dependent AUC for clinically-collected variables and plasma vRNA.

Cohort	Variable[a]		HR (95%CI)	P value	AUC at DSO60[b]	IAUC[c]
Discovery (n=61)	vRNA[d]	Not Adjusted	**3.13 (1.90, 5.17)**	**< 0.001**	**0.84 (0.72, 0.96)**	**0.84**
		Adjusted	**3.53 (2.03, 6.16)**	**< 0.001**	**0.87 (0.76, 0.99)**	**0.90**
	qSOFA[e]	Not Adjusted	**3.25 (1.09, 9.70)**	**0.03**	0.65 (0.43, 0.88)	0.66
		Adjusted	**3.35 (1.10, 10.23)**	**0.03**	**0.73 (0.58, 0.88)**	**0.76**
	P/F[f]	Not Adjusted	**0.91 (0.85, 0.98)**	**0.02**	**0.73 (0.59, 0.86)**	**0.78**
		Adjusted	**0.91 (0.84, 0.98)**	**0.01**	**0.80 (0.68, 0.91)**	**0.84**
	vRNA + qSOFA	Adjusted				
		vRNA	**3.65 (1.79; 7.44)**	**<0.001**	**0.85 (0.73; 0.97)**	**0.85**
		qSOFA	0.61 (0.13; 2.87)	0.53		
	vRNA + P/F	Adjusted				
		vRNA	**2.57 (1.46; 4.50)**	**0.001**	**0.88 (0.75; 1.00)**	**0.87**
		P/F	0.99 (0.99; 1.003)	0.24		
Merged Cohort[g] (n=113, 98 survivor and 15 non-survivor)	vRNA	Not Adjusted	**2.59 (1.78; 3.76)**	**< 0.001**	**0.85 (0.74; 0.96)**	**0.87**
	CRP[d]	Not Adjusted	**4.73 (1.44 ; 15.50)**	**0.01**	**0.71 (0.49; 0.93)**	**0.62**
	vRNA + CRP	Not Adjusted				
		vRNA	**2.69 (1.79; 4.05)**	**< 0.001**	**0.87 (0.75; 0.99)**	**0.86**
		CRP[d]	**4.15 (1.17; 14.68)**	**0.03**		
	vRNA + CRP	Adjusted				
		vRNA	**2.82 (1.72; 4.62)**	**< 0.001**	**0.91 (0.83; 0.99)**	**0.93**
		CRP[d]	**4.01 (0.97; 16.67)**	**0.06**		
		age	**1.05 (1.01; 1.09)**	**0.008**		
		sex	0.39 (0.10; 1.53)	0.18		

Values are Hazard ratio (HR) (95%Confidence interval CI) with p value, and AUC. p<0.05 are in bold.

[a] AUC values given either not adjusted (only variable(s) listed) or adjusted (age and sex). For multivariate models, AUC is given for each parameter *within* the model.

[b] AUC values are given at 60 days after symptom onset

[c] Integrated AUC (IAUC) is the average of all AUC from DSO10-60.

[d] HR value is given for every increase in 1 log unit.

[e] HR value is given for high qSOFA (>=2) vs low qSOFA (<=1) (categorical values).

[f] HR values given for every 10 unit increase.

[g] Includes patients among the three merged cohorts for whom clinical lab CRP measurements were available at DSO11.

Table S3.4 Predictive accuracy of plasma vRNA measured at different times after symptom onset.

Median DSO [range]	Total [#]	Non-survivor	Model[a]	Hazard Ratio		AUC	
				HR(95%CI)	P-value	AUC at DSO60[b]	IAUC[c]
DSO5 [3-7]	80	15	Not-adjusted	2.32 (1.52, 3.55)	0.0001	0.76 (0.63, 0.89)	0.82
			Adjusted	2.03 (1.34, 3.06)	0.0007	0.83 (0.70, 0.96)	0.89
DSO9 [8-11]	164	21	Not-adjusted	3.03 (2.11, 4.34)	< 0.0001	0.86 (0.77, 0.95)	0.87
			Adjusted	2.82 (1.99, 4.00)	< 0.0001	0.89 (0.82, 0.97)	0.90
DSO13 [12-15]	127	17	Not-adjusted	2.88 (1.80, 4.62)	< 0.0001	0.77 (0.64, 0.90)	0.81
			Adjusted	3.37 (2.05, 5.54)	< 0.0001	0.82 (0.68, 0.95)	0.89

[#] Total of 371 samples collected on 279 patients
Values are Hazard ratio (HR) (95%Confidence interval CI) with p value, and AUC. p<0.05 are in bold. All values relate to plasma vRNA (for an increase of 1 unit of copies/mL)
[a] HR and AUC values given either not adjusted (only variable(s) listed) or adjusted (age and sex).
[b] AUC values are given at 60 days after symptom onset
[c] Integrated AUC (IAUC) is the average of all AUC from DSO10-60.

Chapter 4 – Dimensionality reduction for stepwise analysis of immune response dynamics in COVID19

Status: This manuscript is under preparation.

Authors contributions:

Conceptualization: EBR, SM, DEK, GW, KM.

Data Curation: EBR, SM, ML, JB, CO, MMP, CL, DEK, RMR, GBL, DM, TN, SZ

Formal analysis: EBR, SM, HR, LM, SPR, PG, GMB, AD, GBB, AP, RG, JR, DEK

Funding acquisition: DEK, AF, NC, NA, AP, CL, JBR, MT, MD

Investigation/experiments: SPR, PG, EBR, GBB, AP, MB, FP, RG, AL, JR, JP, GG, JN, MN, GS, HM, CB, JDD, MB, GGL

Biostatistical methodology: SM, JB

Patient recruitment and cohort administration: NB, DM, MMP, LL, AP, MD, JBR, MC, DEK

Visualization: EBR, SM, JB, ML, HR

Supervision: GW, KM, DEK, LB, MT, NC, AF

Writing – original draft: EBR, SM, DEK

Authors : Elsa Brunet-Ratnasingham*, Sacha Morin*, Haley Randolph*, Marjorie Labrecque, Xiaoyan Deng, Lorie Marchitto, Amélie Pagliuzza, Rose Cloutier, Dani Vézina, Mélanie Laporte, Nathalie Brassard[1], Guillaume Beaudoin-Bussières[1,2], Mehdi Benlarbi[1], Floriane Point[1], Jérémie Prévost[1,2], Annemarie Laumaea[1], Julia Niessl[1,2,], Manon

Nayrac[1], Gérémy Sannier[1,2], Catherine Orban[1,4], Marc Messier-Peet[1,4], Guillaume Butler-Laporte[5,6], David R. Morrison[5], Sirui Zhou[5,6], Tomoko Nakanishi[5,7,8,9], Marianne Boutin[1,2], Jade Descôteux-Dinelle[1,2], Gabrielle Gendron-Lepage[1], Guillaume Goyette[1], Catherine Bourassa[1], Halima Medjahed[1], Laetitia Laurent[5], J. Brent Richards[5,6,7,11], Michaël Chassé[1,4], Madeleine Durand[1,4], Nicolas Chomont, Andrés Finzi, Morgan Craig, Martine Tétreault[1,10],Michael Hultstrom, **Luis Barreiro**, **Kevin Moon**, **Guy Wolf** and **Daniel E. Kaufmann**

Affiliations :

1Research Centre of the Centre Hospitalier de l'Université de Montréal (CRCHUM), Montréal, QC, Canada.

2Département de Microbiologie, Infectiologie et Immunologie, Université de Montréal, Montréal, QC, Canada.

3Department of Microbiology and Immunology, McGill University, Montréal, Quebec, Canada

4Centre hospitalier de l'Université de Montréal (CHUM), Montréal, QC, Canada

5Lady Davis Institute, Jewish General Hospital, McGill University, Montreal, QC, Canada

6Department of Epidemiology, Biostatistics and Occupational Health, McGill University, Montreal, QC, Canada

7Department of Human Genetics, McGill University, Montreal, QC, Canada

8Kyoto-McGill International Collaborative School in Genomic Medicine, Gaduate School of Medicine, Kyoto University, Kyoto, Japan

9Research Fellow, Japan Society for the Promotion of Science.

10Department of Neuroscience, Université de Montréal, Montréal, QC, Canada

11Department of Twin Research, King's College London, London, UK

12Center for HIV/AIDS Vaccine Immunology and Immunogen Discovery, La Jolla, CA, USA.

†Contributed equally

*Co-corresponding authors. Email: Guy Wolf; Daniel E Kaufmann daniel.kaufmann@umontreal.ca

Abstract

COVID-19 is highly heterogeneous in clinical severity and outcome. Considerable advances have uncovered biomolecular traits associated with fatal outcome. However, novel analytical tools are needed to rapidly and accurately delineate patient subgroups with various immunovirological profiles, analyze diverging disease trajectories and prioritize in-depth molecular studies.

To find how immunovirological features are interrelated, we profiled 12 plasma analytes (SARS-CoV-2 vRNA, SARS-COV-2-specifc antibodies, cytokine and tissue injury markers) in 500 acute longitudinal plasma samples collected from 214 hospitalized COVID-19 patients. We analyzed them simultaneously using PHATE algorithm (potential of heat diffusion for affinity-based transition embedding, Moon et al, Nature Biotech 2019), which can reduce multiple input variables to two salient features for visualization. We performed whole blood transcriptomic analyses to identify molecular signatures associated with survival vs death in a patient cluster identified as being at extreme mortality risk.

PHATE analysis of samples collected 11 days after symptom onset (DSO11) revealed four distinct k-means clusters of patients, which aligned with disease severity and outcome. Two groups were highly enriched in critical patients requiring mechanical ventilation: a high-fatality critical cluster 1 accounted for 67% of fatal outcomes (14/21) by DSO60, while critical cluster 2 had good prognosis. Clusters 3 and 4 consisted almost entirely of non-critical survivors delineated respectively by low and high antibody responses. Averaged trajectories between DSO3 to DSO30 diverged between clusters. All patients of the high-fatality cluster had detectable plasma vRNA, which lingered unlike the critical survivor cluster. Their antibody response had a multiple-day delay, while their cytokine profile diverged from the other clusters by DSO8, remaining distinct until DSO22.

This unbiased approach gives an integrated view of dysregulated immune response components in fatal COVID-19, which may be explained through differences in molecular pathways. This approach allows to efficiently target detailed investigations on very high-risk patient subgroups who may most likely benefit from new therapeutic interventions.

Introduction

COVID-19 is a highly heterogeneous disease which from asymptomatic infection to fatal outcome and is caused by SARS-CoV-2 infection. While pre-existing conditions have been linked to increased COVID-19 severity (Williamson et al., 2020), it is still unclear what mechanisms drive COVID-19 to progress to fatal outcome.

Research addressing how differences in immune responses can contribute to separate outcome has revealed multiple factors likely important. We (Brunet-Ratnasingham et al., 2021) and others (Pujadas et al., 2020) have shown that SARS-CoV-2 plasma viral RNA can predict fatal outcome in COVID-19 patients. However, some patients succombed to their infection in the absence of high plasma vRNA or, in reverse, patients with high vRNA which survived (Brunet-Ratnasingham et al., 2021), suggesting a role for additional factors.

High amount of inflammatory cytokines, which spur on inflammation, have also been linked with fatal outcome (Laing et al., 2020 ; Lucas et al., 2020). These cytokines likely play a role in immupathology, since immunomodulatory treatments such as IL-6R antagonists (Group, 2021), systemic corticosteroids (Group, 2020) and JAK inhibitors (Group, 2021) have a proven benefit for survival. In addition, a delay in antibody response (Zohar et al., 2020), possibly linked to disrupted coordination between virus-specific T and B cell responses (Rydyznski Moderbacker et al., 2020), has also been observed in patients with fatal outcome. However, antibody responses were not as strong predictors as viral RNA, the cohort of COVID-19 survivors did present with a wide range antibody early in their infection (Brunet-Ratnasingham et al., 2021). Furthermore, monoclonal antibodies (Group, 2021) and plasma transfer therapy (Bégin et al., 2021) have not shown

a proven benefit of survival, perhaps reflecting a less decisive role for these proteins than inflammation, at least by the time treatment can be administered.

Although interplay between these compartments have been observed (positive association between plasma vRNA and cytokines, both of which correlate negatively with antibody response), we still lack comprehensive systems biology overview that take into account the timing of the disease, of critical importance given the dynamic nature of the immune response. As such, we aimed to subdivide patients into meaningful clusters, based on their immunovirological plasma profiles early in infection, and track their progression over time. We could identify four distinct patients clusters, with one cluster highly enriched in fatal outcome. These four patient clusters revealed differences in kinetics of antibody development, lingering of plasma vRNA and the amount of inflammatory cytokines and tissue damage markers. This unbiased approach allowed for better understanding of the heterogeneity of hospitalized COVID-19 patients, with implications for choice and timing of therapeutic interventions.

Material and methods

Participants and samples

SARS-CoV-2 positive patients admitted to the Centre Hospitalier de l'Université de Montréal (CHUM) or the Jewish General Hospital (JGH) were recruited into the Biobanque Québécoise de la COVID-19 (BQC19) (58). Samples from CHUM made up the discovery and confirmation cohort, and samples from JGH were the validation cohort. Blood draws were performed at baseline and when possible, at Day 2 (± 3 days) and Day 7 (± 3 days) after enrollment. The study was approved by the respective IRBs and written, informed consent obtained from all participants or, when incapacitated, their legal guardian before enrollment and sample collection. Blood draws were also performed on 50 asymptomatic, NSW PCR negative uninfected controls (UC).

COVID-19 hospitalized patients were stratified based on severity of respiratory support at the DSO11 timepoint: critical patients required mechanical ventilation (endotracheal, non-invasive ventilation, extracorporeal membrane oxygenation - ECMO), and non-critical patients, encompassing patients with moderate disease required no supplemental oxygen and patients with severe disease required nasal cannula for oxygen. Mortality was followed up to 60 days. Medical charts were reviewed by two physicians for data collection on demographics, co-morbidities, risk factors, severity state, time of infection, etc (see Table 1). Median age and range for UC cohort was 37 (32-46), and 30 individuals were males (60%).

In the course of acquiring the datasets of Manuscript 1, we screened multiple timepoints by most of the same techniques. The longitudinal samples were taken at time of

enrollment, and after 2 days, 7 days, 14 days and 30 days, and the measurements were plasma vRNA quantities, ELISA-based measurements of RBD-specific IgG, IgM and IgA, and all 26 analytes acquired by Luminex (*for detailed methods, please see Material and Methods of Manuscript 1*). Viral RNA measurements and ELISA measurements required no correction.

Quantification of SARS-CoV2 RNA

Absolute copy numbers of SARS-CoV-2 RNA (N region) in plasma samples were measured by real time PCR. Total RNA was extracted from 230 µL of plasma collected on ACD using the QIAamp Viral RNA Mini Kit (Qiagen Cat. No. 52906). Two master reaction mixes with specific primers and probes were prepared for quantification of N gene from SARS-CoV-2 and 18S (as a control for efficient extraction and amplification). Absolute copy numbers N region in were measured by real time PCR. A positive and no-template controls were included in all experiments. Purified RNA N transcripts (1328 bp) were quantified by Nanodrop and the RNA copy numbers were calculated using the ENDMEMO online tool (see STAR methods for details).

Measurements of plasma analytes by beads array

Duplicates of SARS-CoV-2-inactivated plasma samples were analyzed using a customized Human Magnetix Luminex Assay (LXSAHM-26, R&D).

While the first set of CHUM samples had been acquired on a BioPlex, first-wave JGH samples and onwards were acquired using a newly-acquired MagPix, as the BioPlex had technical problems. 30 samples acquired on the Bioplex were repeated on the MagPix, and a linear regression was performed for each analyte between both rounds of

acquisition using GraphPad Prism 9. These regressions were then used for batch correction of the samples acquired on the BioPlex samples. For certain analytes, the batch correction could not be performed for all samples given differences in the lower limits of detection between the two machines: there were missing values for the analytes CCL20, CCL3, CCL7, IFNa, GM-CSF, IL-10, IL-17A, IL-1b, IL-2, and IL-33. As PHATE requires complete datasets, we tried imputing these missing data with two different methods (mean imputation and k-Nearest Neighbor Imputation); however, these methods resulted in artificial clustering of samples which had missing values. Thus, these analytes were excluded. Exploratory analyses revealed that retaining only 8 analytes gave the cleanest clusters, as analytes with little discrimination blurred the differences. These 8 final analytes included in the analysis were TNFa, CXCL13, IL-6, IL-23, CXCL8/IL-8, angiopoietin-2, RAGE and Surfactant Protein D, all of which were significantly associated to fatal outcome in our previous work (see Manuscript 1).

Serology measurements

Plasma from uninfected donors were used as negative controls and used to calculate the seropositivity threshold in our ELISA and flow cytometry assays. The monoclonal antibody CR3022(59) was used as a positive control.

RBD-specific ELISA

The SARS-CoV-2 RBD ELISA assay used was recently described (24). The seropositivity threshold was established using the following formula: mean of all COVID-19 negative plasma + (3 standard deviation of the mean of all COVID-19 negative plasma) (see supplemental material for details).

Bio-informatic analyses

We collaborated closely with Sacha Morin and Dr. Guy Wolf at MILA and the Université de Montréal, whom have expertise in exploratory data analysis and applied mathematics.

Dimensionality reduction is a necessary step to visualize and explore high dimensional datasets. While PCA is the standard algorithm to use in such a case, the resulting components are restricted to a linear projection of the input data, thereby limiting the expressiveness of the resulting visualizations. Recent advances in dimensionality reduction techniques instead favor so-called manifold learning algorithms, such as PHATE (Potential of Heat-diffusion for Affinity-based Trajectory Embedding), which can compute a nonlinear transformation of the data to effectively represent the latent structure of a dataset in low dimensions (Moon et al., 2019). PHATE begins by computing a sample-sample affinity graph, i.e., a graph connecting pairs of similar samples to form “neighborhoods”. It then leverages diffusion geometry to propagate similarities along the graph and learn long-range affinities between data points. Data samples are subsequently embedded in a low dimensional space (usually, 2 dimensions) by preserving both the local and long-range pairwise similarities, meaning the distance between “neighborhoods” are meaningful. Intuitively, this can be thought as « unfolding » the sample-sample graph in low dimensions while preserving the graph’s intrinsic structure, as captured by diffusion affinities. PHATE has been notably used to explore single-cell RNA-seq data (Moon *et al.*, 2019) as well as clinical data from SARS-CoV-2 positive patients (https://www.medrxiv.org/content/10.1101/2021.05.29.21257760v1).

When multiple samples are taken from the same patient at different timepoints, as in our

case, one can study the progression of a given patient or a given group of patients on the PHATE embedding in what is called a trajectory analysis. In order to visualize and compare the typical trajectories of groups (e.g., survivors *versus* non-survivors), we used a *rolling window* approach over the PHATE coordinates. Specifically, we slide a 4-day window over the range DSO 0-28 by increment of 1 DSO. At each window step, and for each group separately, we use the average PHATE coordinates of the all samples in that window range as the coordinates of the group trajectory. Windows with fewer than 4 samples in a given group are not displayed. We add the actual DSO marker every 4 days on the visualization to better interpret time progression. This analysis was performed on the longitudinal plasma samples of a total of 500 samples from hospitalized COVID-19+ patients, whom were recruited at the CHUM or the JGH between April 2020 and May 2021. This analysis included all 12 aforementioned variables and the DSO of the sample, which gave the manifold a cleaner structure. The patient clusters were the same as identified in the PHATE manifold generated at DSO11.

In addition to visualizing structure and trajectories, PHATE plots can be useful to visualize variables of interest by using them for coloring. Input variables can be used as color gradients to observe how they are distributed on the visualization (e.g., high antibody and low antibody neighborhoods). Outcome variables can be used in a similar way. Of particular interest to visualize categorical outcome variables is the MELD algorithm (Burkhardt et al., 2021), which performs a low-pass filtering of said variables over the affinity graph in order to smooth them over neighborhoods. The resulting values are used to compute a relative likelihood, i.e., the likelihood of a given sample or neighborhood belonging to a specific condition of the outcome variable over the others. The relative

likelihood of a sample incorporates information from both the condition of said sample and the conditions of neighboring samples, and is practical to determine whether a given region of the visualization is enriched or depleted in a specific condition.

Results

DSO11 patient samples reveal severity and outcome-driven clusters

Clustering of samples taken around 11 days after symptom onset (DSO11) revealed four patient clusters (Figure 4.2A), with distinct plasma profiles (Fig 4.2B). SARS-CoV-2 vRNA was high in Cluster 1 only, although a few positive samples were observed in all clusters. RBD-specific antibody responses were absent in cluster 3, and weaker in cluster 1 than in clusters 2 and 4. While markers of tissue damage and inflammatory cytokines were highest in cluster 1, it was also elevated in cluster 2. Fatal outcome within 60 days of symptom onset was most observed in cluster 1, although all clusters counted at least 1 fatality (Fig 4.2C). MELD confirmed cluster 1's enrichement for fatality (Fig 4.2D), and demonstrated clusters' 1 and 2's enrichment for critical cases.

In summary, the four patient clusters are : a "deceased" cluster (1), characterized by high amounts of SARS-CoV-2 vRNA, cytokines, and tissue damage markers, and low amounts of antibodies ; a critical survivor cluster (2), with similarly high cytokines and tissue damage marker, but lower SARS-CoV-2 vRNA and higher antibody responses ; and two non-critical survivor clusters, with equally low amounts of tissue damage markers, cytokines and plasma SARS-CoV-2 vRNA, but distinguished by either the presence (cluster 4) or absence (cluster 3) of an antibody response.

Trajectory analyses reveal divergences between patient clusters

Building on these observations, we were curious to see what differences these plasma variables could reveal *over time*. As the variables we measured were particularly relevant in the acute phase of the infection - after which they either cleared (vRNA), returned to

baseline levels (cytokines) or plateaued (antibody response) - we limited our analysis to samples collected within 30 days of symptom onset.

We first sought to subdivide the trajectory analysis between categories of analytes, although it was not possible to look at vRNA alone, given it is a single variable. The embedding of the 8 plasma analytes revealed inflammatory-cytokine-high, intermediate and low zones at the top, right and bottom peaks, respectively (Fig 4.3A). While the markers of tissue damage RAGE followed similar patterns, Surfactant Protein D (SP-D) and Angiopoientin-2 (Ang-2) had more diffused expressions, where only the bottom peak had low expression. Within this embedding, trajectory analysis revealed a similar starting point for all three survivor clusters, while the deceased cluster 1 was appart (Fig 4.3F). The distance between the deceased and survivor clusters was further accentuated at DSO8, and only started converging towards the other clusters by DSO20. Meanwhile, the non-critical, high-antibody cluster 4 also distinguished itself from the other two clusters, and was furthest appart from the deceased cluster. These observations suggest that the plasma profile before DSO20 is most discriminatory between fatal and non-fatal outcome, at least with regards to the inflammatory cytokines and tissue damage markers considered.

Next, we looked at how the PHATE embedding using the three measures of antibody response to SARS-CoV-2 drove the trajectories for the four patient clusters. Analysis of local concentrations of the three measurements revealed a low-response zone on the right, which progresses to an intermediate zone on the bottom point, then up to a high-response zone on the left (Fig 4.2B). The patient clusters start their trajectories at different sites: both high-fatality cluster 1 and non-critical survivor cluster 3 start in the low-response

zone, while clusters 2 and 4 are in the intermediate zone early in their disease course. These latter two clusters follow very similar trajectories throughout the disease course, ending in the high zone by DSO20. While the deceased cluster 1 also has a similar trajectory route as these latter two clusters, it initially trails behind, only catching up by DSO16. Finally, the low-antibody cluster 2 remains in the low-response section, and is the only patient cluster not to plateau in the high-zone. While confirming the described delayed antibody response observed in critical cases (Zohar *et al.*, 2020) (Lucas et al., 2021), these observations also reveal a non-fatal group of patients which do not mount an antibody response against RBD in acute COVID-19,

Finally, we combined all variables (Fig 4.2H). This PHATE embedding roughly had 4 regions: the upper tip of the triangle, with low expression of all variables; the lower right tip with high SARS-CoV-2 vRNA, inflammatory cytokines and tissue damage RAGE, and low-to-mid antibody responses; the lower left tip, characterised by high antibody responses and SP-D levels, intermediate amounts of inflammatory cytokines and low vRNA; and finally the center, which was essentially intermediate for all variables (Fig SXZ). The deceased cluster 1's trajectory mostly localized in the high vRNA zone, although this was also the starting point for critical survivor' cluster 2. This latter cluster quickly progressed out of this zone, however, and remained in the middle section, progressing towards the high-antibody region. Conversely, both non-critical clusters were well appart from the vRNA zone, rather travelling from the low to intermediate antibody sections for cluster 3, and the intermediate to high antibody zones for cluster 3. These trajectory analyses revealed the strong association of the inflammatory cytokines with SARS-CoV-2 vRNA, as they colozalize in a single section of the embedding. It is

principally in this region where the fatal-outcome trajectory lies, while the critical survivors are able to extract themselves from it quickly through the generation of an antibody response.

Discussion

Despite the high heterogeneity in outcome following COVID-19, considerable advances have uncovered certain immunovirological traits associated with fatal outcome, including the presence of RNAemia, delayed antibody responses, and high inflammatory profiles. To find how these are interrelated, we profiled 12 analytes in 500 acute longitudinal plasma samples collected from 201 hospitalized COVID-19 patients (shown are the preliminary analyses; we now have over 300 patients with more than 700 samples), and analyzed them simultaneously using PHATE algorithm (potential of heat diffusion for affinity-based transition embedding, Moon et al, Nature Biotech 2019), which can reduce multiple input variables to two salient features for clustering and visualization. Quantities of SARS-CoV-2-specific IgG, IgM, and IgA; TNFa, CXCL13, IL-6, IL-23, CXCL8, angiopoientin-2, RAGE, surfactant protein D and RNAemia in plasma sampled 11 days after symptom onset (DSO11) revealed four distinct clusters of patients which aligned with their disease severities: survivors who required mechanical ventilation (critical), non-critical survivors, subdivided by high or low antibody responses, and a high-fatality cluster which accounted for 67% of all fatal outcomes (14/21) by DSO60. Averaged trajectories between DSO3 to DSO30 diverged between clusters. The high-fatality cluster's antibody response had a 4-day delay– with low antibody-mediated killing and neutralization capacities - but caught up with the survivor groups by DSO12. Conversely, the early cytokine profile (at DSO4) was similar, but the high-fatality cluster diverged by DSO8, and remained distinct until DSO22. The high-fatality cluster also uniquely maintained high vRNA. This approach offers a new, time-sensitive and unbiaised approach to study the characteristics of hospitalised COVID-19 disease and to understand the discting courses

the immune response can take in response to SARS-CoV-2 infection.

In our dataset, we observed that the highest levels of viral RNA were observed at the same time as the highest levels of inflammatory cytokines IL-6, IL-23, TNFa and chemokine IL-8, (which may indicate cDC activation upon microbial sensing), and low amounts of antibodies, a state that was observed in earlier disease. This co-upregulation between cytokines and circulating vRNA supports the hypothesis that viral particles or debris may contribute to systemic inflammation. Intermediate vRNA was seen with intermediate cytokines and chemokines, which could suggest a dose-dependent cytokine activation. Ultimately, all clusters converged towards a similar profile by DSO22, by which time circulating vRNA is cleared in the vast majority of patients. The convergence may be explained by different non-exlusive mechanisms: the analytes included in the analyses which, being acute-related molecules, eventually wained to baseline levels and, specifically for the high-fatality cluster, the patients whom contributed to the analyses were those who survived until at least DSO22, and perhaps had a less inflammatory profile compared to those which succumbed quicker. In all cases, our results confirm that early plasma profiles are more differential than later profiles (Lucas *et al.*, 2020).

The four patient clusters had diverging antibody responses: high response, observed in critical and non-critical survivors (clusters 2 and 4, respectively), and low antibody response in the high fatality cluster 1, and second survivor non-critical cluster 3. High antibody is only observed without vRNA, and either with intermediate or no cytokines, which suggests that the presence of a strong antibody response may help clearing circulating vRNA, thus modulating the cytokine response. Conversely, a delayed antibody response has already been shown in the fatal case, although it does not seem that a lack

of an early response is fatal in all cases. Furthermore, although mild COVID-19 cases have already reported lower antibody responses, presumably due to low antigen exposure from the mild nature of the infection, it is likely not the case here, as these patients were sick enough to be admitted to hospital. There are instances of patients clearing the viral infection in the absence of antibody responses: in cancer patients treated with B-cell-depleting antibodies (anti-CD20), survival was associated to a robust SARS-CoV-2-specific CD8+ T cell response (Bange et al., 2021). In future work, we will characterize the SARS-CoV-2-specific T cell responses per clusters to see if other adaptive immunity mechanisms were key in these patients' survival.

As with any data reduction method and due to data sparcity (specifically, we have few samples per patient for the trajectory analyses), one limitation of our study is that we lose the interpatient variability inherent to any human study. However, this can be partially mitigated by univariate analysis at different times. We are also adding 130-plus samples to the analysis, increasing our clustering power and granularity to our trajectory analyses. An additional current limitation is the descriptive nature of the study: it will be critical to include characterisation of cellular components, for example quantities of SARS-CoV-2-specific CD4, CD8 T and B cells, and transcriptomic profiles of myeloid and NK cells, to elucidate the mechanisms behind the antibody and cytokine kinetics. Although samples of cryopreserved cells are a limitating factor, cell-based assays will be performed on a subset of individuals per cluster. Futhermore, we have sequenced bulk RNA from whole blood which can be used to identify differentially expressed genes (DEGs), and point towards dysregulated molecular pathways behind the slower antibody kinetics observed in clusters 1 and 3. Finally, we have not yet studied how the patients' demographics or

treatment during the time of hospital could have influenced these profiles. However, the impact of immunoregulatory drugs, such as systemic corticosteroids and IL-6r antagonists, on observed trajectories will also be analyzed.

In summary, our unbiased approach gives a “big-picture” view of multiple dysregulated immune response components in fatal COVID-19, and will allow to target detailed investigations of potentially dysredulated immune responses on very high-risk patient subgroups who may most likely benefit from new therapeutic interventions.

Declaration of interest, funding, acknowledgements

Acknowledgements

For sample collection and processing, and clinical data retrieva at the CHUM, we thank Dounia Boumahni, Fatna Benettaib, Ali Ghamraoui, Boaz Lahav, Pascale Arlotto, Nakome Nguissant, Kip Brown, Johann Plantin, Stéphanie Matte, Martine Lebrasseur, Gloria Ortega-Delgado, Mélanie Laporte, Caroline Dufour, Isabelle Turcotte, Syllah Mohammed and Natalia Zamorano. We thank Dr. Stefan Pöhlmann (Georg-August University, Germany) for the plasmid coding for SARS-CoV-2 S glycoproteins and Dr. M. Gordon Joyce (U.S. MHRP) for the monoclonal antibody CR3022. For sample collection and processing at JGH, we thank Meriem Bouab, Danielle Henry, Zaman Afrasiabi, Hershlee Vernet, Branka Vulesevic, Nardin Rezk, Nofar Kimchi, Chris Tselios, Charlotte Guzman, Louis Petitjean, Xiaoqing Xue, Maureen Oliveira and Bluma Brenner. For chart review at JGH, we thank Yara Moussa, Olumide Adeleye, Noor Mamlouk, Tala Abdullah, Michael Palayew and Biswarup Ghosh. For administration at JGH, we thank Vincenzo Forgetta, Darin Adra, Jonathan Afilalo and Marc Afilalo. We also thank the flow cytometry and NC3 platforms at the CRCHUM.

Funding

American Foundation for AIDS Research (amfAR) grant 110068-68-RGCV (DEK, NC, AF)

Canada's COVID-19 Immunity Task Force (CITF), in collaboration with the Canadian Institutes of Health Research (CIHR) grant VR2-173203 (DEK, AF)

CIHR grants 365825 and 409511 (JBR)

Canada Foundation for Innovation (CFI): Exceptional Fund COVID-19 grant #41027 to AF, DEK, NC; CFI leader to JBR

Ministère de l'Économie et de l'Innovation du Québec, Programme de soutien aux organismes de recherche et d'innovation (AF)

CRCHUM Foundation

Fonds de recherche Québec-Santé (FRQS) (BQC-19, JBR)

Génome Québec (BQC-19, JBR)

Public Health Agency of Canada (BQC-19,JBR)

FRQS Merit Research Scholar Award (DEK)

FRQS Salary Award (NC, MD, MC, JBR, CL, MT)

FRQS Clinical Research Scholarship (JBR)

Canada Research Chair (AF, AP)

COVID-19 excellence scholarship from the Université de Montréal (EBR)

CIHR fellowships (SPA, PG)

Lady Davis Institute of the Jewish General Hospital (JBR)

NIH Foundation (JBR)

Cancer Research UK (JBR)

Competing interests

JBR has served as an advisor to GlaxoSmithKline and Deerfield Capital. These agencies had no role in the design, implementation or interpretation of this study. Authors declare that they have no other competing interests.

Data and materials availability

All data are available in the main text or the supplementary materials.

Figures

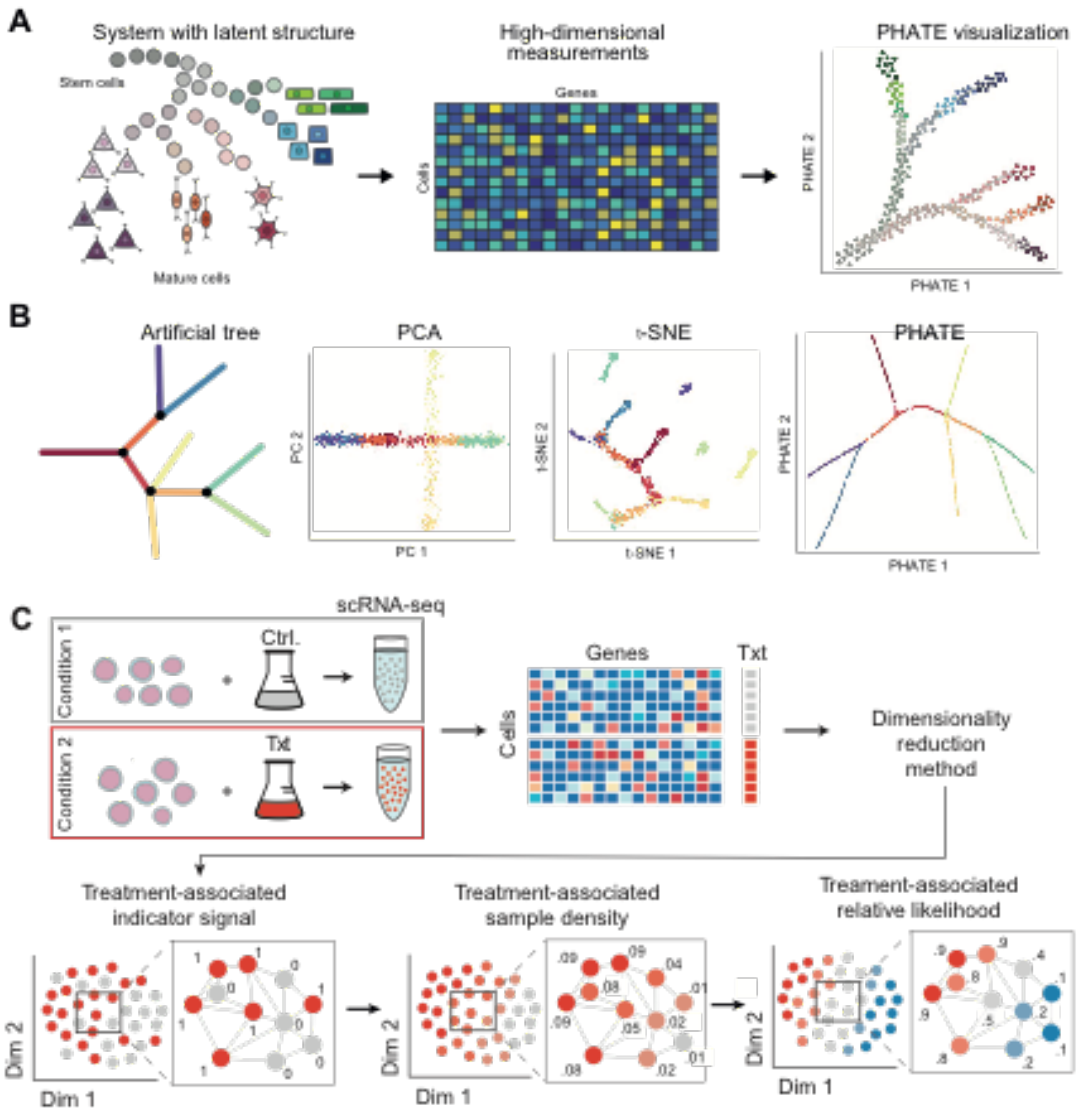

Figure 4.1 **Visualization of complex data using PHATE and MELD. A**) Hypothetical experimental setting, where the progression of stem cells into different cell types is analyzed by single-cell RNA sequencing and rendered as a PHATE visualization. **B**) Hypothetical tree with color-coded branches, and ability of PCA, t-SNE and PHATE to render the structure of this tree. PHATE is superior in revealing global and structure of branches, while PCA cannot reveal local features (branches) and t-SNE breaks the branches appart and shuffles the pieces within the visualization. **C**) Hypothetical experimental setting, whereby the same cell types are treated with a control (grey) or experimental (red) treatment, and perturbations of their transcriptome are analyzed using single-cell RNA sequencing. Application of a dimensionality reduction method allows to reduce the n genes (=dimensions) down to a single coordinate among two dimensions (dim 1/dim 2), where the localisation of the dot is representative of a specific cell state (based on gene expression). Cells which received the treatment (red dots) tend to cluster together in the upper left region of the manifold, while the control-treated cells (grey dots) are mostly in the bottom left section, indicative of the transcriptomic perturbation by the treatment. The sample-associated relative

likelihood measures the probability (in percentage) that a cell in a given region is from the treated (or the control) group. This method allows for more reliable clustering and labelling of samples, despite intrinsic heterogeneity within a given sample. Panels A and B modified from (Moon *et al.*, 2019) and panel C modified from (Burkhardt *et al.*, 2021).

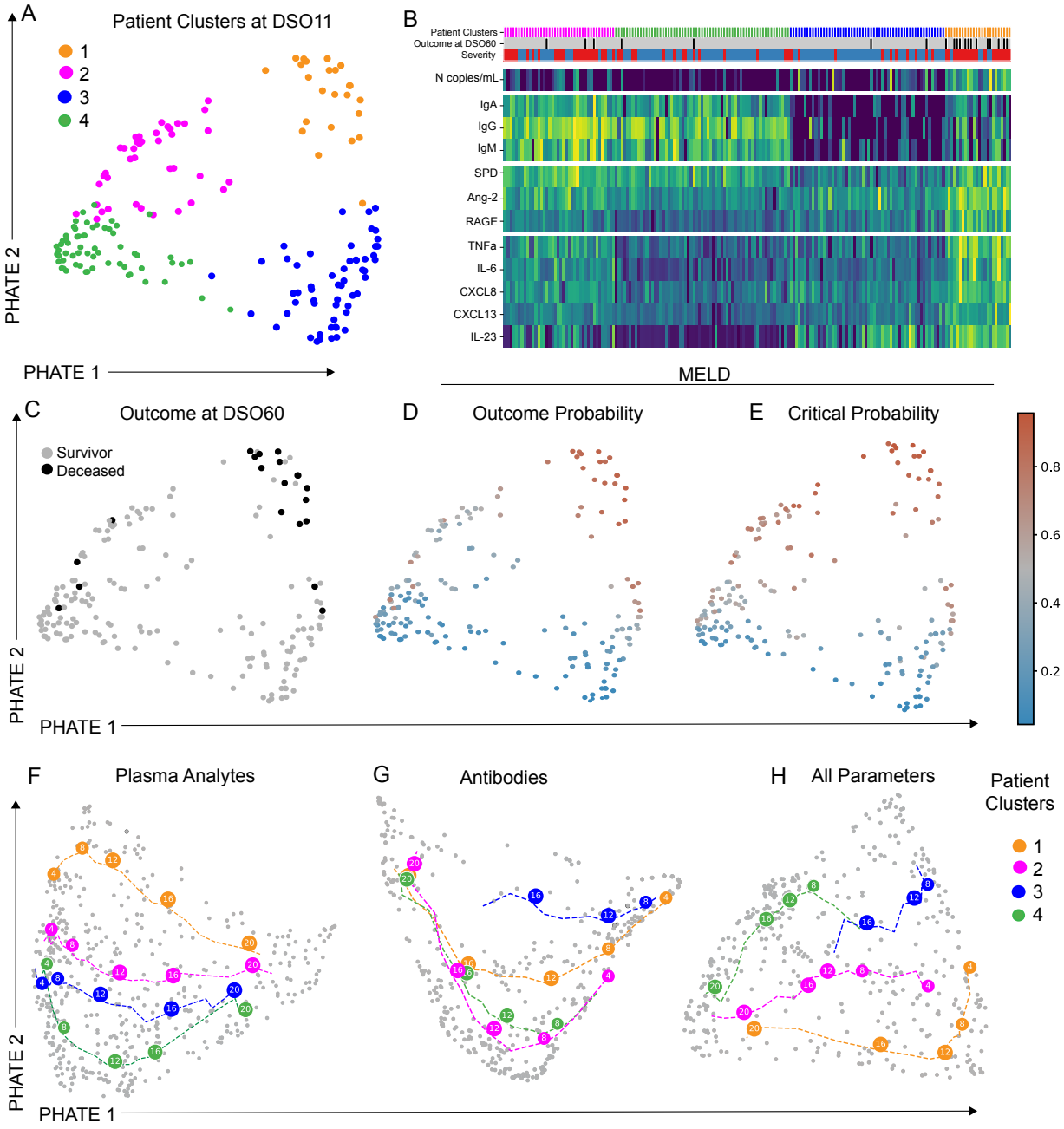

Figure 4.2 **Unsupervised patient clusters and their trajectories vary between outcome and severity**. **A**) PHATE embedding of plasma sample profiles collected at around 11 days after symptom onset (+/- 4-day window, 1 sample per patient) of hospitalized COVID-19 patients. Unsupervised K-means clustering revealed 4 distinct patient clusters, color-coded. N = 195. **B**) Heatmap of relative amounts of variables per patient. Top rows are categories: patient clusters from A (color-coded) ; outcome, where black is deceased, and grey is survival at DSO60 ; and max severity, where critical is red and non-critical, blue. For analytes, each row represents a distinct patient. Within categories, variables are ordered by unsupervised hierarchical cluster. **C**) Patients from PHATE embedding color-coded by outcome, where black os deceased and grey, survival at DSO60. MELD representation of local enrichment of **D**) fatality or **E**) critical disease. Average trajectory per color-coded patient cluster (from A) when PHATE embedding was

performed using **F**) plasma analytes only; **G**) antibody measurements only ; **H**) all measurements. Numbers in the circles represent the days since symptom onset. A-E) n=195 ; F-H) n = 500.

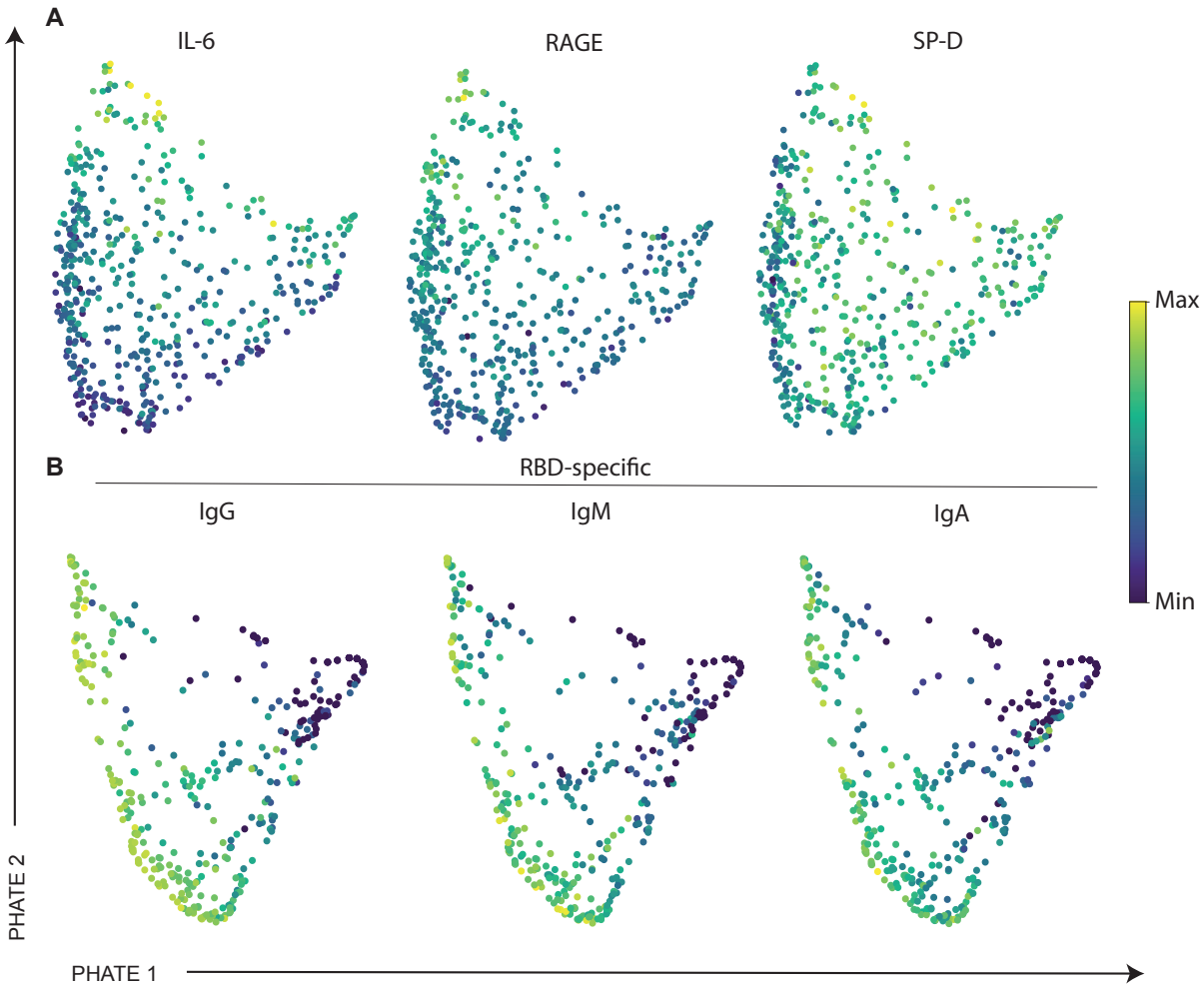

Figure 4.3 Variable expression within category-specific PHATE embeddings. Relative expression of log-transformed concentrations of **A**) representative analytes across PHATE embedding of Fig XF or **B**) of all three antibody measurements across PHATE embedding of Fig 4.2G. N = 500 COVID-19+ samples.

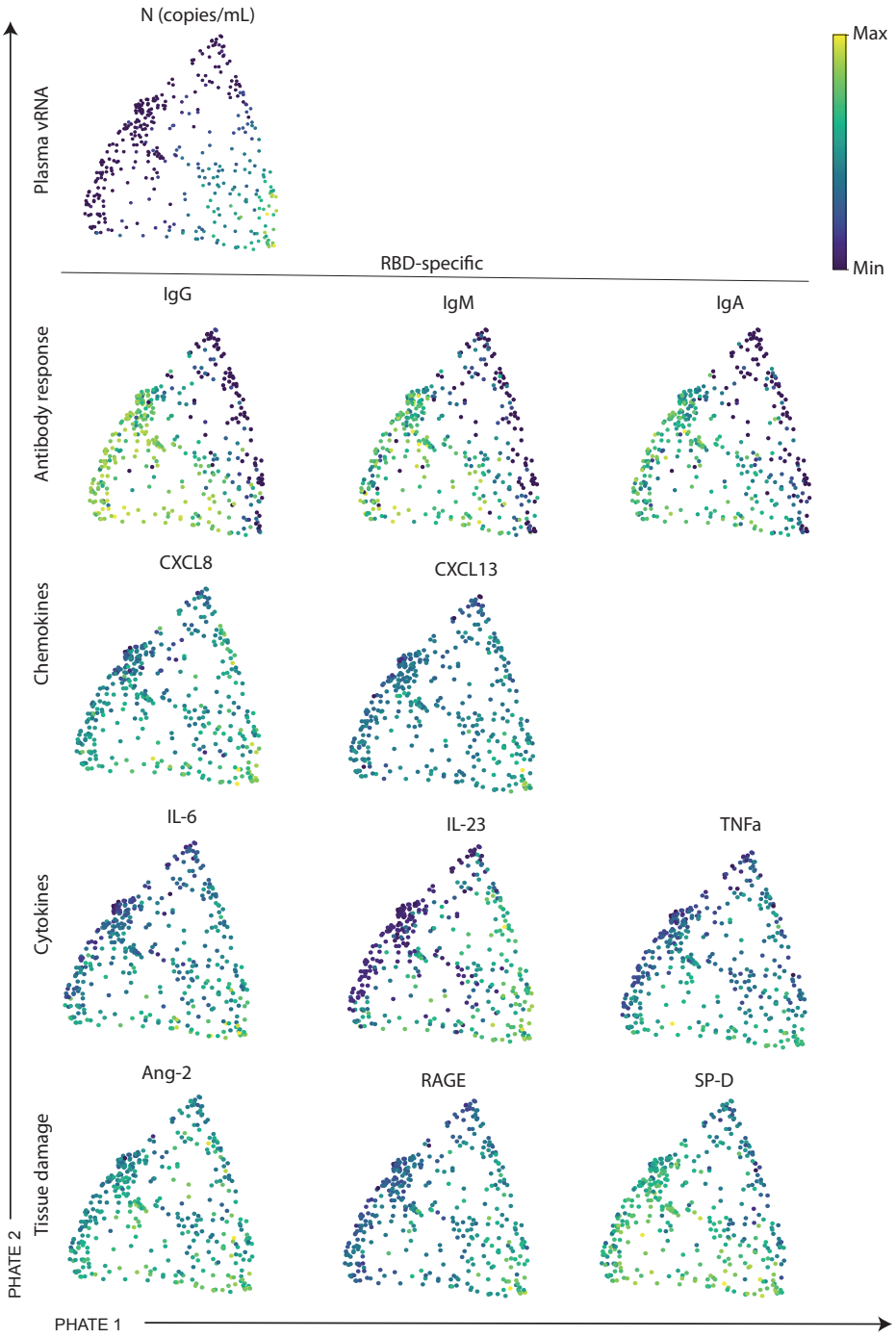

Figure 4.4 Variable expression within global PHATE embedding. Relative expression of log-transformed concentrations of all included variables within PHATE embedding of Fig 4.2. Each row is a distinct category of variables. N = 500 COVID-19+ samples.

Chapter 5 – MANUSCRIPT 2 : Immune checkpoint expression on HIV-specific CD4+ T cells and response to their blockade are dependent on lineage and function

Status : We are currently addressing reviewers' comments at EBioMed.

Author contributions :

Conceptualization: EBR, DEK, AM, MD

Data Curation: EBR, AM, JN

Formal analysis: EBR, AM, OT, DEK

Funding acquisition: DEK, MD

Investigation/experiments: EBR, AM, NB, GOD, RC

Methodology: EBR, AM, JN, AEB

Resources: GJF, JPR, CT

Software: OT

Visualization: EBR, OT

Patient recruitment and cohort administration: NB, CT, JPR

Supervision: DEK, AM, MD, AEB

Writing – original draft: EBR, AEB, DEK

Writing – review and editing: all authors

Title : Immune checkpoint expression on HIV-specific CD4+ T cells and response to their blockade are dependent on lineage and function

Authors: Elsa Brunet-Ratnasingham1,2, Antigoni Morou1,2†, Mathieu Dubé1, Julia Niessl1,2, Amy E. Baxter1,2‡, Olivier Tastet1, Nathalie Brassard1, Gloria Ortega-Delgado1, Roxanne Charlebois1, Gordon J. Freeman3, Cécile Tremblay1,2, Jean-Pierre Routy4, and Daniel E. Kaufmann1,2*

Affiliations:

1Research Centre of the Centre Hospitalier de l'Université de Montréal (CRCHUM), Montreal, Quebec, Canada.

2Université de Montréal, Montreal, Quebec, Canada.

3Department of Medical Oncology, Dana-Farber Cancer Institute, Harvard Medical School, Boston, USA

4Chronic Viral Illnesses Service and Division of Hematology, McGill University Health Centre, Montreal, Quebec, Canada.

†Current affiliation: Roche Diagnostics, Penzberg, Bavaria, Germany

‡Current affiliation: Perelman School of Medicine, University of Pennsylvania, Philadelphia, USA

* Correspondence to: daniel.kaufmann@umontreal.ca

Keywords (4-6): HIV-specific CD4+ T cells, T cell dysfunction, immune checkpoint blockade, PD-1, TOX, CD4+ T cell subsets.

Abstract

Background: Antigen-specific T cell impairment is observed in chronic infections. CD4+ T cells are diverse in phenotype and function; how their different lineages are impacted by inhibitory immune checkpoints (IC) is unknown.

Methods: We examined IC expression and function in HIV-specific CD4+ T cells of viremic individuals prior to ART initiation and persons with spontaneous or therapy-induced viral suppression. We investigated IC patterns associated with exhaustion-related transcription factors and chemokine receptors using cytokine-independent activation-induced marker assays. We determined effector functions representative of TFH, TH1 and TH17/TH22 using ultra-sensitive RNA flow cytometric fluorescence in situ hybridization (FISH), and their response to IC blockade.

Findings: The dysfunction-related transcription factor TOX was elevated in HIV-specific CD4+ T cells of viremic patients, and its expression was associated with lineage differentiation. We observed a hierarchy of PD-1, TIGIT and CD200 expression associated with both infection status and effector profile. In vitro responsiveness to PD-L1 blockade varied with defined CD4+ T cell functions rather than IC expression levels: frequencies of cells with TH1- and TH17/TH22-, but not TFH-related functions, increased. Response to PD-L1 blockade was strongest in viremic participants and reduced after ART initiation.

Interpretation: Our data highlight a polarization-specific regulation of IC expression and differing sensitivities of antigen-specific Thelper subsets to PD-1-mediated inhibition. This heterogeneity may direct ICB efficacy on CD4+ T cells in HIV infection.

Context of research

Combination antiretroviral therapy (ART) is highly effective in controlling HIV but requires life-long medication due to the latent viral reservoir, and does not restore suppressive immune responses. In particular, there is no generation of effective HIV-specific T cell responses, which are thought to play an important role in controlling HIV in the rare individuals who can spontaneously control the virus. Inhibitory immune checkpoints (IC) such as PD-1 contribute to T cell dysfunction and failure to control viral infections, including HIV, and IC blockade (ICB) represents a potential adjuvant to ART through restoration of T cell functions. While most studies have focused on CD8+ T cells, increasing evidence shows that the remarkable impact of ICB therapy in a subset of cancer patients is enhanced by functional CD4+ T cell help, which can be directly affected by ICB. While effective virus-specific CD4+ T cell responses are also thought to be important for immune control of HIV, these cells are highly heterogenous. How IC expression and function differs across CD4+ T cell lineages and the consequences of this diversity for IC blockade (ICB) strategies are still poorly understood.

To compare various stages of immune dysfunction, we examined people living with HIV (PLWH) with different levels of viral control pre-ART (including elite controllers who spontaneously control virus) and followed a cohort longitudinally post-ART. We used a panel of assays to characterize HIV-specific CD4+ T cell subsets, including activation-induced marker (AIM) assays and flow cytometric detection of mRNAs coding for a wider variety of HIV-specific CD4+ T cell functions than what is detected by standard procedures. Our experiments indicate a hierarchy of IC (PD-1, TIGIT, CD200) expression

on blood HIV-specific CD4+ T cells that depends not only on the person's infection status but also on expression of lineage differentiation markers and effector functions representative of CD4+ T cell subsets critical for antiviral responses (TFH, TH1 and TH17/TH22 cells). This hierarchy was also present in the putatively functional cells of elite controllers. We characterized the expression of the dysfunction-related transcription factor TOX, and saw that its association with the key IC PD-1 in the setting of viremia varied across CD4+ T cell polarizations. Response to blockade of the PD-1 pathway resulted in increased antiviral and mucosal-protective functions, but did not affect TFH-related functions. Response to ICB was most prominent in viremic patients, and subdued but not fully abrogated in the setting of viral suppression.

These results highlight a previously unrecognized impact of ICB on mucosal immunity-related CD4+ functions, which are known to be depleted upon HIV infection and not restored by ART, and strong links between IC expression patterns and HIV-specific CD4+ T cell differentiation. The impact of ICB on CD4+ T cells in HIV infection has primarily been studied in the context of viral reservoir reactivation, which are preferentially harbored in IC+ cells. Our work emphasizes the importance of considering the differentiation profile of the virus-specific CD4+ T cells in studies of ICB blockade, as it may direct ICB efficacy in HIV infection. This data may also have implications for CD4+ T cell help in other infectious and non-infectious chronic human diseases.

Introduction

CD4+ T helper (TH) cells orchestrate the immune responses against pathogens (1, 2) and defects in T helper responses contribute to lack of viral immune control in HIV infection. This diverse cell population polarizes towards lineages characterized by expression of chemokine receptors and transcription factors (TF), and produce distinct sets of cytokines (3). Beyond the prototypical antiviral TH1 subset, HIV-specific CD4+ T cells also include mucosal-related TH17/TH22 and B-cell helper TFH, the proportions of which are differentially related to spontaneous viral control (4).

In chronic infections such as HIV, sustained antigenic exposure and inflammation alter both CD4+ and CD8+ T cell function. CD8+ T cell exhaustion follows a gradient enforced by epigenetic remodeling with limited reversibility (5, 6). TOX is a central transcription factor (TF) involved in the development and maintenance of exhausted CD8+ T cells in mice (7) and humans (8), although its role in human CD8+ T cells is not limited to exhaustion (9). Dysfunctional CD4+ T cells differ from exhausted CD8+ T cells in that they present prominent features of altered differentiation: loss of antiviral and mucosal-protective functions and a skewing towards a T follicular helper (TFH)-like profile (4). Little is known about TFs implicated in CD4+ T cells dysfunction, although some, increased in mice models, overlap with exhaustion-related TF (10). Another commonality between dysfunctional CD4+ and CD8+ T cells is the upregulation of inhibitory immune checkpoints (IC) (11), however with some notable differences in the IC hierarchy between the two subsets (10, 12-14). IC have dual roles as physiologic regulators of T cell activation and mediators of exhaustion (15). PD-1 is the best characterized IC contributing to both HIV-specific CD4+ and CD8+ T cell dysfunction (16), and correlates with disease progression

(12, 14) and loss of antiviral function (16).

Immune checkpoint blockade (ICB) can partially rescue CD8+ T cell exhaustion, in particular blockade of the PD-1 signaling pathway. A population of mildly exhausted CD8+ T cells, called “progenitor exhausted”, with stem-like properties and intermediate levels of PD-1, respond to ICB(17-19), while terminally exhausted CD8+ T cells, with high PD-1 and Tim3+ expression, have poor response to ICB (19). Responsiveness of CD4+ T cells to ICB is understudied due to their heterogeneity and the paucity of tools to identify them in an antigen-specific manner. Although PD-1’s effect on CD4+ T cell function in vivo was classically described as IL-2 inhibition (20, 21), studies in animal and human chronic infections support broader ramifications. PD-1 blockade enhanced IFNg+ TH1-responses specific to Mycobacterium tuberculosis in murine models (22) and patients undergoing ICB for cancer therapy (23), and moderately increased IFNg secretion by SIV-specific CD4+ T in non-human primates (24). These primates had replenished TH17 in the gut and improved gut integrity, which may explain their improved survival through reduced immune hyperactivation (25, 26). In vitro, PD-1 blockade enhanced HIV-specific CD4+ T cell proliferation as well as IFNg, IL-2, IL-13 and IL-21 production (14). However, the links between IC expression among the heterogeneous polarizations of CD4+ T cells and the impact of ICB on various effector functions of these cells are still lacking.

Here, we define the relationships between dysfunction-related characteristics and the lineages of HIV-specific CD4+ T cells across disease and treatment status. We pinpoint a previously underappreciated heterogeneity across types of CD4+ T cells in both their IC and exhaustion-related TF expression patterns, as well as their capacity to respond to PD-1 blockade. Greater understanding of ICB’s impact on CD4+ T cells can foster new

therapeutic uses for immunotherapeutic interventions.

Materials and Methods

Study Design

Leukaphereses were obtained from study participants at the Montreal General Hospital, Montreal, Canada and at the Centre Hospitalier de l'Université de Montréal (CHUM) in Montreal, Canada. The study was approved by the respective IRBs (IRB CHUM: 17.335) and participants gave written informed consent prior to enrollment. Samples were collected between 2013 and 2019 as part of a multicentric study (MP-37-2018-4029). Subject characteristics are summarized in Supplementary Table 1. Chronic Progressors (CP) had plasma viral loads of at least 5000 copies/ml and were infected and infected/off treatment for at least 3 months at the time of collection of the "Pre-ART" sample. Longitudinal "Post-ART" samples were collected in these same subjects, after at least 3 months on ART and undetectable viral loads. Elite controllers (EC) had spontaneously controlled viremia (< 40 viral copies/ml) in the absence of ART. PBMCs were isolated by the Ficoll density gradient method and stored in gas phase of a liquid nitrogen tank in 90%FBS with 10% DMSO.

Antibodies

All antibodies are listed in Supplementary Tables 2-5. Antibodies are monoclonal and raised in mice. All antibodies were validated by manufacturer and titrated with biological and/or isotype controls.

Activation-induced marker (AIM) assay

As previously described (4), cryopreserved peripheral blood mononuclear cells (PBMCs) were thawed and rested in cell culture media (RPMI supplemented with 10% Human AB serum and PenStrep – 50 U/ml of penicillin and 50 µg/ml of streptomycin) at 37°C for 3 hours at a density of 10M/ml in 24-well plates. 15 minutes prior to stimulation, CD40 blocking antibody (clone HB14, Miltenyi, cat #: 130-094-133) was added to each well at 0.5 µg/ml, as well as antibodies staining CXCR5, CXCR3 and CCR6. Cells were either left unstimulated or stimulated with overlapping peptide pools of HIV Gag (JPT, PM-HIV-Gag ULTRA), at a final concentration of 0.5 µg/ml/peptide. Alternatively, 1µg/ml of Staphylococcal Enterotoxin B (SEB, Toxin Technology) was used to stimulated the cells as a positive control. Cells were stimulated for 9 hours, collected, washed and stained with LIVE/DEAD™ Fixable Aqua Dead Cell Stain Kit (20 mins, 4°C; Thermofisher, #L34965). After washing, cells were incubated with FcR block (10mins, 4°C; Miltenyi) then stained with a cocktail of surface markers (30 mins, 4°C; See panel in Supplementary Table 2). Washed cells were then fixed with 2% paraformaldehyde (PFA) for 20 mins at RT, then washed and resuspended in PBS-2% FBS for flow acquisition on a 5-laser LSRII (BD BioSciences). For experiments with intranuclear transcription factor staining, fixation and permeabilisation were done using eBioscience™ Foxp3 / Transcription Factor Staining Buffer Set (cat#: 00-5523-00) following kit instructions: surface-stained cells were fixed with 1x Fixation/Permeabilisation for 30 min at RT in the dark, then washed and resuspended in 1X Permeabilization buffer with intranuclear antibody cocktail for 1h at RT in the dark. Analysis was performed using FlowJo (Treestar, V10). Gates were set on the unstimulated controls.

Combined cytokine/chemokine mRNA-Flow-FISH and protein staining assays

As previously described(4), PBMCs were thawed and rested for 2-3 hours in 48-well plates at 5M in 0.5ml in cell culture medium. 15 minutes prior to stimulation, a PD-L1 blocking antibody (29E.2A3(27)) or an isotypic control (IgG2b, clone MPC-11, BioXcell, # BE0086) at a concentration of 10 µg/ml were added into culture, along with antibodies staining CXCR5, CXCR3 and CCR6. PBMCs were then either left unstimulated or were stimulated with an HIV Gag peptide pool (JPT) or SEB for 12 hours. After incubation, cells were stained with Fixable Viability Dye eFluor™ 506 (20 min, 4oC; eBioscience, # 65-0866-14) before labeling of surface markers with surface antibodies (30 min, 4oC; See panel in Supplementary Table 3). Samples were next subjected to the PrimeFlow RNA® assay (ThermoFisher) for specific mRNA detection in a 96-well plate as per manufacturer's instructions. All buffers and fixation reagents were provided with the kit, with the exception of flow cytometry staining buffer (PBS - 2% FBS). Briefly, after fixation and permeabilization, cytokine/chemokine mRNAs were labelled with one of five combinations of probes as listed in Supplementary Table 4. The probes were each diluted 1:20 in probe diluent and hybridized to the target mRNA for 2 hr at 40oC. Samples were washed to remove excess probes and stored overnight in the presence of RNAse inhibitor 1X (RNAsin). Signal amplification was achieved by sequential 1.5 hr incubations at 40oC with the pre-amplification and amplification mixes. Amplified mRNA was labelled with fluorescently-tagged probes for 1 hr at 40oC. Samples were acquired on a BD LSRFortessa™. Analysis was performed using FlowJo (Treestar, V10). Gates were set on unstimulated controls (see Fig S3b). Net frequencies of HIV-specific responses were calculated by subtracting the background expression in the absence of exogenous stimulation from the value measured after Gag antigen stimulation. HIV-specific

responses were considered positive when the frequency obtained with Gag stimulation was at least twice that obtained in the absence of exogenous stimulation. Responses not meeting this criterion were characterized as negative.

Delayed Intracellular cytokine staining

As previously described(28), thawed, rested PBMCs were either left unstimulated or were stimulated with an HIV Gag peptide pool (JPT) or SEB. After a 9h stimulation, 1.25 µg/ml of brefeldin A (BD GolgiPlug) was added to culture and cells were further incubated for 12 hours. Cells were collected, washed and stained with AquaVivid Viability dye (20 mins, 4°C). After washing, cells were incubated with FcR block (10mins, 4°C) then stained for cocktail of surface markers (30 mins, 4°C; see supplementary table 5 for panel). Cells were washed and fixed with Fixation Solution (eBioscience, #88-8824-00) for 15 mins at RT, following which they were washed and stained for intracellular proteins with 1X Permeabilization Buffer (eBioscience, #00-8333-56) (30 mins, 4°C). Cells were washed once more with 1X Permeabilization buffer, then with PBS – 2%FBS and acquired on the BD LSRFortessa. Analysis was performed using FlowJo (Treestar, V10). Gates were set on unstimulated controls.

qRT PCR analysis of HIV-specific CD4+ T cells

These data were collected in a previously published study (4). Briefly, AIM assay was conducted as previously explained and CD69+CD40L+CD4+ T cells were live-sorted on a FACS Aria cell sorter (BD BioSciences) equipped for handling of biohazardous material,

operated at 70 pounds per square inch with a 70-um nozzle (for gating strategy, please refer to (4). 5000 cells were collected directly into RLT lysis buffer (Qiagen) and vigorously vortexed before flash-freezing. Total RNA was purified using the RNeasy Plus Micro Kit (Qiagen). cDNA was synthesized using all RNA available (or 1-5 ng) with the High-Capacity Reverse Transcription Kit with RNase Inhibitor (Life Technologies) (250 C for 10 min, 370 C for 120 min, 850 C for 5 min). cDNA equivalent to 1000 sorted cells was subjected to gene-specific preamplification using Taqman Preamp MasterMix (Applied Biosystems) and 96 pooled TaqMan Assays (Applied Biosystems – for full panels, please refer to (4) at final concentration 0.2X (95°C for 10 min, followed by 16 cycles of 95°C for 15 s and 60°C for 4 min). The preamplified cDNA was diluted 5-fold in DNA suspension buffer (Teknova) and was mixed with TaqMan Universal PCR Master mix (Life Technologies) and 20X GE sample loading reagent (Fluidigm). 20X Taqman assays were diluted 1:1 with 2X assay loading buffer (Fluidigm). Taqman assays mixtures were loaded onto a primed 96.96 Dynamic Array chip (Fluidigm). The chip was loaded into the IFC Controller, where each sample was mixed with each assay in every possible combination. The chip was transferred in a Biomark (Fluidigm) for real-time PCR amplification and fluorescence acquisition using single probe (FAM-MGB, reference: ROX) settings and the default hot-start protocol with 40 cycles. Cycle thresholds (Ct) were calculated using the Fluidigm BioMark software.

Analysis of the qRT-PCR data obtained on the microfluidic platform was carried out using GenEx software (MultiD Analyses, URL: http://www.multid.se). Five endogenous control genes were included in the Fluidigm run and the stability of endogenous control genes across all experimental samples was evaluated applying the NormFinder algorithm50 in

GenEx. The mean expression of the most stable endogenous control genes was used for normalization and calculation of -ΔCt values. Principal component analysis and biplots were created using the prcomp and fviz_pca_biplot functions in R programming language.

Statistical analyses

Statistical analyses were performed with Prism v6.0 (GraphPad) using non-parametric tests. The type of statistical test is specified in the figure legends. Permutation test (10 000 permutations) was calculated using the SPICE software (https://niaid.github.io/spice/). Statistical tests were considered two-sided and $p<0.05$ was considered significant. The heatmap, dendrogram and PCA were generated using the fold change between the net value of the frequency of a cytokine mRNA detected with PD-L1 blockade over that seen for the same cytokine with the isotypic control. The prcomp function was used for the PCA, and the ggfortify and pheatmap packages were used for the dendrogram and heatmap, respectively.

Results

Exhaustion-related transcription factor TOX correlates with PD-1 expression

To explore dysfunction among the heterogeneous T helper (TH) populations, we compared dysfunctional HIV-specific CD4+ T cells from viremic chronic progressors with high viral burden prior to ART (CP; VL > 5000 viral RNA copies/ml) to the relatively functional HIV-specific CD4+ T cells from elite controllers who spontaneously suppress virus (EC; VL < 40 copies/ml) (patient characteristics in Supplemental Table 1)(4). Upregulation of activation-induced markers (AIM) following peptide stimulation allows the capture of a broader antigen-specific CD4+ T cell population than cytokine-based techniques (29). We stained for co-expression of CD69 and CD40L, an activation-induced co-signaling molecule expressed on multiple polarizations but low on bystander activated cells (4, 29), after a 9-hour ex vivo stimulation with a peptide pool of HIV's immunodominant antigen, Gag (Fig 1a and Fig S1a). Both cohorts had similar frequencies of AIM+ HIV-specific CD4+ T cells (Fig 1b), and PD-1 expression was higher on HIV-specific CD4+ T cells from CP than EC (Fig 1c, and Fig S1b), as previously reported (12, 14).

We considered the exhaustion-related TF TOX, given its association with T cell exhaustion(7), and TFs reported in mouse dysfunctional CD4+ T cells (10): Blimp-1 (Prdm1), Helios, Nfatc1, Batf, Eomes and Tbet. Our previously published high-throughput qRT-PCR assay data on sorted HIV-specific CD4+ T cells from CP or EC (4) showed increased TOX (Fig 1d), IKZF2 (HELIOS), NFATC1, and PRDM1 (BLIMP-1) (Fig S1c) in

HIV-specific CD4+ T cells of CP compared to EC, while BATF and TBX21 were higher in EC. EOMES was similar in both cohorts.

We next performed intra-nuclear protein staining for the TF (which were largely increased in CP compared to EC) in HIV-specific CD4+ T cells using the 9h AIM assay (Fig S1d). HELIOS was undetectable in the AIM+ population, whereas both NFATc1 and TOX were increased in the CP compared to the EC. TOX was most differential based on varying viral loads (Fig S1d). As CD4+ T cell dysfunction and viral load are strongly associated in HIV infection (4), TOX was best candidate for assessment of dysfunction by flow cytometry.

We set the TOX+ gate on naïve CD4+ T cells (Fig 1e), and confirmed a greater frequency of TOX+ cells in AIM+ HIV-specific CD4+ T cells of the CP cohort compared to EC (Fig 1f). TOX correlated significantly with PD-1 expression at the patient level (Fig 1g) and at the single-cell level (Fig 1h). Of note, EC had a population of TOX+PD-1low cells not observed in CP (Fig 1g), losing the correlation between PD-1 and TOX single cell expression. These observations suggest TOX and PD-1 are increased jointly in the setting of dysfunction, perhaps from common upregulating signals.

Differential PD-1 expression in polarized HIV-specific CD4+ T cells

Among AIM+ HIV-specific CD4+ T cells, we characterized three polarizations based on chemokine-receptors expression: CXCR3, CCR6 and CXCR5, enriched on antiviral TH1, mucosal-related TH17/TH22 and B-cell helper TFH, respectively (Fig 2a). Proportions were comparable between CP and EC, with the exception of a decreased CCR6+ fraction in CP (Fig S2a), as previously reported(4). TOX expression varied among polarizations

and the hierarchy was not maintained between both cohorts: while in CP, the CXCR3+ polarization had significantly greater TOX levels than CCR6+ and CXCR5+, in EC TOX levels were greater in CCR6+ than CXCR5+, and intermediate in CXCR3+ (Fig 2b).

PD-1 expression also varied among polarizations, mimicking TOX's pattern in CP: highest PD-1 was again observed on CXCR3+, while CXCR5+ and CCR6+ had comparable levels (Fig 2cd). In EC, the hierarchy of PD-1 was similar to that of CP, but contrasted with the hierarchy of TOX in EC: CXCR3+ cells had the greatest PD-1 levels, although only significantly greater when compared to CCR6+ cells. This is in line with the absence of correlation for EC between single-cell expression PD-1 and TOX, and further emphasizes that PD-1 and TOX expression are specifically linked in the context of dysfunction.

CXCR3, CCR6 and CXCR5 can be co-expressed in various patterns, in line with the plastic nature of TH (Fig 2eg). PD-1 expression was highest on the CXCR3+ CCR6- subsets (Fig 2fh). We further examined co-expression of classical "master" TFs with chemokine receptors, identifying TH1 as CXCR3+ T-BET+EOMES+, TH17 as CCR6+ROR-gt+CXCR3- and TH1/TH17 as CCR6+ROR-gt+CXCR3+(Fig S2e) (30). TFH's master regulator BCL-6 was largely undetectable in peripheral CD4+ T cells (Fig S2e), as previously reported (31). Among the AIM+ HIV-specific CD4+ T cells, the proportions of TH17 and TH1/TH17 were significantly higher in EC, but similar for TH1 (Fig S2f). PD-1 expression in CP always exceeded that in EC (Fig 2i) and, in both cohorts, TH1 cells had greater PD-1 expression than a CCR6+ polarization (Fig 2jk).

Thus, TOX and PD-1 expression follow similar patterns in the setting of dysfunction only ; however, the differing hierarchy of PD-1 expression among subsets of HIV-specific CD4+ T cells is observed both in CP and in EC.

PD-1 levels differ according to HIV-specific CD4+ T cell functions

We further identified HIV-specific CD4+ T cell subsets by cytokine expression and cytotoxic functions. Flow cytometric RNA fluorescent in situ hybridization (RNA-Flow-FISH) assay can capture hard-to-detect cytokines transcribed by HIV-specific CD4+ T upon cognate antigen stimulation, with fluorescence intensity giving a semi-quantitative measurement of the number of RNA copies per cell (32). We examined eight cytokines plus granzyme B (GZMB) that spanned five functional categories: IFNg and IL-2 for TH1-associated functions; GZMB for cytotoxic activity; IL-22 and IL-17F for mucosal-related TH17/TH22 functions; IL-21, CXCL13 and IL-4 for TFH-associated functions; and IL-10, a pleiotropic molecule with mostly inhibitory functions (Fig 3a, Fig S3a). CD69 served as a surrogate for recent activation to increase specificity for HIV antigen-induced cytokine mRNA (Fig S3b). HIV-specific CD4+ T cells producing IL-4 and IL-10 mRNA had low or undetectable frequencies in most participants and were not pursued (Fig S3bc). CPs had lower frequencies of IL22 mRNA+ cells, with a trend for lower IL17F and GZMB mRNA+ cells (Fig 3b), and fewer mucosal-related cytokine transcripts per cell (Fig 3C). Conversely, CP exhibited increased frequencies of TFH-related cytokines IL21 and CXCL13 mRNA+ cells (Fig 3b). Polyfunctional cells were observed in both cohorts, with only the GZMB+IL2+ populations rarely detected (Fig S3d). The other combinations followed the expected trends (Fig 3b): GZMB single-positive cells and all combinations of mucosal cytokines were greater in EC, whereas the CP had higher frequencies of TFH-related cytokines combinations. IFNG single-positive cells were increased in the response of CP, consistent with the reported loss of polyfunctionality in HIV-specific TH1 (33).

Chemokine receptors expression among cytokine mRNA+ HIV-specific CD4+ T cells

revealed complex associations between phenotype and function (Fig S3e). While CXCR3 was expressed on a large majority of GZMB, IL2 and IFNG mRNA+ cells (Fig S4a-c), it was also present on most IL21 and CXCL13+ mRNA cells. A minority of TFH-associated cytokine+ cells expressed CXCR5, with this proportion being smaller in CP. In contrast, almost all IL22 or IL17F mRNA+ cells expressed CCR6.

Among defined T helper functions, PD-1's hierarchy was similar to that observed on chemokine-receptor-identified polarizations: low on cells producing GZMB and mucosal-associated cytokines IL22 and IL17F, and high on TH1 (IFNG, IL2) and TFH (IL21, CXCL13) cytokine mRNA+ cells (Fig 3d-f). The hierarchy was similar in both cohorts, with the exception of particularly low PD-1 on IFNG mRNA+ cells in EC (Fig 3f).

These results demonstrate that HIV-specific CD4+ T cells can retain at least part of their functionality despite high PD-1 expression. Viremia leads to upregulation of this IC on functional cells, although the extent of its increase varies among T helper functions.

Differential responsiveness of individual cytokines to PD-1 blockade

Given the hierarchical expression of PD-1 among CD4+ T cells of different functions, we speculated that responsiveness of these cells to blockade of PD-L1, the major ligand for PD-1 in PBMCs, would be heterogeneous as well. On cells from CP, PD-L1 blockade increased frequencies of HIV-specific cytokine mRNA+ CD4+ T cells for mucosal and antiviral functions (Fig 4ab), only slightly impacted IL21, and no effect on CXCL13 mRNA+ cells. Blockade in EC had a globally smaller impact on HIV-specific CD4+ T cells (Fig

4cd), with increased frequencies only detected for IL2, IFNG, and IL22. Fold increases upon blockade of the 7 functions classified the participants relative to their cohort by unsupervised hierarchical clustering (Fig 4e), and in principal component analysis (PCA), clearly depicts disease status as the main source of variation (Fig 4f). CP were heterogeneous in which type of cytokine-producing cells were increased upon blockade, suggesting PD-L1 blockade does not result in a consistent profile of response even for one same antigen specificity. Many combinatory subpopulations increased in frequencies upon PD-L1 blockade in CP, with the notable exception of CXCL13 mRNA+ cells (Fig 4ghi). EC had overall lower responses (Fig S4efg). For most constellations, there was at least a trend for greater response in CP than in EC in terms of fold change, although the spread in our relatively small cohorts did not allow to rank responsiveness to PD-L1 blockade among subsets.

To study whether the effects observed on mRNA translated to protein, we performed delayed intracellular cytokine staining (d-ICS) following Gag stimulation. Extended stimulation before the addition of brefeldin A allows to capture the expression of both cytokines produced early, like IL-2 and IFNg as well as molecules induced later, namely CXCL13 and IL-21 (28). IL-17F and IL-22 were not detectable (Fig S4ab). Cytokine protein and cytokine mRNA expression correlated significantly for the IFNg IL-2 and CXCL13, but not for IL-21 (Fig S4c). Frequencies of IFNg+ and IL2+ HIV-specific CD4+ T cells were increased upon blockade, but not CXCL13+ cells (Fig S4d), reflecting the lack of response to anti-PD-L1 seen at the mRNA level.

These data demonstrate a heterogeneous capacity of functionally-distinct HIV-specific CD4+ T cells to respond to PD-L1 blockade at the transcriptional and translational level,

including for polyfunctional cells.

IC co-expression on HIV-specific CD4+ T cells is lineage- and function- specific

To understand the low responsiveness to blockade seen in TFH, we examined expression of the other ICs TIGIT and CD200, which are also frequently expressed on TFH cells (34). Similar to PD-1, expression of these IC was higher on AIM+ HIV-specific CD4+ T cells of CP than EC (Fig 5a-d), and correlated positively with viremia (Fig S5a), demonstrating an association between antigen burden and their accumulation, as previously shown for PD-1 (16) and TIGIT (35). Single-cell expression of TIGIT and CD200 was directly correlated with that of PD-1 (Fig 5ef), as well as with each other (Fig S5b). Almost half of AIM+ HIV-specific CD4+ T cells of CP co-expressed all three IC, whereas only a small fraction was triple-positive in EC (Fig 5g), in line with IC co-upregulation in conditions of elevated CD4+ T cell dysfunction (10). These IC varied according to subsets of HIV-specific CD4+ T cells (Fig S5cd). TIGIT was high on CXCR5+ cells and low on CCR6+ cells in both cohorts, and high on the CXCR3+ of CP only (Fig S5e). CD200 expression followed very similar patterns (Fig S5f). Consistently, IC expression differed between HIV-specific cytokine mRNA+ CD4+ T cells of CP, with high expression on IL21, CXCL13, IFNG and IL2 mRNA+ cells, and low IC levels on GZMB, IL17F and IL22 mRNA+ cells (Fig 5hi). Notably, CD200 was undetectable on mucosal-related cytokine mRNA+ cells. These patterns were conserved in EC (Fig S5ef), with once again the exception of IFNG mRNA+ cells, on which TIGIT and CD200 levels were low. Thus, TIGIT and CD200 are highly expressed on HIV-specific CD4+ T cells producing IL-2 or TFH-associated cytokines even in the absence of

high viral loads, yet IC accumulate on other cytokine+ cells only in the setting of dysfunction, in particular for functions reduced in CP compared to EC.

Combined ICB strategies targeting different molecules can be more potent than single blockade (10, 11). We examined the impact of two clinical-grade ICB antibodies developed for immunotherapy, the anti-PD-L1 antibody BMS-936559 and the anti-TIGIT antibody BMS-g86207-Ab (Bristol-Myers Squibb) using d-ICS, allowing us to multiplex the four cytokines IFNg IL-2, IL-21 and CXCL13 (Fig S5i). Single TIGIT blockade did not increase cytokine+ responses for any of the functions studied (Fig S5j). Responses were heterogeneous within the CP cohort: depending on the participant, we observed limited response to any blockade strategy (Fig S5h, left), detectable responses in the co-blockade condition only (Fig S5h, middle) or modest to no benefit of co-blockade compared to single PD-1 blockade (Fig S5h, right). Our data suggests co-blockade strategies may generate responses in a larger fraction of individuals than single-blockade, although some subjects may remain unresponsive.

Because of the differential response of IFNg and CXCL13 to blockade, we compared its impact between monofunctional cells and the population co-expressing CXCL13 and IFNg which represented roughly 20% of the overall cytokine-producing populations (Fig S5i). The frequency of IFNg single-positive and or double-positive CD4+ T cells increased upon PD-L1 blockade, whereas CXCL13 single-positive cells remained refractory (Fig S5jk). The double-positive population are also increased upon blockade, highlighting that CXCL13 transcription can be susceptible to ICB. The pattern was the same with co-blockade, at a slightly greater magnitude.

These observations highlight the accumulation of ICs TIGIT and CD200 on subsets other

than TFH in the context of dysfunction. However, high co-expression of TIGIT and PD-1 does not result in enhanced response to TIGIT and PD-L1 co-blockade compared to single PD-L1 blockade in most individuals.

ART-induced viral suppression differentially affects HIV-specific CD4+ T cell response to ICB

As ICB in HIV infection is predominantly being evaluated in ART-suppressed individuals, we compared responses in longitudinal samples obtained before and after ART (Fig 6a, Fig S6a). ART initiation led to a consistent decrease of the preferentially TFH-associated functions IL-21 and CXCL13 in HIV-specific CD4+ T cells (Fig 6b). With the exception of the frequency of IL2 mRNA+ CD4+ T cells, which remained constant between both time points, the effect of ART was heterogeneous and subject-dependent, with some subjects experiencing an increase or a decrease, and others still maintaining stable responses (Fig 6b). Post-ART, IC expression decreased on all cytokine mRNA+ CD4+ T cells, except for the IL2+, on which IC expression was maintained (Fig S6b-d). These results highlight a correction of the high IC expression and TFH-like skewing acquired in viremia towards a profile more similar to that observed in EC, while other functions are inconsistently recovered.

The increase of IL2 mRNA+ CD4+ T cells upon PD-L1 blockade was also seen following ART treatment (Fig 6c), and of similar magnitude to that observed in both CP (Fig 6d) and EC (Fig 4d). However, the increases for IFNG and mucosal-related cytokine expression were generally less pronounced after ART initiation, albeit with inter-subject variability (Fig

6cd). No effect on the frequency of TFH-cytokine+ CD4+ T cells was observed upon blockade during ART.

These data suggest that increased IL-2 production is a maintained benefit of PD-L1 blockade, while the increase in IFNG and mucosal-related cytokines upon ICB is subdued once ART is initiated.

Discussion

Immune checkpoints inhibit T cell activation through multiple mechanisms (36, 37). Although recent findings have partially elucidated the molecular features behind these effects (5, 37), an understudied topic remains if and how these immune checkpoints operate differently among the heterogeneous lineages of CD4+ T cells. Using high-parameter flow cytometry combining protein and FISH mRNA staining, we assessed HIV-specific CD4+ T cells of an array of T helper phenotypes and functions otherwise difficult to measure. We focused on a palette of TFH, TH1 and TH17/TH22-associated traits. These phenotypes, as identified by canonical chemokine receptors and transcription factors or by production of effector molecules, presented a hierarchy of relative expression levels of TOX, PD-1, TIGIT and CD200. This differential expression was present at all HIV disease stages, although the magnitude of expression was associated with viral load. Responsiveness to PD-L1 blockade varied according to a defined function of CD4+ T cells rather than their levels of IC expression. PD-L1 blockade had more limited effects in individuals with spontaneous or therapeutic control of viral replication than in people with high antigen load. These data highlight a previously unappreciated heterogeneity of responsiveness to ICB among HIV-specific CD4+ T cells.

TOX expression was greater in HIV-specific CD4+ T cells of CP compared to EC, in line with their greater state of dysfunction linked with ongoing antigen stimulation in CP, and greater functionality in EC(4). TOX expression is linked to repeated TCR stimulation (7, 38), a central driver of T cell exhaustion, and was strongly associated to PD-1 levels in the presence of viremia. HIV-specific CD4+ T cells from a same subject expressed different amounts of IC depending on their polarization, consistent across function-

dependent (ICS) and function-agnostic (AIM) methods of identification. High expression or co-expression of IC did not prevent effector functions, as observed with IC-high CXCL13+, IL-21+ and IL-2+ cells. IL-2 markedly increased with PD-L1 blockade, consistent with an inhibitory effect by PD-1, while no effect was observed for IL-21 and CXCL13. The hierarchy of IC expression between polarizations of HIV-specific CD4+ T cells suggest IC may not equally regulate the respective' CD4+ T cell function. As shown in a TCR transfection model system of primary human PBMCs, some T cell functions are more resistant to PD-1-mediated inhibition than others (39), while a recent study using mouse and human T cell lines demonstrated different sensitivities of gene expression to PD-1 inhibition (40). IC may not be inhibitory in all instances: TFH express lower amounts of IL-21 and IL-4 following PD-1 ablation in mice (41); TIGIT, although inhibitory when expressed on CD8+ or TH1 T cells (42, 43), is associated with strong B cell help and cytokine expression in TFH (44); CD200 is associated with lack of pro-inflammatory cytokines, yet high IL-4 production in CD4+ T cells (45). Although these reports often find IC not inhibiting TFH-related functions, our observation that CXCL13+IFNg+ cells increased in frequency upon ICB indicates this TFH function can be negatively modulated by PD-1. Co-expression of CXCL13+ cells with a TH1-associated cytokine may correspond to a transition into a more plastic cell state which is responsive to ICB, while the absence of response in CXCL13 single-positive cells suggest that the cell-intrinsic state is associated with response to blockade, rather than single cytokine pathways or IC expression.

Response to PD-L1 blockade was stronger in both breadth and magnitude for the dysfunctional HIV-specific CD4+ T cells of the CP compared to the EC and ART cohorts,

suggesting that antigen presence sensitizes antigen-specific CD4+ T cells to ICB. Co-blockade with a TIGIT-blocking antibody further enhanced the effect of PD-L1 blockade only in some patients, consistent with the reported varying sensitivity to co-blockade among subjects (12, 35, 46), and highlighting the central inhibitory role of PD-1. Of note, HIV-specific CD4+T cells may respond directly to ICB by blockade of autologous PD-1 molecules, as we have shown with live-sorted CD4 T cells subsets and add back co-culture experiments(14), or indirectly by paracrine mechanisms, like the feed forward loop of soluble factors between T cells and antigen-presenting cells (47). While their respective contributions would be extremely challenging to delineate on primary human T cells, the critical observation remains that different HIV-specific CD4 T cell subsets have a differential ability to respond to PD-1 blockade.

CD4+ T cells expressing mucosal cytokines responded well to PD-L1 blockade, despite the low levels of PD-1 expression on these cells overall. This suggests the replenished gut in the chronic SIV model may be linked to responsiveness of TH17/TH22 cells (25, 26), the primary CD4+ T cell population of that anatomical site. In this scenario, bacteria-specific TH17 may also have responded to ICB (48). Taken together, our data suggests that polarizations nudging towards TH1 and TH17 may undergo a more direct inhibition by PD-1, explaining their strong responsiveness to ICB. This can procure benefits such as direct antiviral control and restored gut integrity, even under conditions of persistent antigen.

As rapid initiation of ART is now the standard of care upon HIV diagnosis, it is crucial to know whether the response to PD-L1 blockade changes once viremia is therapeutically suppressed. IL-2 response reached the same magnitude as observed at the pre-ART time

point, comparable to that seen in EC, in line with the direct inhibitory role PD-1 plays in regulating IL-2 (20). Conversely, responses of CD4+ T cells expressing IFNg and mucosal-related cytokines to ICB decreased in magnitude once ART was initiated. The general lowering of reactivity to ICB in contexts of controlled viremia strongly support a role of ongoing antigen presence in sensitizing these cells to this type of treatment. In addition, ART may block de novo virus-specific CD4+ T cells, which may be more responsive to ICB (49). These observations highlight the important role timing may play to maximize benefits of ICB in the context of HIV.

Although more comprehensive than previous studies looking at HIV-specific CD4+ T cells, our observational study focused on a selected set of T helper functions. Furthermore, while we utilized in vitro blockade of PBMCs to interrogate the response of multiple CD4+ T cell subsets to PD-L1 blockade, most HIV-specific CD4+ T cells reside in tissues, where IC can play distinct roles, and cannot address the actively-researched in vivo role of ICB(50). Addressing such questions would require tissue samples or animal models. Indeed, a clinical safety trial of anti-PD-L1 in ART-treated revealed 2 of 6 HIV-infected individuals had increased HIV-specific CD8+ T cell responses in blood (51). In the non-human primate model (NHP) of Simian Immunodeficiency Virus (SIV) infection, PD-1 blockade did significantly decreased viral load in chronically-infected NHPs (24). In ART-treated NHPs, PD-1 blockade and PD-1/CTLA dual blockade resulted in a 5-day delay in viral rebound following ART cessation, but was not sufficient to achieve viral control (52), suggesting ICB may have to be combined with additional strategies. Indeed, combination of ART, an anti-SIV-boosting vaccine and PD-1 blockade was recently shown to suppress rebound after ART interruption in rhesus macaques (53). These approaches should be

considered with precaution, as restoring function of virus-specific T cells can cause depletion of lymphoid organs harboring infected cells, impeding the generation of new immune responses (54).

In summary, we highlight an intrinsic heterogeneity in IC expression among different polarizations of HIV-specific CD4+ T cells, revealing a disconnect between classical notions of IC and their relevance among CD4+ T cells lineages. This data also shows that functional lineages of HIV-specific CD4+ T cells have different capacities to respond to IC blockade, with CD4+ T cells expressing mucosal-protective and antiviral-associated cytokines responding well, whereas TFH-associated cytokines responded poorly. These results emphasize the importance of considering CD4+ T cell differentiation in studies of IC blockade in the context of T cell dysfunction, and may have implications for CD4+ T cell help in other infectious and non-infectious chronic human diseases.

Declaration of Competing Interests

GJF has patents/pending royalties on the PD-1/PD-L1 pathway from Roche, Merck MSD, Bristol-Myers-Squibb, Merck KGA, Boehringer-Ingelheim, AstraZeneca, Dako, Leica, Mayo Clinic, and Novartis. GJF has served on advisory boards for Roche, Bristol-Myers-Squibb, Xios, Origimed, Triursus, iTeos, and NextPoint. GJF has equity in Nextpoint, Triursus, and Xios. Data and materials availability: The anti-PD-L1 antibody BMS-936559 and the anti-TIGIT antibody BMS-g86207-Ab were given by Bristol-Myers Squibb. The company had no implications in the design and interpretation of the experiments performed in this manuscript.

Ackowledgements

We thank Josée Girouard, the clinical staff at the McGill University Health Centre in Montreal and all study participants for their invaluable role in this project. We also thank Ms. Alina Dyachenko for help with statistical analyses.

Function sources

This study was supported by the National Institutes of Health (HL092565, to D.E.K; R37AI112787 to G.J.F); the Canadian Institutes for Health Research (grants 137694 and 152977 to D.E.K.; grant MOP-93770 to C.T), Canada Foundation for Innovation Program Leader grants (grants #31756 and 37521 to D.E.K.), the FRQS AIDS and Infectious Diseases Network. D.E.K is a Merit Research Scholar of the Quebec Health Research

Fund (FRQS). J.P.R is the holder of Louis Lowenstein Chair in Hematology & Oncology, McGill University. E. B. R. received a scholarship from the Faculté des Études Supérieures (FESP) of the Université de Montréal.

References :

1. Laidlaw BJ, Craft JE, Kaech SM. The multifaceted role of CD4(+) T cells in CD8(+) T cell memory. Nat Rev Immunol. 2016;16(2):102-11.

2. Swain SL, McKinstry KK, Strutt TM. Expanding roles for CD4(+) T cells in immunity to viruses. Nat Rev Immunol. 2012;12(2):136-48.

3. Becattini S, Latorre D, Mele F, Foglierini M, De Gregorio C, Cassotta A, et al. T cell immunity. Functional heterogeneity of human memory CD4(+) T cell clones primed by pathogens or vaccines. Science. 2015;347(6220):400-6.

4. Morou A, Brunet-Ratnasingham E, Dube M, Charlebois R, Mercier E, Darko S, et al. Altered differentiation is central to HIV-specific CD4(+) T cell dysfunction in progressive disease. Nat Immunol. 2019;20(8):1059-70.

5. Sen DR, Kaminski J, Barnitz RA, Kurachi M, Gerdemann U, Yates KB, et al. The epigenetic landscape of T cell exhaustion. Science. 2016;354(6316):1165-9.

6. Pauken KE, Sammons MA, Odorizzi PM, Manne S, Godec J, Khan O, et al. Epigenetic stability of exhausted T cells limits durability of reinvigoration by PD-1 blockade. Science. 2016;354(6316):1160-5.

7. Khan O, Giles JR, McDonald S, Manne S, Ngiow SF, Patel KP, et al. TOX transcriptionally and epigenetically programs CD8(+) T cell exhaustion. Nature. 2019;571(7764):211-8.

8. Heim K, Binder B, Sagar, Wieland D, Hensel N, Llewellyn-Lacey S, et al. TOX defines the degree of CD8+ T cell dysfunction in distinct phases of chronic HBV infection. Gut. 2020.

9. Sekine T, Perez-Potti A, Nguyen S, Gorin JB, Wu VH, Gostick E, et al. TOX is expressed by exhausted and polyfunctional human effector memory CD8(+) T cells. Sci Immunol. 2020;5(49).

10. Crawford A, Angelosanto JM, Kao C, Doering TA, Odorizzi PM, Barnett BE, et al. Molecular and transcriptional basis of CD4(+) T cell dysfunction during chronic infection. Immunity. 2014;40(2):289-302.

11. Wherry EJ, Kurachi M. Molecular and cellular insights into T cell exhaustion. Nat Rev Immunol. 2015;15(8):486-99.

12. Kaufmann DE, Kavanagh DG, Pereyra F, Zaunders JJ, Mackey EW, Miura T, et al. Upregulation of CTLA-4 by HIV-specific CD4+ T cells correlates with disease progression and defines a reversible immune dysfunction. Nat Immunol. 2007;8(11):1246-54.

13. Kassu A, Marcus RA, D'Souza MB, Kelly-McKnight EA, Golden-Mason L, Akkina R, et al. Regulation of virus-specific CD4+ T cell function by multiple costimulatory receptors during chronic HIV infection. J Immunol. 2010;185(5):3007-18.

14. Porichis F, Kwon DS, Zupkosky J, Tighe DP, McMullen A, Brockman MA, et al. Responsiveness of HIV-specific CD4 T cells to PD-1 blockade. Blood. 2011;118(4):965-74.

15. Schildberg FA, Klein SR, Freeman GJ, Sharpe AH. Coinhibitory Pathways in the B7-CD28 Ligand-Receptor Family. Immunity. 2016;44(5):955-72.

16. Day CL, Kaufmann DE, Kiepiela P, Brown JA, Moodley ES, Reddy S, et al. PD-1 expression on HIV-specific T cells is associated with T-cell exhaustion and disease progression. Nature. 2006;443(7109):350-4.

17. Im SJ, Hashimoto M, Gerner MY, Lee J, Kissick HT, Burger MC, et al. Defining CD8+ T cells that provide the proliferative burst after PD-1 therapy. Nature. 2016;537(7620):417-21.

18. Kamphorst AO, Pillai RN, Yang S, Nasti TH, Akondy RS, Wieland A, et al. Proliferation of PD-1+ CD8 T cells in peripheral blood after PD-1-targeted therapy in lung cancer patients. Proc Natl Acad Sci U S

A. 2017;114(19):4993-8.

19. Miller BC, Sen DR, Al Abosy R, Bi K, Virkud YV, LaFleur MW, et al. Subsets of exhausted CD8(+) T cells differentially mediate tumor control and respond to checkpoint blockade. Nat Immunol. 2019;20(3):326-36.

20. Quigley M, Pereyra F, Nilsson B, Porichis F, Fonseca C, Eichbaum Q, et al. Transcriptional analysis of HIV-specific CD8+ T cells shows that PD-1 inhibits T cell function by upregulating BATF. Nat Med. 2010;16(10):1147-51.

21. Zuazo M, Arasanz H, Fernandez-Hinojal G, Garcia-Granda MJ, Gato M, Bocanegra A, et al. Functional systemic CD4 immunity is required for clinical responses to PD-L1/PD-1 blockade therapy. EMBO Mol Med. 2019;11(7):e10293.

22. Sakai S, Kauffman KD, Sallin MA, Sharpe AH, Young HA, Ganusov VV, et al. CD4 T Cell-Derived IFN-gamma Plays a Minimal Role in Control of Pulmonary Mycobacterium tuberculosis Infection and Must Be Actively Repressed by PD-1 to Prevent Lethal Disease. PLoS Pathog. 2016;12(5):e1005667.

23. Barber DL, Sakai S, Kudchadkar RR, Fling SP, Day TA, Vergara JA, et al. Tuberculosis following PD-1 blockade for cancer immunotherapy. Sci Transl Med. 2019;11(475).

24. Velu V, Titanji K, Zhu B, Husain S, Pladevega A, Lai L, et al. Enhancing SIV-specific immunity in vivo by PD-1 blockade. Nature. 2009;458(7235):206-10.

25. Dyavar Shetty R, Velu V, Titanji K, Bosinger SE, Freeman GJ, Silvestri G, et al. PD-1 blockade during chronic SIV infection reduces hyperimmune activation and microbial translocation in rhesus macaques. J Clin Invest. 2012;122(5):1712-6.

26. Mylvaganam GH, Chea LS, Tharp GK, Hicks S, Velu V, Iyer SS, et al. Combination anti-PD-1 and antiretroviral therapy provides therapeutic benefit against SIV. JCI Insight. 2018;3(18).

27. Brown JA, Dorfman DM, Ma FR, Sullivan EL, Munoz O, Wood CR, et al. Blockade of programmed death-1 ligands on dendritic cells enhances T cell activation and cytokine production. J Immunol. 2003;170(3):1257-66.

28. Niessl J, Baxter AE, Morou A, Brunet-Ratnasingham E, Sannier G, Gendron-Lepage G, et al. Persistent expansion and Th1-like skewing of HIV-specific circulating T follicular helper cells during antiretroviral therapy. EBioMedicine. 2020;54:102727.

29. Reiss S, Baxter AE, Cirelli KM, Dan JM, Morou A, Daigneault A, et al. Comparative analysis of activation induced marker (AIM) assays for sensitive identification of antigen-specific CD4 T cells. PLoS One. 2017;12(10):e0186998.

30. O'Shea JJ, Paul WE. Mechanisms underlying lineage commitment and plasticity of helper CD4+ T cells. Science. 2010;327(5969):1098-102.

31. Locci M, Havenar-Daughton C, Landais E, Wu J, Kroenke MA, Arlehamn CL, et al. Human circulating PD-1+CXCR3-CXCR5+ memory Tfh cells are highly functional and correlate with broadly neutralizing HIV antibody responses. Immunity. 2013;39(4):758-69.

32. Porichis F, Hart MG, Griesbeck M, Everett HL, Hassan M, Baxter AE, et al. High-throughput detection of miRNAs and gene-specific mRNA at the single-cell level by flow cytometry. Nat Commun. 2014;5:5641.

33. Vella LA, Herati RS, Wherry EJ. CD4(+) T Cell Differentiation in Chronic Viral Infections: The Tfh Perspective. Trends Mol Med. 2017;23(12):1072-87.

34. Sade-Feldman M, Yizhak K, Bjorgaard SL, Ray JP, de Boer CG, Jenkins RW, et al. Defining T Cell States Associated with Response to Checkpoint Immunotherapy in Melanoma. Cell. 2018;175(4):998-1013 e20.

35. Chew GM, Fujita T, Webb GM, Burwitz BJ, Wu HL, Reed JS, et al. TIGIT Marks Exhausted T Cells, Correlates with Disease Progression, and Serves as a Target for Immune Restoration in HIV and SIV Infection. PLoS Pathog. 2016;12(1):e1005349.

36. Chen L, Flies DB. Molecular mechanisms of T cell co-stimulation and co-inhibition. Nat Rev Immunol. 2013;13(4):227-42.

37. Hui E, Cheung J, Zhu J, Su X, Taylor MJ, Wallweber HA, et al. T cell costimulatory receptor CD28 is a primary target for PD-1-mediated inhibition. Science. 2017;355(6332):1428-33.

38. Alfei F, Kanev K, Hofmann M, Wu M, Ghoneim HE, Roelli P, et al. TOX reinforces the phenotype and longevity of exhausted T cells in chronic viral infection. Nature. 2019;571(7764):265-9.

39. Wei F, Zhong S, Ma Z, Kong H, Medvec A, Ahmed R, et al. Strength of PD-1 signaling differentially affects T-cell effector functions. Proc Natl Acad Sci U S A. 2013;110(27):E2480-9.

40. Shimizu K, Sugiura, D., Okazaki, I., Maruhashi, T., Takegami, Y., Cheng, C., Ozaki, S., Okazaki, T. PD-1 Imposes Qualitative Control of Cellular Transcriptomes in Response to T Cell Activation. Molecular Cell. 2020(77):1-14.

41. Good-Jacobson KL, Szumilas CG, Chen L, Sharpe AH, Tomayko MM, Shlomchik MJ. PD-1 regulates germinal center B cell survival and the formation and affinity of long-lived plasma cells. Nat Immunol. 2010;11(6):535-42.

42. Tauriainen J, Scharf L, Frederiksen J, Naji A, Ljunggren HG, Sonnerborg A, et al. Perturbed CD8+ T cell TIGIT/CD226/PVR axis despite early initiation of antiretroviral treatment in HIV infected individuals. Sci Rep. 2017;7:40354.

43. Joller N, Lozano E, Burkett PR, Patel B, Xiao S, Zhu C, et al. Treg cells expressing the coinhibitory molecule TIGIT selectively inhibit proinflammatory Th1 and Th17 cell responses. Immunity. 2014;40(4):569-81.

44. Godefroy E, Zhong H, Pham P, Friedman D, Yazdanbakhsh K. TIGIT-positive circulating follicular helper T cells display robust B-cell help functions: potential role in sickle cell alloimmunization. Haematologica. 2015;100(11):1415-25.

45. Caserta S, Nausch N, Sawtell A, Drummond R, Barr T, Macdonald AS, et al. Chronic infection drives expression of the inhibitory receptor CD200R, and its ligand CD200, by mouse and human CD4 T cells. PLoS One. 2012;7(4):e35466.

46. Grabmeier-Pfistershammer K, Stecher C, Zettl M, Rosskopf S, Rieger A, Zlabinger GJ, et al. Antibodies targeting BTLA or TIM-3 enhance HIV-1 specific T cell responses in combination with PD-1 blockade. Clin Immunol. 2017;183:167-73.

47. Porichis F, Hart MG, Zupkosky J, Barblu L, Kwon DS, McMullen A, et al. Differential impact of PD-1 and/or interleukin-10 blockade on HIV-1-specific CD4 T cell and antigen-presenting cell functions. J Virol. 2014;88(5):2508-18.

48. Perreau M, Vigano S, Bellanger F, Pellaton C, Buss G, Comte D, et al. Exhaustion of bacteria-specific CD4 T cells and microbial translocation in common variable immunodeficiency disorders. J Exp Med. 2014;211(10):2033-45.

49. Snell LM, Osokine I, Yamada DH, De la Fuente JR, Elsaesser HJ, Brooks DG. Overcoming CD4 Th1 Cell Fate Restrictions to Sustain Antiviral CD8 T Cells and Control Persistent Virus Infection. Cell Rep. 2016;16(12):3286-96.

50. Fromentin R, DaFonseca S, Costiniuk CT, El-Far M, Procopio FA, Hecht FM, et al. PD-1 blockade potentiates HIV latency reversal ex vivo in CD4(+) T cells from ART-suppressed individuals. Nat Commun. 2019;10(1):814.

51. Gay CL, Bosch RJ, Ritz J, Hataye JM, Aga E, Tressler RL, et al. Clinical Trial of the Anti-PD-L1

Antibody BMS-936559 in HIV-1 Infected Participants on Suppressive Antiretroviral Therapy. J Infect Dis. 2017.

52. Harper J, Gordon S, Chan CN, Wang H, Lindemuth E, Galardi C, et al. CTLA-4 and PD-1 dual blockade induces SIV reactivation without control of rebound after antiretroviral therapy interruption. Nat Med. 2020;26(4):519-28.

53. Rahman SA, Yagnik, B., Bally, A.P., Morrow, K. N., Wang, S., Vanderford, T. H., Freeman, G. J., Ahmend, R., Amara, R.R. PD-1 blockade and vaccination provide therapeutic benefit against SIV by inducing broad and functional CD8+ T cells in lymphoid tissue. Sci Immunol. 2021;6(63).

54. Elsaesser HJ, Mohtashami M, Osokine I, Snell LM, Cunningham CR, Boukhaled GM, et al. Chronic virus infection drives CD8 T cell-mediated thymic destruction and impaired negative selection. Proc Natl Acad Sci U S A. 2020;117(10):5420-9.

Figures

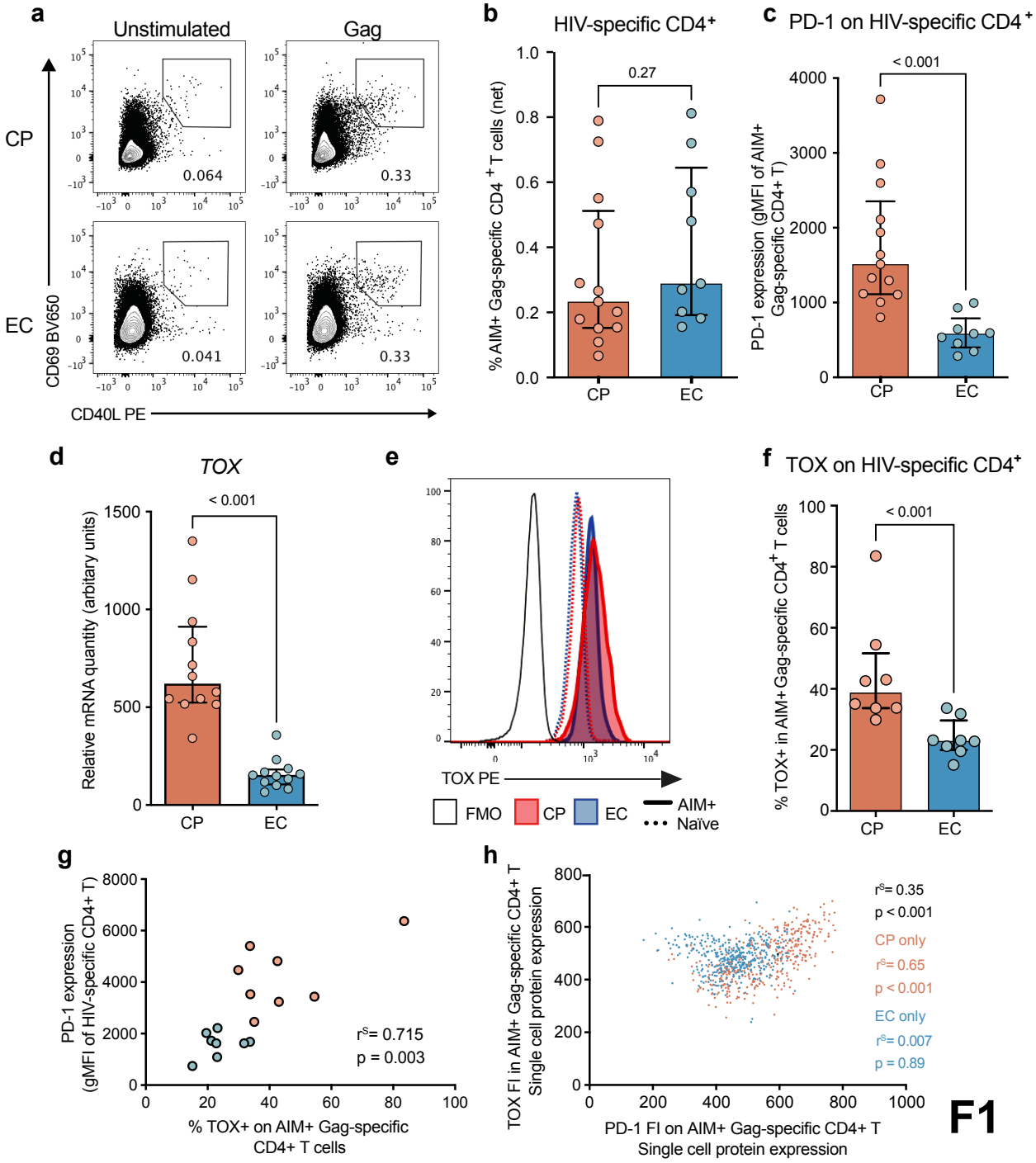

Figure 5.1 Increased expression of exhaustion-related transcription factors in HIV-specific CD4+ T cells of CP compared to EC. a) Representative flow cytometry plots and b) cumulative data of AIM+ Gag-specific CD4+ T cells detection via upregulation of the activation-induced markers (AIM) CD69 and CD40L in a CP (top) and an EC (bottom) 9 hours after stimulation with a HIV Gag peptide pool. c) Comparison of PD-1 expression on AIM+ HIV-specific CD4+ T cells in the CP (orange) and EC (blue)

cohorts. Representative flow cytometry plot of TCF-1 and TOX staining on total CD4+ T cell (top) or Gag-specific AIM+ CD4+ T cells (bottom). d) Relative *Tox* mRNA expression among sorted Gag-specific CD4+ T cells of CP (red) or EC (blue), as captured by high-throughput RT-PCR (Fluidigm® - for details, please see (Morou *et al.*, 2019). e) Representative example of TOX expression in AIM+ HIV-specific CD4+ T cells (shaded) or unstimulated naïve CD4+T cells (dotted line) of both cohorts. Black line is FMO control. f) Cumulative data of the frequency of TOX+ cells among AIM+ Gag-specific CD4+ T cells (right) of CP (blue) or EC (red), using gating strategy depicted in A. g) Correlation between the frequency of TOX and PD-1 expression level among AIM+ Gag-specific CD4+ T cells. h) Correlation between the single cell expression (as captured by flow cytometry – FI = fluorescence intensity) of TOX and PD-1. Correlation done using 100 cells per patient for 4 CP and 4 EC. bc) n = 13 CP and 9 EC. d) n = 9 CP and 9 EC. fg) n = 8 CP & 8 EC. bcdf) Stats = Mann-Whitney test. GH) Spearman correlation.

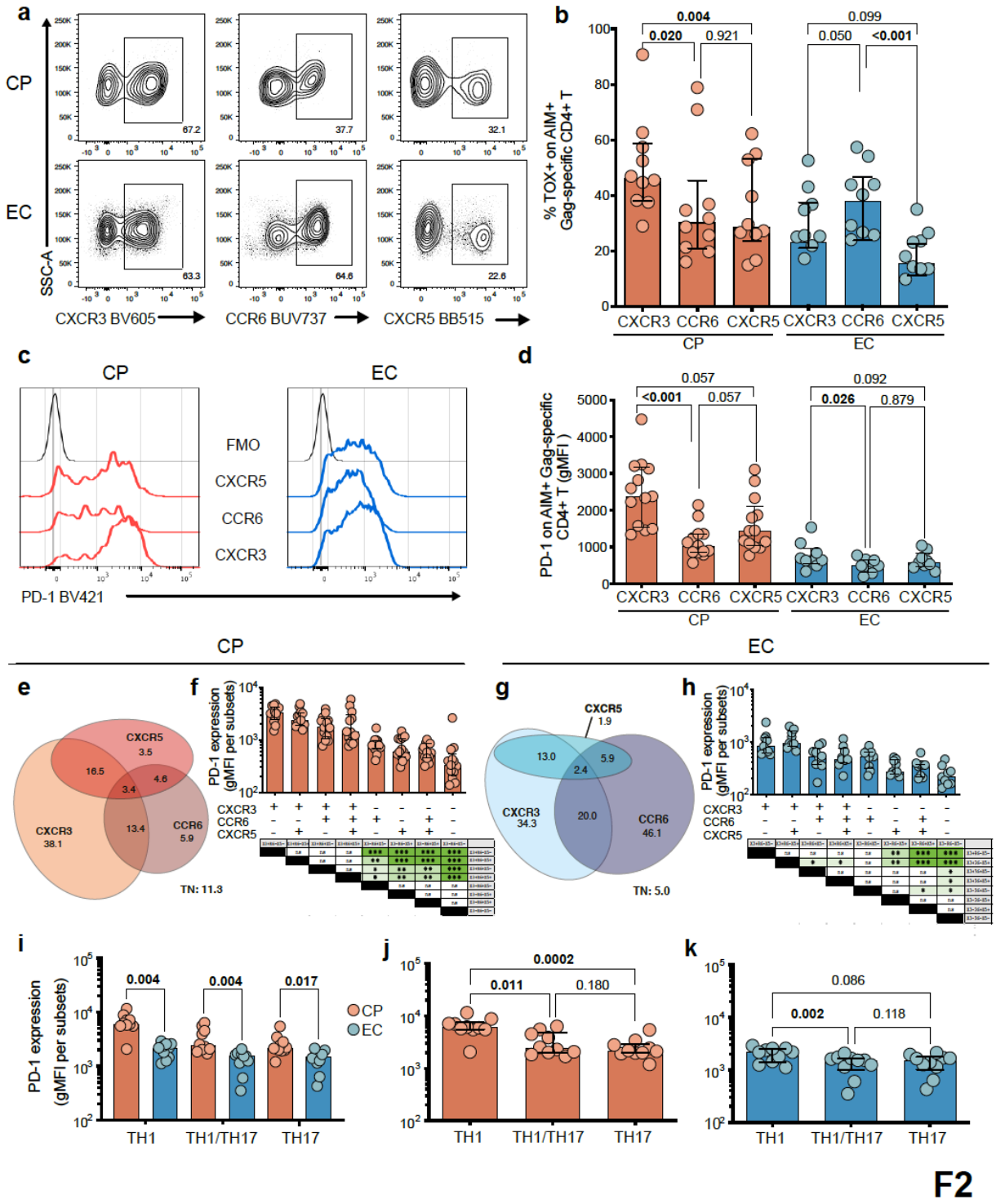

Figure 5.2 PD-1 expression on HIV-specific CD4+ T cells depends on their polarization. **a**) Representative flow cytometry plots of expression of the chemokine receptors CXCR3, CCR6 and CXCR5 on AIM+ Gag-specific CD4+ T cells of a CP (top) and an EC (bottom). **b**) Expression of TOX among chemokine-receptor-identified polarizations of Gag-specific CD4+ T cells among CP (red) or EC (blue). **c**) Representative example and **d**) cumulative data of PD-1 expression among chemokine-receptor-identified polarizations of Gag-specific CD4+ T cells. Euler graphs of co-expression for CXCR3, CCR6 and CXCR5 on

AIM+ Gag-specific CD4+ T cells in **e**) CP or **g**) EC. Values represent median frequencies of subsets within total AIM+ Gag-specific CD4+ T cells. TN: triple negative for all three chemokine receptors. PD-1 expression in AIM+ HIV-specific CD4+ T cells subsets, as identified by chemokine co-expression patterns in **f**) CP or **h**) EC. Statistics appear in tables below, with p values < 0.05 highlighted in green. PD-1 expression on CD4+ T cell subsets identified by chemokine receptor and master transcription factors, **i**) in CP vs EC; between polarizations of **j**) CP or **k**) EC. In D-H n= 13 CP and 9 EC. I-J n = 8 CP and 8 EC. Columns correspond to median values with interquartile range. dfhjk) Friedman test with Dunn's post-test. i) Mann-Whitney test. Geo MFI: Geometric Mean of Fluorescence Intensity.

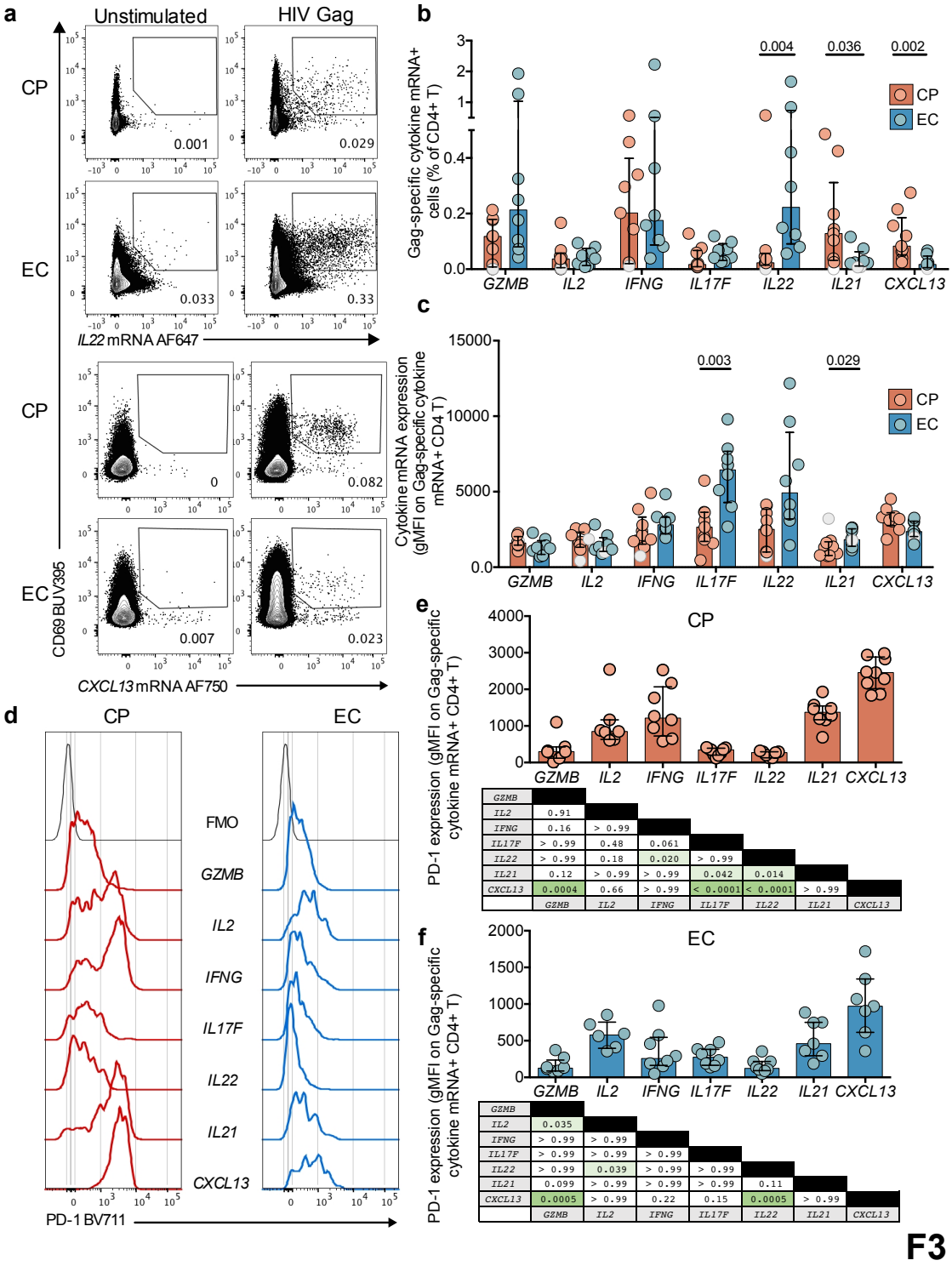

Figure 5.3 Heterogeneous PD-1 expression among cytokine-producing HIV-specific CD4+ T cells. a) Representative flow cytometry plots of IL22 mRNA and CXCL13 mRNA detection in a CP and an EC. Cumulative data of the **b**) net frequencies or **c**) geometric mean fluorescence intensity of Gag-specific cytokine mRNA+ CD4+ T cells in both cohorts. **d**) Representative examples and cumulative data of PD-1

expression on Gag-specific cytokine mRNA+ CD4+ T cells in **e**) CP or **f**) EC. Statistics appear in tables below, with p values < 0.05 highlighted in green. All mRNA data were acquired following a 12-hour stimulation with HIV Gag peptide pool. In bcef, n = 9 CP and 8 EC. In ef) only positive responses (at least 2 fold greater than unstimulated) are considered. Negative responses identified by grey shapes in bc. Bars represent medians with interquartile range. bc) Mann Whitney test. ef) Kruskall Wallis, with Dunn's multiple comparisons tests.

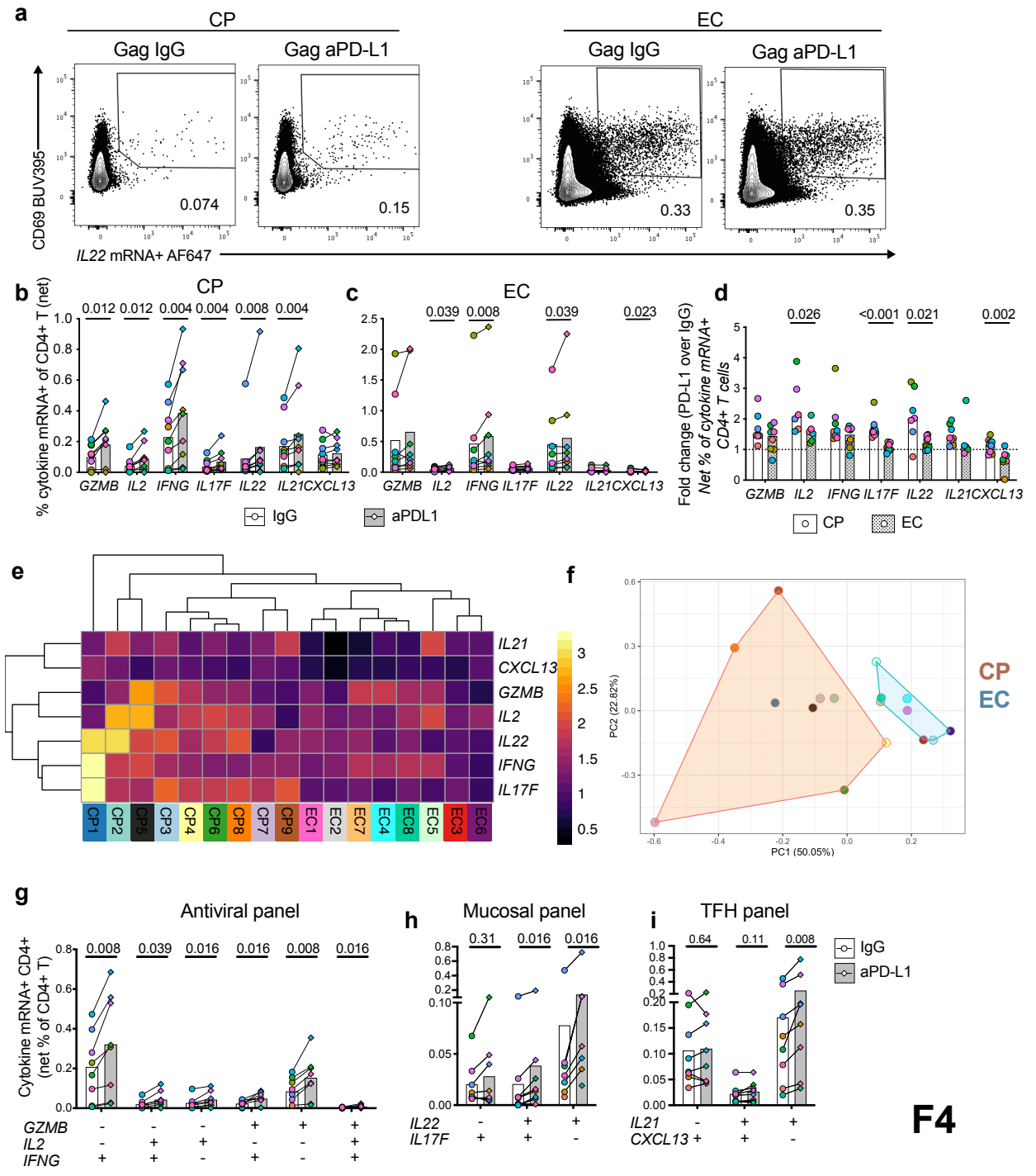

Figure 5.4 Differential responsiveness of individual HIV-specific CD4+ T cell cytokines to PD-1 blockade. **a**) Representative flow cytometry plots of *IL22* mRNA following Gag stimulation with PD-L1 blocking antibody (aPD-L1) or isotypic control (IgG) in a CP and an EC. Cumulative net frequency for all cytokine mRNA+ CD4+ T cells in **b**) CP and **c**) EC. **d**) Fold change in the net frequencies of cytokine mRNA+ HIV-specific CD4+ T cells upon PD-L1 blockade compared to isotypic control for both cohorts. CP in orange and EC in blue. **e**) Unsupervised hierarchical clustering analysis and heatmap of fold changes per cytokine across subjects, with warmer colors representing stronger fold changes. Bottom row corresponds to

individual subject IDs. **f**) Principal component analysis (PCA) representation of CP (orange) and EC (blue) responses based on cytokine mRNA fold changes upon PD-L1 blockade. Length of lines to cytokines represent contribution to variance of each cytokine; angle of line represents their contribution to either PC1 and PC2. Red or blue shading regroups CP or EC, respectively. The numbers in parentheses are the percentage of variance explained by each principal component. Response of all cytokine mRNA combinations to PD-L1 blockade, upon Gag-stimulation among CP, for **g**) antiviral panel; **h**) mucosal panel or **i**) TFH panel. n = 9 CP and 8 EC. Columns correspond to median values with interquartile range. bcghi) Wilcoxon test. d) Mann-Whitney test. Each donor within a cohort has been separately color coded.

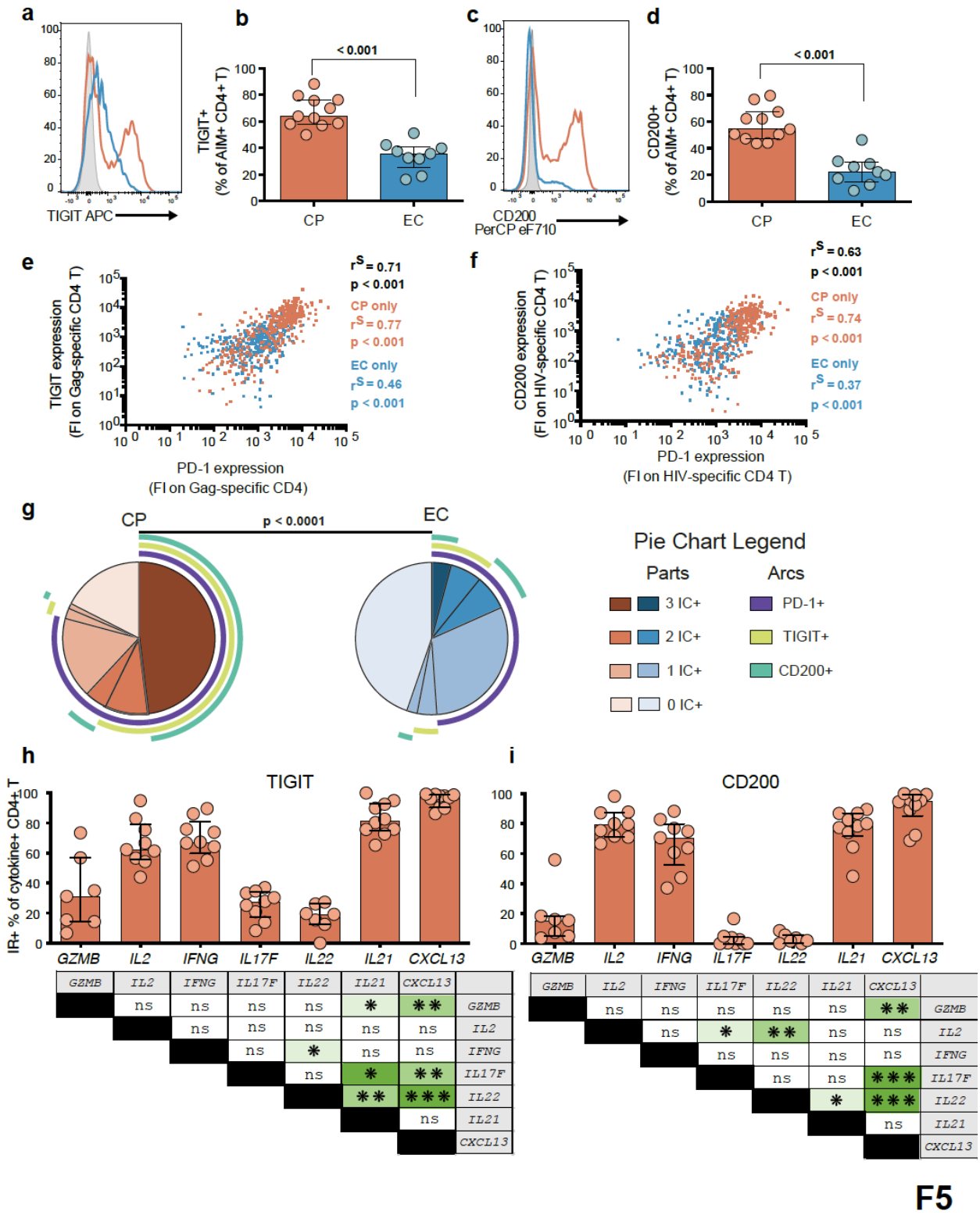

Figure 5.5 Differential expression of ICs among functionally-distinct subsets of HIV-specific CD4+ T cells. Representative histogram overlays of **a**) TIGIT or **c**) CD200 expression on AIM+ Gag-specific CD4+ T cells from a CP (red) or an EC (blue). Grey shaded outline represents PD-1 FMO. Fraction of AIM+ Gag-specific CD4+ T cells expressing **b**) TIGIT or **d**) CD200 of either cohort. Correlation between single-

cell expression of PD-1 and **e**) TIGIT or **f**) CD200 on AIM+ Gag-specific CD4+ T cells from 4 CP and 4 EC (100 cells per subject). **g**) Co-expression patterns between the ICs PD-1, TIGIT and CD200 on AIM+ HIV-specific CD4+ T cells from both cohorts. Shades of pie parts represent number of ICs; arcs represent IC expressed in pie part. Cumulative data of **h**) TIGIT and **i**) CD200 expression on cytokine mRNA+ Gag-specific CD4+ T cells from CP. Statistics appear in tables below, with p values < 0.05 highlighted in green. bd) n = 13 CP and 8 EC, only positive responses (at least 2 fold greater than unstimulated) were considered; g) n = 9 CP, only positive responses were considered. Columns and pie chart fractions correspond to median values, with interquartile range for columns. bd) Mann-Whitney test; ef) Spearman correlation; g) permutation test with 10 000 permutations; hi) Friedman test with Dunn's post-test. FI = Fluorescence Intensity.

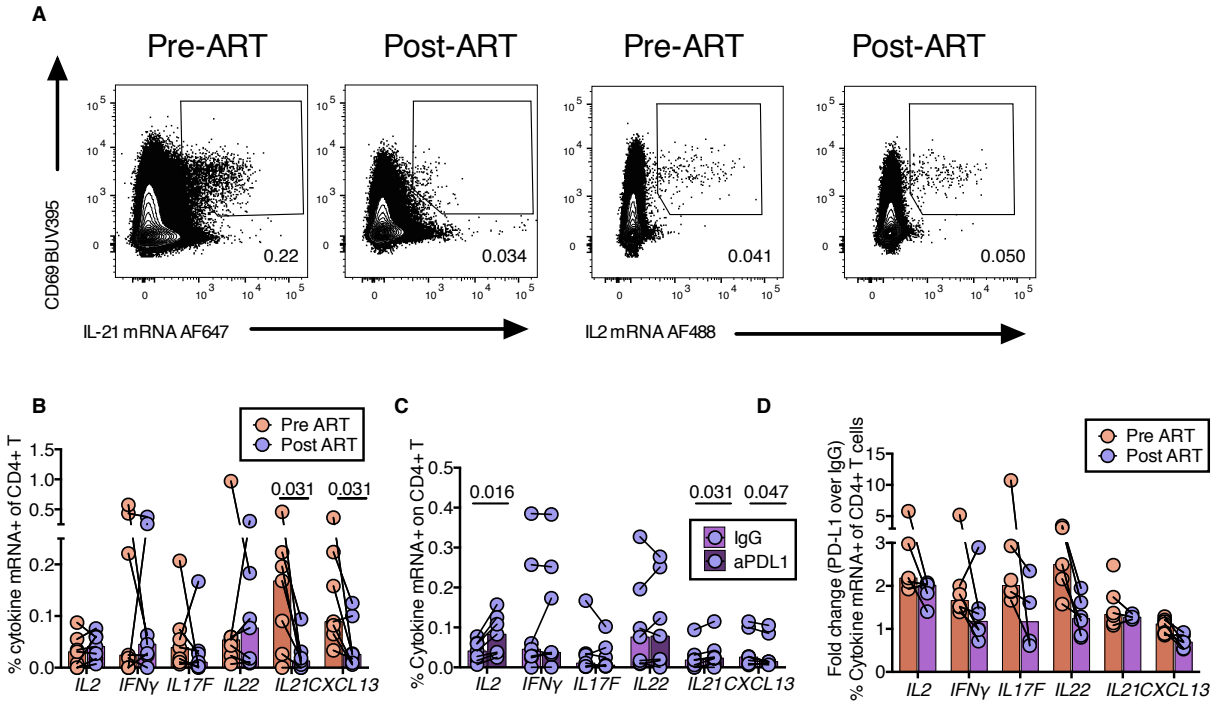

Figure 5.6 Viral suppression on ART differentially affects responsiveness of effector functions to PD-L1 blockade. a) Representative examples and **b)** summary data of net frequency of Gag-specific cytokine mRNA+ CD4+ T cells from matched subjects prior to ART (orange) and after ART (purple) following a 9hr in vitro stimulation with Gag peptide pool. **c**) Summary net frequencies of Gag-specific cytokine mRNA+ CD4+ T cells stimulated with PD-L1 blocking antibody or isotypic control (IgG) among ART-treated individuals. **d**) Comparison of the fold changes upon PD-L1 blockade between longitudinal samples pre- (orange) and post-ART (purple). N = 7 longitudinal samples. Bars represent medians. bcd) Wilcoxon test.

Supplementary Materials

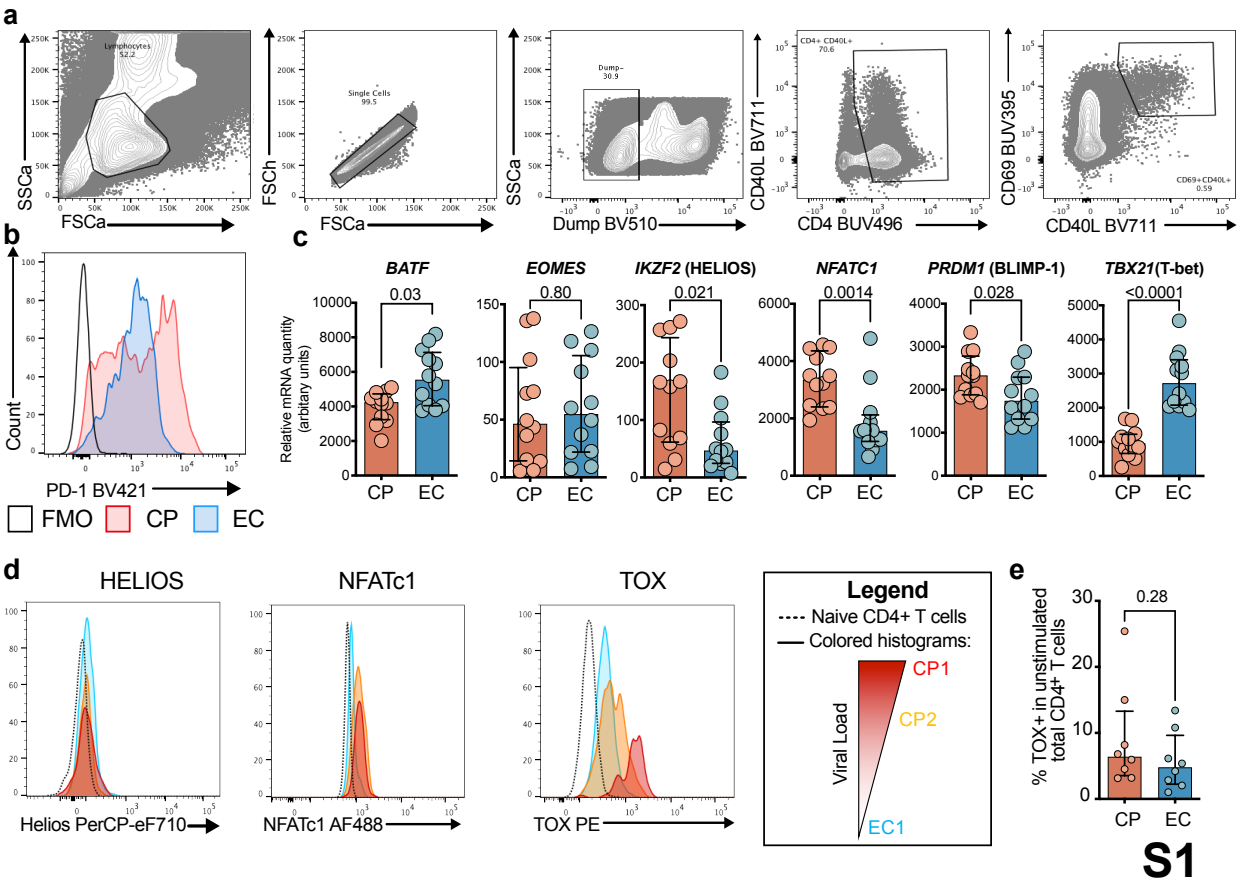

Figure S5.1 Transcriptomic analysis of exhaustion-related transcription factors in HIV-specific CD4+ T cells. a) Representative flow cytometry plots of the full gating strategy for the AIM panel on HIV Gag-stimulated cells from a CP. Gating strategy includes CD3-low CD69+ as CD3 expression can be downregulated following TCR stimulation. **b**) Representative example of PD-1 expression on AIM+ Gag-specific CD4+ T cells. Black line is FMO. **c**) Relative mRNA expression of exhaustion-related TF among sorted Gag-specific CD4+ T cells of CP (red) or EC (blue), as captured by high-throughput RT-PCR (Fluidigm® - for details, please see (Morou *et al.*, 2019). n = 12 CP and 12 EC. **d**) Histogram overlay of flow cytometry data showing the expression of TF in AIM+ Gag-specific CD4+ T cells of two CP of varying viral loads (red, orange) and one EC (blue). Dotted line is expression in unstimulated naïve CD4+ T cells. E) Expression of TOX among total unstimulated CD4+ T cells per cohort. c) n = 12 CP and 12 EC. e) n = 8 CP and 8 EC. ce) Stats = Mann-Whitney test.

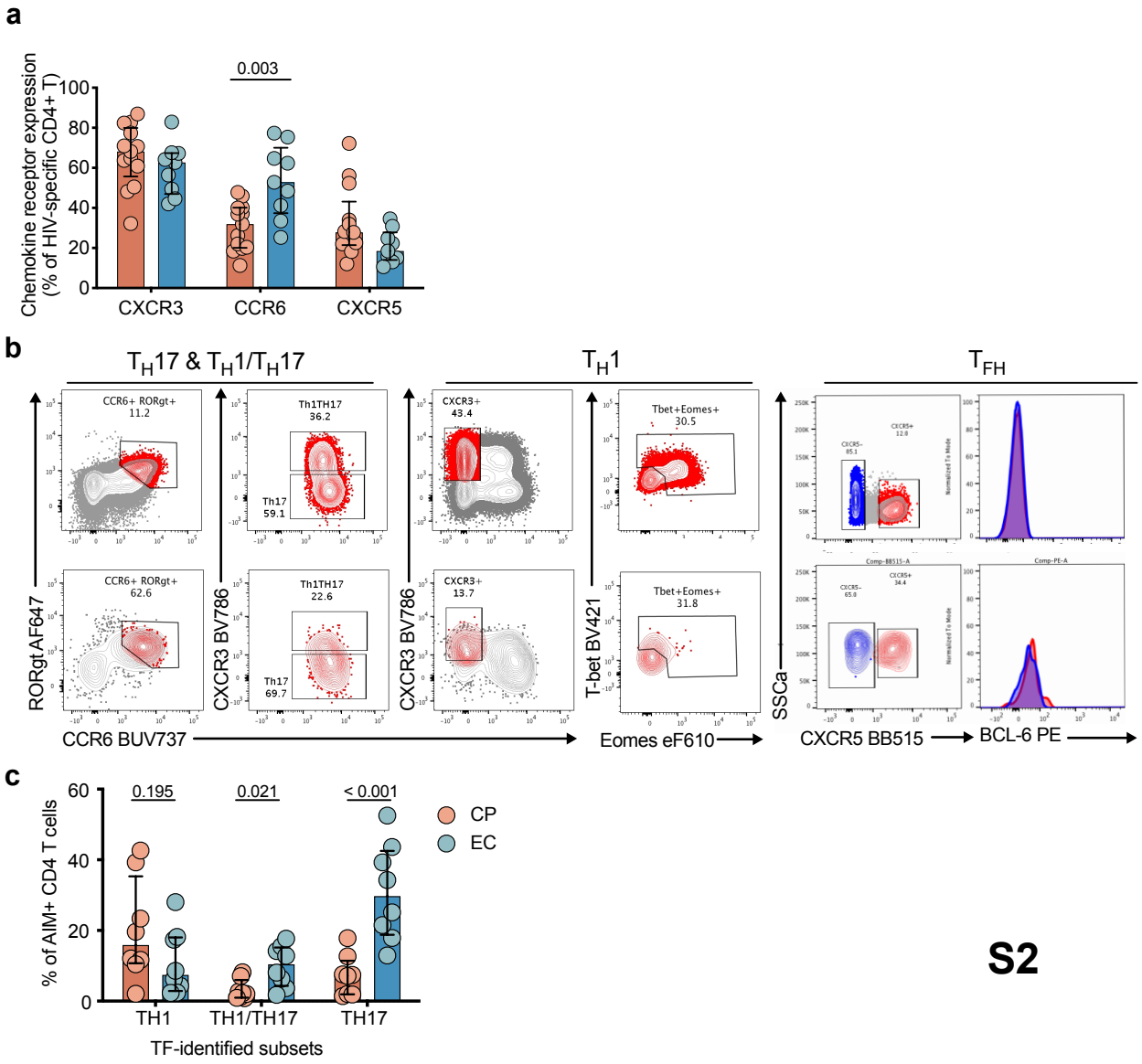

Figure S5.2 PD-1 expression on subsets of AIM+ HIV-specific CD4+ T cells. **a**) Summary of expression of the chemokine receptors CXCR3, CCR6 and CXCR5 on AIM+ Gag-specific CD4+ T cells from CP (orange) or EC (blue). **b**) Representative flow cytometry plots depicting gating strategy to identify TH17 (CCR6+RORgt+CXCR3-), TH1/TH17 (CCR6+RORgt+CXCR3+), TH1 (CXCR3+CCR6-Tbet+Eomes+) or TFH (CXCR5+BCL-6+), either in total CD4+ (top row) or AIM+ Gag-specific CD4+ T (bottom row). **c**) Cumulative data of the frequency of TF-identified subsets among AIM+ Gag-specific CD4+ T cells. a) n= 13 CP and 9 EC; c) n = 8 CP and 8 EC. Columns correspond to median values with interquartile range. ac) Mann-Whitney test.

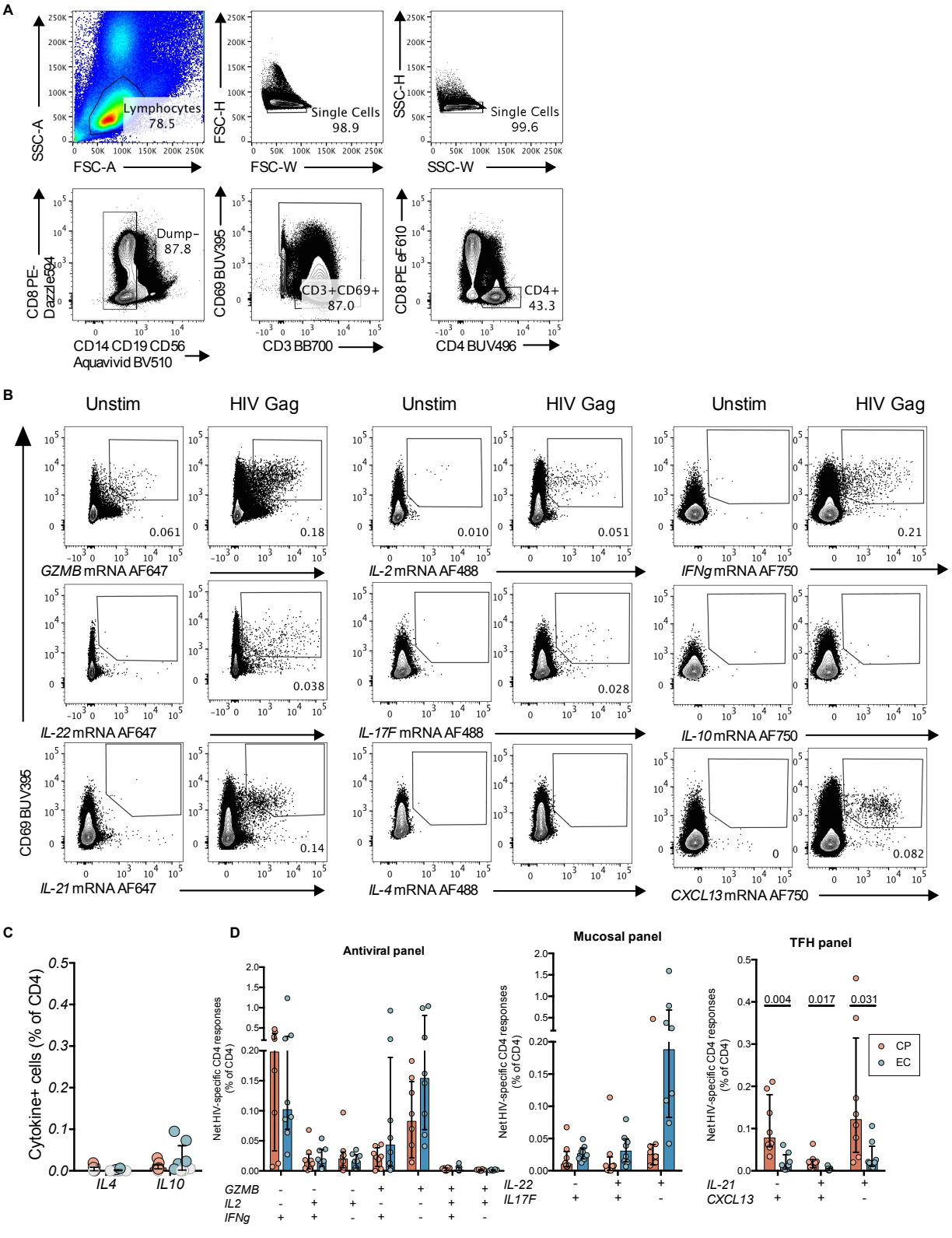

Figure S5.3 Transcription of multiple Thelper cytokines is detected by RNA-Flow-FISH following HIV peptide stimulation. a) Representative flow cytometry plots of the full gating strategy for the RNA-Flow-FISH panels (see methods for details). b) Representative examples of cytokine mRNA+ Gag-specific

CD4+ T cells as detected by RNA-Flow-FISH following a 12hr Gag stimulation for a CP. Gates set on unstimulated (Unstim) conditions. c) Cumulative data for detection of *IL4* mRNA and *IL10* mRNA production following Gag stimulation in both cohorts. Negative responses (less than 2 fold over unstimulated condition) are identified by grey symbols. d) Response of all cytokine mRNA combinations per panel to Gag-stimulation in CP compared to EC. e) Euler diagrams of chemokine receptor expression among HIV-specific CD4+ T cells identified by production of *GZMB*, *IL2*, *IFNG*, *IL17F*, *IL22*, *IL21* or *CXCL13* mRNA. Values represent median frequencies of subsets among cytokine mRNA+ Gag-specific CD4+ T cells from 9 CP (red hues) or 8 EC (blue hues). n = 9 CP and 8 EC. Columns correspond to median values with interquartile range. Mann-Whitney, n= 9 CP and 8 EC.

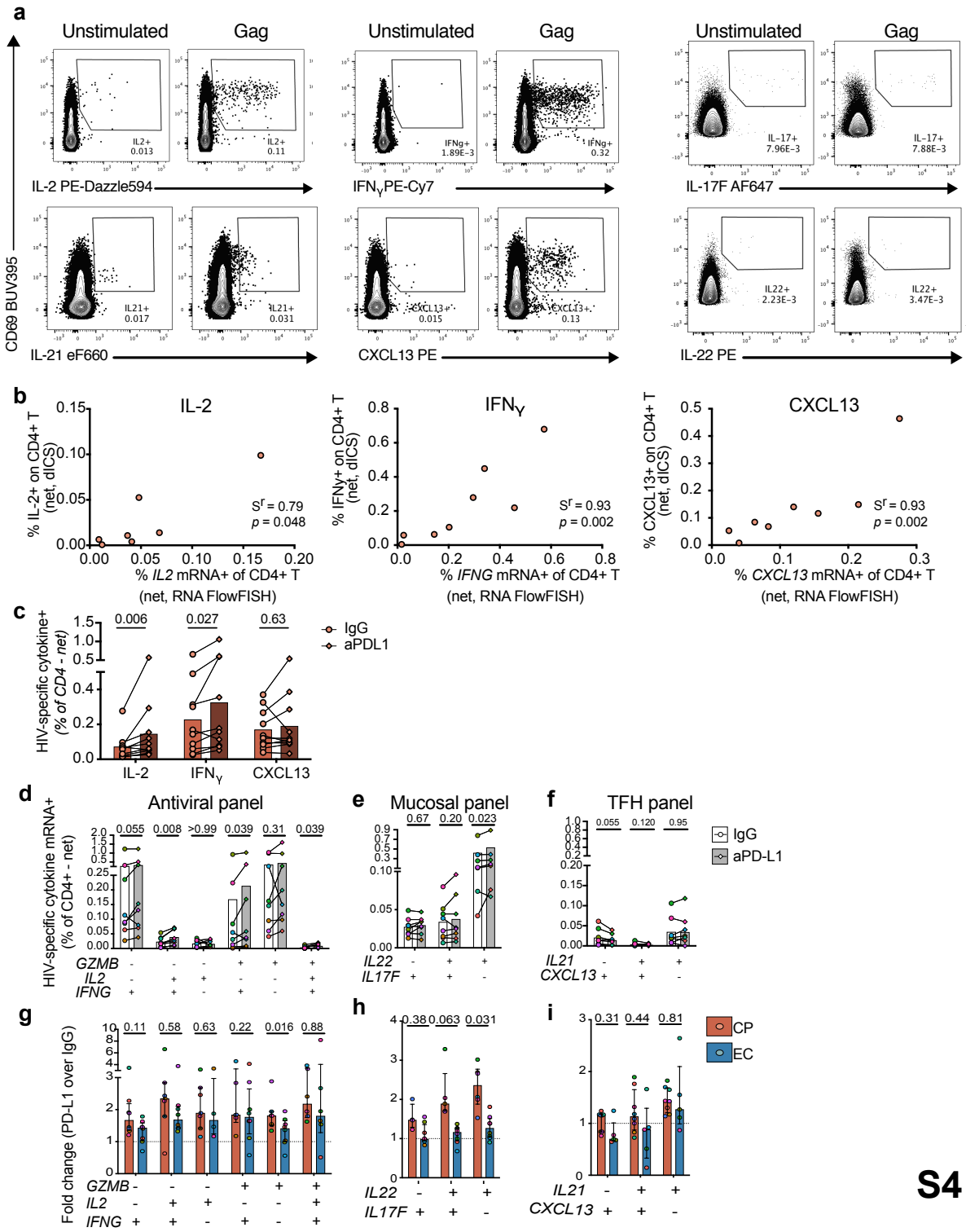

Figure S5. 4 Protein data corroborates cytokine mRNA responses of HIV-specific CD4+ T cells. a) Representative flow cytometry plots showing detection of protein cytokine production by delayed ICS following stimulation with a HIV Gag peptide pool in a CP. **b**) Correlation between the net frequency of Gag-specific CD4+ T cells, as detected by cytokine mRNA+ cells by RNA FlowFISH (x axis) or by protein cytokine

assessed by delayed ICS (y axis) for IL-2 (left), IFNγ (midde) or CXCL13 (right) in CP. n= 8 CP (only donors with Gag-specific responses at least 2-fold over unstimulated are shown). Statistical comparison: Spearman correlation. **d**) Frequency of protein cytokine+ cells detected by delayed ICS upon Gag stimulation, either with isotype control (IgG) or with PD-L1 blocking antibody (aPD-L1). Response of all cytokine mRNA combinations to PD-L1 blockade, upon Gag-stimulation among EC, for **e**) antiviral panel, **f**) mucosal panel, or **g**) TFH panel. n = 8 EC. Statistical comparison: Wilcoxon test. Fold change in the net frequencies of cytokine mRNA+ Gag-specific CD4+ T cells detected upon PD-L1 blockade compared to isotypic control for both cohorts for **h**) antiviral panel, **i**) mucosal panel, or **j**) TFH panel. CP in orange and EC in blue. n= 9 CP and 8 EC (only donors with Gag-specific responses at least 2-fold over unstimulated are shown). Statistical comparison: Mann-Whitney test. Each donor within a cohort has been separately color coded. Columns correspond to median values with interquartile range.n = 10 CP. Stats : Wilcoxon test.

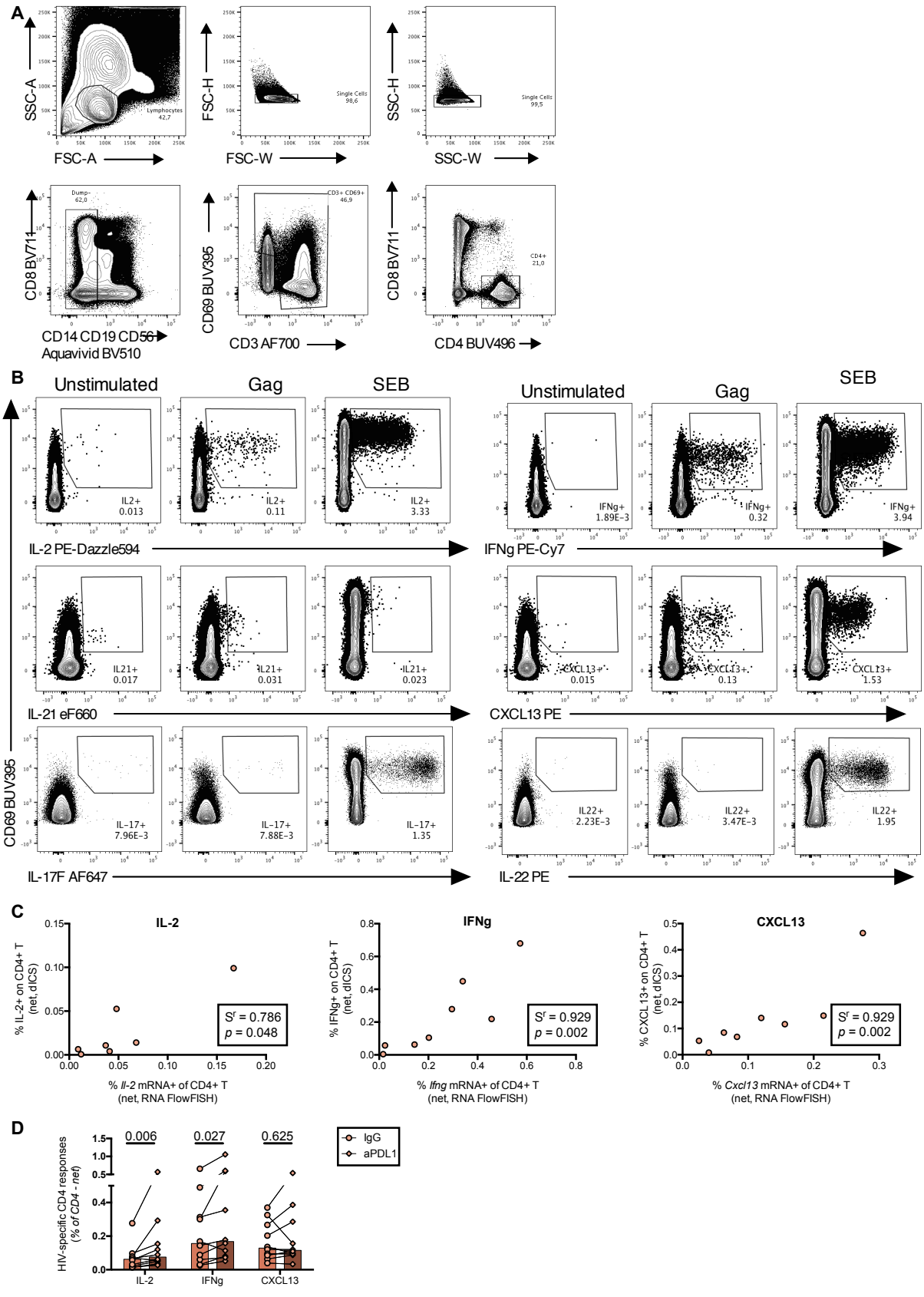
A
SSC-A
FSC-A
Lymphocytes
42,7
FSC-H
FSC-W
Single Cells
96,6
SSC-H
SSC-W
Single Cells
99,5
CD8 BV711
CD14 CD19 CD56
Aquavivid BV510
Dump-
62,0
CD69 BUV395
CD3 AF700
CD3+ CD69+
46,9
CD8 BV711
CD4 BUV496
CD4+
21,0
B
Unstimulated
Gag
SEB
IL-2 PE-Dazzle594
IL2+
0.013
IL2+
0.11
IL2+
3.33
IFNg PE-Cy7
IFNg+
1.89E-3
IFNg+
0.32
IFNg+
3.94
IL-21 eF660
IL21+
0.017
IL21+
0.031
IL21+
0.023
CXCL13 PE
CXCL13+
0.015
CXCL13+
0.13
CXCL13+
1.53
CD69 BUV395
IL-17F AF647
IL-17+
7.96E-3
IL-17+
7.88E-3
IL-17+
1.35
IL-22 PE
IL22+
2.23E-3
IL22+
3.47E-3
IL22+
1.95
C
IL-2
% IL-2+ on CD4+ T
(net, dICS)
Sr = 0.786
p = 0.048
% Il-2 mRNA+ of CD4+ T
(net, RNA FlowFISH)
IFNg
% IFNg+ on CD4+ T
(net, dICS)
Sr = 0.929
p = 0.002
% Ifng mRNA+ of CD4+ T
(net, RNA FlowFISH)
CXCL13
% CXCL13+ on CD4+ T
(net, dICS)
Sr = 0.929
p = 0.002
% Cxcl13 mRNA+ of CD4+ T
(net, RNA FlowFISH)
D
HIV-specific CD4 responses
(% of CD4 - net)
0.006
0.027
0.625
IgG
aPDL1
IL-2
IFNg
CXCL13

Figure S5. 5 Despite high ICs' TIGIT and CD200 expression among polarizations of HIV-specific CD4+T cells, co-blockade of PD-1 and TIGIT does not increase responsiveness to ICB. a) Correlations between viral load of CP and their IC expression (PD-1 gMFI on left, % TIGIT+ in middle and % CD200+ on right) Gag-specific AIM+ CD4+ T cells. b) Correlation between single-cell expression of TIGIT and CD200 on AIM+ HIV-specific CD4+ T cells from 4 CP and 4 EC (100 cells per subject). Frequency of c) TIGIT+ or d) CD200+ among the three polarizations of the AIM+ Gag-specific CD4+ T cells defined by CXCR3, CCR6 and CXCR5 expression in both cohorts – CP (red) and EC (blue). Grey circles represent negative responses (less than 2 fold over unstimulated condition). Cumulative data of e) TIGIT and f) CD200 expression on cytokine mRNA+ Gag-specific CD4+ T cells from EC cohort. Statistics appear in tables below, with p values < 0.05 highlighted in green. g) Response (fold change compared to IgG) to all blocking strategies as detected by delayed ICS in CP. h) Responses of individuals' responses (fold change compared to IgG) with no benefit of dual blockade over single PD-L1 blockade (left), further enhancement of cytokine production by dual blockade over single PD-L1 blockade (middle), or no (or modest) effect of either blockade strategy (right). i) Venn representation of IFNγ and CXCL13 median co-expression in the CP cohort. j) Net frequencies of IFNγ single-positive (SP), CXCL13 SP or IFNγ/CXCL13 double-positive Gag-specific CD4+ T cells following stimulation in the presence of IgG or aPD-L1. Statistical comparison by Wilcoxon test. k) Fold change of blocking conditions (compared to IgG) for IFNγ SP, CXCL13 SP or DP. bh) Statistical comparison by 2-way ANOVA with Tukey's multiple comparison test. a, c-f) n= 13 CP, 9 EC. g-k) N = 10 CP. Bars represent medians with interquartile range. de) N = 13 CP and 8 EC; fg) n = 8 EC, where only positive responses are considered. Friedman's test with Dunn's correction. abc) Spearman R correlation. Viral load was Log10 transformed.

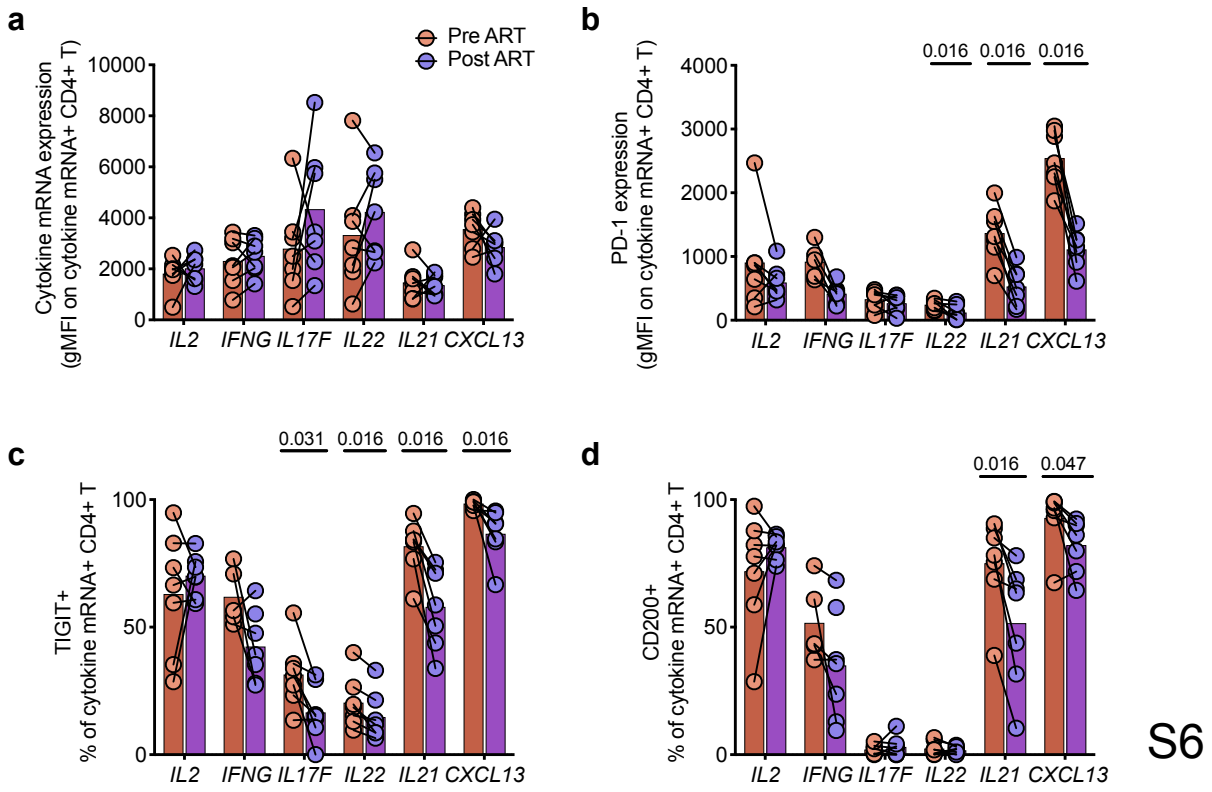

Figure S5.6 ART initiation causes a decrease of IC upon HIV-specific cytokine mRNA+ CD4+ T cells. a) gMFI of cytokine mRNA+ in Gag-specific cytokine mRNA+ CD4+ T cells from matched subjects prior to ART (ored) and after ART (purple) following a 9hr *in vitro* stimulation with Gag peptide pool. Comparison of IC expression among Gag-specific cytokine mRNA+ CD4+ T from matched donors: **b**) PD-1 gMFI, **c**) frequency of TIGIT+, or **d**) frequency of CD200+. Only positive responses (at least 2 fold over unstimulated condition) were considered. bcd) Wilcoxon test, n = 7 longitudinal samples. gMFI = geometric mean fluorescence intensity.

Table S5.1 Subject characteristics

Characteristic	CP	EC	ART
Number of subjects	13	9	7
Median (IQR) Viral load (copies/ml)	19067	< 40	< 40
	(6235 - 1 000 000)	(< 40 - 49)	(< 20 - 44)
Median (IQR) CD4 Count (cells/ul)	329	591	640
	(138 - 1036)	(369 - 744)	(361-940)
Median (IQR) documented years of HIV infection	8.5	16.4	9.2
	(0.25 - 23.9)	(1.2 - 28.5)	(0.9 - 24.9)
Median (IQR) age (years)	41	46	43
	(22 - 51)	(33 - 59)	(37 - 52)
Gender			
Number of Males (%)	11 (85%)	4 (44%)	6 (86%)
Number of Females (%)	2 (15%)	5 (56%)	1 (14%)

Table S5.2 Flow cytometry panel used in AIM assay

Antigen/Reagent	Fluorochrome	Clone	Manufacturer	Cat #	Volume/test (ul)*
Brilliant Stain buffer	-	-	BD	563794	50
LIVE/DEAD	Aquavivid	-	eBioscience	L34966	1
CD14	V500	M5E2	BD	561391	2
CD19	V500	H1B19	BD	561121	2
CD8	V500	SK1	BD	561618	4
CD3	BUV395	UCHT1	BD	563546	6
CD4	BUV496	SK3	BD	564651	8
CD69	BV650	FN05	Biolegend	310934	7.5
CD154	PE	TRAP1	BD	555700	20
TIGIT	APC	MBSA43	eBioscience	17-9500	7.5
PD-1	BV421	EH12.2H75	Biolegend	329920	6
ICOS	PE-Cy7	ISA-3	eBioscience	25-9948	10
CD200	PerCP-efluor710	OX104	eBioscience	46-9200	7.5
CD45RA	BUV737	H1100	BD	564442	4
CCR6**	APC-R700	11A9	BD	565173	7.5
CXCR3**	BV605	G025H7	Biolegend	353728	10
CXCR5**	BB515	RF8B2	BD	564624	10

* one test : 10M PBMC in 200ul staining buffer

** added in cull culture (0.5ml) 15 min prior to stimulation

Table S5.3 Variants of the Flow cytometry panels used in intra-nuclear transcription factor staining

	Antigen/Reagent	Fluorochrome	Clone	Manufacturer	Cat #	Volume/test (ul)*
	Brilliant Stain buffer	-	-	BD	563794	10
	LIVE/DEAD	Aquavivid	-	eBioscience	L34966	0.5
	CD14	BV480	M5E2	BD	746304	1
	CD19	BV480	HIB19	BD	746457	0.5
	CD8	BV480	RPA-T8	BD	566121	0.5
	CD4	BUV496	SK3	BD	564651	4
	CD69	BUV395	FN50	BD	564364	2.5
	CD154	BV711	24-31	Biolegend	310838	5
	TIGIT	PE-Cy7	MBSA43	eBioscience	25-9500	2
	PD-1	BV605	EH12.2H7	Biolegend	329924	5
	T-BET	BV421	O4-46	BD	563318	5
	CD45RA	APC-Fire 750	HI100	Biolegend	304151	0.5
	CCR7**	BB700	3D12	BD	566438	5
	CCR6**	BUV737	11A9	BD	564377	0.5
	CXCR3**	BV785	G025H7	Biolegend	353738	0.5
TF exhaustion	NFATc1	AF488	7A6	Biolegend	649604	5
	CXCR5**	PE-Dazzle 594	J252D4	Biolegend	356928	5
	TOX	PE	TXRX10	eBioscience	12-6502-82	5
	TCF-1	AF647	7F11A10	Biolegend	655204	5
TF Pol	CXCR5**	BB515	RF8B2	BD	564624	2
	Eomes	PE-eF610	WD1928	eBioscience	61-4877-42	5
	CD200	PE	OXS-104	Biolegend	329206	3
	RORgt	AF647	Q21-559	BD	563620	5
Optimization	Helios	PerCP eFluor710	22F6	eBioscience	46-9883	5
	BATF	eFluor660	MBM7C7	ThermoFisher	50-9860-42	5
	Bcl6	PE	K112-91	BD	561522	5

Supplementary Table 4: Flow cytometry panel used in mRNA-Flow-FISH assay

Antigen/Reagent	Fluorochrome	Clone	Manufacturer	Cat #	Volume/test (ul)*
Brilliant Stain buffer	-	-	BD	563794	25
LIVE/DEAD	Efluor-506	-	Invitrogen	65-0866	0.5
CD14	BV510	M5E2	Biolegend	301842	3
CD19	BV510	H1B19	Biolegend	302242	3
CD56	BV510	NCM16.2	BD	563041	0.5
CD3	BB700	HIT3a	BD	742207	0.5
CD4	BUV496	SK3	BD	564651	4
CD8	PE-efluor610	RPA-T8	eBioscience	61-0088	0.5
CD69	BUV395	FN50	BD	564364	2.5
TIGIT	PE-Cy7	MBSA43	eBioscience	25-9500	5
PD1	BV711	EH12.2H7	Biolegend	329928	5
CD200	PE	OX-104	Biolegend	329206	3
CCR6**	BUV737	11A9	BD	564377	2
CXCR3**	BV421	G025H7	Biolegend	353716	1
CXCR5**	BV605	J252D4	Biolegend	356929	2

* one test : 5M PBMC in 100ul staining buffer

** added in cull culture (0.5ml) 15 min prior to stimulation

Table S5.5 Probe panel combination used in mRNA-Flow-FISH assay

	Proble	Fluoro.	Manufacturer	Cat #	Volume/test (ul)*
Probe combinations	Antiviral panel				
	GZMB mRNA	Type 1	ThermoFisher	VA1-3084452	5
	IL2 mRNA	Type 4	ThermoFisher	VA4-14454	5
	IFNG mRNA	Type 6	ThermoFisher	VA6-13121	5
	Mucosal panel				
	IL22 mRNA	Type 1	ThermoFisher	VA1-14439	5
	IL17F mRNA	Type 4	ThermoFisher	VA4-11185	5
	IL10 mRNA	Type 6	ThermoFisher	VA6-13016	5
	TFH Panel				
	IL21 mRNA	Type 1	ThermoFisher	VA1-14117	5
	IL4 mRNA	Type 4	ThermoFisher	VA4-3082434	5
	CXCL13 mRNA	Type 6	ThermoFisher	VA6-15752	5
	Modified Mucosal panel				
	IL22 mRNA	Type 1	ThermoFisher	VA1-14439	5
	IL17F mRNA	Type 4	ThermoFisher	VA4-11185	5
	IFNG mRNA	Type 6	ThermoFisher	VA6-13121	5
	Modified TFH Panel				
	IL21 mRNA	Type 1	ThermoFisher	VA1-14117	5
	IL2 mRNA	Type 4	ThermoFisher	VA4-14454	5
	CXCL13 mRNA	Type 6	ThermoFisher	VA6-15752	5

* one test : 5M PBMC in 100ul staining buffer

Table S5.6 Flow cytometry panel used in delayed intracellular cytokine staining (d-ICS)

Antigen/Reagent	Fluorochrome	Clone	Manufacturer	Cat #	Volume/test (ul)*
Brilliant Stain buffer	-	-	BD	563794	25
LIVE/DEAD	Aquavivid	-	eBioscience	L34957	0.5
CD14	BV510	M5E2	Biolegend	301842	3
CD19	BV510	H1B19	Biolegend	302242	3
CD56	BV510	NCAM16.2	BD	563041	0.5
CD8	BV711	RPA-T8	BioLegend	301044	2
CD69	BUV395	FN50	BD	564364	2.5
CD4	BUV496	SK3	BD	564651	4
CCR7**	BV650	G043H7	Biolegend	353234	5
CD45RA	APC-Fire750	HI100	Biolegend	304151	1
CXCR5**	BV421	J252D4	Biolegend	356920	2.5
IFNγ***	PE-Cy7	B27	BD	557643	4
IL-2***	PE-Dazzle594	MQ1-17H12	Biolegend	500344	3.5
TNFa***	AF488	MAb11	Biolegend	502915	2
IL-21***	eFluor660	eBio3A3-n2	eBioscience	50-7219-42	5
CXCL13***	PE	53610	R&D	IC801P	10

* one test : 5M PBMC in 100ul staining buffer

** added in cell culture (0.5ml) 15 min prior to stimulation

*** Stained for intracellularly

Chapter 6 – Discussion

Two separate pandemic-causing viruses have been covered in this thesis: SARS-CoV-2 and HIV. These viruses differ considerably in terms of origin, genetic make-up, replication cycle, and pathology. In both cases, patient outcome can differ greatly, with the same diversity also found in the immune response to the virus. The study of these differences give us an opportunity to understand patient-specific pathophysiology. This discussion is separated in three parts, with the first two about the two viruses covered in this thesis. The third part will contrast both these viruses.

PART 1: CHARACTERISTICS OF ACUTE SARS-COV-2 INFECTION

The worldwide effort to understand SARS-CoV-2 infection led to an enormous amount of evidence quickly becoming available. As a consequence, researchers sometimes had diverging conclusions due to different cohorts, inconsistent sampling times, subtle divergences in sample processing or protocols, etc. For these reasons, the scientific community initially had a hard time getting a clear picture of COVID-19.

We set off to identify a robust and reproducible predictor of fatality, even among the critical subgroup of patients. At the start of this project, we hypothesized that different mechanisms could explain a poor outcome (and thus serve as biomarkers): the cytokine storm (already linked to severe COVID-19, and reminiscent of sepsis), ARDS (already associated to COVID-19), plasma vRNA (linked to severe disease for other respiratory viruses (Kim et al., 2016)) and a faulty antibody response (linked to poor outcome for other viruses). The sequential sampling, in-depth clinical characterization, and the immunovirological plasma profiling of the cohort allowed us to narrow our analysis down to a specific timeframe. It turned out to be opportune, as it simultaneously captured the lingering plasma vRNA, the delay in antibody response, and the strong association of ARDS markers with fatality. As reports before us, we found that high levels of SARS-CoV-2 viral RNA, cytokines, and markers of ARDS were significantly associated to fatal

outcome, as well as low antibody responses. By pitting the fatality-associated markers against each other in a multivariate model, we found that plasma vRNA systematically was the superior predictor. Testing the models in multiple cohorts underscored the robustness of our model as, among the cytokines associated to fatality in our discovery cohort, some lost their association in the validation cohort. The robustness of viral RNA was validated in two independent cohorts and across different early sampling time points, confirming its robustness in predicting fatality, even among the critical subgroup.

All early longitudinal samples were characterized in the same fashion. Since all this had been done on longitudinal samples, we could study the interplay between these aspects across disease severity and outcome. This was done by using a combination of dimensionality reduction tools, such as PHATE and knn clustering, leading to insights about the pathology and dysregulated immune responses in COVID-19. Through this approach, we grouped patients not based on clinical features but rather on the progression of their immune response to COVID-19, and found that these patients fell among four clusters. This type of approach is powerful, in that it can combine different types of measures to subcluster patients, bringing us closer to personalized medicine.

What do our findings suggest about the pathology of COVID-19?

The significance of SARS-CoV-2 plasma vRNA

We sequenced the N and E genes of SARS-CoV-2 in plasma. This vRNA is likely not complete, as *in vitro* testing revealed no evidence of infectious virus in the plasma (however, the tested samples had low amounts of SARS-CoV-2 vRNA) (Andersson *et al.*, 2020). We saw a strong non-perfect correlation between both probes (where detection with the E probe was slightly inferior), which could suggest fragments of the virus. Circulating viral microRNA have been detected early in SARS-CoV-2 infection, and may play a role in immune dysregulation in these patients (Meng et al., 2021). However, microRNAs are less than 30 nucleotides, much shorter than the 1328 base pairs N transcripts we quantified by Nanodrop.

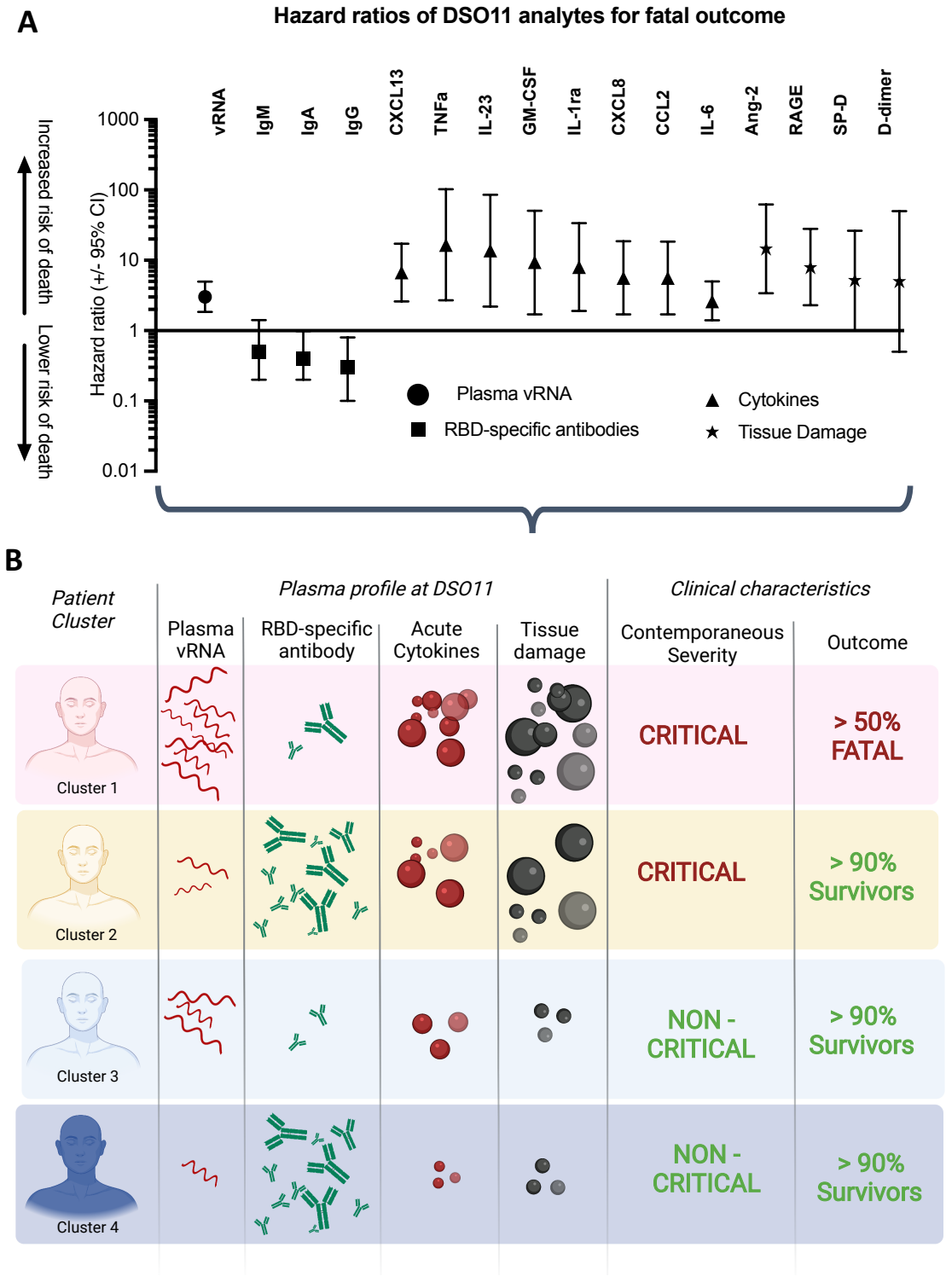
A
Hazard ratios of DSO11 analytes for fatal outcome
vRNA
IgM
IgA
IgG
CXCL13
TNFa
IL-23
GM-CSF
IL-1ra
CXCL8
CCL2
IL-6
Ang-2
RAGE
SP-D
D-dimer
1000
100
10
1
0.1
0.01
Hazard ratio (+/- 95% CI)
Increased risk of death
Lower risk of death
Plasma vRNA
RBD-specific antibodies
Cytokines
Tissue Damage
B
Patient Cluster
Plasma profile at DSO11
Plasma vRNA
RBD-specific antibody
Acute Cytokines
Tissue damage
Clinical characteristics
Contemporaneous Severity
Outcome
Cluster 1
CRITICAL
> 50% FATAL
Cluster 2
CRITICAL
> 90% Survivors
Cluster 3
NON - CRITICAL
> 90% Survivors
Cluster 4
NON - CRITICAL
> 90% Survivors

Figure 6.1 Integrative DSO11 plasma profile reveals four types of immune response to SARS-COV-2. A) Hazard Ratios (HR) showing the risk of mortality within 60 days of symptom onset (DSO60) for very increase in 1 log unit of the measurement. Only significant measurements included in PHATE embedding are shown. **B)** Overview of immunovirological plasma profiles and clinical features of each patient cluster identified.

Plasma vRNA correlated poorly with that of nasopharygeal swabs (NSW) (Prebensen *et al.*, 2020). While this points to a disconnect between viral quantities in the upper respiratory tract and the blood, our findings had a number of parallels with saliva vRNA detected by N-specific probes (Silva et al., 2021) Like plasma vRNA, saliva vRNA was higher in critical than non-critical cases, and generally greater in deceased than survivors. It also correlated strongly with markers of inflammation such as IL1ra, TNFa, IL-6 and CXCL10. The authors speculate that the saliva vRNA may come from SARS-CoV-2-replication in minor salivary glands, as seen with SARS-CoV-1 (Liu et al., 2011) or from viral invasion in the lower respiratory tract (where the virus is then expeled into the oral cavity through coughing and mixed with saliva). It is unclear whether saliva and plasma vRNA correlate, but there are some differences: saliva vRNA at DSO11 is similar between survivors and deceased within the critical subgroup, while we see a significant difference with plasma vRNA. Also, it is the absence of clearance rather than higher levels of saliva vRNA which is associated to fatal outcome. This suggests that the vRNA quantified in the saliva may not come exclusively from the same source as plasma vRNA.

New evidence indicates that kidneys are directly infected by SARS-CoV-2 *in vivo* (Diao et al., 2021). It is possible that a small fraction of plasma vRNA is indeed infectious, and the study which saw no infectivity of plasma SARS-CoV-2 did not test enough samples to detect this rare occurrence (Andersson et al., 2020). Once infected, the kidneys may also serve as a source of viral RNA, as infectious particles have been detected in the urine of an infected COVID-19 patient (Sun et al., 2020). Rather than a surrogate of viral replication in the respiratory tract, it may be a sign of viral replication in other organs of the body.

Whether the virus is infectious or not, wandering pieces of virus across the body can prime immune responses, for example through pattern-recognition-receptors or through activation of the complement cascade, and sustain the immunopathology seen in COVID-

19.

Plasma vRNA as a superior predictor to markers of inflammation and tissue damage

Although initiated by SARS-CoV-2's infection, COVID-19 cases are fatal because of the exaggerated immunopathology. IL-6 and TNFa, some of the "favourite" markers of inflammation, have often been cited as predictive of fatality (Del Valle et al., 2020), and we saw the same in our data. Similarly, hypercoagulability and, in consequence, thrombosis are also linked to fatal COVID-19, like high levels of their biomarker D-dimer (Xu et al., 2021). Of note, D-dimer was not predictive of fatality in our cohort nor in others (Laing et al., 2020), perhaps due to the early timeframe.

Why is it then that plasma vRNA has a superior predictive value than these other markers?

We must consider what we mean by "superior". Many of the other cytokine markers of inflammation or ARDS had a significant hazard ratio (HR) over 1, meaning that for every 1 log increase in the plasma concentration of those markers, there was an increase in risk of fatality. When we combined these measurements in a multivariate model, only vRNA remained significant: this means that the predictive value of high levels of IL-6, for example, is accounted for in the information given by vRNA, likely because of the correlation between vRNA and IL-6. Furthermore, high levels of IL-6 falsely predicted a death (a survivor with high IL-6 concentrations) and/or falsely predicted a survival (a deceased patient with low IL-6) more often than did plasma vRNA. This indicates that vRNA is a more *accurate* biomarker of fatality than IL-6.

The only biomarkers for whom higher levels predicted survival were RBD-specific antibody responses.

Causes of delayed antibody responses in fatal cases.

We saw that at DSO11, low amounts of SARS-Cov-2 RBD-specific antibodies were associated with an increased risk of fatality. Our subsequent longitudinal study showed that it was not an absence, but rather a *delay* in antibody production. This delay did not

affect the levels of IgM, suggesting normal initial recognition of SARS-CoV-2 by B cells. It was specifically the antibodies issued from class switching (IgG), which were delayed in our data and others (Zohar et al., 2020).

This delay in class switching may arise from a defect in B cells. Although cytopenia is restricted to T cells in severe COVID-19 (Laing et al., 2020), depletion of circulating IgM+ memory B cells had also been associated to fatal COVID-19 (Lenti et al., 2020). However, this latter study did not ascertain the specificity of these B cells cells, nor perform correlations with SARS-CoV-2-specific antibody titers. The depletion of SARS-CoV-2-specific B cells would more likely result in an ablated, or at least diminished antibody response. Conversely, we only observed a delay in our fatal cohort: IgG titers ultimately plateaued to the same extent in survivors and deceased, suggesting another mechanism.

Class-switching from IgM to IgG is a T-helper-dependent process; the delay may then be due to a defect in CD4+ T cells. Germinal centre formation, where most class switching and high affinity maturation occurs (Maehara et al., 2018), was defective in early SARS-CoV-2 due to blocked differentiation of CD4+ T cells into TFH (Kaneko et al., 2020). This block was associated to high TNFa production by TH1 in the extra-follicular milieu (Kaneko et al., 2020). It is also plausible that the abundant levels of circulating CXCL13 disrupted proper recruitment of CXCR5+ cells, which may partially explain the negative correlation we observed between this chemokine and antibody responses.

In addition to this subset-specific effect, global SARS-CoV-2-specific CD4+ T cell responses may be affected, as early virus-specific T cell responses were seen in milder disease (Tan et al., 2021), (Zhou et al., 2020a). Delayed T cell priming may itself be explained by impaired cDC function in acute SARS-CoV-2 (Zhou et al., 2020a). Normally the most potent antigen-presenters, the cDC collected in acute COVID-19 patients have decreased expression of co-stimulatory molecules and of type I IFNs, and could not induce CD4 and CD8 T cell proliferation *in vitro* (Zhou et al., 2020a). If the clonal expansion of SARS-CoV-2-specific CD4+ T cells is delayed, this would indeed also delay the production of SARS-CoV-2-specific IgG antibodies.

While our cross-sectional study identified the fatal cases as lacking an RBD-specific IgG response at DSO11, the longitudinal project revealed two separate patient clusters with

low antibody responses: the fatal cluster (the same one as identified in the cross-sectional study) and a second non-critical survivor cluster. This latter cluster's qualitative SARS-CoV-2-specific antibody response seems to also have lower IgM levels. This would imply not a defect in class-switching, but rather a low priming of B cells. This is seen in cases of mild COVID-19, which have lower SARS-CoV-2-specific antibody titers than critical cases (Long et al., 2020), a difference that persists over 1 year after recovery (Yan et al., 2021). However, it is not known why some non-critical cases generate antibodies while others do not.

Thus, antibody responses are delayed in fatal cases, although they eventually do produce these antibodies.

What are the implications of our observations for treatment of SARS-CoV-2?

Proper identification of subgroups which may benefit from treatment

As discussed in Chapter 1, many large clinical trials of therapeutic interventions had disappointing results. Given the delay in antibody response in fatal cases, the lack of effect from treatments involving passive transfer of humoral immunity, either as convalescent plasma (Bégin et al., 2021) or from monoclonal antibodies (Group, 2021), was unexpected.

Among hospitalized COVID-19 patients, the delay was observed in a small proportion of cases which were critical, where most deaths occurred. Unfortunately, as many of these trials measured disease progression as well (sometimes as the primary outcome), they excluded by design patients already on mechanical ventilation. The survival benefit may have been greater if the trials had different selection criteria.

These trials sometimes included additional makers to identify patients with high inflammation. Our data showed that while these markers are frequently associated to critical disease (over non-critical) and to fatal outcome, they are not as accurate as plasma SARS-CoV-2 viral RNA (vRNA). In addition, we also observed that vRNA remained predictive of fatality even among second and third-wave cases, by which time treatment

with dexamethasone and, to a lesser extent, IL-6R blockers, were already implemented in Quebec's clinics. It was also predictive of fatality when sampled earlier than 11 days after symptom onset, and remained predictive when only considering critical cases. The robustness, flexibility, and simplicity of this measurement makes it a very advantageous measurement to identify high-risk patients, perhaps even with dexamethasone and IL-6R blockade therapies.

Beyond clinical trials, implementation of this measurement in clinic may allow for targeted treatments. For example, plasma vRNA correlates with inflammatory cytokines, and can be used as a proxy of high inflammation. This is relevant since all therapies with proven benefits in clinical trials are thought to increase survival through immunomodulation.

In summary, plasma vRNA may help objectively identify cases with high potential of benefiting from immunotherapies.

Timing in the administration of treatments

Among treatments with proven efficacy (in terms of benefit for survival), there were often differences based on when the treatment was first administered in the course of the infection. In the largest RECOVERY trials, dexamethasone showed survival benefit if administered at or after 7 days after symptom onset, while IL-6R blockers were most beneficial when administered before DSO7, with a similar trend for convalescent plasma. Survival benefit of treating with JAK inhibitor Batricinib was not affected by the treatment initiation time, and antivirals never increased survival. Our trajectory analysis using PHATE may shed some light on these time-dependent different outcomes.

People generally present at hospital for their COVID-19 infection around 7 days after symptom onset (Huang et al., 2020). At this time, peak viral replication has likely already passed. We were not able to study the effect on antiviral administration of plasma vRNA, as remdesivir was not administered as standard care, except in immunosuppressed individuals with extended viral shedding. However, we do know that plasma vRNA is detectable before DSO7. If we consider that the high predictive value of vRNA is because it may indicate viral dissemination and/or serious damage to lung tissue, then already by DSO7 a big extent of the damage directly due to the viral replication is done, and non-

viral mechanisms maintain the inflammatory loop. Thus, antivirals may not lower fatal outcome as it cannot be administered soon *enough*.

The survival benefit of IL-6R blockade is greater in moderate cases of COVID-19. We saw that these cases had lower levels of IL-6 than critical patients (although still 10-fold greater quantities than in the uninfected control cohort). Thus, it is not patients with the highest levels of IL-6 which benefit from this treatment. IL-6 correlated strongly with a number of other inflammatory processes and the CytoScore, and weaker with markers of ARDS (except for RAGE). This may mean that, under a certain threshold, blocking the IL-6 signalling pathway can be sufficient to attenuate immunopathology, but over that threshold, other inflammatory mechanisms significantly contribute to the immunopathology. This is also supported by the fact the IL-6R blockade therapy is only beneficial when administered before DSO7 (before the hyperinflammatory phase) in conjunction with dexamethasone, suggesting a role for IL-6 is spurring on inflammation.

Dexamethasone benefited critical cases of COVID-19 and if administered after DSO7 – i.e. during the hyperinflammatory phase (Group, 2021). This is in line with dexamethasone's anti-inflammatory effect directly upstream of cytokine production. Likely important as well is its capacity to reduce edema, key to lung deterioration later in the acute disease course. Of note, there was a synergistic effect between dexamethasone and IL-6R blockade administration: perhaps when dexamethasone reduces more general mechanisms of inflammation, IL-6R blockade has a therapeutic effect. Early administration of dexamethasone, by hampering the immune response, may increase replication of the virus.

Finally, the JAK inhibitor Baricitinib had a survival benefit of severe cases of COVID-19, no matter the time of administration. This treatment also impedes inflammation, but did not affect antibody production, indicating that the adaptive immune response is not affected. Even if the immune-mediated control of viral replication is reduced by the drug, this may be palliated by its direct antiviral effect.

These observations highlight how a better understand of COVID-19's pathology of a can help direct treatment.

PART II : CHARACTERISTICS OF CHRONIC HIV INFECTION

Uncontrolled human immunodeficiency virus (HIV) infection is fatal in the majority of cases and, although combination antiretroviral therapy (ART) halts this progression, infected individuals require life-long treatment. These individuals generate HIV-specific T cell responses, however only in a small minority is there spontaneous control of viral replication. The highly heterogeneous CD4+ T cells are a central part of this response, but the chronic nature of this infection induces their dysfunction, impeding their antiviral capabilities by favouring a skewing away from the antiviral TH1 and mucosal-protective TH17/TH22 phenotypes, and towards the B-cell helping TFH polarization (Morou et al., 2019). Dysfunctional CD4+ T cells are also characterized by high levels of immune checkpoints (IC) which modulate their effector functions. Signalling through these IC can be therapeutically blocked using immune checkpoint blockade (ICB), and can increase antiviral potential of dysfunctional CD4+ T cells. However, how ICB impacts the different polarizations of CD4+ T cells is still incompletely understood.

Here, we studied the response of various HIV-specific CD4+ T cell functions to ICB. First, we characterized the expression of dysfunction-related transcription factor TOX, and saw that it correlated with key IC PD-1 in a setting of viremia. Furthermore, both TOX and PD-1's expression varied across CD4+ T cell polarizations. This shows similarities with CD8+ T cells, whereby TOX and PD-1 expression are correlated (Sekine et al., 2020), but with a CD4 polarization-specific regulation atop of it. Response to blockade of PD-1 signaling cascade resulted in increased antiviral and mucosal-protective functions, but did not affect TFH-related functions, similar to recent observations in the mouse LCMV clone 13 model (at least for Th1 vs TFH) (Snell et al., 2021). Similar observations were made when two IC were simultaneously blocked. Response to ICB was most prominent in viremic patients, and largely subdued upon ART initiation, suggesting a role of high antigen burden in the responsiveness of CD4+ T cells.

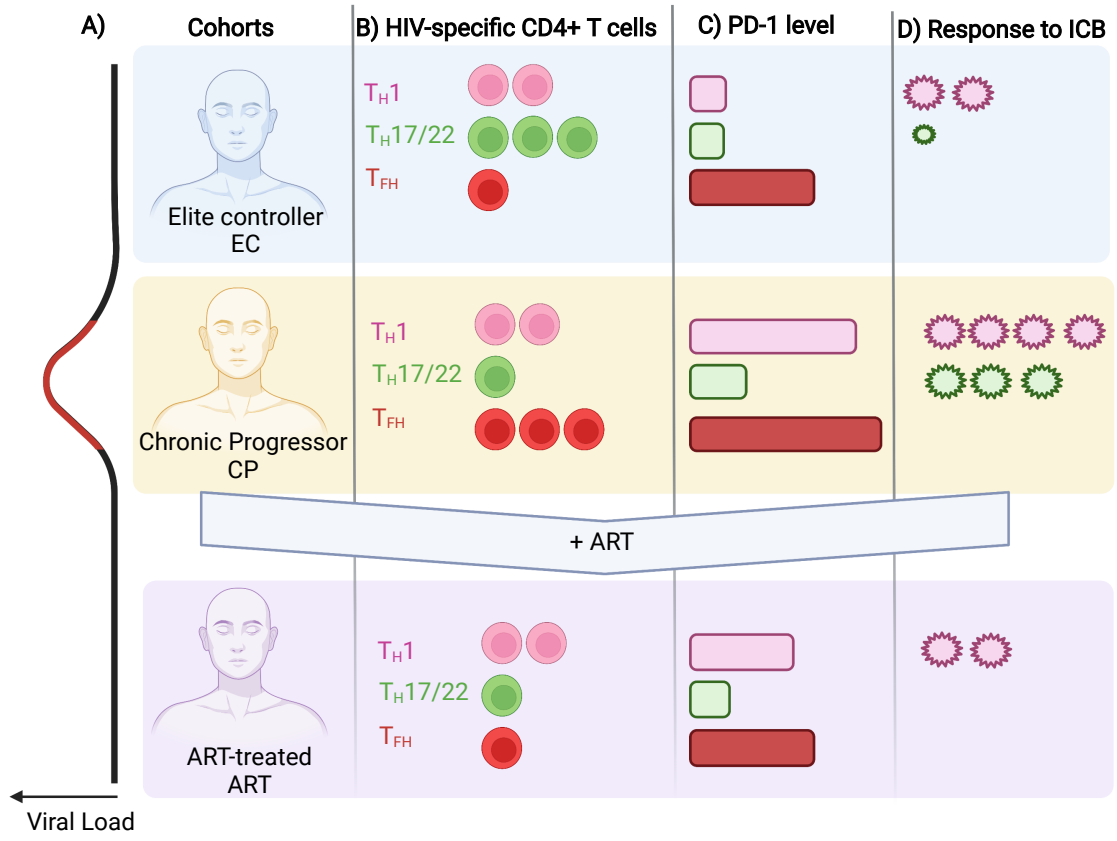

Figure 6.2 Differential expression of PD-1 on subsets of HIV-specific CD4+ T cells, and their respective responses to PD-L1 blockade. A) Characteristics of HIV-infected cohorts, with amount of virus in plasma (viral load) represented by curve on the left. Elite controllers (EC, top, blue) have undetectable VL without ART. Chronic progressors (CP, middle, orange) have high VL without ART. ART-treated individuals (ART, bottom, purple) have therapeutically-suppressed undetectable VL. **B)** Relative proportion of subsets which make up the total pool of HIV-specific CD4+ T cells per cohort. **C)** Relative levels of PD-1 per HIV-specific CD4+ T cell subset. Colour-coded to cell types presented in B. **D)** Response to immune checkpoint blockade (ICB, in this case, blockade of PD-L1), as measured by increased subset-specific cytokine production. More stars mean greater increase of cytokine upon blockade.

What are the implications for the timing of ICB in HIV?

Timing of ICB administration

The recommendation for all people living with HIV (PLWH) is to start ART as soon as possible, as early ART reduces the deleterious effects on the immune response, is associated with a greater chance of complete CD4+ T cell count restoration, and can

reduce the size of the reservoir (Le et al., 2013). These effects can translate to fewer co-morbidities (namely the non-AIDS-related events) and fewer side effects of the infection. Of notable importance for HIV research, early-treated individuals may achieve a functional cure easier, as their immune system is less impacted by the virus (Saez-Cirion et al., 2013).

For these reasons, the use of ICB *in vivo* in humans has been studied only in the context of ART, where the results have been underwhelming (for example, only 2/6 PD-1-inhibitor treated individuals had greater HIV-specific T cell responses). In SIV models, the most encouraging results were observed in chronically-infected RM, which had decreased viral load and, most importantly, improved survival (Velu et al., 2009). In contrast, antviral responses were only modestly enhanced following short-term ART (Mylvaganam *et al.*, 2018), and not at all following long-term ART (Bekerman et al., 2019) in RM.

These contrasts suggest that a recent exposure to high virus amounts, and thus of antigens, may favour a greater response to ICB. This would mimic ICB response in cancer research, where clearance of “hot” tumours (i.e. highly inflamed tumour, with T cell infiltration – signifying that there is T-cell recognition of the tumour) is greater than that of “cold” tumours (no inflammation, no T cell infiltration) (Bonaventura et al., 2019). This was also seen in our *in vitro* PD-L1-blockade treatment, where chronic progressors had greater responses prior to ART therapy. It is not clear whether it is the presence of antigens *per se*, or rather the accompanying inflammatory milieu, which drive this better response.

In summary, administration of ICB with the goal of a lasting enhancement of HIV-specific T cell function may be most beneficial (or potentially, *only* beneficial) either before the initiation of ART or during treatment interruption. This is reminiscent of broadly-neutralizing antibody therapy, where enhanced T-cell responses were only observed if ART was interrupted (Niessl et al., 2020a).

How may the effect of ICB on HIV-specific CD4+ T cells synergize with other effects?

Reactivation of latent reservoir

In HIV, CD4+ T cells are most studied for their role as principal hosts of the HIV reservoir. Reactivation of a latent reservoir can occur through activation of the host CD4+T cell. Immune checkpoint receptors, which effectively diminish T cell activation, are enriched in HIV-harbouring CD4+ T cells during ART (Ryan et al., 2016). Recently, the engagement of PD-1 with its ligand was shown to directly inhibit HIV-transcription following TCR engagement *in vitro* (Fromentin et al., 2019). The contrary was also true: blocking PD-1-ligand interaction increases HIV production, even in settings where T cell activation is not increased (for example, with the use of latency-reversing agents) (Fromentin et al., 2019). Furthermore, T_{FH} in the lymph nodes of ART-treated PLWH, which express high levels of PD-1, are a key source of inducible, replication-competent HIV (Perreau et al., 2013). All these observations highlight the latency-reversal potential of ICB.

Cases of ART-treated PLWH receiving ICB as treatment for cancer are now emerging, but with contradictory results. PD-1 blockade alone has shown an important decrease in HIV-DNA of one treated patient (Guihot et al., 2018). However, another study with three patients did not see a consistent effect of different measurements of HIV reservoir, no matter whether the patient's cancer responded to the treatment or not (Scully et al., 2018). Of note, this latter study did see spikes of HIV RNA in blood, highlighting that there was indeed reactivation of the reservoir, but this did not lead to a clearance over time.

Studies have also tested the effect of combined PD-1 and CTLA-4 co-blockade, as they inhibit T cell activation through different mechanisms and have both been associated to viral reactivation *in vivo* in humans (Wightman et al., 2015). A recent SIV study created a long-term ART-treated model, which received ICB during ART, then underwent ART-treatment interruption (Harper et al., 2020). The authors compared single PD-1 and CTLA-4 blockades, and the combined treatment. Both PD-1 and CTLA-4 did reactivate latent reservoir, but of different clones, suggesting that reservoirs do not have the same sensitivity to all ICB (with CTLA-4 blockade reactivating a larger diversity of clones than PD-1 blockade). This highlights why a better understanding of which CD4+ T cell subsets responds to a given treatment regimen is key to finding the combination best for a greater reactivation of the viral reservoir. Unfortunately, none of the regimens were sufficient to

prevent viral rebound, underscoring that ICB alone is not enough to achieve a functional cure.

Another key observation of this latter study was that all regimens with PD-1 blockade delayed viral rebound by 5 days, while no such delay was observed with CTLA-4 single blockade (Harper et al., 2020). Since anti-CTLA-4 reactivated more latent virus than anti-PD-1 (and decrease of SIV DNA), this delay cannot be due to a greater depletion of the reservoir with PD-1 blockade. This suggests that PD-1's role in enhancing a dysregulated immune response probably played a greater part in the delay than the depletion of the reservoir.

Effect of other adaptive immune cells

The best-characterized function of ICB is the reversal of CD8+ T cell . Antigen-specific CD8+ T cells in a chronic setting incrementally lose antiviral functions, and are ultimately clonally depleted. PD-1 blockade can reverse the effect of exhaustion in HIV-specific CD8+ T cells *in vitro* (Day et al., 2006), and *in vivo* in SIV models (Velu et al., 2009) and humans (Gay et al., 2017).

A functional CD4+ T cell help has been shown to be indispensable response to ICB in CD8+ T cells in patients with cancer (Zuazo et al., 2019) and, in a model of chronic viral infection in mice, in virus-specific CD8+ T cells (West et al., 2013).

Furthermore, increased CD4+ T cell function through blockade of the PD-1 and IL-10 pathways resulted in increased IFNg production from NK cells stimulated with HIV antigens (Porichis et al., 2018).

Of note, the SIV study also measured improved memory B cell responses, with increased titers of SIV-specific antibodies upon PD-L1 blockade (Velu et al., 2009). Indeed, PD-1 expression is increased on HIV-specific B cells, also characterized as dysfunctional. PD-1 blockade *in vitro* led to greater activation of these B cells (Nicholas et al., 2013). Thus, the increased antibody response seen in the RM may be due to direct response from B cells. However, as TFH function did not seem affected by blockade in our data, it is

possible that ICB may not translate to better quality B cell responses.

Taken together, these reports show how boosting CD4+ T cell help directly favours antiviral responses in other immune effector cell populations.

Contribution of the gut microbiome in response to ICB

A recent paper linked microbiome to the response to ICB (Routy et al., 2018). They transplanted fecal matter (FMT) into mice models of cancer patients which either responded or not to ICB and then inoculated them with the same tumour, and found that mice with the FMT from responders responded to ICB, but not those which received FMT from non-responders. That microbiome is key was also reflected in humans, where antibiotics during ICB were associated with reduced clinical benefit from ICB (Derosa et al., 2018). The exact mechanism of why microbiome influences tumouricidal responses induced by ICB are unknown. However, other lines of evidence link bacterium-derived products with ICB efficacy. Combined administration of PD-L1 blockade and LPS resulted in an increase of functionally-active virus-specific CD8+ T cells in an LCMV model of chronic infection (Wang et al., 2019). In this model, LPS through TLR-4 signalling increased the antigen-presenting capacities of DCs.

In addition, an *in vitro* study showed that bacteria-specific CD4+ T cells can also succumb to exhaustion in the context of increased bacterial translocation in common variable immunodeficiency (also characterized by a “leaky gut”) (Perreau et al., 2014). These cells can be reinvigorated by ICB, as evident by increased frequencies of TH1-specific cytokines IFNg and IL-2, but also the mucosal-associated cytokine IL-17A. This indicates that the reinvigoration we saw of TH17-associated functions are not limited to HIV-specificity.

Thus, there are at least two mechanisms whereby the gut microbiome influences the response to ICB: i) activating APC’s antigen-presenting capacities; ii) reversing bacteria-specific exhaustion, which can contribute to priming virus-specific cells and reactivate the HIV reservoirs in the gut.

How can we use co-blockade in HIV?

PD-1 with TIGIT co-blockade.

Accumulation of multiple immune checkpoints is one of the key features of T cell exhaustion. Each IC signals through a different pathway; it was a logical progression then to assume that by blocking multiple IC pathways, one can further enhance the restoration of the T cell function.

Multiple studies have investigated the effect of simultaneously blocking PD-1 and CTLA-4 pathways. Mice tumour models showed that these ICB caused the expansion of different T cell subsets (Wei et al., 2019; Wei et al., 2017), which is concordant with the ICB reactivating different clones of reservoir (see above).

In contrast, our data from the PD-1 and TIGIT co-blockades do not suggest that each blocking strategy reinvigorated different HIV-specific CD4+ T cell. We saw no measurable effect with TIGIT blockade alone, and when applied in combination with PD-1, the profile of response was very similar to what was observed with single PD-1 blockade, but enhanced. These observations are reminiscent of other *in vitro* studies, where PD-1 blockade was the only blockade strategy to reinvigorate HIV-specific T cell function when used alone, but could be further enhanced from combined strategies (Grabmeier-Pfistershammer et al., 2017).

These observations suggest that PD-1 is the central IC in HIV-specific T cell exhaustion, and the first block that must be overcome, before being able to observe any benefits from other blockade strategies – at least for ICs which signal *after* TCR binding.

What non-beneficial effects may ICB have in HIV infection?

Limited duration of effect

Epigenetic analysis of T cell responses following ICB revealed no changes in the epigenetic state of the responding cells using a CD4-depleted mouse model of chronic

infection (Pauken et al., 2016). They saw that the beneficial effect of ICB on exhausted virus-specific CD8+ T, specifically increased proliferative capacity and effector functions, were lost within 11 weeks of infection. Even after transfer of ICB-boosted exhausted CD8+ T cells into antigen-free mice, they did not survive for a long time, in line with the differences they had compared to the epigenetic landscape to memory T cells. They linked this specifically to NFAT signalling without AP-1 (Bengsch and Wherry, 2015; Martinez et al., 2015). This would support PD-1's role in sustaining exhaustion, since PD-1 signalling induces BATF, a negative regulator of AP-1 (Quigley et al., 2010).

Due to the depletion of the CD4+ T cells, the duration of the effect of ICB on dysfunctional CD4+ T cells was not assessed (Pauken et al., 2016). However, increased expression of BATF was also observed in dysfunctional virus-specific CD4+ T cells (Crawford et al., 2014). Exhausted CD8+ T cells are epigenetically similar to (presumably) dysfunctional CD4+ T cells (Satpathy et al., 2019) (presumably, since this paper identifies dysfunctional cells as TFH – but it is the population of CD4+ T cells enriched in tumour microenvironment). They also observed no changes in the epigenetic profiles of these dysfunctional CD4+ T cells, only their expansion. Since the inflexibility of the epigenetic profile upon ICB is the reason that ICB-driven reinvigoration of exhausted CD8+ T cells is short-lived, and the same inflexibility is observed in dysfunctional CD4+ T cells, it is likely that the beneficial effect ICB can have of CD4+ T cells is also limited in duration. Thus, ICB cannot not be used as a long-term therapy to sustain antiviral CD4+ T cells.

Overt immunopathology and secondary effects of ICB

Outside chronic disease, PD-1 plays a pivotal role in modulating immune responses: deletion of PD-1 is a mouse model sets off a number of autoimmune-driven pathologies (Nishimura et al., 1999). In the context of cancer therapy, inhibition of the PD-1 pathway, immune-related adverse events were reported in 16% of individuals, and up to 55% when used in combination with CLTA-4 blockade (Larkin et al., 2015). These events can affect the dermatological (rash), gastrointestinal (colitis), endocrine (hypothyroidism), pulmonary (pneumonitis), joints (inflammatory arthritis), neurological, ocular, renal and cardiac systems (Marin-Acevedo et al., 2019). The gut microbiota has as well been associated to

ICB-related toxicity (Andrews et al., 2021) – although the strains associated with it were not the same as those linked to response to PD-1 blockade (Routy et al., 2018) (Gopalakrishnan et al., 2018) (of note, the types of cancers and the treatments observed were not the same, which strongly impacts the efficacy of ICB). In addition, a recent study demonstrated that anti-CTLA-4-induced enterocolitis could be avoided by deleting FcyR interactions (through mutation of the antagonistic antibody), while preserving the beneficial antitumor activity (Bauche et al., 2020). Taken together, these reports propose modifying the microbiota (probiotics) or modifying the antagonists used for the blockades as strategies to reduce ICB-mediated adverse events.

Luckily, administration of ICB specifically to PLWH, in the context of cancer treatment, seemed well tolerated. A clinical trial with 20 patients treated with durvalumab (PD-L1 blockade) (Gonzalez-Cao et al., 2020) reported no grade 3 or 4 drug-related adverse events, and a second with 30 such patients (pembrolizumab, PD-1 blockade) reported the same amount of such events as in a non-infected population (Uldrick et al., 2019). Of note, viral blips were common occurrences in these trials. In PLWH without cancer, PD-L1 blockade also showed low toxicity in the 6 individuals included in the trial (Gay et al., 2017).

As discussed previously, non-virus-specific T cells can also respond to ICB. However, some chronic viral infection can also reach sites of immune maturation, notably the thymus, as is the case for LCMV clone 13 in mice. Initial LCMV clone 13 infection causes infiltration of virus-specifc CD8+ T cells in the thymus, which deplete thymocytes. While thymocytes are normally reconstituted over time, PD-L1 blockade depletes them anew (Elsaesser et al., 2020). The ongoing viral replication in the thymus also resulted in lower stringency for negative selection; as a consequence, autoreactive T cells were released from the thymus. A similar mechanism of depletion due to chronic infection likely explains the thymus depletion in HIV (Davis, 1984). Thus, ICB could lead to the presence of more autoreactive cells when administered to PLWH, and potentially of autoimmunity.

In summary, ICB-associated adverse events are observed in similar frequency in infected and non-infected individuals, and future research will likely develop strategies to minimize them. However, potential problems specifically associated to ICB in PLWH may be

reactivating latent reservoir without subsequent reduction in reservoir, and further hampering the already-affected thymus environment. For these reasons, strategies using ICB should aim at being short, and only in combination with other therapies, if used as an HIV-treatment strategy.

The impact of ICB on CD4+ T cells have primarily been studied in the context of reactivation of viral reservoirs, which are preferentially harboured in IC+ cells. However, we show that HIV-specific CD4+ T cells also functionally respond to ICB in multiple ways. We also show that the degree of response depends on the polarization of the CD4+ T cell. Our work highlights the relevance of considering CD4+ T cell differentiation in studies of ICB in HIV, but perhaps as well for other infectious and non-infectious chronic human diseases, as understanding which cell types respond to ICB could allow for a more targeted usage. Future studies still may study their functional contribution *in vivo*, as well as that of CD4+ T cells of other specificities, whose function may also benefit from ICB. While recent studies indicate that ICB may not be sufficient in a cure of HIV, they have highlighted significant benefits and open new synergistic opportunities.

PART III : CONTRASTS BETWEEN HIV AND SARS-COV-2

Both viruses can cause sizeable immunopathology in the host they have infected. As we have described, there is notable heterogeneity in the immunopathology following infection of both SARS-CoV-2 and HIV.

As with most viral infections, there are similarities in the initial immune response against the virus, in terms of the innate response. They are also vulnerable to some overlapping pathways. For example, both infections show evidence that a delayed type I IFN response is bad, while a rapid, robust T cell response is beneficial.

Since SARS-CoV-2 is ultimately cleared, there is no exhaustion observed in SARS-CoV-2-specific T cells. While high PD-1 expression is observed on SARS-CoV-2-specific T cells early in infection (led some to think there was exhaustion), it was later shown to be simply associated to the cell's activation (Shahbaz et al., 2021). It would be interesting to study whether this phenomenon occurs in immunocompromised individuals with extended viral shedding. However, important confounding factors, namely the cause of immunosuppression, would likely make interpretation difficult.

In both studies, the responses of the patients to the virus diverged greatly. Part of it can likely be explained by the usual demographic suspects: differences between age groups, sexes, co-morbidities, etc. – although our restricted cohorts' sizes prevented these types of analyses. However, it would also be interesting to consider genotypic differences between patients. For example, certain polymorphisms were highly associated to fatal outcome in COVID-19 (Zhou et al*.,* 2021); does this association stem from inherent differences in the immune response? Taking that a step further, genetic ancestry (where multiple polymorphisms tend to be passed down together) has recently been linked to cell-specific differences in response to influenza virus (Randolph et al., 2021). How do such differences affect other viral infections? Indeed, considering multiple layers of data concomitantly, such as plasmatic profile and genotype, will allow scientists to parse apart the granularity among the patients. This is a key step for any outlook on personalized medicine.

Chapter 7 – Limitations and perspectives

Both studies have given insight into two separate human viral infections. However, the nature of the samples available and/or technical difficulties were sometimes limitations, highlighting the opportunity to expand on these findings in future studies.

SARS-CoV-2

Blood vs tissues

Given the pandemic context, our lab was only able to obtain small quantities of blood from the infected individuals, which were taken at the same time as routine clinical sampling. Given the huge time pressure of the pandemic on healthcare workers, their contact with infected patients was kept to strict minimum.

Although we do detect SARS-CoV-2 in the blood and there are coagulopathies, most of the aspects of the disease, particularly the immune response, would be most accurately captured in tissues such as the respiratory tract. Indeed, samples of lung tissue *post-mortem* or bronchoalveolar lavage fluid could have allowed us to link the early immunovirological plasma profiles we observed to specific immunopathologies, such as whether high amonts of plasma vRNA was indeed linked to the reported infection of the kidneys (Farkash et al., 2020). Of equally great interest would have been to collect biopsies from secondary lymphoid tissues, for example through fine needle aspirate (FNA), where we could have studied the qualitative features of interactions between SARS-CoV-2-specific CD4+ T and B cells, to find mechanistic explanations behind the different types of aberrant early antibody responses we observed in two of four types of patients. For example, a loss of TFH differentiation, with accompagnying absence of GC, was linked to fewer SARS-CoV-2-specific B cells (Kaneko *et al.*, 2020), but whether that would translate to the delay we observed in the high-fatality cluster, or rather the atypical antibody response of the non-critical low antibody cluster, is unclear. While not possible to address this is human patients, these question could also be studied using an animal

model of SARS-CoV-2 infection.

Anti-SARS-CoV-2 antibody response

In our studies, we focused on early RBD-specific antibodies as they can be measured quickly and easily by ELISA. We were also able to compare the neutralization and ADCC capacities of only a select few samples, since these assays are labour-intensive. The few samples we analyzed revealed that reduced ADCC, but not neutralization, was observed in fatal COVID-19 cases. Neutralization in SARS-CoV-2 immunity is primarily driven by IgM (Gasser *et al.*, 2021), while ADCC is only possible with IgG. The different kinetics we observed between the isotypes of RBD-specific antibodies may very well extend to the functionality of the humoral response, and this longitudinal information could allow us to pick apart which functional profile is most important early in SARS-CoV-2 infection. While this has already been partially eluded using a highly-pathogenic mouse model (Ullah et al., 2021), the parallel information is lacking in humans. To fully understand a favourable humoral response, more antibody-mediated functions should also be studied.

Once we have identified what traits are associated to fatal outcome, we could also contrast it against the humoral response of the patients in the non-critical low-antibody response cluster which survive their infection. This may allow us to separate what aspects of the faltering humoral response in the fatal cases would truly aid in clearing the virus.

Once the advantageous humoral response profile identified, we can then look into why it is lacking in the fatal cases of COVID-19, which brings us back to the usefulness of tissue samples and/or animal models. Building on this, comparing the individual transcriptomic profile of these cells through single-cell RNA Seq of cells extracted from tissues, such as the antigen-presenting cells and effector T and B cells, may allow us to identify the mechanisms behind these different antibody profiles, and may lead to new therapeutic strategies.

Mechanisms behind therapeutic efficacy

While there has been a survival benefit with dexamethasone, IL-6R antagonists and batricinib, the mechanisms by which they operate is not fully understood. Similarly, the reason why monoclonal antibody therapies did not show the same efficacy is not known.

Although our cohort did include some patients which received dexamethasone, IL-6R antagonists and even a few with plasma transfer therapy, we have not sampled enough patients for these analyses. Given the heterogeneity of COVID-19, this would likely require a very large multi-centric collaboration, with normalized monitoring strategies and implementation of unbiased patient identification. Monitoring the immunovirological plasma profile of treated individuals, for example by observing changes in the expected trajectories (i.e. the immunovirological traits associated with progression of fatal COVID-19) could pinpoint the beneficial mechanisms of therapies, and perhaps allow the development for more targeted treatments.

HIV

Working with PBMCs

Given the absence of small-animal models of HIV infection as well as the difficulty of working with large animals which can be infected with SIV, we were limited to *ex vivo* samples and *in vitro* testing of immune checkpoint blockade. The drawback of this was that we could not take into account the systemic effects of ICB, nor of its effect on CD4+ T cells in the tissue. Future work which could isolate the response of specific T helper subsets' to ICB may help elucidate the observed benefits of ICB beyond increased antiviral control, namely increased survival. It is telling though that a recent report has found similarly subset-dependent responses to PD-L1 blockade using the LCMV clone 13 model, suggesting that our *in vitro* observation would also translate to *in vitro* systems.

In addition, the *in vitro* set-up we used, whereby PBMCs were exposed to ICB *in vitro*, is not one found *in vivo.* Thus, we cannot be certain that the effects we observed will have biologically-relevant impacts *in vivo*, a reccuring limitation of *in vitro* experimentation. Nonetheless, *in vitro* testing is a much more controllable setting, which can be fine-tuned to isolate almost a single variable at a time (for example, (Wei et al., 2013)). While our current studied focused on the phenotype and corresponding response to ICB of subsets of CD4+ T cells, our *in vitro* setup could be further refined to also control the signals received by the CD4+ T cells from APCs. For example, a recent Nature Protocols paper describes APC-mimetic scaffolds (APC-ms), liposome-coated silica microrods at the

surface of which co-stimulatory molecules are added (Zhang et al., 2020). While the authors of this article developed this system for *ex vivo* amplification of antigen-specific T cells for adoptive cell transfer, one can picture using such a system to finely tune the co-stimulatory molecules received by the CD4+ T cells. Such approaches would help elucidate the mechanisms behind response to ICB, such as the contribution of activating ligands or immune checkpoints other than PD-1, the effect of varying TCR strengths, the contribution of signal 3 molecules (cytokines), etc.

An additional difficulty with working with PBMCs is our inability to track, at a single-cell level, which CD4+ T cell responds to ICB. In our work, we looked at “bulk” increases in response to ICB, and deduced what cells it came from based on the phenotype of all responding cells. However, with the advent of more powerful single-cell methods such as single cell RNA sequencing and single cell ATAC sequencing, the ability to specifically identify the cells responding to ICB would allow us to only look at their transcriptome and epigenetic profiles, and confirm “bulk” observations. This could be applied to confirm that CD8+ T cells responding to ICB are the progenitor-exhausted CD8+ T cells, and see whether only a similar “lowly” dysfunctional CD4+ T cell population can respond to ICB.

The rarity of untreated HIV patients

Fortunately, few PLWH in Montreal remain untreated. However, the low amount of patients we were able to recruit does limit the characterization we were able to accomplish. Indeed, the pattern of responsiveness to ICB has high interpatient variability. Environmental-related factors have already been observed to affect responsiveness to ICB (for example, the microbiome (Routy et al., 2018)). However, we did not have the power to identify homogeneous groups of patients in terms of responsiveness to ICB (for example, subgroups of patients which responded strongly for certains cytokines, and not for others). Such subgrouping, as we were able to do with the PHATE analysis in our cohort of COVID-19 patients, could have allowed us to find features beyond the phenotype of circulating CD4+ T cells that may have a link with the responsiveness to ICB. The increasing number of clinical trials on PLWH receiving ICB for treatment of cancers now offer a remarkable opportunity to better understand what influences the response to ICB, and whether it is similar in HIV-negative and HIV-positive individuals.

Chapter 8 – Significance

The projects were conducted very much with the optic that patients would benefit clinically from the results.

Our COVID-19 project has not only confirmed previous findings' association of high amounts of plasma SARS-CoV-2 vRNA, cytokines, and tissue damage markers to fatal outcome, but has validated across three cohorts, the superior predictive value of vRNA. This easily-measured variable can quickly be integrated into clinical, and may help direct therapeutic efforts. In the context of clinical trials, inclusion of this metric to subgroup patients may highlight the efficacy of new treatments by focusing exclusively on high-risk patients. This metric also proved superior to other clinical metrics used to gage the severity of ARDS, highlighting that measures which specifically target the virus are better suited to predict fatal outcome, than those used to measure severity of symptoms. Furthermore, concomitant consideration of these fatality-associated plasma analytes segregate hospitalized individuals into four distinct types of immune responses to SARS-CoV-2. For example, high inflammation or delay in antibody response only occurs in some patients. Our observations highlight inherent heterogeneity in immune responses, which translates to different outcomes in these patients.

Our immune checkpoint blockade project of HIV-specific CD4+ T cells has highlighted that not all responses to ICB are equal in dysfunctional CD4+ T cells. Specifically, TFH cells, most akin transcriptomically to the progenitor-exhausted CD8+ T cells that *do* respond to ICB, are the most refractory of all studied CD4+ T cell subsets to ICB. These findings underscore important differences between CD4+ and CD8+ T cells, and highlight the

importance of considering the CD4+ T cells when studying efficacy and side effects, specially given the recent inclusion of ICB as treatment for diverse cancers in PLWH.

Taken together, this work has sought to characterize what the diversity in immune responses mean for efficacy of immune therapies. Through a better understanding of patient-specific immunopathology, we can tailor treatment to each separate case, serving as the first steps towards personalized medicine in viral infections. These studies are all the more relevant now, as more and more therapies leveraging the immune system are being used in humans.

References

Abram, M.E., Ferris, A.L., Shao, W., Alvord, W.G., and Hughes, S.H. (2010). Nature, position, and frequency of mutations made in a single cycle of HIV-1 replication. J Virol *84*, 9864-9878. 10.1128/JVI.00915-10.

Ackermann, M., Verleden, S.E., Kuehnel, M., Haverich, A., Welte, T., Laenger, F., Vanstapel, A., Werlein, C., Stark, H., Tzankov, A., et al. (2020). Pulmonary Vascular Endothelialitis, Thrombosis, and Angiogenesis in Covid-19. N Engl J Med *383*, 120-128. 10.1056/NEJMoa2015432.

Adams, N.M., Grassmann, S., and Sun, J.C. (2020). Clonal expansion of innate and adaptive lymphocytes. Nat Rev Immunol *20*, 694-707. 10.1038/s41577-020-0307-4.

Agostini, M.L., Andres, E.L., Sims, A.C., Graham, R.L., Sheahan, T.P., Lu, X., Smith, E.C., Case, J.B., Feng, J.Y., Jordan, R., et al. (2018). Coronavirus Susceptibility to the Antiviral Remdesivir (GS-5734) Is Mediated by the Viral Polymerase and the Proofreading Exoribonuclease. mBio *9*. 10.1128/mBio.00221-18.

Ahmed, R., Byrne, J.A., and Oldstone, M.B. (1984). Virus specificity of cytotoxic T lymphocytes generated during acute lymphocytic choriomeningitis virus infection: role of the H-2 region in determining cross-reactivity for different lymphocytic choriomeningitis virus strains. J Virol *51*, 34-41. 10.1128/JVI.51.1.34-41.1984.

Alfei, F., Kanev, K., Hofmann, M., Wu, M., Ghoneim, H.E., Roelli, P., Utzschneider, D.T., von Hoesslin, M., Cullen, J.G., Fan, Y., et al. (2019). TOX reinforces the phenotype and longevity of exhausted T cells in chronic viral infection. Nature *571*, 265-269. 10.1038/s41586-019-1326-9.

Altfeld, M., and Gale, M., Jr. (2015). Innate immunity against HIV-1 infection. Nat Immunol *16*, 554-562. 10.1038/ni.3157.

Ananworanich, J., and Robb, M.L. (2014). The transient HIV remission in the Mississippi baby: why is this good news? J Int AIDS Soc *17*, 19859. 10.7448/IAS.17.1.19859.

Andersson, M.I., Arancibia-Carcamo, C.V., Auckland, K., Baillie, J.K., Barnes, E., Beneke, T., Bibi, S., Brooks, T., Carroll, M., Crook, D., et al. (2020). SARS-CoV-2 RNA detected in blood products from patients with COVID-19 is not associated with infectious virus. Wellcome Open Res *5*, 181. 10.12688/wellcomeopenres.16002.2.

Andrews, M.C., Duong, C.P.M., Gopalakrishnan, V., Iebba, V., Chen, W.S., Derosa, L., Khan, M.A.W., Cogdill, A.P., White, M.G., Wong, M.C., et al. (2021). Gut microbiota signatures are associated with toxicity to combined CTLA-4 and PD-1 blockade. Nat Med *27*, 1432-1441. 10.1038/s41591-021-01406-6.

Angelosanto, J.M., Blackburn, S.D., Crawford, A., and Wherry, E.J. (2012). Progressive loss of memory T cell potential and commitment to exhaustion during chronic viral infection. J Virol *86*, 8161-8170. 10.1128/JVI.00889-12.

Angus, D.C., Derde, L., Al-Beidh, F., Annane, D., Arabi, Y., Beane, A., van Bentum-Puijk, W., Berry, L., Bhimani, Z., Bonten, M., et al. (2020). Effect of Hydrocortisone on Mortality and Organ Support in Patients With Severe COVID-19: The REMAP-CAP COVID-19 Corticosteroid Domain Randomized Clinical Trial. JAMA *324*, 1317-1329. 10.1001/jama.2020.17022.

Apetrei, C., Kaur, A., Lerche, N.W., Metzger, M., Pandrea, I., Hardcastle, J., Falkenstein, S., Bohm,

R., Koehler, J., Traina-Dorge, V., et al. (2005). Molecular epidemiology of simian immunodeficiency virus SIVsm in U.S. primate centers unravels the origin of SIVmac and SIVstm. J Virol *79*, 8991-9005. 10.1128/JVI.79.14.8991-9005.2005.
Arabi, Y.M., Mandourah, Y., Al-Hameed, F., Sindi, A.A., Almekhlafi, G.A., Hussein, M.A., Jose, J., Pinto, R., Al-Omari, A., Kharaba, A., et al. (2018). Corticosteroid Therapy for Critically Ill Patients with Middle East Respiratory Syndrome. Am J Respir Crit Care Med *197*, 757-767. 10.1164/rccm.201706-1172OC.
Arts, E.J., and Hazuda, D.J. (2012). HIV-1 antiretroviral drug therapy. Cold Spring Harb Perspect Med *2*, a007161. 10.1101/cshperspect.a007161.
Arunachalam, P.S., Wimmers, F., Mok, C.K.P., Perera, R., Scott, M., Hagan, T., Sigal, N., Feng, Y., Bristow, L., Tak-Yin Tsang, O., et al. (2020). Systems biological assessment of immunity to mild versus severe COVID-19 infection in humans. Science *369*, 1210-1220. 10.1126/science.abc6261.
Aubert, R.D., Kamphorst, A.O., Sarkar, S., Vezys, V., Ha, S.J., Barber, D.L., Ye, L., Sharpe, A.H., Freeman, G.J., and Ahmed, R. (2011). Antigen-specific CD4 T-cell help rescues exhausted CD8 T cells during chronic viral infection. Proc Natl Acad Sci U S A *108*, 21182-21187. 10.1073/pnas.1118450109.
Austin, J.W., Lu, P., Majumder, P., Ahmed, R., and Boss, J.M. (2014). STAT3, STAT4, NFATc1, and CTCF regulate PD-1 through multiple novel regulatory regions in murine T cells. J Immunol *192*, 4876-4886. 10.4049/jimmunol.1302750.
Autran, B., Carcelain, G., Li, T.S., Blanc, C., Mathez, D., Tubiana, R., Katlama, C., Debre, P., and Leibowitch, J. (1997). Positive effects of combined antiretroviral therapy on CD4+ T cell homeostasis and function in advanced HIV disease. Science *277*, 112-116. 10.1126/science.277.5322.112.
Ayers, M., Lunceford, J., Nebozhyn, M., Murphy, E., Loboda, A., Kaufman, D.R., Albright, A., Cheng, J.D., Kang, S.P., Shankaran, V., et al. (2017). IFN-gamma-related mRNA profile predicts clinical response to PD-1 blockade. J Clin Invest *127*, 2930-2940. 10.1172/JCI91190.
Baksh, K., and Weber, J. (2015). Immune checkpoint protein inhibition for cancer: preclinical justification for CTLA-4 and PD-1 blockade and new combinations. Semin Oncol *42*, 363-377. 10.1053/j.seminoncol.2015.02.015.
Bally, A.P., Austin, J.W., and Boss, J.M. (2016). Genetic and Epigenetic Regulation of PD-1 Expression. J Immunol *196*, 2431-2437. 10.4049/jimmunol.1502643.
Bange, E.M., Han, N.A., Wileyto, P., Kim, J.Y., Gouma, S., Robinson, J., Greenplate, A.R., Hwee, M.A., Porterfield, F., Owoyemi, O., et al. (2021). CD8(+) T cells contribute to survival in patients with COVID-19 and hematologic cancer. Nat Med *27*, 1280-1289. 10.1038/s41591-021-01386-7.
Barber, D.L., Wherry, E.J., Masopust, D., Zhu, B., Allison, J.P., Sharpe, A.H., Freeman, G.J., and Ahmed, R. (2006). Restoring function in exhausted CD8 T cells during chronic viral infection. Nature *439*, 682-687. 10.1038/nature04444.
Battivelli, E., Dahabieh, M.S., Abdel-Mohsen, M., Svensson, J.P., Tojal Da Silva, I., Cohn, L.B., Gramatica, A., Deeks, S., Greene, W.C., Pillai, S.K., and Verdin, E. (2018). Distinct chromatin functional states correlate with HIV latency reactivation in infected primary CD4(+) T cells. Elife *7*. 10.7554/eLife.34655.
Bauche, D., Mauze, S., Kochel, C., Grein, J., Sawant, A., Zybina, Y., Blumenschein, W., Yang, P., Annamalai, L., Yearley, J.H., et al. (2020). Antitumor efficacy of combined CTLA4/PD-1 blockade

without intestinal inflammation is achieved by elimination of FcgammaR interactions. J Immunother Cancer *8*. 10.1136/jitc-2020-001584.
Bbosa, N., Kaleebu, P., and Ssemwanga, D. (2019). HIV subtype diversity worldwide. Curr Opin HIV AIDS *14*, 153-160. 10.1097/COH.0000000000000534.
Becattini, S., Latorre, D., Mele, F., Foglierini, M., De Gregorio, C., Cassotta, A., Fernandez, B., Kelderman, S., Schumacher, T.N., Corti, D., et al. (2015). T cell immunity. Functional heterogeneity of human memory CD4(+) T cell clones primed by pathogens or vaccines. Science *347*, 400-406. 10.1126/science.1260668.
Begin, P., Callum, J., Jamula, E., Cook, R., Heddle, N.M., Tinmouth, A., Zeller, M.P., Beaudoin-Bussieres, G., Amorim, L., Bazin, R., et al. (2021). Convalescent plasma for hospitalized patients with COVID-19: an open-label, randomized controlled trial. Nat Med *27*, 2012-2024. 10.1038/s41591-021-01488-2.
Beigel, J.H., Tomashek, K.M., Dodd, L.E., Mehta, A.K., Zingman, B.S., Kalil, A.C., Hohmann, E., Chu, H.Y., Luetkemeyer, A., Kline, S., et al. (2020). Remdesivir for the Treatment of Covid-19 - Final Report. N Engl J Med *383*, 1813-1826. 10.1056/NEJMoa2007764.
Bekerman, E., Hesselgesser, J., Carr, B., Nagel, M., Hung, M., Wang, A., Stapleton, L., von Gegerfelt, A., Elyard, H.A., Lifson, J.D., and Geleziunas, R. (2019). PD-1 Blockade and TLR7 Activation Lack Therapeutic Benefit in Chronic Simian Immunodeficiency Virus-Infected Macaques on Antiretroviral Therapy. Antimicrob Agents Chemother *63*. 10.1128/AAC.01163-19.
Benati, D., Galperin, M., Lambotte, O., Gras, S., Lim, A., Mukhopadhyay, M., Nouel, A., Campbell, K.A., Lemercier, B., Claireaux, M., et al. (2016). Public T cell receptors confer high-avidity CD4 responses to HIV controllers. J Clin Invest *126*, 2093-2108. 10.1172/JCI83792.
Bengsch, B., and Wherry, E.J. (2015). The importance of cooperation: partnerless NFAT induces T cell exhaustion. Immunity *42*, 203-205. 10.1016/j.immuni.2015.01.023.
Bevan, M.J. (2004). Helping the CD8(+) T-cell response. Nat Rev Immunol *4*, 595-602. 10.1038/nri1413.
Bjorkstrom, N.K., Strunz, B., and Ljunggren, H.G. (2021). Natural killer cells in antiviral immunity. Nat Rev Immunol. 10.1038/s41577-021-00558-3.
Blank, C., Brown, I., Peterson, A.C., Spiotto, M., Iwai, Y., Honjo, T., and Gajewski, T.F. (2004). PD-L1/B7H-1 inhibits the effector phase of tumor rejection by T cell receptor (TCR) transgenic CD8+ T cells. Cancer Res *64*, 1140-1145. 10.1158/0008-5472.can-03-3259.
Blankson, J.N., Bailey, J.R., Thayil, S., Yang, H.C., Lassen, K., Lai, J., Gandhi, S.K., Siliciano, J.D., Williams, T.M., and Siliciano, R.F. (2007). Isolation and characterization of replication-competent human immunodeficiency virus type 1 from a subset of elite suppressors. J Virol *81*, 2508-2518. 10.1128/JVI.02165-06.
Bonaventura, P., Shekarian, T., Alcazer, V., Valladeau-Guilemond, J., Valsesia-Wittmann, S., Amigorena, S., Caux, C., and Depil, S. (2019). Cold Tumors: A Therapeutic Challenge for Immunotherapy. Front Immunol *10*, 168. 10.3389/fimmu.2019.00168.
Bonnet, F., Lewden, C., May, T., Heripret, L., Jougla, E., Bevilacqua, S., Costagliola, D., Salmon, D., Chene, G., Morlat, P., and Mortalite Study, G. (2005). Opportunistic infections as causes of death in HIV-infected patients in the HAART era in France. Scand J Infect Dis *37*, 482-487. 10.1080/00365540510035328.
Borrow, P., Lewicki, H., Wei, X., Horwitz, M.S., Peffer, N., Meyers, H., Nelson, J.A., Gairin, J.E., Hahn, B.H., Oldstone, M.B., and Shaw, G.M. (1997). Antiviral pressure exerted by HIV-1-specific

cytotoxic T lymphocytes (CTLs) during primary infection demonstrated by rapid selection of CTL escape virus. Nat Med *3*, 205-211. 10.1038/nm0297-205.
Boufassa, F., Saez-Cirion, A., Lechenadec, J., Zucman, D., Avettand-Fenoel, V., Venet, A., Rouzioux, C., Delfraissy, J.F., Lambotte, O., Meyer, L., and Group, A.E.H.C.S. (2011). CD4 dynamics over a 15 year-period among HIV controllers enrolled in the ANRS French observatory. PLoS One *6*, e18726. 10.1371/journal.pone.0018726.
Boussiotis, V.A., Chatterjee, P., and Li, L. (2014). Biochemical signaling of PD-1 on T cells and its functional implications. Cancer J *20*, 265-271. 10.1097/PPO.0000000000000059.
Brenchley, J.M., Price, D.A., Schacker, T.W., Asher, T.E., Silvestri, G., Rao, S., Kazzaz, Z., Bornstein, E., Lambotte, O., Altmann, D., et al. (2006). Microbial translocation is a cause of systemic immune activation in chronic HIV infection. Nat Med *12*, 1365-1371. 10.1038/nm1511.
Brenchley, J.M., Schacker, T.W., Ruff, L.E., Price, D.A., Taylor, J.H., Beilman, G.J., Nguyen, P.L., Khoruts, A., Larson, M., Haase, A.T., and Douek, D.C. (2004). CD4+ T cell depletion during all stages of HIV disease occurs predominantly in the gastrointestinal tract. J Exp Med *200*, 749-759. 10.1084/jem.20040874.
Brodin, P. (2021). Immune determinants of COVID-19 disease presentation and severity. Nat Med *27*, 28-33. 10.1038/s41591-020-01202-8.
Bronte, V., Ugel, S., Tinazzi, E., Vella, A., De Sanctis, F., Cane, S., Batani, V., Trovato, R., Fiore, A., Petrova, V., et al. (2020). Baricitinib restrains the immune dysregulation in patients with severe COVID-19. J Clin Invest *130*, 6409-6416. 10.1172/JCI141772.
Brooks, D.G., Trifilo, M.J., Edelmann, K.H., Teyton, L., McGavern, D.B., and Oldstone, M.B. (2006). Interleukin-10 determines viral clearance or persistence in vivo. Nat Med *12*, 1301-1309. 10.1038/nm1492.
Bruel, T., Hadjadj, J., Maes, P., Planas, D., Seve, A., Staropoli, I., Guivel-Benhassine, F., Porrot, F., Bolland, W.H., Nguyen, Y., et al. (2022). Serum neutralization of SARS-CoV-2 Omicron sublineages BA.1 and BA.2 in patients receiving monoclonal antibodies. Nat Med. 10.1038/s41591-022-01792-5.
Bucks, C.M., Norton, J.A., Boesteanu, A.C., Mueller, Y.M., and Katsikis, P.D. (2009). Chronic antigen stimulation alone is sufficient to drive CD8+ T cell exhaustion. J Immunol *182*, 6697-6708. 10.4049/jimmunol.0800997.
Burkhardt, D.B., Stanley, J.S., 3rd, Tong, A., Perdigoto, A.L., Gigante, S.A., Herold, K.C., Wolf, G., Giraldez, A.J., van Dijk, D., and Krishnaswamy, S. (2021). Quantifying the effect of experimental perturbations at single-cell resolution. Nat Biotechnol *39*, 619-629. 10.1038/s41587-020-00803-5.
Cano-Gamez, E., Soskic, B., Roumeliotis, T.I., So, E., Smyth, D.J., Baldrighi, M., Wille, D., Nakic, N., Esparza-Gordillo, J., Larminie, C.G.C., et al. (2020). Single-cell transcriptomics identifies an effectorness gradient shaping the response of CD4(+) T cells to cytokines. Nat Commun *11*, 1801. 10.1038/s41467-020-15543-y.
Carissimo, G., Xu, W., Kwok, I., Abdad, M.Y., Chan, Y.H., Fong, S.W., Puan, K.J., Lee, C.Y., Yeo, N.K., Amrun, S.N., et al. (2020). Whole blood immunophenotyping uncovers immature neutrophil-to-VD2 T-cell ratio as an early marker for severe COVID-19. Nat Commun *11*, 5243. 10.1038/s41467-020-19080-6.
Carsana, L., Sonzogni, A., Nasr, A., Rossi, R.S., Pellegrinelli, A., Zerbi, P., Rech, R., Colombo, R., Antinori, S., Corbellino, M., et al. (2020). Pulmonary post-mortem findings in a series of COVID-

19 cases from northern Italy: a two-centre descriptive study. Lancet Infect Dis *20*, 1135-1140. 10.1016/S1473-3099(20)30434-5.
Carvelli, J., Demaria, O., Vely, F., Batista, L., Chouaki Benmansour, N., Fares, J., Carpentier, S., Thibult, M.L., Morel, A., Remark, R., et al. (2020). Association of COVID-19 inflammation with activation of the C5a-C5aR1 axis. Nature *588*, 146-150. 10.1038/s41586-020-2600-6.
Chahroudi, A., Bosinger, S.E., Vanderford, T.H., Paiardini, M., and Silvestri, G. (2012). Natural SIV hosts: showing AIDS the door. Science *335*, 1188-1193. 10.1126/science.1217550.
Chaplin, D.D. (2010). Overview of the immune response. J Allergy Clin Immunol *125*, S3-23. 10.1016/j.jaci.2009.12.980.
Chen, F., Chan, K.H., Jiang, Y., Kao, R.Y., Lu, H.T., Fan, K.W., Cheng, V.C., Tsui, W.H., Hung, I.F., Lee, T.S., et al. (2004). In vitro susceptibility of 10 clinical isolates of SARS coronavirus to selected antiviral compounds. J Clin Virol *31*, 69-75. 10.1016/j.jcv.2004.03.003.
Chen, X., Pan, Z., Yue, S., Yu, F., Zhang, J., Yang, Y., Li, R., Liu, B., Yang, X., Gao, L., et al. (2020). Disease severity dictates SARS-CoV-2-specific neutralizing antibody responses in COVID-19. Signal Transduct Target Ther *5*, 180. 10.1038/s41392-020-00301-9.
Chikanza, I.C. (2002). Mechanisms of corticosteroid resistance in rheumatoid arthritis: a putative role for the corticosteroid receptor beta isoform. Ann N Y Acad Sci *966*, 39-48. 10.1111/j.1749-6632.2002.tb04200.x.
Cho, H.Y., Lee, S.W., Seo, S.K., Choi, I.W., Choi, I., and Lee, S.W. (2008). Interferon-sensitive response element (ISRE) is mainly responsible for IFN-alpha-induced upregulation of programmed death-1 (PD-1) in macrophages. Biochim Biophys Acta *1779*, 811-819. 10.1016/j.bbagrm.2008.08.003.
Chomont, N., El-Far, M., Ancuta, P., Trautmann, L., Procopio, F.A., Yassine-Diab, B., Boucher, G., Boulassel, M.R., Ghattas, G., Brenchley, J.M., et al. (2009). HIV reservoir size and persistence are driven by T cell survival and homeostatic proliferation. Nat Med *15*, 893-900. 10.1038/nm.1972.
Choy, K.T., Wong, A.Y., Kaewpreedee, P., Sia, S.F., Chen, D., Hui, K.P.Y., Chu, D.K.W., Chan, M.C.W., Cheung, P.P., Huang, X., et al. (2020). Remdesivir, lopinavir, emetine, and homoharringtonine inhibit SARS-CoV-2 replication in vitro. Antiviral Res *178*, 104786. 10.1016/j.antiviral.2020.104786.
Cohen, M.S., Shaw, G.M., McMichael, A.J., and Haynes, B.F. (2011). Acute HIV-1 Infection. N Engl J Med *364*, 1943-1954. 10.1056/NEJMra1011874.
Collin, M., and Bigley, V. (2018). Human dendritic cell subsets: an update. Immunology *154*, 3-20. 10.1111/imm.12888.
Connor, R.I., Sheridan, K.E., Ceradini, D., Choe, S., and Landau, N.R. (1997). Change in coreceptor use correlates with disease progression in HIV-1--infected individuals. J Exp Med *185*, 621-628. 10.1084/jem.185.4.621.
Crawford, A., Angelosanto, J.M., Kao, C., Doering, T.A., Odorizzi, P.M., Barnett, B.E., and Wherry, E.J. (2014). Molecular and transcriptional basis of CD4(+) T cell dysfunction during chronic infection. Immunity *40*, 289-302. 10.1016/j.immuni.2014.01.005.
Crotty, S. (2011). Follicular helper CD4 T cells (TFH). Annu Rev Immunol *29*, 621-663. 10.1146/annurev-immunol-031210-101400.
Cummins, N.W., and Badley, A.D. (2010). Mechanisms of HIV-associated lymphocyte apoptosis: 2010. Cell Death Dis *1*, e99. 10.1038/cddis.2010.77.
Curtsinger, J.M., and Mescher, M.F. (2010). Inflammatory cytokines as a third signal for T cell

activation. Curr Opin Immunol *22*, 333-340. 10.1016/j.coi.2010.02.013.
D'Alessandro, A., Thomas, T., Dzieciatkowska, M., Hill, R.C., Francis, R.O., Hudson, K.E., Zimring, J.C., Hod, E.A., Spitalnik, S.L., and Hansen, K.C. (2020). Serum Proteomics in COVID-19 Patients: Altered Coagulation and Complement Status as a Function of IL-6 Level. J Proteome Res *19*, 4417-4427. 10.1021/acs.jproteome.0c00365.
Davis, A.E., Jr. (1984). The histopathological changes in the thymus gland in the acquired immune deficiency syndrome. Ann N Y Acad Sci *437*, 493-502. 10.1111/j.1749-6632.1984.tb37173.x.
Day, C.L., Kaufmann, D.E., Kiepiela, P., Brown, J.A., Moodley, E.S., Reddy, S., Mackey, E.W., Miller, J.D., Leslie, A.J., DePierres, C., et al. (2006). PD-1 expression on HIV-specific T cells is associated with T-cell exhaustion and disease progression. Nature *443*, 350-354. 10.1038/nature05115.
Deacon, N.J., Tsykin, A., Solomon, A., Smith, K., Ludford-Menting, M., Hooker, D.J., McPhee, D.A., Greenway, A.L., Ellett, A., Chatfield, C., et al. (1995). Genomic structure of an attenuated quasi species of HIV-1 from a blood transfusion donor and recipients. Science *270*, 988-991. 10.1126/science.270.5238.988.
Deeks, S.G., Lewin, S.R., and Havlir, D.V. (2013). The end of AIDS: HIV infection as a chronic disease. Lancet *382*, 1525-1533. 10.1016/S0140-6736(13)61809-7.
Deeks, S.G., Overbaugh, J., Phillips, A., and Buchbinder, S. (2015). HIV infection. Nat Rev Dis Primers *1*, 15035. 10.1038/nrdp.2015.35.
Deeks, S.G., and Walker, B.D. (2007). Human immunodeficiency virus controllers: mechanisms of durable virus control in the absence of antiretroviral therapy. Immunity *27*, 406-416. 10.1016/j.immuni.2007.08.010.
Del Alcazar, D., Wang, Y., He, C., Wendel, B.S., Del Rio-Estrada, P.M., Lin, J., Ablanedo-Terrazas, Y., Malone, M.J., Hernandez, S.M., Frank, I., et al. (2019). Mapping the Lineage Relationship between CXCR5(+) and CXCR5(-) CD4(+) T Cells in HIV-Infected Human Lymph Nodes. Cell Rep *28*, 3047-3060 e3047. 10.1016/j.celrep.2019.08.037.
Del Valle, D.M., Kim-Schulze, S., Huang, H.H., Beckmann, N.D., Nirenberg, S., Wang, B., Lavin, Y., Swartz, T.H., Madduri, D., Stock, A., et al. (2020). An inflammatory cytokine signature predicts COVID-19 severity and survival. Nat Med *26*, 1636-1643. 10.1038/s41591-020-1051-9.
Dequin, P.F., Heming, N., Meziani, F., Plantefeve, G., Voiriot, G., Badie, J., Francois, B., Aubron, C., Ricard, J.D., Ehrmann, S., et al. (2020). Effect of Hydrocortisone on 21-Day Mortality or Respiratory Support Among Critically Ill Patients With COVID-19: A Randomized Clinical Trial. JAMA *324*, 1298-1306. 10.1001/jama.2020.16761.
Derosa, L., Hellmann, M.D., Spaziano, M., Halpenny, D., Fidelle, M., Rizvi, H., Long, N., Plodkowski, A.J., Arbour, K.C., Chaft, J.E., et al. (2018). Negative association of antibiotics on clinical activity of immune checkpoint inhibitors in patients with advanced renal cell and non-small-cell lung cancer. Ann Oncol *29*, 1437-1444. 10.1093/annonc/mdy103.
Dhont, S., Derom, E., Van Braeckel, E., Depuydt, P., and Lambrecht, B.N. (2020). The pathophysiology of 'happy' hypoxemia in COVID-19. Respir Res *21*, 198. 10.1186/s12931-020-01462-5.
Diagnosis and Treatment Protocol for Novel Coronavirus Pneumonia (Trial Version 7). (2020). Chin Med J (Engl) *133*, 1087-1095. 10.1097/CM9.0000000000000819.
Diao, B., Wang, C., Wang, R., Feng, Z., Zhang, J., Yang, H., Tan, Y., Wang, H., Wang, C., Liu, L., et

al. (2021). Human kidney is a target for novel severe acute respiratory syndrome coronavirus 2 infection. Nat Commun *12*, 2506. 10.1038/s41467-021-22781-1.
Ding, L., and Chen, F. (2019). Predicting Tumor Response to PD-1 Blockade. N Engl J Med *381*, 477-479. 10.1056/NEJMcibr1906340.
Doitsh, G., Galloway, N.L., Geng, X., Yang, Z., Monroe, K.M., Zepeda, O., Hunt, P.W., Hatano, H., Sowinski, S., Munoz-Arias, I., and Greene, W.C. (2014). Cell death by pyroptosis drives CD4 T-cell depletion in HIV-1 infection. Nature *505*, 509-514. 10.1038/nature12940.
Doitsh, G., and Greene, W.C. (2016). Dissecting How CD4 T Cells Are Lost During HIV Infection. Cell Host Microbe *19*, 280-291. 10.1016/j.chom.2016.02.012.
Donaghy, H., Pozniak, A., Gazzard, B., Qazi, N., Gilmour, J., Gotch, F., and Patterson, S. (2001). Loss of blood CD11c(+) myeloid and CD11c(-) plasmacytoid dendritic cells in patients with HIV-1 infection correlates with HIV-1 RNA virus load. Blood *98*, 2574-2576. 10.1182/blood.v98.8.2574.
Dunkelberger, J.R., and Song, W.C. (2010). Role and mechanism of action of complement in regulating T cell immunity. Mol Immunol *47*, 2176-2186. 10.1016/j.molimm.2010.05.008.
Dyavar Shetty, R., Velu, V., Titanji, K., Bosinger, S.E., Freeman, G.J., Silvestri, G., and Amara, R.R. (2012). PD-1 blockade during chronic SIV infection reduces hyperimmune activation and microbial translocation in rhesus macaques. J Clin Invest *122*, 1712-1716. 10.1172/JCI60612.
Edler, C., Schroder, A.S., Aepfelbacher, M., Fitzek, A., Heinemann, A., Heinrich, F., Klein, A., Langenwalder, F., Lutgehetmann, M., Meissner, K., et al. (2020). Dying with SARS-CoV-2 infection-an autopsy study of the first consecutive 80 cases in Hamburg, Germany. Int J Legal Med *134*, 1275-1284. 10.1007/s00414-020-02317-w.
Ehre, C. (2020). SARS-CoV-2 Infection of Airway Cells. N Engl J Med *383*, 969. 10.1056/NEJMicm2023328.
Elhed, A., and Unutmaz, D. (2010). Th17 cells and HIV infection. Curr Opin HIV AIDS *5*, 146-150. 10.1097/COH.0b013e32833647a8.
Elsaesser, H., Sauer, K., and Brooks, D.G. (2009). IL-21 is required to control chronic viral infection. Science *324*, 1569-1572. 10.1126/science.1174182.
Emu, B., Sinclair, E., Favre, D., Moretto, W.J., Hsue, P., Hoh, R., Martin, J.N., Nixon, D.F., McCune, J.M., and Deeks, S.G. (2005). Phenotypic, functional, and kinetic parameters associated with apparent T-cell control of human immunodeficiency virus replication in individuals with and without antiretroviral treatment. J Virol *79*, 14169-14178. 10.1128/JVI.79.22.14169-14178.2005.
Estes, J.D. (2013). Pathobiology of HIV/SIV-associated changes in secondary lymphoid tissues. Immunol Rev *254*, 65-77. 10.1111/imr.12070.
Fahey, L.M., Wilson, E.B., Elsaesser, H., Fistonich, C.D., McGavern, D.B., and Brooks, D.G. (2011). Viral persistence redirects CD4 T cell differentiation toward T follicular helper cells. J Exp Med *208*, 987-999. 10.1084/jem.20101773.
Fajnzylber, J., Regan, J., Coxen, K., Corry, H., Wong, C., Rosenthal, A., Worrall, D., Giguel, F., Piechocka-Trocha, A., Atyeo, C., et al. (2020). SARS-CoV-2 viral load is associated with increased disease severity and mortality. Nat Commun *11*, 5493. 10.1038/s41467-020-19057-5.
Fanelli, G., Romano, M., Nova-Lamperti, E., Werner Sunderland, M., Nerviani, A., Scotta, C., Bombardieri, M., Quezada, S.A., Sacks, S.H., Noelle, R.J., et al. (2021). PD-L1 signaling on human memory CD4+ T cells induces a regulatory phenotype. PLoS Biol *19*, e3001199. 10.1371/journal.pbio.3001199.

Farkash, E.A., Wilson, A.M., and Jentzen, J.M. (2020). Ultrastructural Evidence for Direct Renal Infection with SARS-CoV-2. J Am Soc Nephrol *31*, 1683-1687. 10.1681/ASN.2020040432.
Fassati, A., Gorlich, D., Harrison, I., Zaytseva, L., and Mingot, J.M. (2003). Nuclear import of HIV-1 intracellular reverse transcription complexes is mediated by importin 7. EMBO J *22*, 3675-3685. 10.1093/emboj/cdg357.
Fehrenbach, H. (2001). Alveolar epithelial type II cell: defender of the alveolus revisited. Respir Res *2*, 33-46. 10.1186/rr36.
Ferreira-Gomes, M., Kruglov, A., Durek, P., Heinrich, F., Tizian, C., Heinz, G.A., Pascual-Reguant, A., Du, W., Mothes, R., Fan, C., et al. (2021). SARS-CoV-2 in severe COVID-19 induces a TGF-beta-dominated chronic immune response that does not target itself. Nat Commun *12*, 1961. 10.1038/s41467-021-22210-3.
Fife, B.T., and Bluestone, J.A. (2008). Control of peripheral T-cell tolerance and autoimmunity via the CTLA-4 and PD-1 pathways. Immunol Rev *224*, 166-182. 10.1111/j.1600-065X.2008.00662.x.
Fletcher, C.V., Staskus, K., Wietgrefe, S.W., Rothenberger, M., Reilly, C., Chipman, J.G., Beilman, G.J., Khoruts, A., Thorkelson, A., Schmidt, T.E., et al. (2014). Persistent HIV-1 replication is associated with lower antiretroviral drug concentrations in lymphatic tissues. Proc Natl Acad Sci U S A *111*, 2307-2312. 10.1073/pnas.1318249111.
Folkesson, H.G., Norlin, A., Wang, Y., Abedinpour, P., and Matthay, M.A. (2000). Dexamethasone and thyroid hormone pretreatment upregulate alveolar epithelial fluid clearance in adult rats. J Appl Physiol (1985) *88*, 416-424. 10.1152/jappl.2000.88.2.416.
Francisco, L.M., Salinas, V.H., Brown, K.E., Vanguri, V.K., Freeman, G.J., Kuchroo, V.K., and Sharpe, A.H. (2009). PD-L1 regulates the development, maintenance, and function of induced regulatory T cells. J Exp Med *206*, 3015-3029. 10.1084/jem.20090847.
Fromentin, R., Bakeman, W., Lawani, M.B., Khoury, G., Hartogensis, W., DaFonseca, S., Killian, M., Epling, L., Hoh, R., Sinclair, E., et al. (2016). CD4+ T Cells Expressing PD-1, TIGIT and LAG-3 Contribute to HIV Persistence during ART. PLoS Pathog *12*, e1005761. 10.1371/journal.ppat.1005761.
Fromentin, R., DaFonseca, S., Costiniuk, C.T., El-Far, M., Procopio, F.A., Hecht, F.M., Hoh, R., Deeks, S.G., Hazuda, D.J., Lewin, S.R., et al. (2019). PD-1 blockade potentiates HIV latency reversal ex vivo in CD4(+) T cells from ART-suppressed individuals. Nat Commun *10*, 814. 10.1038/s41467-019-08798-7.
Galani, I.E., Rovina, N., Lampropoulou, V., Triantafyllia, V., Manioudaki, M., Pavlos, E., Koukaki, E., Fragkou, P.C., Panou, V., Rapti, V., et al. (2021). Untuned antiviral immunity in COVID-19 revealed by temporal type I/III interferon patterns and flu comparison. Nat Immunol *22*, 32-40. 10.1038/s41590-020-00840-x.
Garon, E.B., Rizvi, N.A., Hui, R., Leighl, N., Balmanoukian, A.S., Eder, J.P., Patnaik, A., Aggarwal, C., Gubens, M., Horn, L., et al. (2015). Pembrolizumab for the treatment of non-small-cell lung cancer. N Engl J Med *372*, 2018-2028. 10.1056/NEJMoa1501824.
Gasper, D.J., Tejera, M.M., and Suresh, M. (2014). CD4 T-cell memory generation and maintenance. Crit Rev Immunol *34*, 121-146. 10.1615/critrevimmunol.2014010373.
Gasser, R., Cloutier, M., Prevost, J., Fink, C., Ducas, E., Ding, S., Dussault, N., Landry, P., Tremblay, T., Laforce-Lavoie, A., et al. (2021). Major role of IgM in the neutralizing activity of convalescent plasma against SARS-CoV-2. Cell Rep, 108790. 10.1016/j.celrep.2021.108790.
Gaunsbaek, M.Q., Rasmussen, K.J., Beers, M.F., Atochina-Vasserman, E.N., and Hansen, S.

(2013). Lung surfactant protein D (SP-D) response and regulation during acute and chronic lung injury. Lung *191*, 295-303. 10.1007/s00408-013-9452-x.
Gay, C.L., Bosch, R.J., Ritz, J., Hataye, J.M., Aga, E., Tressler, R.L., Mason, S.W., Hwang, C.K., Grasela, D.M., Ray, N., et al. (2017). Clinical Trial of the Anti-PD-L1 Antibody BMS-936559 in HIV-1 Infected Participants on Suppressive Antiretroviral Therapy. J Infect Dis. 10.1093/infdis/jix191.
Ghosh, S., Dellibovi-Ragheb, T.A., Kerviel, A., Pak, E., Qiu, Q., Fisher, M., Takvorian, P.M., Bleck, C., Hsu, V.W., Fehr, A.R., et al. (2020). beta-Coronaviruses Use Lysosomes for Egress Instead of the Biosynthetic Secretory Pathway. Cell *183*, 1520-1535 e1514. 10.1016/j.cell.2020.10.039.
Gonzalez-Cao, M., Moran, T., Dalmau, J., Garcia-Corbacho, J., Bracht, J.W.P., Bernabe, R., Juan, O., de Castro, J., Blanco, R., Drozdowskyj, A., et al. (2020). Assessment of the Feasibility and Safety of Durvalumab for Treatment of Solid Tumors in Patients With HIV-1 Infection: The Phase 2 DURVAST Study. JAMA Oncol *6*, 1063-1067. 10.1001/jamaoncol.2020.0465.
Goodman, A.M., Kato, S., Bazhenova, L., Patel, S.P., Frampton, G.M., Miller, V., Stephens, P.J., Daniels, G.A., and Kurzrock, R. (2017). Tumor Mutational Burden as an Independent Predictor of Response to Immunotherapy in Diverse Cancers. Mol Cancer Ther *16*, 2598-2608. 10.1158/1535-7163.MCT-17-0386.
Gopalakrishnan, V., Spencer, C.N., Nezi, L., Reuben, A., Andrews, M.C., Karpinets, T.V., Prieto, P.A., Vicente, D., Hoffman, K., Wei, S.C., et al. (2018). Gut microbiome modulates response to anti-PD-1 immunotherapy in melanoma patients. Science *359*, 97-103. 10.1126/science.aan4236.
Gorbalenya, A.E., Enjuanes, L., Ziebuhr, J., and Snijder, E.J. (2006). Nidovirales: evolving the largest RNA virus genome. Virus Res *117*, 17-37. 10.1016/j.virusres.2006.01.017.
Gottlinger, H.G., Dorfman, T., Sodroski, J.G., and Haseltine, W.A. (1991). Effect of mutations affecting the p6 gag protein on human immunodeficiency virus particle release. Proc Natl Acad Sci U S A *88*, 3195-3199. 10.1073/pnas.88.8.3195.
Goulder, P.J., and Walker, B.D. (2012). HIV and HLA class I: an evolving relationship. Immunity *37*, 426-440. 10.1016/j.immuni.2012.09.005.
Grabmeier-Pfistershammer, K., Stecher, C., Zettl, M., Rosskopf, S., Rieger, A., Zlabinger, G.J., and Steinberger, P. (2017). Antibodies targeting BTLA or TIM-3 enhance HIV-1 specific T cell responses in combination with PD-1 blockade. Clin Immunol *183*, 167-173. 10.1016/j.clim.2017.09.002.
Grasselli, G., Tonetti, T., Protti, A., Langer, T., Girardis, M., Bellani, G., Laffey, J., Carrafiello, G., Carsana, L., Rizzuto, C., et al. (2020). Pathophysiology of COVID-19-associated acute respiratory distress syndrome: a multicentre prospective observational study. Lancet Respir Med *8*, 1201-1208. 10.1016/S2213-2600(20)30370-2.
Greczmiel, U., Krautler, N.J., Pedrioli, A., Bartsch, I., Agnellini, P., Bedenikovic, G., Harker, J., Richter, K., and Oxenius, A. (2017). Sustained T follicular helper cell response is essential for control of chronic viral infection. Sci Immunol *2*. 10.1126/sciimmunol.aam8686.
Greczmiel, U., and Oxenius, A. (2018). The Janus Face of Follicular T Helper Cells in Chronic Viral Infections. Front Immunol *9*, 1162. 10.3389/fimmu.2018.01162.
Greenwald, R.J., Boussiotis, V.A., Lorsbach, R.B., Abbas, A.K., and Sharpe, A.H. (2001). CTLA-4 regulates induction of anergy in vivo. Immunity *14*, 145-155. 10.1016/s1074-7613(01)00097-8.
Grifoni, A., Weiskopf, D., Ramirez, S.I., Mateus, J., Dan, J.M., Moderbacher, C.R., Rawlings, S.A., Sutherland, A., Premkumar, L., Jadi, R.S., et al. (2020). Targets of T Cell Responses to SARS-CoV-2

Coronavirus in Humans with COVID-19 Disease and Unexposed Individuals. Cell *181*, 1489-1501 e1415. 10.1016/j.cell.2020.05.015.
Group, A.-T.L.-C.S., Lundgren, J.D., Grund, B., Barkauskas, C.E., Holland, T.L., Gottlieb, R.L., Sandkovsky, U., Brown, S.M., Knowlton, K.U., Self, W.H., et al. (2021a). A Neutralizing Monoclonal Antibody for Hospitalized Patients with Covid-19. N Engl J Med *384*, 905-914. 10.1056/NEJMoa2033130.
Group, R.C. (2020). Lopinavir-ritonavir in patients admitted to hospital with COVID-19 (RECOVERY): a randomised, controlled, open-label, platform trial. Lancet *396*, 1345-1352. 10.1016/S0140-6736(20)32013-4.
Group, R.C. (2021a). Convalescent plasma in patients admitted to hospital with COVID-19 (RECOVERY): a randomised controlled, open-label, platform trial. Lancet *397*, 2049-2059. 10.1016/S0140-6736(21)00897-7.
Group, R.C. (2021b). Tocilizumab in patients admitted to hospital with COVID-19 (RECOVERY): a randomised, controlled, open-label, platform trial. Lancet *397*, 1637-1645. 10.1016/S0140-6736(21)00676-0.
Group, R.C. (2022). Casirivimab and imdevimab in patients admitted to hospital with COVID-19 (RECOVERY): a randomised, controlled, open-label, platform trial. Lancet *399*, 665-676. 10.1016/S0140-6736(22)00163-5.
Group, R.C., Horby, P., Lim, W.S., Emberson, J.R., Mafham, M., Bell, J.L., Linsell, L., Staplin, N., Brightling, C., Ustianowski, A., et al. (2021b). Dexamethasone in Hospitalized Patients with Covid-19. N Engl J Med *384*, 693-704. 10.1056/NEJMoa2021436.
Group, W.H.O.R.E.A.f.C.-T.W., Shankar-Hari, M., Vale, C.L., Godolphin, P.J., Fisher, D., Higgins, J.P.T., Spiga, F., Savovic, J., Tierney, J., Baron, G., et al. (2021c). Association Between Administration of IL-6 Antagonists and Mortality Among Patients Hospitalized for COVID-19: A Meta-analysis. JAMA *326*, 499-518. 10.1001/jama.2021.11330.
Group, W.H.O.R.E.A.f.C.-T.W., Sterne, J.A.C., Murthy, S., Diaz, J.V., Slutsky, A.S., Villar, J., Angus, D.C., Annane, D., Azevedo, L.C.P., Berwanger, O., et al. (2020). Association Between Administration of Systemic Corticosteroids and Mortality Among Critically Ill Patients With COVID-19: A Meta-analysis. JAMA *324*, 1330-1341. 10.1001/jama.2020.17023.
Guan, W.J., Ni, Z.Y., Hu, Y., Liang, W.H., Ou, C.Q., He, J.X., Liu, L., Shan, H., Lei, C.L., Hui, D.S.C., et al. (2020). Clinical Characteristics of Coronavirus Disease 2019 in China. N Engl J Med *382*, 1708-1720. 10.1056/NEJMoa2002032.
Guihot, A., Bourgarit, A., Carcelain, G., and Autran, B. (2011). Immune reconstitution after a decade of combined antiretroviral therapies for human immunodeficiency virus. Trends Immunol *32*, 131-137. 10.1016/j.it.2010.12.002.
Guihot, A., Marcelin, A.G., Massiani, M.A., Samri, A., Soulie, C., Autran, B., and Spano, J.P. (2018). Drastic decrease of the HIV reservoir in a patient treated with nivolumab for lung cancer. Ann Oncol *29*, 517-518. 10.1093/annonc/mdx696.
Gupta, A., Madhavan, M.V., Sehgal, K., Nair, N., Mahajan, S., Sehrawat, T.S., Bikdeli, B., Ahluwalia, N., Ausiello, J.C., Wan, E.Y., et al. (2020). Extrapulmonary manifestations of COVID-19. Nat Med *26*, 1017-1032. 10.1038/s41591-020-0968-3.
Gutierrez-Martinez, E., Planes, R., Anselmi, G., Reynolds, M., Menezes, S., Adiko, A.C., Saveanu, L., and Guermonprez, P. (2015). Cross-Presentation of Cell-Associated Antigens by MHC Class I in Dendritic Cell Subsets. Front Immunol *6*, 363. 10.3389/fimmu.2015.00363.

Gutmann, C., Takov, K., Burnap, S.A., Singh, B., Ali, H., Theofilatos, K., Reed, E., Hasman, M., Nabeebaccus, A., Fish, M., et al. (2021). SARS-CoV-2 RNAemia and proteomic trajectories inform prognostication in COVID-19 patients admitted to intensive care. Nat Commun *12*, 3406. 10.1038/s41467-021-23494-1.
Hadjadj, J., Yatim, N., Barnabei, L., Corneau, A., Boussier, J., Smith, N., Pere, H., Charbit, B., Bondet, V., Chenevier-Gobeaux, C., et al. (2020). Impaired type I interferon activity and inflammatory responses in severe COVID-19 patients. Science *369*, 718-724. 10.1126/science.abc6027.
Hargadon, K.M., Johnson, C.E., and Williams, C.J. (2018). Immune checkpoint blockade therapy for cancer: An overview of FDA-approved immune checkpoint inhibitors. Int Immunopharmacol *62*, 29-39. 10.1016/j.intimp.2018.06.001.
Harouse, J.M., Gettie, A., Tan, R.C., Blanchard, J., and Cheng-Mayer, C. (1999). Distinct pathogenic sequela in rhesus macaques infected with CCR5 or CXCR4 utilizing SHIVs. Science *284*, 816-819. 10.1126/science.284.5415.816.
Harper, J., Gordon, S., Chan, C.N., Wang, H., Lindemuth, E., Galardi, C., Falcinelli, S.D., Raines, S.L.M., Read, J.L., Nguyen, K., et al. (2020). CTLA-4 and PD-1 dual blockade induces SIV reactivation without control of rebound after antiretroviral therapy interruption. Nat Med *26*, 519-528. 10.1038/s41591-020-0782-y.
Harr, M.W., Rong, Y., Bootman, M.D., Roderick, H.L., and Distelhorst, C.W. (2009). Glucocorticoid-mediated inhibition of Lck modulates the pattern of T cell receptor-induced calcium signals by down-regulating inositol 1,4,5-trisphosphate receptors. J Biol Chem *284*, 31860-31871. 10.1074/jbc.M109.005579.
Harrigan, P.R., Whaley, M., and Montaner, J.S. (1999). Rate of HIV-1 RNA rebound upon stopping antiretroviral therapy. AIDS *13*, F59-62. 10.1097/00002030-199905280-00001.
Harvey, W.T., Carabelli, A.M., Jackson, B., Gupta, R.K., Thomson, E.C., Harrison, E.M., Ludden, C., Reeve, R., Rambaut, A., Consortium, C.-G.U., et al. (2021). SARS-CoV-2 variants, spike mutations and immune escape. Nat Rev Microbiol *19*, 409-424. 10.1038/s41579-021-00573-0.
Hastings, R.H., Grady, M., Sakuma, T., and Matthay, M.A. (1992). Clearance of different-sized proteins from the alveolar space in humans and rabbits. J Appl Physiol (1985) *73*, 1310-1316. 10.1152/jappl.1992.73.4.1310.
Hatziioannou, T., and Evans, D.T. (2012). Animal models for HIV/AIDS research. Nat Rev Microbiol *10*, 852-867. 10.1038/nrmicro2911.
He, R., Hou, S., Liu, C., Zhang, A., Bai, Q., Han, M., Yang, Y., Wei, G., Shen, T., Yang, X., et al. (2016). Follicular CXCR5- expressing CD8(+) T cells curtail chronic viral infection. Nature *537*, 412-428. 10.1038/nature19317.
Hellman, U., Karlsson, M.G., Engstrom-Laurent, A., Cajander, S., Dorofte, L., Ahlm, C., Laurent, C., and Blomberg, A. (2020). Presence of hyaluronan in lung alveoli in severe Covid-19: An opening for new treatment options? J Biol Chem *295*, 15418-15422. 10.1074/jbc.AC120.015967.
Hodi, F.S., Mihm, M.C., Soiffer, R.J., Haluska, F.G., Butler, M., Seiden, M.V., Davis, T., Henry-Spires, R., MacRae, S., Willman, A., et al. (2003). Biologic activity of cytotoxic T lymphocyte-associated antigen 4 antibody blockade in previously vaccinated metastatic melanoma and ovarian carcinoma patients. Proc Natl Acad Sci U S A *100*, 4712-4717. 10.1073/pnas.0830997100.
Hoffmann, M., Kleine-Weber, H., Schroeder, S., Kruger, N., Herrler, T., Erichsen, S., Schiergens,

T.S., Herrler, G., Wu, N.H., Nitsche, A., et al. (2020). SARS-CoV-2 Cell Entry Depends on ACE2 and TMPRSS2 and Is Blocked by a Clinically Proven Protease Inhibitor. Cell *181*, 271-280 e278. 10.1016/j.cell.2020.02.052.
Hogan, C.A., Stevens, B.A., Sahoo, M.K., Huang, C., Garamani, N., Gombar, S., Yamamoto, F., Murugesan, K., Kurzer, J., Zehnder, J., and Pinsky, B.A. (2020). High Frequency of SARS-CoV-2 RNAemia and Association With Severe Disease. Clin Infect Dis. 10.1093/cid/ciaa1054.
Hou, T.Z., Qureshi, O.S., Wang, C.J., Baker, J., Young, S.P., Walker, L.S., and Sansom, D.M. (2015). A transendocytosis model of CTLA-4 function predicts its suppressive behavior on regulatory T cells. J Immunol *194*, 2148-2159. 10.4049/jimmunol.1401876.
Hou, Y.J., Okuda, K., Edwards, C.E., Martinez, D.R., Asakura, T., Dinnon, K.H., 3rd, Kato, T., Lee, R.E., Yount, B.L., Mascenik, T.M., et al. (2020). SARS-CoV-2 Reverse Genetics Reveals a Variable Infection Gradient in the Respiratory Tract. Cell *182*, 429-446 e414. 10.1016/j.cell.2020.05.042.
Hryniewicz, A., Boasso, A., Edghill-Smith, Y., Vaccari, M., Fuchs, D., Venzon, D., Nacsa, J., Betts, M.R., Tsai, W.P., Heraud, J.M., et al. (2006). CTLA-4 blockade decreases TGF-beta, IDO, and viral RNA expression in tissues of SIVmac251-infected macaques. Blood *108*, 3834-3842. 10.1182/blood-2006-04-010637.
Hsu, D.C., Sereti, I., and Ananworanich, J. (2013). Serious Non-AIDS events: Immunopathogenesis and interventional strategies. AIDS Res Ther *10*, 29. 10.1186/1742-6405-10-29.
Hu, L.R., Li, D., Chu, Q., Wang, Y.C., Zhou, L., Yu, Y., Zhang, Y., Zhang, S.L., Usman, T., Xie, Z.Q., et al. (2021). Selection and implementation of single nucleotide polymorphism markers for parentage analysis in crossbred cattle population. Animal *15*, 100066. 10.1016/j.animal.2020.100066.
Huang, B., Wang, D.X., and Deng, W. (2014). Protective effects of dexamethasone on early acute lung injury induced by oleic acid in rats. Int J Clin Exp Med *7*, 4698-4709.
Huang, C., Wang, Y., Li, X., Ren, L., Zhao, J., Hu, Y., Zhang, L., Fan, G., Xu, J., Gu, X., et al. (2020). Clinical features of patients infected with 2019 novel coronavirus in Wuhan, China. Lancet *395*, 497-506. 10.1016/S0140-6736(20)30183-5.
Hui, E., Cheung, J., Zhu, J., Su, X., Taylor, M.J., Wallweber, H.A., Sasmal, D.K., Huang, J., Kim, J.M., Mellman, I., and Vale, R.D. (2017). T cell costimulatory receptor CD28 is a primary target for PD-1-mediated inhibition. Science *355*, 1428-1433. 10.1126/science.aaf1292.
Hung, I.F., To, K.K., Lee, C.K., Lee, K.L., Chan, K., Yan, W.W., Liu, R., Watt, C.L., Chan, W.M., Lai, K.Y., et al. (2011). Convalescent plasma treatment reduced mortality in patients with severe pandemic influenza A (H1N1) 2009 virus infection. Clin Infect Dis *52*, 447-456. 10.1093/cid/ciq106.
Hunt, P.W., Brenchley, J., Sinclair, E., McCune, J.M., Roland, M., Page-Shafer, K., Hsue, P., Emu, B., Krone, M., Lampiris, H., et al. (2008). Relationship between T cell activation and CD4+ T cell count in HIV-seropositive individuals with undetectable plasma HIV RNA levels in the absence of therapy. J Infect Dis *197*, 126-133. 10.1086/524143.
Hunt, P.W., Lee, S.A., and Siedner, M.J. (2016). Immunologic Biomarkers, Morbidity, and Mortality in Treated HIV Infection. J Infect Dis *214 Suppl 2*, S44-50. 10.1093/infdis/jiw275.
Hunt, P.W., Sinclair, E., Rodriguez, B., Shive, C., Clagett, B., Funderburg, N., Robinson, J., Huang, Y., Epling, L., Martin, J.N., et al. (2014). Gut epithelial barrier dysfunction and innate immune activation predict mortality in treated HIV infection. J Infect Dis *210*, 1228-1238.

10.1093/infdis/jiu238.
Iacob, S.A., Iacob, D.G., and Jugulete, G. (2017). Improving the Adherence to Antiretroviral Therapy, a Difficult but Essential Task for a Successful HIV Treatment-Clinical Points of View and Practical Considerations. Front Pharmacol *8*, 831. 10.3389/fphar.2017.00831.
Ignatieva, A., Lyngso, R.B., Jenkins, P.A., and Hein, J. (2021). KwARG: Parsimonious reconstruction of ancestral recombination graphs with recurrent mutation. Bioinformatics. 10.1093/bioinformatics/btab351.
Im, S.J., and Ha, S.J. (2020). Re-defining T-Cell Exhaustion: Subset, Function, and Regulation. Immune Netw *20*, e2. 10.4110/in.2020.20.e2.
Im, S.J., Hashimoto, M., Gerner, M.Y., Lee, J., Kissick, H.T., Burger, M.C., Shan, Q., Hale, J.S., Lee, J., Nasti, T.H., et al. (2016). Defining CD8+ T cells that provide the proliferative burst after PD-1 therapy. Nature *537*, 417-421. 10.1038/nature19330.
Investigators, R.-C., Gordon, A.C., Mouncey, P.R., Al-Beidh, F., Rowan, K.M., Nichol, A.D., Arabi, Y.M., Annane, D., Beane, A., van Bentum-Puijk, W., et al. (2021). Interleukin-6 Receptor Antagonists in Critically Ill Patients with Covid-19. N Engl J Med *384*, 1491-1502. 10.1056/NEJMoa2100433.
Ip, W.K., Chan, K.H., Law, H.K., Tso, G.H., Kong, E.K., Wong, W.H., To, Y.F., Yung, R.W., Chow, E.Y., Au, K.L., et al. (2005). Mannose-binding lectin in severe acute respiratory syndrome coronavirus infection. J Infect Dis *191*, 1697-1704. 10.1086/429631.
Ishida, Y., Agata, Y., Shibahara, K., and Honjo, T. (1992). Induced expression of PD-1, a novel member of the immunoglobulin gene superfamily, upon programmed cell death. EMBO J *11*, 3887-3895.
Iwai, Y., Ishida, M., Tanaka, Y., Okazaki, T., Honjo, T., and Minato, N. (2002). Involvement of PD-L1 on tumor cells in the escape from host immune system and tumor immunotherapy by PD-L1 blockade. Proc Natl Acad Sci U S A *99*, 12293-12297. 10.1073/pnas.192461099.
Iwai, Y., Terawaki, S., Ikegawa, M., Okazaki, T., and Honjo, T. (2003). PD-1 inhibits antiviral immunity at the effector phase in the liver. J Exp Med *198*, 39-50. 10.1084/jem.20022235.
Janssen, E.M., Lemmens, E.E., Wolfe, T., Christen, U., von Herrath, M.G., and Schoenberger, S.P. (2003). CD4+ T cells are required for secondary expansion and memory in CD8+ T lymphocytes. Nature *421*, 852-856. 10.1038/nature01441.
Jiang, C., Lian, X., Gao, C., Sun, X., Einkauf, K.B., Chevalier, J.M., Chen, S.M.Y., Hua, S., Rhee, B., Chang, K., et al. (2020). Distinct viral reservoirs in individuals with spontaneous control of HIV-1. Nature *585*, 261-267. 10.1038/s41586-020-2651-8.
Jin, X., Bauer, D.E., Tuttleton, S.E., Lewin, S., Gettie, A., Blanchard, J., Irwin, C.E., Safrit, J.T., Mittler, J., Weinberger, L., et al. (1999). Dramatic rise in plasma viremia after CD8(+) T cell depletion in simian immunodeficiency virus-infected macaques. J Exp Med *189*, 991-998. 10.1084/jem.189.6.991.
Jirak, P., Larbig, R., Shomanova, Z., Frob, E.J., Dankl, D., Torgersen, C., Frank, N., Mahringer, M., Butkiene, D., Haake, H., et al. (2021). Myocardial injury in severe COVID-19 is similar to pneumonias of other origin: results from a multicentre study. ESC Heart Fail *8*, 37-46. 10.1002/ehf2.13136.
Joseph, S.B., Swanstrom, R., Kashuba, A.D., and Cohen, M.S. (2015). Bottlenecks in HIV-1 transmission: insights from the study of founder viruses. Nat Rev Microbiol *13*, 414-425. 10.1038/nrmicro3471.

Joyner, M.J., Carter, R.E., Senefeld, J.W., Klassen, S.A., Mills, J.R., Johnson, P.W., Theel, E.S., Wiggins, C.C., Bruno, K.A., Klompas, A.M., et al. (2021). Convalescent Plasma Antibody Levels and the Risk of Death from Covid-19. N Engl J Med *384*, 1015-1027. 10.1056/NEJMoa2031893.
Justiz Vaillant, A.A., and Qurie, A. (2021). Interleukin. In StatPearls.
Kaech, S.M., and Cui, W. (2012). Transcriptional control of effector and memory CD8+ T cell differentiation. Nat Rev Immunol *12*, 749-761. 10.1038/nri3307.
Kalil, A.C., Patterson, T.F., Mehta, A.K., Tomashek, K.M., Wolfe, C.R., Ghazaryan, V., Marconi, V.C., Ruiz-Palacios, G.M., Hsieh, L., Kline, S., et al. (2021). Baricitinib plus Remdesivir for Hospitalized Adults with Covid-19. N Engl J Med *384*, 795-807. 10.1056/NEJMoa2031994.
Kallies, A., Xin, A., Belz, G.T., and Nutt, S.L. (2009). Blimp-1 transcription factor is required for the differentiation of effector CD8(+) T cells and memory responses. Immunity *31*, 283-295. 10.1016/j.immuni.2009.06.021.
Kamphorst, A.O., Pillai, R.N., Yang, S., Nasti, T.H., Akondy, R.S., Wieland, A., Sica, G.L., Yu, K., Koenig, L., Patel, N.T., et al. (2017a). Proliferation of PD-1+ CD8 T cells in peripheral blood after PD-1-targeted therapy in lung cancer patients. Proc Natl Acad Sci U S A *114*, 4993-4998. 10.1073/pnas.1705327114.
Kamphorst, A.O., Wieland, A., Nasti, T., Yang, S., Zhang, R., Barber, D.L., Konieczny, B.T., Daugherty, C.Z., Koenig, L., Yu, K., et al. (2017b). Rescue of exhausted CD8 T cells by PD-1-targeted therapies is CD28-dependent. Science *355*, 1423-1427. 10.1126/science.aaf0683.
Kaneko, N., Kuo, H.H., Boucau, J., Farmer, J.R., Allard-Chamard, H., Mahajan, V.S., Piechocka-Trocha, A., Lefteri, K., Osborn, M., Bals, J., et al. (2020). Loss of Bcl-6-Expressing T Follicular Helper Cells and Germinal Centers in COVID-19. Cell *183*, 143-157 e113. 10.1016/j.cell.2020.08.025.
Kao, C., Oestreich, K.J., Paley, M.A., Crawford, A., Angelosanto, J.M., Ali, M.A., Intlekofer, A.M., Boss, J.M., Reiner, S.L., Weinmann, A.S., and Wherry, E.J. (2011). Transcription factor T-bet represses expression of the inhibitory receptor PD-1 and sustains virus-specific CD8+ T cell responses during chronic infection. Nat Immunol *12*, 663-671. 10.1038/ni.2046.
Kaplan, M.H. (2013). STAT signaling in inflammation. JAKSTAT *2*, e24198. 10.4161/jkst.24198.
Kaslow, R.A., Carrington, M., Apple, R., Park, L., Munoz, A., Saah, A.J., Goedert, J.J., Winkler, C., O'Brien, S.J., Rinaldo, C., et al. (1996). Influence of combinations of human major histocompatibility complex genes on the course of HIV-1 infection. Nat Med *2*, 405-411. 10.1038/nm0496-405.
Keele, B.F., Van Heuverswyn, F., Li, Y., Bailes, E., Takehisa, J., Santiago, M.L., Bibollet-Ruche, F., Chen, Y., Wain, L.V., Liegeois, F., et al. (2006). Chimpanzee reservoirs of pandemic and nonpandemic HIV-1. Science *313*, 523-526. 10.1126/science.1126531.
Kennedy, A.D., and DeLeo, F.R. (2009). Neutrophil apoptosis and the resolution of infection. Immunol Res *43*, 25-61. 10.1007/s12026-008-8049-6.
Kim, S.Y., Park, S.J., Cho, S.Y., Cha, R.H., Jee, H.G., Kim, G., Shin, H.S., Kim, Y., Jung, Y.M., Yang, J.S., et al. (2016). Viral RNA in Blood as Indicator of Severe Outcome in Middle East Respiratory Syndrome Coronavirus Infection. Emerg Infect Dis *22*, 1813-1816. 10.3201/eid2210.160218.
Kiner, E., Willie, E., Vijaykumar, B., Chowdhary, K., Schmutz, H., Chandler, J., Schnell, A., Thakore, P.I., LeGros, G., Mostafavi, S., et al. (2021). Gut CD4(+) T cell phenotypes are a continuum molded by microbes, not by TH archetypes. Nat Immunol *22*, 216-228. 10.1038/s41590-020-00836-7.

Klein, S., Cortese, M., Winter, S.L., Wachsmuth-Melm, M., Neufeldt, C.J., Cerikan, B., Stanifer, M.L., Boulant, S., Bartenschlager, R., and Chlanda, P. (2020). SARS-CoV-2 structure and replication characterized by in situ cryo-electron tomography. Nat Commun *11*, 5885. 10.1038/s41467-020-19619-7.
Klok, F.A., Kruip, M., van der Meer, N.J.M., Arbous, M.S., Gommers, D., Kant, K.M., Kaptein, F.H.J., van Paassen, J., Stals, M.A.M., Huisman, M.V., and Endeman, H. (2020). Incidence of thrombotic complications in critically ill ICU patients with COVID-19. Thromb Res *191*, 145-147. 10.1016/j.thromres.2020.04.013.
Kohler, S.L., Pham, M.N., Folkvord, J.M., Arends, T., Miller, S.M., Miles, B., Meditz, A.L., McCarter, M., Levy, D.N., and Connick, E. (2016). Germinal Center T Follicular Helper Cells Are Highly Permissive to HIV-1 and Alter Their Phenotype during Virus Replication. J Immunol *196*, 2711-2722. 10.4049/jimmunol.1502174.
Konno, Y., Kimura, I., Uriu, K., Fukushi, M., Irie, T., Koyanagi, Y., Sauter, D., Gifford, R.J., Consortium, U.-C., Nakagawa, S., and Sato, K. (2020). SARS-CoV-2 ORF3b Is a Potent Interferon Antagonist Whose Activity Is Increased by a Naturally Occurring Elongation Variant. Cell Rep *32*, 108185. 10.1016/j.celrep.2020.108185.
Koup, R.A. (1994). Virus escape from CTL recognition. J Exp Med *180*, 779-782. 10.1084/jem.180.3.779.
Krause, P.R., Fleming, T.R., Longini, I.M., Peto, R., Briand, S., Heymann, D.L., Beral, V., Snape, M.D., Rees, H., Ropero, A.M., et al. (2021). SARS-CoV-2 Variants and Vaccines. N Engl J Med *385*, 179-186. 10.1056/NEJMsr2105280.
Kreider, T., Anthony, R.M., Urban, J.F., Jr., and Gause, W.C. (2007). Alternatively activated macrophages in helminth infections. Curr Opin Immunol *19*, 448-453. 10.1016/j.coi.2007.07.002.
Kreuzberger, N., Hirsch, C., Chai, K.L., Tomlinson, E., Khosravi, Z., Popp, M., Neidhardt, M., Piechotta, V., Salomon, S., Valk, S.J., et al. (2021). SARS-CoV-2-neutralising monoclonal antibodies for treatment of COVID-19. Cochrane Database Syst Rev *9*, CD013825. 10.1002/14651858.CD013825.pub2.
Krummel, M.F., and Allison, J.P. (1995). CD28 and CTLA-4 have opposing effects on the response of T cells to stimulation. J Exp Med *182*, 459-465. 10.1084/jem.182.2.459.
Kuller, L.H., Tracy, R., Belloso, W., De Wit, S., Drummond, F., Lane, H.C., Ledergerber, B., Lundgren, J., Neuhaus, J., Nixon, D., et al. (2008). Inflammatory and coagulation biomarkers and mortality in patients with HIV infection. PLoS Med *5*, e203. 10.1371/journal.pmed.0050203.
Kuo, H.H., and Lichterfeld, M. (2018). Recent progress in understanding HIV reservoirs. Curr Opin HIV AIDS *13*, 137-142. 10.1097/COH.0000000000000441.
Kwong, P.D., Wyatt, R., Robinson, J., Sweet, R.W., Sodroski, J., and Hendrickson, W.A. (1998). Structure of an HIV gp120 envelope glycoprotein in complex with the CD4 receptor and a neutralizing human antibody. Nature *393*, 648-659. 10.1038/31405.
Lafon, E., Diem, G., Witting, C., Zaderer, V., Bellmann-Weiler, R.M., Reindl, M., Bauer, A., Griesmacher, A., Fux, V., Hoermann, G., et al. (2021). Potent SARS-CoV-2-Specific T Cell Immunity and Low Anaphylatoxin Levels Correlate With Mild Disease Progression in COVID-19 Patients. Front Immunol *12*, 684014. 10.3389/fimmu.2021.684014.
Laing, A.G., Lorenc, A., Del Molino Del Barrio, I., Das, A., Fish, M., Monin, L., Munoz-Ruiz, M., McKenzie, D.R., Hayday, T.S., Francos-Quijorna, I., et al. (2020). A dynamic COVID-19 immune

signature includes associations with poor prognosis. Nat Med *26*, 1623-1635. 10.1038/s41591-020-1038-6.
Larkin, J., Chiarion-Sileni, V., Gonzalez, R., Grob, J.J., Cowey, C.L., Lao, C.D., Schadendorf, D., Dummer, R., Smylie, M., Rutkowski, P., et al. (2015). Combined Nivolumab and Ipilimumab or Monotherapy in Untreated Melanoma. N Engl J Med *373*, 23-34. 10.1056/NEJMoa1504030.
Le, T., Wright, E.J., Smith, D.M., He, W., Catano, G., Okulicz, J.F., Young, J.A., Clark, R.A., Richman, D.D., Little, S.J., and Ahuja, S.K. (2013). Enhanced CD4+ T-cell recovery with earlier HIV-1 antiretroviral therapy. N Engl J Med *368*, 218-230. 10.1056/NEJMoa1110187.
Lee, N., Allen Chan, K.C., Hui, D.S., Ng, E.K., Wu, A., Chiu, R.W., Wong, V.W., Chan, P.K., Wong, K.T., Wong, E., et al. (2004). Effects of early corticosteroid treatment on plasma SARS-associated Coronavirus RNA concentrations in adult patients. J Clin Virol *31*, 304-309. 10.1016/j.jcv.2004.07.006.
Lee, N., Chan, P.K., Hui, D.S., Rainer, T.H., Wong, E., Choi, K.W., Lui, G.C., Wong, B.C., Wong, R.Y., Lam, W.Y., et al. (2009). Viral loads and duration of viral shedding in adult patients hospitalized with influenza. J Infect Dis *200*, 492-500. 10.1086/600383.
Lei, X., Dong, X., Ma, R., Wang, W., Xiao, X., Tian, Z., Wang, C., Wang, Y., Li, L., Ren, L., et al. (2020). Activation and evasion of type I interferon responses by SARS-CoV-2. Nat Commun *11*, 3810. 10.1038/s41467-020-17665-9.
Lenti, M.V., Aronico, N., Pellegrino, I., Boveri, E., Giuffrida, P., Borrelli de Andreis, F., Morbini, P., Vanelli, L., Pasini, A., Ubezio, C., et al. (2020). Depletion of circulating IgM memory B cells predicts unfavourable outcome in COVID-19. Sci Rep *10*, 20836. 10.1038/s41598-020-77945-8.
Letko, M., Marzi, A., and Munster, V. (2020). Functional assessment of cell entry and receptor usage for SARS-CoV-2 and other lineage B betacoronaviruses. Nat Microbiol *5*, 562-569. 10.1038/s41564-020-0688-y.
Lewis, P., Hensel, M., and Emerman, M. (1992). Human immunodeficiency virus infection of cells arrested in the cell cycle. EMBO J *11*, 3053-3058.
Li, C., Jiang, P., Wei, S., Xu, X., and Wang, J. (2020). Regulatory T cells in tumor microenvironment: new mechanisms, potential therapeutic strategies and future prospects. Mol Cancer *19*, 116. 10.1186/s12943-020-01234-1.
Liang, S.C., Tan, X.Y., Luxenberg, D.P., Karim, R., Dunussi-Joannopoulos, K., Collins, M., and Fouser, L.A. (2006). Interleukin (IL)-22 and IL-17 are coexpressed by Th17 cells and cooperatively enhance expression of antimicrobial peptides. J Exp Med *203*, 2271-2279. 10.1084/jem.20061308.
Liao, M., Liu, Y., Yuan, J., Wen, Y., Xu, G., Zhao, J., Cheng, L., Li, J., Wang, X., Wang, F., et al. (2020). Single-cell landscape of bronchoalveolar immune cells in patients with COVID-19. Nat Med *26*, 842-844. 10.1038/s41591-020-0901-9.
Lindqvist, M., van Lunzen, J., Soghoian, D.Z., Kuhl, B.D., Ranasinghe, S., Kranias, G., Flanders, M.D., Cutler, S., Yudanin, N., Muller, M.I., et al. (2012). Expansion of HIV-specific T follicular helper cells in chronic HIV infection. J Clin Invest *122*, 3271-3280. 10.1172/JCI64314.
Linsley, P.S., Greene, J.L., Brady, W., Bajorath, J., Ledbetter, J.A., and Peach, R. (1994). Human B7-1 (CD80) and B7-2 (CD86) bind with similar avidities but distinct kinetics to CD28 and CTLA-4 receptors. Immunity *1*, 793-801. 10.1016/s1074-7613(94)80021-9.
Lippi, G., and Plebani, M. (2020). Laboratory abnormalities in patients with COVID-2019 infection. Clin Chem Lab Med *58*, 1131-1134. 10.1515/cclm-2020-0198.

Litjens, N.H., Huisman, M., van den Dorpel, M., and Betjes, M.G. (2008). Impaired immune responses and antigen-specific memory CD4+ T cells in hemodialysis patients. J Am Soc Nephrol *19*, 1483-1490. 10.1681/ASN.2007090971.
Liu, F., Han, K., Blair, R., Kenst, K., Qin, Z., Upcin, B., Worsdorfer, P., Midkiff, C.C., Mudd, J., Belyaeva, E., et al. (2021). SARS-CoV-2 Infects Endothelial Cells In Vivo and In Vitro. Front Cell Infect Microbiol *11*, 701278. 10.3389/fcimb.2021.701278.
Liu, L., Wei, Q., Alvarez, X., Wang, H., Du, Y., Zhu, H., Jiang, H., Zhou, J., Lam, P., Zhang, L., et al. (2011). Epithelial cells lining salivary gland ducts are early target cells of severe acute respiratory syndrome coronavirus infection in the upper respiratory tracts of rhesus macaques. J Virol *85*, 4025-4030. 10.1128/JVI.02292-10.
Long, Q.X., Liu, B.Z., Deng, H.J., Wu, G.C., Deng, K., Chen, Y.K., Liao, P., Qiu, J.F., Lin, Y., Cai, X.F., et al. (2020). Antibody responses to SARS-CoV-2 in patients with COVID-19. Nat Med *26*, 845-848. 10.1038/s41591-020-0897-1.
Lucas, C., Klein, J., Sundaram, M.E., Liu, F., Wong, P., Silva, J., Mao, T., Oh, J.E., Mohanty, S., Huang, J., et al. (2021). Delayed production of neutralizing antibodies correlates with fatal COVID-19. Nat Med *27*, 1178-1186. 10.1038/s41591-021-01355-0.
Lucas, C., Wong, P., Klein, J., Castro, T.B.R., Silva, J., Sundaram, M., Ellingson, M.K., Mao, T., Oh, J.E., Israelow, B., et al. (2020). Longitudinal analyses reveal immunological misfiring in severe COVID-19. Nature *584*, 463-469. 10.1038/s41586-020-2588-y.
Ma, A., Cheng, J., Yang, J., Dong, M., Liao, X., and Kang, Y. (2020). Neutrophil-to-lymphocyte ratio as a predictive biomarker for moderate-severe ARDS in severe COVID-19 patients. Crit Care *24*, 288. 10.1186/s13054-020-03007-0.
Ma, Y.J., Doni, A., Skjoedt, M.O., Honore, C., Arendrup, M., Mantovani, A., and Garred, P. (2011). Heterocomplexes of mannose-binding lectin and the pentraxins PTX3 or serum amyloid P component trigger cross-activation of the complement system. J Biol Chem *286*, 3405-3417. 10.1074/jbc.M110.190637.
MacLennan, I.C., Toellner, K.M., Cunningham, A.F., Serre, K., Sze, D.M., Zuniga, E., Cook, M.C., and Vinuesa, C.G. (2003). Extrafollicular antibody responses. Immunol Rev *194*, 8-18. 10.1034/j.1600-065x.2003.00058.x.
Maehara, T., Mattoo, H., Mahajan, V.S., Murphy, S.J., Yuen, G.J., Ishiguro, N., Ohta, M., Moriyama, M., Saeki, T., Yamamoto, H., et al. (2018). The expansion in lymphoid organs of IL-4(+) BATF(+) T follicular helper cells is linked to IgG4 class switching in vivo. Life Sci Alliance *1*. 10.26508/lsa.201800050.
Mantlo, E., Bukreyeva, N., Maruyama, J., Paessler, S., and Huang, C. (2020). Antiviral activities of type I interferons to SARS-CoV-2 infection. Antiviral Res *179*, 104811. 10.1016/j.antiviral.2020.104811.
Marconi, V.C., Ramanan, A.V., de Bono, S., Kartman, C.E., Krishnan, V., Liao, R., Piruzeli, M.L.B., Goldman, J.D., Alatorre-Alexander, J., de Cassia Pellegrini, R., et al. (2021). Efficacy and safety of baricitinib for the treatment of hospitalised adults with COVID-19 (COV-BARRIER): a randomised, double-blind, parallel-group, placebo-controlled phase 3 trial. Lancet Respir Med *9*, 1407-1418. 10.1016/S2213-2600(21)00331-3.
Marin-Acevedo, J.A., Chirila, R.M., and Dronca, R.S. (2019). Immune Checkpoint Inhibitor Toxicities. Mayo Clin Proc *94*, 1321-1329. 10.1016/j.mayocp.2019.03.012.
Martinez, F.O., Helming, L., and Gordon, S. (2009). Alternative activation of macrophages: an

immunologic functional perspective. Annu Rev Immunol *27*, 451-483. 10.1146/annurev.immunol.021908.132532.
Martinez, G.J., Pereira, R.M., Aijo, T., Kim, E.Y., Marangoni, F., Pipkin, M.E., Togher, S., Heissmeyer, V., Zhang, Y.C., Crotty, S., et al. (2015). The transcription factor NFAT promotes exhaustion of activated CD8(+) T cells. Immunity *42*, 265-278. 10.1016/j.immuni.2015.01.006.
Martinez-Picado, J., and Deeks, S.G. (2016). Persistent HIV-1 replication during antiretroviral therapy. Curr Opin HIV AIDS *11*, 417-423. 10.1097/COH.0000000000000287.
Masopust, D., and Schenkel, J.M. (2013). The integration of T cell migration, differentiation and function. Nat Rev Immunol *13*, 309-320. 10.1038/nri3442.
Matano, T., Shibata, R., Siemon, C., Connors, M., Lane, H.C., and Martin, M.A. (1998). Administration of an anti-CD8 monoclonal antibody interferes with the clearance of chimeric simian/human immunodeficiency virus during primary infections of rhesus macaques. J Virol *72*, 164-169. 10.1128/JVI.72.1.164-169.1998.
Mathew, D., Giles, J.R., Baxter, A.E., Oldridge, D.A., Greenplate, A.R., Wu, J.E., Alanio, C., Kuri-Cervantes, L., Pampena, M.B., D'Andrea, K., et al. (2020). Deep immune profiling of COVID-19 patients reveals distinct immunotypes with therapeutic implications. Science *369*. 10.1126/science.abc8511.
Matloubian, M., Concepcion, R.J., and Ahmed, R. (1994). CD4+ T cells are required to sustain CD8+ cytotoxic T-cell responses during chronic viral infection. J Virol *68*, 8056-8063. 10.1128/JVI.68.12.8056-8063.1994.
McNab, F., Mayer-Barber, K., Sher, A., Wack, A., and O'Garra, A. (2015). Type I interferons in infectious disease. Nat Rev Immunol *15*, 87-103. 10.1038/nri3787.
McVay, L.D., and Carding, S.R. (1996). Extrathymic origin of human gamma delta T cells during fetal development. J Immunol *157*, 2873-2882.
Meckiff, B.J., Ramirez-Suastegui, C., Fajardo, V., Chee, S.J., Kusnadi, A., Simon, H., Eschweiler, S., Grifoni, A., Pelosi, E., Weiskopf, D., et al. (2020a). Imbalance of Regulatory and Cytotoxic SARS-CoV-2-Reactive CD4(+) T Cells in COVID-19. Cell *183*, 1340-1353 e1316. 10.1016/j.cell.2020.10.001.
Meckiff, B.J., Ramirez-Suastegui, C., Fajardo, V., Chee, S.J., Kusnadi, A., Simon, H., Grifoni, A., Pelosi, E., Weiskopf, D., Sette, A., et al. (2020b). Single-Cell Transcriptomic Analysis of SARS-CoV-2 Reactive CD4 (+) T Cells. SSRN, 3641939. 10.2139/ssrn.3641939.
Meng, F., Siu, G.K., Mok, B.W., Sun, J., Fung, K.S.C., Lam, J.Y., Wong, N.K., Gedefaw, L., Luo, S., Lee, T.M.H., et al. (2021). Viral MicroRNAs Encoded by Nucleocapsid Gene of SARS-CoV-2 Are Detected during Infection, and Targeting Metabolic Pathways in Host Cells. Cells *10*. 10.3390/cells10071762.
Messner, C.B., Demichev, V., Wendisch, D., Michalick, L., White, M., Freiwald, A., Textoris-Taube, K., Vernardis, S.I., Egger, A.S., Kreidl, M., et al. (2020). Ultra-High-Throughput Clinical Proteomics Reveals Classifiers of COVID-19 Infection. Cell Syst *11*, 11-24 e14. 10.1016/j.cels.2020.05.012.
Mestas, J., and Hughes, C.C. (2004). Of mice and not men: differences between mouse and human immunology. J Immunol *172*, 2731-2738. 10.4049/jimmunol.172.5.2731.
Metzemaekers, M., Cambier, S., Blanter, M., Vandooren, J., de Carvalho, A.C., Malengier-Devlies, B., Vanderbeke, L., Jacobs, C., Coenen, S., Martens, E., et al. (2021). Kinetics of peripheral blood neutrophils in severe coronavirus disease 2019. Clin Transl Immunology *10*,

e1271. 10.1002/cti2.1271.
Michot, J.M., Bigenwald, C., Champiat, S., Collins, M., Carbonnel, F., Postel-Vinay, S., Berdelou, A., Varga, A., Bahleda, R., Hollebecque, A., et al. (2016). Immune-related adverse events with immune checkpoint blockade: a comprehensive review. Eur J Cancer *54*, 139-148. 10.1016/j.ejca.2015.11.016.
Miura, T., Brockman, M.A., Schneidewind, A., Lobritz, M., Pereyra, F., Rathod, A., Block, B.L., Brumme, Z.L., Brumme, C.J., Baker, B., et al. (2009). HLA-B57/B*5801 human immunodeficiency virus type 1 elite controllers select for rare gag variants associated with reduced viral replication capacity and strong cytotoxic T-lymphocyte [corrected] recognition. J Virol *83*, 2743-2755. 10.1128/JVI.02265-08.
Montero-Escribano, P., Matias-Guiu, J., Gomez-Iglesias, P., Porta-Etessam, J., Pytel, V., and Matias-Guiu, J.A. (2020). Anti-CD20 and COVID-19 in multiple sclerosis and related disorders: A case series of 60 patients from Madrid, Spain. Mult Scler Relat Disord *42*, 102185. 10.1016/j.msard.2020.102185.
Moon, K.R., van Dijk, D., Wang, Z., Gigante, S., Burkhardt, D.B., Chen, W.S., Yim, K., Elzen, A.V.D., Hirn, M.J., Coifman, R.R., et al. (2019). Visualizing structure and transitions in high-dimensional biological data. Nat Biotechnol *37*, 1482-1492. 10.1038/s41587-019-0336-3.
Morou, A., Brunet-Ratnasingham, E., Dube, M., Charlebois, R., Mercier, E., Darko, S., Brassard, N., Nganou-Makamdop, K., Arumugam, S., Gendron-Lepage, G., et al. (2019). Altered differentiation is central to HIV-specific CD4(+) T cell dysfunction in progressive disease. Nat Immunol *20*, 1059-1070. 10.1038/s41590-019-0418-x.
Mosser, D.M., and Edwards, J.P. (2008). Exploring the full spectrum of macrophage activation. Nat Rev Immunol *8*, 958-969. 10.1038/nri2448.
Mueller, S.N., Matloubian, M., Clemens, D.M., Sharpe, A.H., Freeman, G.J., Gangappa, S., Larsen, C.P., and Ahmed, R. (2007). Viral targeting of fibroblastic reticular cells contributes to immunosuppression and persistence during chronic infection. Proc Natl Acad Sci U S A *104*, 15430-15435. 10.1073/pnas.0702579104.
Murray, S.M., Zhang, Y., Douek, D.C., and Sekaly, R.P. (2020). Myeloid Cells Enriched for a Dendritic Cell Population From People Living With HIV Have Altered Gene Expression Not Restored by Antiretroviral Therapy. Front Immunol *11*, 261. 10.3389/fimmu.2020.00261.
Mylvaganam, G.H., Chea, L.S., Tharp, G.K., Hicks, S., Velu, V., Iyer, S.S., Deleage, C., Estes, J.D., Bosinger, S.E., Freeman, G.J., et al. (2018). Combination anti-PD-1 and antiretroviral therapy provides therapeutic benefit against SIV. JCI Insight *3*. 10.1172/jci.insight.122940.
Nakanishi, Y., Lu, B., Gerard, C., and Iwasaki, A. (2009). CD8(+) T lymphocyte mobilization to virus-infected tissue requires CD4(+) T-cell help. Nature *462*, 510-513. 10.1038/nature08511.
Navarrete-Munoz, M.A., Restrepo, C., Benito, J.M., and Rallon, N. (2020). Elite controllers: A heterogeneous group of HIV-infected patients. Virulence *11*, 889-897. 10.1080/21505594.2020.1788887.
Nayak, A., Dodagatta-Marri, E., Tsolaki, A.G., and Kishore, U. (2012). An Insight into the Diverse Roles of Surfactant Proteins, SP-A and SP-D in Innate and Adaptive Immunity. Front Immunol *3*, 131. 10.3389/fimmu.2012.00131.
Nepom, G.T. (2012). MHC class II tetramers. J Immunol *188*, 2477-2482. 10.4049/jimmunol.1102398.
Nicholas, K.J., Zern, E.K., Barnett, L., Smith, R.M., Lorey, S.L., Copeland, C.A., Sadagopal, S., and

Kalams, S.A. (2013). B cell responses to HIV antigen are a potent correlate of viremia in HIV-1 infection and improve with PD-1 blockade. PLoS One *8*, e84185. 10.1371/journal.pone.0084185.
Niessl, J., Baxter, A.E., Mendoza, P., Jankovic, M., Cohen, Y.Z., Butler, A.L., Lu, C.L., Dube, M., Shimeliovich, I., Gruell, H., et al. (2020a). Combination anti-HIV-1 antibody therapy is associated with increased virus-specific T cell immunity. Nat Med *26*, 222-227. 10.1038/s41591-019-0747-1.
Niessl, J., Baxter, A.E., Morou, A., Brunet-Ratnasingham, E., Sannier, G., Gendron-Lepage, G., Richard, J., Delgado, G.G., Brassard, N., Turcotte, I., et al. (2020b). Persistent expansion and Th1-like skewing of HIV-specific circulating T follicular helper cells during antiretroviral therapy. EBioMedicine *54*, 102727. 10.1016/j.ebiom.2020.102727.
Nishijima, T.F., Shachar, S.S., Nyrop, K.A., and Muss, H.B. (2017). Safety and Tolerability of PD-1/PD-L1 Inhibitors Compared with Chemotherapy in Patients with Advanced Cancer: A Meta-Analysis. Oncologist *22*, 470-479. 10.1634/theoncologist.2016-0419.
Nishimura, H., Nose, M., Hiai, H., Minato, N., and Honjo, T. (1999). Development of lupus-like autoimmune diseases by disruption of the PD-1 gene encoding an ITIM motif-carrying immunoreceptor. Immunity *11*, 141-151. 10.1016/s1074-7613(00)80089-8.
Obi, A.T., Pannucci, C.J., Nackashi, A., Abdullah, N., Alvarez, R., Bahl, V., Wakefield, T.W., and Henke, P.K. (2015). Validation of the Caprini Venous Thromboembolism Risk Assessment Model in Critically Ill Surgical Patients. JAMA Surg *150*, 941-948. 10.1001/jamasurg.2015.1841.
Odorizzi, P.M., and Wherry, E.J. (2012). Inhibitory receptors on lymphocytes: insights from infections. J Immunol *188*, 2957-2965. 10.4049/jimmunol.1100038.
Okazaki, T., Maeda, A., Nishimura, H., Kurosaki, T., and Honjo, T. (2001). PD-1 immunoreceptor inhibits B cell receptor-mediated signaling by recruiting src homology 2-domain-containing tyrosine phosphatase 2 to phosphotyrosine. Proc Natl Acad Sci U S A *98*, 13866-13871. 10.1073/pnas.231486598.
Okoye, A.A., and Picker, L.J. (2013). CD4(+) T-cell depletion in HIV infection: mechanisms of immunological failure. Immunol Rev *254*, 54-64. 10.1111/imr.12066.
Okulicz, J.F., Boufassa, F., Costagliola, D., Ganesan, A., and Lambotte, O. (2016). Cancers in elite controllers: appropriate follow-up is essential. AIDS *30*, 1852-1855. 10.1097/QAD.0000000000001154.
Ortiz, A.M., Klatt, N.R., Li, B., Yi, Y., Tabb, B., Hao, X.P., Sternberg, L., Lawson, B., Carnathan, P.M., Cramer, E.M., et al. (2011). Depletion of CD4(+) T cells abrogates post-peak decline of viremia in SIV-infected rhesus macaques. J Clin Invest *121*, 4433-4445. 10.1172/JCI46023.
Osokine, I., Snell, L.M., Cunningham, C.R., Yamada, D.H., Wilson, E.B., Elsaesser, H.J., de la Torre, J.C., and Brooks, D. (2014). Type I interferon suppresses de novo virus-specific CD4 Th1 immunity during an established persistent viral infection. Proc Natl Acad Sci U S A *111*, 7409-7414. 10.1073/pnas.1401662111.
Osuchowski, M.F., Winkler, M.S., Skirecki, T., Cajander, S., Shankar-Hari, M., Lachmann, G., Monneret, G., Venet, F., Bauer, M., Brunkhorst, F.M., et al. (2021). The COVID-19 puzzle: deciphering pathophysiology and phenotypes of a new disease entity. Lancet Respir Med *9*, 622-642. 10.1016/S2213-2600(21)00218-6.
Ou, J., Lan, W., Wu, X., Zhao, T., Duan, B., Yang, P., Ren, Y., Quan, L., Zhao, W., Seto, D., et al. (2022). Tracking SARS-CoV-2 Omicron diverse spike gene mutations identifies multiple inter-variant recombination events. Signal Transduct Target Ther *7*, 138. 10.1038/s41392-022-00992-

2.
Oxenius, A., Bachmann, M.F., Zinkernagel, R.M., and Hengartner, H. (1998). Virus-specific MHC-class II-restricted TCR-transgenic mice: effects on humoral and cellular immune responses after viral infection. Eur J Immunol *28*, 390-400. 10.1002/(SICI)1521-4141(199801)28:01<390::AID-IMMU390>3.0.CO;2-O.
Paley, M.A., Kroy, D.C., Odorizzi, P.M., Johnnidis, J.B., Dolfi, D.V., Barnett, B.E., Bikoff, E.K., Robertson, E.J., Lauer, G.M., Reiner, S.L., and Wherry, E.J. (2012). Progenitor and terminal subsets of CD8+ T cells cooperate to contain chronic viral infection. Science *338*, 1220-1225. 10.1126/science.1229620.
Pan, Y., Zhang, D., Yang, P., Poon, L.L.M., and Wang, Q. (2020). Viral load of SARS-CoV-2 in clinical samples. Lancet Infect Dis *20*, 411-412. 10.1016/S1473-3099(20)30113-4.
Patsoukis, N., Bardhan, K., Chatterjee, P., Sari, D., Liu, B., Bell, L.N., Karoly, E.D., Freeman, G.J., Petkova, V., Seth, P., et al. (2015). PD-1 alters T-cell metabolic reprogramming by inhibiting glycolysis and promoting lipolysis and fatty acid oxidation. Nat Commun *6*, 6692. 10.1038/ncomms7692.
Pauken, K.E., Sammons, M.A., Odorizzi, P.M., Manne, S., Godec, J., Khan, O., Drake, A.M., Chen, Z., Sen, D.R., Kurachi, M., et al. (2016). Epigenetic stability of exhausted T cells limits durability of reinvigoration by PD-1 blockade. Science *354*, 1160-1165. 10.1126/science.aaf2807.
Peiffer-Smadja, N., Bridier-Nahmias, A., Ferre, V.M., Charpentier, C., Gare, M., Rioux, C., Allemand, A., Lavallee, P., Ghosn, J., Kramer, L., et al. (2021). Emergence of E484K Mutation Following Bamlanivimab Monotherapy among High-Risk Patients Infected with the Alpha Variant of SARS-CoV-2. Viruses *13*. 10.3390/v13081642.
Penaloza-MacMaster, P., Barber, D.L., Wherry, E.J., Provine, N.M., Teigler, J.E., Parenteau, L., Blackmore, S., Borducchi, E.N., Larocca, R.A., Yates, K.B., et al. (2015). Vaccine-elicited CD4 T cells induce immunopathology after chronic LCMV infection. Science *347*, 278-282. 10.1126/science.aaa2148.
Pentcheva-Hoang, T., Egen, J.G., Wojnoonski, K., and Allison, J.P. (2004). B7-1 and B7-2 selectively recruit CTLA-4 and CD28 to the immunological synapse. Immunity *21*, 401-413. 10.1016/j.immuni.2004.06.017.
Pereyra, F., Addo, M.M., Kaufmann, D.E., Liu, Y., Miura, T., Rathod, A., Baker, B., Trocha, A., Rosenberg, R., Mackey, E., et al. (2008). Genetic and immunologic heterogeneity among persons who control HIV infection in the absence of therapy. J Infect Dis *197*, 563-571. 10.1086/526786.
Pereyra, F., Lo, J., Triant, V.A., Wei, J., Buzon, M.J., Fitch, K.V., Hwang, J., Campbell, J.H., Burdo, T.H., Williams, K.C., et al. (2012). Increased coronary atherosclerosis and immune activation in HIV-1 elite controllers. AIDS *26*, 2409-2412. 10.1097/QAD.0b013e32835a9950.
Perez-Zsolt, D., Cantero-Perez, J., Erkizia, I., Benet, S., Pino, M., Serra-Peinado, C., Hernandez-Gallego, A., Castellvi, J., Tapia, G., Arnau-Saz, V., et al. (2019). Dendritic Cells From the Cervical Mucosa Capture and Transfer HIV-1 via Siglec-1. Front Immunol *10*, 825. 10.3389/fimmu.2019.00825.
Pernas, M., Tarancon-Diez, L., Rodriguez-Gallego, E., Gomez, J., Prado, J.G., Casado, C., Dominguez-Molina, B., Olivares, I., Coiras, M., Leon, A., et al. (2018). Factors Leading to the Loss of Natural Elite Control of HIV-1 Infection. J Virol *92*. 10.1128/JVI.01805-17.
Perreau, M., Savoye, A.L., De Crignis, E., Corpataux, J.M., Cubas, R., Haddad, E.K., De Leval, L., Graziosi, C., and Pantaleo, G. (2013). Follicular helper T cells serve as the major CD4 T cell

compartment for HIV-1 infection, replication, and production. J Exp Med *210*, 143-156. 10.1084/jem.20121932.
Perreau, M., Vigano, S., Bellanger, F., Pellaton, C., Buss, G., Comte, D., Roger, T., Lacabaratz, C., Bart, P.A., Levy, Y., and Pantaleo, G. (2014). Exhaustion of bacteria-specific CD4 T cells and microbial translocation in common variable immunodeficiency disorders. J Exp Med *211*, 2033-2045. 10.1084/jem.20140039.
Pirmez, C., Yamamura, M., Uyemura, K., Paes-Oliveira, M., Conceicao-Silva, F., and Modlin, R.L. (1993). Cytokine patterns in the pathogenesis of human leishmaniasis. J Clin Invest *91*, 1390-1395. 10.1172/JCI116341.
Platanias, L.C. (2005). Mechanisms of type-I- and type-II-interferon-mediated signalling. Nat Rev Immunol *5*, 375-386. 10.1038/nri1604.
Poles, M.A., Elliott, J., Taing, P., Anton, P.A., and Chen, I.S. (2001). A preponderance of CCR5(+) CXCR4(+) mononuclear cells enhances gastrointestinal mucosal susceptibility to human immunodeficiency virus type 1 infection. J Virol *75*, 8390-8399. 10.1128/jvi.75.18.8390-8399.2001.
Porichis, F., Hart, M.G., Massa, A., Everett, H.L., Morou, A., Richard, J., Brassard, N., Veillette, M., Hassan, M., Ly, N.L., et al. (2018). Immune Checkpoint Blockade Restores HIV-Specific CD4 T Cell Help for NK Cells. J Immunol *201*, 971-981. 10.4049/jimmunol.1701551.
Porichis, F., Kwon, D.S., Zupkosky, J., Tighe, D.P., McMullen, A., Brockman, M.A., Pavlik, D.F., Rodriguez-Garcia, M., Pereyra, F., Freeman, G.J., et al. (2011). Responsiveness of HIV-specific CD4 T cells to PD-1 blockade. Blood *118*, 965-974. 10.1182/blood-2010-12-328070.
Poropatich, K., and Sullivan, D.J., Jr. (2011). Human immunodeficiency virus type 1 long-term non-progressors: the viral, genetic and immunological basis for disease non-progression. J Gen Virol *92*, 247-268. 10.1099/vir.0.027102-0.
Prasad, V., Kaestner, V., and Mailankody, S. (2018). Cancer Drugs Approved Based on Biomarkers and Not Tumor Type-FDA Approval of Pembrolizumab for Mismatch Repair-Deficient Solid Cancers. JAMA Oncol *4*, 157-158. 10.1001/jamaoncol.2017.4182.
Prebensen, C., Hre, P.L.M., Jonassen, C., Rangberg, A., Blomfeldt, A., Svensson, M., Omland, T., and Berdal, J.E. (2020). SARS-CoV-2 RNA in plasma is associated with ICU admission and mortality in patients hospitalized with COVID-19. Clin Infect Dis. 10.1093/cid/ciaa1338.
Presicce, P., Orsborn, K., King, E., Pratt, J., Fichtenbaum, C.J., and Chougnet, C.A. (2011). Frequency of circulating regulatory T cells increases during chronic HIV infection and is largely controlled by highly active antiretroviral therapy. PLoS One *6*, e28118. 10.1371/journal.pone.0028118.
Prevost, J., Gasser, R., Beaudoin-Bussieres, G., Richard, J., Duerr, R., Laumaea, A., Anand, S.P., Goyette, G., Benlarbi, M., Ding, S., et al. (2020). Cross-Sectional Evaluation of Humoral Responses against SARS-CoV-2 Spike. Cell Rep Med *1*, 100126. 10.1016/j.xcrm.2020.100126.
Prlic, M., and Bevan, M.J. (2008). Exploring regulatory mechanisms of CD8+ T cell contraction. Proc Natl Acad Sci U S A *105*, 16689-16694. 10.1073/pnas.0808997105.
Quigley, M., Pereyra, F., Nilsson, B., Porichis, F., Fonseca, C., Eichbaum, Q., Julg, B., Jesneck, J.L., Brosnahan, K., Imam, S., et al. (2010). Transcriptional analysis of HIV-specific CD8+ T cells shows that PD-1 inhibits T cell function by upregulating BATF. Nat Med *16*, 1147-1151. 10.1038/nm.2232.
Quinti, I., Lougaris, V., Milito, C., Cinetto, F., Pecoraro, A., Mezzaroma, I., Mastroianni, C.M.,

Turriziani, O., Bondioni, M.P., Filippini, M., et al. (2020). A possible role for B cells in COVID-19? Lesson from patients with agammaglobulinemia. J Allergy Clin Immunol *146*, 211-213 e214. 10.1016/j.jaci.2020.04.013.
Qureshi, O.S., Zheng, Y., Nakamura, K., Attridge, K., Manzotti, C., Schmidt, E.M., Baker, J., Jeffery, L.E., Kaur, S., Briggs, Z., et al. (2011). Trans-endocytosis of CD80 and CD86: a molecular basis for the cell-extrinsic function of CTLA-4. Science *332*, 600-603. 10.1126/science.1202947.
Radziewicz, H., Ibegbu, C.C., Fernandez, M.L., Workowski, K.A., Obideen, K., Wehbi, M., Hanson, H.L., Steinberg, J.P., Masopust, D., Wherry, E.J., et al. (2007). Liver-infiltrating lymphocytes in chronic human hepatitis C virus infection display an exhausted phenotype with high levels of PD-1 and low levels of CD127 expression. J Virol *81*, 2545-2553. 10.1128/JVI.02021-06.
Ranasinghe, S., Cutler, S., Davis, I., Lu, R., Soghoian, D.Z., Qi, Y., Sidney, J., Kranias, G., Flanders, M.D., Lindqvist, M., et al. (2013). Association of HLA-DRB1-restricted CD4(+) T cell responses with HIV immune control. Nat Med *19*, 930-933. 10.1038/nm.3229.
Reiss, S., Baxter, A.E., Cirelli, K.M., Dan, J.M., Morou, A., Daigneault, A., Brassard, N., Silvestri, G., Routy, J.P., Havenar-Daughton, C., et al. (2017). Comparative analysis of activation induced marker (AIM) assays for sensitive identification of antigen-specific CD4 T cells. PLoS One *12*, e0186998. 10.1371/journal.pone.0186998.
Rhodes, J.W., Tong, O., Harman, A.N., and Turville, S.G. (2019). Human Dendritic Cell Subsets, Ontogeny, and Impact on HIV Infection. Front Immunol *10*, 1088. 10.3389/fimmu.2019.01088.
Robert, C., Schachter, J., Long, G.V., Arance, A., Grob, J.J., Mortier, L., Daud, A., Carlino, M.S., McNeil, C., Lotem, M., et al. (2015). Pembrolizumab versus Ipilimumab in Advanced Melanoma. N Engl J Med *372*, 2521-2532. 10.1056/NEJMoa1503093.
Rodger, A.J., Lodwick, R., Schechter, M., Deeks, S., Amin, J., Gilson, R., Paredes, R., Bakowska, E., Engsig, F.N., Phillips, A., and Insight Smart, E.S.G. (2013). Mortality in well controlled HIV in the continuous antiretroviral therapy arms of the SMART and ESPRIT trials compared with the general population. AIDS *27*, 973-979. 10.1097/QAD.0b013e32835cae9c.
Rosas-Umbert, M., Llano, A., Bellido, R., Olvera, A., Ruiz-Riol, M., Rocafort, M., Fernandez, M.A., Cobarsi, P., Crespo, M., Dorrell, L., et al. (2019). Mechanisms of Abrupt Loss of Virus Control in a Cohort of Previous HIV Controllers. J Virol *93*. 10.1128/JVI.01436-18.
Routy, B., Le Chatelier, E., Derosa, L., Duong, C.P.M., Alou, M.T., Daillere, R., Fluckiger, A., Messaoudene, M., Rauber, C., Roberti, M.P., et al. (2018). Gut microbiome influences efficacy of PD-1-based immunotherapy against epithelial tumors. Science *359*, 91-97. 10.1126/science.aan3706.
Ryan, E.S., Micci, L., Fromentin, R., Paganini, S., McGary, C.S., Easley, K., Chomont, N., and Paiardini, M. (2016). Loss of Function of Intestinal IL-17 and IL-22 Producing Cells Contributes to Inflammation and Viral Persistence in SIV-Infected Rhesus Macaques. PLoS Pathog *12*, e1005412. 10.1371/journal.ppat.1005412.
Rydyznski Moderbacher, C., Ramirez, S.I., Dan, J.M., Grifoni, A., Hastie, K.M., Weiskopf, D., Belanger, S., Abbott, R.K., Kim, C., Choi, J., et al. (2020). Antigen-Specific Adaptive Immunity to SARS-CoV-2 in Acute COVID-19 and Associations with Age and Disease Severity. Cell *183*, 996-1012 e1019. 10.1016/j.cell.2020.09.038.
Sadegh Beigee, F., Pourabdollah Toutkaboni, M., Khalili, N., Nadji, S.A., Dorudinia, A., Rezaei, M., Askari, E., Farzanegan, B., Marjani, M., and Rafiezadeh, A. (2020). Diffuse alveolar damage and thrombotic microangiopathy are the main histopathological findings in lung tissue biopsy

samples of COVID-19 patients. Pathol Res Pract *216*, 153228. 10.1016/j.prp.2020.153228.
Sallusto, F. (2016). Heterogeneity of Human CD4(+) T Cells Against Microbes. Annu Rev Immunol *34*, 317-334. 10.1146/annurev-immunol-032414-112056.
Sallusto, F., Lenig, D., Forster, R., Lipp, M., and Lanzavecchia, A. (1999). Two subsets of memory T lymphocytes with distinct homing potentials and effector functions. Nature *401*, 708-712. 10.1038/44385.
Sanchez, G.A.M., Reinhardt, A., Ramsey, S., Wittkowski, H., Hashkes, P.J., Berkun, Y., Schalm, S., Murias, S., Dare, J.A., Brown, D., et al. (2018). JAK1/2 inhibition with baricitinib in the treatment of autoinflammatory interferonopathies. J Clin Invest *128*, 3041-3052. 10.1172/JCI98814.
Sandu, I., Cerletti, D., Claassen, M., and Oxenius, A. (2020). Exhausted CD8(+) T cells exhibit low and strongly inhibited TCR signaling during chronic LCMV infection. Nat Commun *11*, 4454. 10.1038/s41467-020-18256-4.
Satpathy, A.T., Granja, J.M., Yost, K.E., Qi, Y., Meschi, F., McDermott, G.P., Olsen, B.N., Mumbach, M.R., Pierce, S.E., Corces, M.R., et al. (2019). Massively parallel single-cell chromatin landscapes of human immune cell development and intratumoral T cell exhaustion. Nat Biotechnol *37*, 925-936. 10.1038/s41587-019-0206-z.
Satpathy, A.T., Kc, W., Albring, J.C., Edelson, B.T., Kretzer, N.M., Bhattacharya, D., Murphy, T.L., and Murphy, K.M. (2012). Zbtb46 expression distinguishes classical dendritic cells and their committed progenitors from other immune lineages. J Exp Med *209*, 1135-1152. 10.1084/jem.20120030.
Schachter, J., Ribas, A., Long, G.V., Arance, A., Grob, J.J., Mortier, L., Daud, A., Carlino, M.S., McNeil, C., Lotem, M., et al. (2017). Pembrolizumab versus ipilimumab for advanced melanoma: final overall survival results of a multicentre, randomised, open-label phase 3 study (KEYNOTE-006). Lancet *390*, 1853-1862. 10.1016/S0140-6736(17)31601-X.
Schacker, T.W., Brenchley, J.M., Beilman, G.J., Reilly, C., Pambuccian, S.E., Taylor, J., Skarda, D., Larson, M., Douek, D.C., and Haase, A.T. (2006). Lymphatic tissue fibrosis is associated with reduced numbers of naive CD4+ T cells in human immunodeficiency virus type 1 infection. Clin Vaccine Immunol *13*, 556-560. 10.1128/CVI.13.5.556-560.2006.
Schadendorf, D., Hodi, F.S., Robert, C., Weber, J.S., Margolin, K., Hamid, O., Patt, D., Chen, T.T., Berman, D.M., and Wolchok, J.D. (2015). Pooled Analysis of Long-Term Survival Data From Phase II and Phase III Trials of Ipilimumab in Unresectable or Metastatic Melanoma. J Clin Oncol *33*, 1889-1894. 10.1200/JCO.2014.56.2736.
Schaefer, I.M., Padera, R.F., Solomon, I.H., Kanjilal, S., Hammer, M.M., Hornick, J.L., and Sholl, L.M. (2020). In situ detection of SARS-CoV-2 in lungs and airways of patients with COVID-19. Mod Pathol *33*, 2104-2114. 10.1038/s41379-020-0595-z.
Schmidt, T., and Sester, M. (2013). Detection of antigen-specific T cells based on intracellular cytokine staining using flow-cytometry. Methods Mol Biol *1064*, 267-274. 10.1007/978-1-62703-601-6_19.
Schroeder, H.W., Jr., and Cavacini, L. (2010). Structure and function of immunoglobulins. J Allergy Clin Immunol *125*, S41-52. 10.1016/j.jaci.2009.09.046.
Schulien, I., Kemming, J., Oberhardt, V., Wild, K., Seidel, L.M., Killmer, S., Sagar, Daul, F., Salvat Lago, M., Decker, A., et al. (2021). Characterization of pre-existing and induced SARS-CoV-2-specific CD8(+) T cells. Nat Med *27*, 78-85. 10.1038/s41591-020-01143-2.
Scully, E.P., Rutishauser, R.L., Simoneau, C.R., Delagreverie, H., Euler, Z., Thanh, C., Li, J.Z.,

Hartig, H., Bakkour, S., Busch, M., et al. (2018). Inconsistent HIV reservoir dynamics and immune responses following anti-PD-1 therapy in cancer patients with HIV infection. Ann Oncol *29*, 2141-2142. 10.1093/annonc/mdy259.
Seki, S., and Matano, T. (2011). CTL Escape and Viral Fitness in HIV/SIV Infection. Front Microbiol *2*, 267. 10.3389/fmicb.2011.00267.
Sekine, T., Perez-Potti, A., Nguyen, S., Gorin, J.B., Wu, V.H., Gostick, E., Llewellyn-Lacey, S., Hammer, Q., Falck-Jones, S., Vangeti, S., et al. (2020). TOX is expressed by exhausted and polyfunctional human effector memory CD8(+) T cells. Sci Immunol *5*. 10.1126/sciimmunol.aba7918.
Sen, D.R., Kaminski, J., Barnitz, R.A., Kurachi, M., Gerdemann, U., Yates, K.B., Tsao, H.W., Godec, J., LaFleur, M.W., Brown, F.D., et al. (2016). The epigenetic landscape of T cell exhaustion. Science *354*, 1165-1169. 10.1126/science.aae0491.
Senejani, A.G., Dalal, S., Liu, Y., Nottoli, T.P., McGrath, J.M., Clairmont, C.S., and Sweasy, J.B. (2012). Y265C DNA polymerase beta knockin mice survive past birth and accumulate base excision repair intermediate substrates. Proc Natl Acad Sci U S A *109*, 6632-6637. 10.1073/pnas.1200800109.
Sereti, I., Sheikh, V., Shaffer, D., Phanuphak, N., Gabriel, E., Wang, J., Nason, M.C., Roby, G., Ngeno, H., Kirui, F., et al. (2020). Prospective International Study of Incidence and Predictors of Immune Reconstitution Inflammatory Syndrome and Death in People Living With Human Immunodeficiency Virus and Severe Lymphopenia. Clin Infect Dis *71*, 652-660. 10.1093/cid/ciz877.
Sette, A., and Crotty, S. (2021). Adaptive immunity to SARS-CoV-2 and COVID-19. Cell *184*, 861-880. 10.1016/j.cell.2021.01.007.
Sharma, N., Vacher, J., and Allison, J.P. (2019). TLR1/2 ligand enhances antitumor efficacy of CTLA-4 blockade by increasing intratumoral Treg depletion. Proc Natl Acad Sci U S A *116*, 10453-10462. 10.1073/pnas.1819004116.
Sharpe, A.H., Wherry, E.J., Ahmed, R., and Freeman, G.J. (2007). The function of programmed cell death 1 and its ligands in regulating autoimmunity and infection. Nat Immunol *8*, 239-245. 10.1038/ni1443.
Sheahan, T.P., Sims, A.C., Leist, S.R., Schafer, A., Won, J., Brown, A.J., Montgomery, S.A., Hogg, A., Babusis, D., Clarke, M.O., et al. (2020). Comparative therapeutic efficacy of remdesivir and combination lopinavir, ritonavir, and interferon beta against MERS-CoV. Nat Commun *11*, 222. 10.1038/s41467-019-13940-6.
Shedlock, D.J., and Shen, H. (2003). Requirement for CD4 T cell help in generating functional CD8 T cell memory. Science *300*, 337-339. 10.1126/science.1082305.
Siddiqi, H.K., and Mehra, M.R. (2020). COVID-19 illness in native and immunosuppressed states: A clinical-therapeutic staging proposal. J Heart Lung Transplant *39*, 405-407. 10.1016/j.healun.2020.03.012.
Siegal, F.P., Kadowaki, N., Shodell, M., Fitzgerald-Bocarsly, P.A., Shah, K., Ho, S., Antonenko, S., and Liu, Y.J. (1999). The nature of the principal type 1 interferon-producing cells in human blood. Science *284*, 1835-1837. 10.1126/science.284.5421.1835.
Siliciano, J.D., Kajdas, J., Finzi, D., Quinn, T.C., Chadwick, K., Margolick, J.B., Kovacs, C., Gange, S.J., and Siliciano, R.F. (2003). Long-term follow-up studies confirm the stability of the latent reservoir for HIV-1 in resting CD4+ T cells. Nat Med *9*, 727-728. 10.1038/nm880.

Silva, J., Lucas, C., Sundaram, M., Israelow, B., Wong, P., Klein, J., Tokuyama, M., Lu, P., Venkataraman, A., Liu, F., et al. (2021). Saliva viral load is a dynamic unifying correlate of COVID-19 severity and mortality. medRxiv, 2021.2001.2004.21249236. 10.1101/2021.01.04.21249236.
Simon, S., Vignard, V., Varey, E., Parrot, T., Knol, A.C., Khammari, A., Gervois, N., Lang, F., Dreno, B., and Labarriere, N. (2017). Emergence of High-Avidity Melan-A-Specific Clonotypes as a Reflection of Anti-PD-1 Clinical Efficacy. Cancer Res *77*, 7083-7093. 10.1158/0008-5472.CAN-17-1856.
Siswanto, Gani, M., Fauzi, A.R., Yuliyanti, R.E., Inggriani, M.P., Nugroho, B., Agustiningsih, D., and Gunadi (2020). Possible silent hypoxemia in a COVID-19 patient: A case report. Ann Med Surg (Lond) *60*, 583-586. 10.1016/j.amsu.2020.11.053.
Smith-Franklin, B.A., Keele, B.F., Tew, J.G., Gartner, S., Szakal, A.K., Estes, J.D., Thacker, T.C., and Burton, G.F. (2002). Follicular dendritic cells and the persistence of HIV infectivity: the role of antibodies and Fcgamma receptors. J Immunol *168*, 2408-2414. 10.4049/jimmunol.168.5.2408.
Snell, L.M., MacLeod, B.L., Law, J.C., Osokine, I., Elsaesser, H.J., Hezaveh, K., Dickson, R.J., Gavin, M.A., Guidos, C.J., McGaha, T.L., and Brooks, D.G. (2018). CD8(+) T Cell Priming in Established Chronic Viral Infection Preferentially Directs Differentiation of Memory-like Cells for Sustained Immunity. Immunity *49*, 678-694 e675. 10.1016/j.immuni.2018.08.002.
Snell, L.M., Xu, W., Abd-Rabbo, D., Boukhaled, G., Guo, M., Macleod, B.L., Elsaesser, H.J., Hezaveh, K., Alsahafi, N., Lukhele, S., et al. (2021). Dynamic CD4(+) T cell heterogeneity defines subset-specific suppression and PD-L1-blockade-driven functional restoration in chronic infection. Nat Immunol *22*, 1524-1537. 10.1038/s41590-021-01060-7.
Snyder, A., Makarov, V., Merghoub, T., Yuan, J., Zaretsky, J.M., Desrichard, A., Walsh, L.A., Postow, M.A., Wong, P., Ho, T.S., et al. (2014). Genetic basis for clinical response to CTLA-4 blockade in melanoma. N Engl J Med *371*, 2189-2199. 10.1056/NEJMoa1406498.
Sorbello, M., El-Boghdadly, K., Di Giacinto, I., Cataldo, R., Esposito, C., Falcetta, S., Merli, G., Cortese, G., Corso, R.M., Bressan, F., et al. (2020). The Italian coronavirus disease 2019 outbreak: recommendations from clinical practice. Anaesthesia *75*, 724-732. 10.1111/anae.15049.
Sorensen, G.L. (2018). Surfactant Protein D in Respiratory and Non-Respiratory Diseases. Front Med (Lausanne) *5*, 18. 10.3389/fmed.2018.00018.
Staron, M.M., Gray, S.M., Marshall, H.D., Parish, I.A., Chen, J.H., Perry, C.J., Cui, G., Li, M.O., and Kaech, S.M. (2014). The transcription factor FoxO1 sustains expression of the inhibitory receptor PD-1 and survival of antiviral CD8(+) T cells during chronic infection. Immunity *41*, 802-814. 10.1016/j.immuni.2014.10.013.
Stebbing, J., Krishnan, V., de Bono, S., Ottaviani, S., Casalini, G., Richardson, P.J., Monteil, V., Lauschke, V.M., Mirazimi, A., Youhanna, S., et al. (2020). Mechanism of baricitinib supports artificial intelligence-predicted testing in COVID-19 patients. EMBO Mol Med *12*, e12697. 10.15252/emmm.202012697.
Stertz, S., Reichelt, M., Spiegel, M., Kuri, T., Martinez-Sobrido, L., Garcia-Sastre, A., Weber, F., and Kochs, G. (2007). The intracellular sites of early replication and budding of SARS-coronavirus. Virology *361*, 304-315. 10.1016/j.virol.2006.11.027.
Stieh, D.J., Matias, E., Xu, H., Fought, A.J., Blanchard, J.L., Marx, P.A., Veazey, R.S., and Hope, T.J. (2016). Th17 Cells Are Preferentially Infected Very Early after Vaginal Transmission of SIV in Macaques. Cell Host Microbe *19*, 529-540. 10.1016/j.chom.2016.03.005.

Su, Y.C.F., Anderson, D.E., Young, B.E., Linster, M., Zhu, F., Jayakumar, J., Zhuang, Y., Kalimuddin, S., Low, J.G.H., Tan, C.W., et al. (2020). Discovery and Genomic Characterization of a 382-Nucleotide Deletion in ORF7b and ORF8 during the Early Evolution of SARS-CoV-2. mBio *11*. 10.1128/mBio.01610-20.
Suleyman, G., Fadel, R.A., Malette, K.M., Hammond, C., Abdulla, H., Entz, A., Demertzis, Z., Hanna, Z., Failla, A., Dagher, C., et al. (2020). Clinical Characteristics and Morbidity Associated With Coronavirus Disease 2019 in a Series of Patients in Metropolitan Detroit. JAMA Netw Open *3*, e2012270. 10.1001/jamanetworkopen.2020.12270.
Sun, J., Zhu, A., Li, H., Zheng, K., Zhuang, Z., Chen, Z., Shi, Y., Zhang, Z., Chen, S.B., Liu, X., et al. (2020). Isolation of infectious SARS-CoV-2 from urine of a COVID-19 patient. Emerg Microbes Infect *9*, 991-993. 10.1080/22221751.2020.1760144.
Sundquist, W.I., and Krausslich, H.G. (2012). HIV-1 assembly, budding, and maturation. Cold Spring Harb Perspect Med *2*, a006924. 10.1101/cshperspect.a006924.
Suthar, M.S., Zimmerman, M.G., Kauffman, R.C., Mantus, G., Linderman, S.L., Hudson, W.H., Vanderheiden, A., Nyhoff, L., Davis, C.W., Adekunle, O., et al. (2020). Rapid Generation of Neutralizing Antibody Responses in COVID-19 Patients. Cell Rep Med *1*, 100040. 10.1016/j.xcrm.2020.100040.
Tan, A.T., Linster, M., Tan, C.W., Le Bert, N., Chia, W.N., Kunasegaran, K., Zhuang, Y., Tham, C.Y.L., Chia, A., Smith, G.J.D., et al. (2021). Early induction of functional SARS-CoV-2-specific T cells associates with rapid viral clearance and mild disease in COVID-19 patients. Cell Rep *34*, 108728. 10.1016/j.celrep.2021.108728.
Tazi, J., Bakkour, N., Marchand, V., Ayadi, L., Aboufirassi, A., and Branlant, C. (2010). Alternative splicing: regulation of HIV-1 multiplication as a target for therapeutic action. FEBS J *277*, 867-876. 10.1111/j.1742-4658.2009.07522.x.
Tecchio, C., Micheletti, A., and Cassatella, M.A. (2014). Neutrophil-derived cytokines: facts beyond expression. Front Immunol *5*, 508. 10.3389/fimmu.2014.00508.
Teijaro, J.R., Ng, C., Lee, A.M., Sullivan, B.M., Sheehan, K.C., Welch, M., Schreiber, R.D., de la Torre, J.C., and Oldstone, M.B. (2013). Persistent LCMV infection is controlled by blockade of type I interferon signaling. Science *340*, 207-211. 10.1126/science.1235214.
Tenorio, A.R., Zheng, Y., Bosch, R.J., Krishnan, S., Rodriguez, B., Hunt, P.W., Plants, J., Seth, A., Wilson, C.C., Deeks, S.G., et al. (2014). Soluble markers of inflammation and coagulation but not T-cell activation predict non-AIDS-defining morbid events during suppressive antiretroviral treatment. J Infect Dis *210*, 1248-1259. 10.1093/infdis/jiu254.
Thachil, J., Tang, N., Gando, S., Falanga, A., Cattaneo, M., Levi, M., Clark, C., and Iba, T. (2020). ISTH interim guidance on recognition and management of coagulopathy in COVID-19. J Thromb Haemost *18*, 1023-1026. 10.1111/jth.14810.
Tham, E.L., Shrikant, P., and Mescher, M.F. (2002). Activation-induced nonresponsiveness: a Th-dependent regulatory checkpoint in the CTL response. J Immunol *168*, 1190-1197. 10.4049/jimmunol.168.3.1190.
Thome, J.J., and Farber, D.L. (2015). Emerging concepts in tissue-resident T cells: lessons from humans. Trends Immunol *36*, 428-435. 10.1016/j.it.2015.05.003.
Thoms, M., Buschauer, R., Ameismeier, M., Koepke, L., Denk, T., Hirschenberger, M., Kratzat, H., Hayn, M., Mackens-Kiani, T., Cheng, J., et al. (2020). Structural basis for translational shutdown and immune evasion by the Nsp1 protein of SARS-CoV-2. Science *369*, 1249-1255.

10.1126/science.abc8665.
Toccafondi, E., Lener, D., and Negroni, M. (2021). HIV-1 Capsid Core: A Bullet to the Heart of the Target Cell. Front Microbiol *12*, 652486. 10.3389/fmicb.2021.652486.
Tomazini, B.M., Maia, I.S., Cavalcanti, A.B., Berwanger, O., Rosa, R.G., Veiga, V.C., Avezum, A., Lopes, R.D., Bueno, F.R., Silva, M., et al. (2020). Effect of Dexamethasone on Days Alive and Ventilator-Free in Patients With Moderate or Severe Acute Respiratory Distress Syndrome and COVID-19: The CoDEX Randomized Clinical Trial. JAMA *324*, 1307-1316. 10.1001/jama.2020.17021.
Trautmann, L., Janbazian, L., Chomont, N., Said, E.A., Gimmig, S., Bessette, B., Boulassel, M.R., Delwart, E., Sepulveda, H., Balderas, R.S., et al. (2006). Upregulation of PD-1 expression on HIV-specific CD8+ T cells leads to reversible immune dysfunction. Nat Med *12*, 1198-1202. 10.1038/nm1482.
Tuccori, M., Convertino, I., Ferraro, S., Cappello, E., Valdiserra, G., de Luca, G., Franchini, M., and Focosi, D. (2022). Preclinical discovery and development of the casirivimab + imdevimab cocktail for the treatment of novel coronavirus infection: the rise and fall. Expert Opin Drug Discov, 1-16. 10.1080/17460441.2022.2058486.
Tumeh, P.C., Harview, C.L., Yearley, J.H., Shintaku, I.P., Taylor, E.J., Robert, L., Chmielowski, B., Spasic, M., Henry, G., Ciobanu, V., et al. (2014). PD-1 blockade induces responses by inhibiting adaptive immune resistance. Nature *515*, 568-571. 10.1038/nature13954.
Uldrick, T.S., Goncalves, P.H., Abdul-Hay, M., Claeys, A.J., Emu, B., Ernstoff, M.S., Fling, S.P., Fong, L., Kaiser, J.C., Lacroix, A.M., et al. (2019). Assessment of the Safety of Pembrolizumab in Patients With HIV and Advanced Cancer-A Phase 1 Study. JAMA Oncol *5*, 1332-1339. 10.1001/jamaoncol.2019.2244.
Ullah, I., Prevost, J., Ladinsky, M.S., Stone, H., Lu, M., Anand, S.P., Beaudoin-Bussieres, G., Symmes, K., Benlarbi, M., Ding, S., et al. (2021). Live imaging of SARS-CoV-2 infection in mice reveals that neutralizing antibodies require Fc function for optimal efficacy. Immunity *54*, 2143-2158 e2115. 10.1016/j.immuni.2021.08.015.
Urbani, S., Amadei, B., Tola, D., Massari, M., Schivazappa, S., Missale, G., and Ferrari, C. (2006). PD-1 expression in acute hepatitis C virus (HCV) infection is associated with HCV-specific CD8 exhaustion. J Virol *80*, 11398-11403. 10.1128/JVI.01177-06.
Utzschneider, D.T., Charmoy, M., Chennupati, V., Pousse, L., Ferreira, D.P., Calderon-Copete, S., Danilo, M., Alfei, F., Hofmann, M., Wieland, D., et al. (2016). T Cell Factor 1-Expressing Memory-like CD8(+) T Cells Sustain the Immune Response to Chronic Viral Infections. Immunity *45*, 415-427. 10.1016/j.immuni.2016.07.021.
Utzschneider, D.T., Legat, A., Fuertes Marraco, S.A., Carrie, L., Luescher, I., Speiser, D.E., and Zehn, D. (2013). T cells maintain an exhausted phenotype after antigen withdrawal and population reexpansion. Nat Immunol *14*, 603-610. 10.1038/ni.2606.
V'Kovski, P., Kratzel, A., Steiner, S., Stalder, H., and Thiel, V. (2021). Coronavirus biology and replication: implications for SARS-CoV-2. Nat Rev Microbiol *19*, 155-170. 10.1038/s41579-020-00468-6.
Vaidyanathan, B., and Chaudhuri, J. (2015). Epigenetic Codes Programing Class Switch Recombination. Front Immunol *6*, 405. 10.3389/fimmu.2015.00405.
Van Laethem, F., Baus, E., Smyth, L.A., Andris, F., Bex, F., Urbain, J., Kioussis, D., and Leo, O. (2001). Glucocorticoids attenuate T cell receptor signaling. J Exp Med *193*, 803-814.

10.1084/jem.193.7.803.
van Lelyveld, S.F., Gras, L., Kesselring, A., Zhang, S., De Wolf, F., Wensing, A.M., Hoepelman, A.I., and study, A.n.o.c. (2012). Long-term complications in patients with poor immunological recovery despite virological successful HAART in Dutch ATHENA cohort. AIDS *26*, 465-474. 10.1097/QAD.0b013e32834f32f8.
Van Lint, C., Bouchat, S., and Marcello, A. (2013). HIV-1 transcription and latency: an update. Retrovirology *10*, 67. 10.1186/1742-4690-10-67.
van Rooij, N., van Buuren, M.M., Philips, D., Velds, A., Toebes, M., Heemskerk, B., van Dijk, L.J., Behjati, S., Hilkmann, H., El Atmioui, D., et al. (2013). Tumor exome analysis reveals neoantigen-specific T-cell reactivity in an ipilimumab-responsive melanoma. J Clin Oncol *31*, e439-442. 10.1200/JCO.2012.47.7521.
Varga, Z., Flammer, A.J., Steiger, P., Haberecker, M., Andermatt, R., Zinkernagel, A.S., Mehra, M.R., Schuepbach, R.A., Ruschitzka, F., and Moch, H. (2020). Endothelial cell infection and endotheliitis in COVID-19. Lancet *395*, 1417-1418. 10.1016/S0140-6736(20)30937-5.
Velazquez-Salinas, L., Verdugo-Rodriguez, A., Rodriguez, L.L., and Borca, M.V. (2019). The Role of Interleukin 6 During Viral Infections. Front Microbiol *10*, 1057. 10.3389/fmicb.2019.01057.
Velu, V., Titanji, K., Zhu, B., Husain, S., Pladevega, A., Lai, L., Vanderford, T.H., Chennareddi, L., Silvestri, G., Freeman, G.J., et al. (2009). Enhancing SIV-specific immunity in vivo by PD-1 blockade. Nature *458*, 206-210. 10.1038/nature07662.
Viana, R., Moyo, S., Amoako, D.G., Tegally, H., Scheepers, C., Althaus, C.L., Anyaneji, U.J., Bester, P.A., Boni, M.F., Chand, M., et al. (2022). Rapid epidemic expansion of the SARS-CoV-2 Omicron variant in southern Africa. Nature *603*, 679-686. 10.1038/s41586-022-04411-y.
Waldman, A.D., Fritz, J.M., and Lenardo, M.J. (2020). A guide to cancer immunotherapy: from T cell basic science to clinical practice. Nat Rev Immunol *20*, 651-668. 10.1038/s41577-020-0306-5.
Wang, C., Xie, J., Zhao, L., Fei, X., Zhang, H., Tan, Y., Nie, X., Zhou, L., Liu, Z., Ren, Y., et al. (2020a). Alveolar macrophage dysfunction and cytokine storm in the pathogenesis of two severe COVID-19 patients. EBioMedicine *57*, 102833. 10.1016/j.ebiom.2020.102833.
Wang, F., Hou, H., Yao, Y., Wu, S., Huang, M., Ran, X., Zhou, H., Liu, Z., and Sun, Z. (2020b). Systemically comparing host immunity between survived and deceased COVID-19 patients. Cell Mol Immunol *17*, 875-877. 10.1038/s41423-020-0483-y.
Wang, M., Cao, R., Zhang, L., Yang, X., Liu, J., Xu, M., Shi, Z., Hu, Z., Zhong, W., and Xiao, G. (2020c). Remdesivir and chloroquine effectively inhibit the recently emerged novel coronavirus (2019-nCoV) in vitro. Cell Res *30*, 269-271. 10.1038/s41422-020-0282-0.
Wang, W., Xu, Y., Gao, R., Lu, R., Han, K., Wu, G., and Tan, W. (2020d). Detection of SARS-CoV-2 in Different Types of Clinical Specimens. JAMA *323*, 1843-1844. 10.1001/jama.2020.3786.
Wang, Y., Chung, Y.R., Eitzinger, S., Palacio, N., Gregory, S., Bhattacharyya, M., and Penaloza-MacMaster, P. (2019). TLR4 signaling improves PD-1 blockade therapy during chronic viral infection. PLoS Pathog *15*, e1007583. 10.1371/journal.ppat.1007583.
Wang, Y., Zhang, D., Du, G., Du, R., Zhao, J., Jin, Y., Fu, S., Gao, L., Cheng, Z., Lu, Q., et al. (2020e). Remdesivir in adults with severe COVID-19: a randomised, double-blind, placebo-controlled, multicentre trial. Lancet *395*, 1569-1578. 10.1016/S0140-6736(20)31022-9.
Wang, Y., Zhang, L., Sang, L., Ye, F., Ruan, S., Zhong, B., Song, T., Alshukairi, A.N., Chen, R., Zhang, Z., et al. (2020f). Kinetics of viral load and antibody response in relation to COVID-19

severity. J Clin Invest *130*, 5235-5244. 10.1172/JCI138759.
Waterhouse, P., Penninger, J.M., Timms, E., Wakeham, A., Shahinian, A., Lee, K.P., Thompson, C.B., Griesser, H., and Mak, T.W. (1995). Lymphoproliferative disorders with early lethality in mice deficient in Ctla-4. Science *270*, 985-988. 10.1126/science.270.5238.985.
Wei, F., Zhong, S., Ma, Z., Kong, H., Medvec, A., Ahmed, R., Freeman, G.J., Krogsgaard, M., and Riley, J.L. (2013). Strength of PD-1 signaling differentially affects T-cell effector functions. Proc Natl Acad Sci U S A *110*, E2480-2489. 10.1073/pnas.1305394110.
Wei, S.C., Anang, N.A.S., Sharma, R., Andrews, M.C., Reuben, A., Levine, J.H., Cogdill, A.P., Mancuso, J.J., Wargo, J.A., Pe'er, D., and Allison, J.P. (2019). Combination anti-CTLA-4 plus anti-PD-1 checkpoint blockade utilizes cellular mechanisms partially distinct from monotherapies. Proc Natl Acad Sci U S A *116*, 22699-22709. 10.1073/pnas.1821218116.
Wei, S.C., Levine, J.H., Cogdill, A.P., Zhao, Y., Anang, N.A.S., Andrews, M.C., Sharma, P., Wang, J., Wargo, J.A., Pe'er, D., and Allison, J.P. (2017). Distinct Cellular Mechanisms Underlie Anti-CTLA-4 and Anti-PD-1 Checkpoint Blockade. Cell *170*, 1120-1133 e1117. 10.1016/j.cell.2017.07.024.
Weinreich, D.M., Sivapalasingam, S., Norton, T., Ali, S., Gao, H., Bhore, R., Musser, B.J., Soo, Y., Rofail, D., Im, J., et al. (2021). REGN-COV2, a Neutralizing Antibody Cocktail, in Outpatients with Covid-19. N Engl J Med *384*, 238-251. 10.1056/NEJMoa2035002.
Weiskopf, D., Schmitz, K.S., Raadsen, M.P., Grifoni, A., Okba, N.M.A., Endeman, H., van den Akker, J.P.C., Molenkamp, R., Koopmans, M.P.G., van Gorp, E.C.M., et al. (2020). Phenotype and kinetics of SARS-CoV-2-specific T cells in COVID-19 patients with acute respiratory distress syndrome. Sci Immunol *5*. 10.1126/sciimmunol.abd2071.
West, E.E., Jin, H.T., Rasheed, A.U., Penaloza-Macmaster, P., Ha, S.J., Tan, W.G., Youngblood, B., Freeman, G.J., Smith, K.A., and Ahmed, R. (2013). PD-L1 blockade synergizes with IL-2 therapy in reinvigorating exhausted T cells. J Clin Invest *123*, 2604-2615. 10.1172/JCI67008.
Wherry, E.J. (2011). T cell exhaustion. Nat Immunol *12*, 492-499.
Wherry, E.J., Barber, D.L., Kaech, S.M., Blattman, J.N., and Ahmed, R. (2004). Antigen-independent memory CD8 T cells do not develop during chronic viral infection. Proc Natl Acad Sci U S A *101*, 16004-16009. 10.1073/pnas.0407192101.
Whitney, J.B., Hill, A.L., Sanisetty, S., Penaloza-MacMaster, P., Liu, J., Shetty, M., Parenteau, L., Cabral, C., Shields, J., Blackmore, S., et al. (2014). Rapid seeding of the viral reservoir prior to SIV viraemia in rhesus monkeys. Nature *512*, 74-77. 10.1038/nature13594.
Wigenstam, E., Elfsmark, L., Agren, L., Akfur, C., Bucht, A., and Jonasson, S. (2018). Anti-inflammatory and anti-fibrotic treatment in a rodent model of acute lung injury induced by sulfur dioxide. Clin Toxicol (Phila) *56*, 1185-1194. 10.1080/15563650.2018.1479527.
Wightman, F., Solomon, A., Kumar, S.S., Urriola, N., Gallagher, K., Hiener, B., Palmer, S., McNeil, C., Garsia, R., and Lewin, S.R. (2015). Effect of ipilimumab on the HIV reservoir in an HIV-infected individual with metastatic melanoma. AIDS *29*, 504-506. 10.1097/QAD.0000000000000562.
Wilen, C.B., Tilton, J.C., and Doms, R.W. (2012). HIV: cell binding and entry. Cold Spring Harb Perspect Med *2*. 10.1101/cshperspect.a006866.
Wilk, A.J., Rustagi, A., Zhao, N.Q., Roque, J., Martinez-Colon, G.J., McKechnie, J.L., Ivison, G.T., Ranganath, T., Vergara, R., Hollis, T., et al. (2020). A single-cell atlas of the peripheral immune response in patients with severe COVID-19. Nat Med *26*, 1070-1076. 10.1038/s41591-020-0944-y.
Wilson, E.B., Yamada, D.H., Elsaesser, H., Herskovitz, J., Deng, J., Cheng, G., Aronow, B.J., Karp,

C.L., and Brooks, D.G. (2013). Blockade of chronic type I interferon signaling to control persistent LCMV infection. Science *340*, 202-207. 10.1126/science.1235208.
Wilson, M.S., and Wynn, T.A. (2009). Pulmonary fibrosis: pathogenesis, etiology and regulation. Mucosal Immunol *2*, 103-121. 10.1038/mi.2008.85.
Wilson, N.M., Norton, A., Young, F.P., and Collins, D.W. (2020). Airborne transmission of severe acute respiratory syndrome coronavirus-2 to healthcare workers: a narrative review. Anaesthesia *75*, 1086-1095. 10.1111/anae.15093.
Wolfel, R., Corman, V.M., Guggemos, W., Seilmaier, M., Zange, S., Muller, M.A., Niemeyer, D., Jones, T.C., Vollmar, P., Rothe, C., et al. (2020). Virological assessment of hospitalized patients with COVID-2019. Nature *581*, 465-469. 10.1038/s41586-020-2196-x.
Wolff, G., Melia, C.E., Snijder, E.J., and Barcena, M. (2020). Double-Membrane Vesicles as Platforms for Viral Replication. Trends Microbiol *28*, 1022-1033. 10.1016/j.tim.2020.05.009.
Wong, J.K., and Yukl, S.A. (2016). Tissue reservoirs of HIV. Curr Opin HIV AIDS *11*, 362-370. 10.1097/COH.0000000000000293.
Xiao, F., Tang, M., Zheng, X., Liu, Y., Li, X., and Shan, H. (2020). Evidence for Gastrointestinal Infection of SARS-CoV-2. Gastroenterology *158*, 1831-1833 e1833. 10.1053/j.gastro.2020.02.055.
Xu, D., Zhou, F., Sun, W., Chen, L., Lan, L., Li, H., Xiao, F., Li, Y., Kolachalama, V.B., Li, Y., et al. (2021). Relationship Between Serum Severe Acute Respiratory Syndrome Coronavirus 2 Nucleic Acid and Organ Damage in Coronavirus 2019 Patients: A Cohort Study. Clin Infect Dis *73*, 68-75. 10.1093/cid/ciaa1085.
Xu, G., Qi, F., Li, H., Yang, Q., Wang, H., Wang, X., Liu, X., Zhao, J., Liao, X., Liu, Y., et al. (2020). The differential immune responses to COVID-19 in peripheral and lung revealed by single-cell RNA sequencing. Cell Discov *6*, 73. 10.1038/s41421-020-00225-2.
Yan, X., Chen, G., Jin, Z., Zhang, Z., Zhang, B., He, J., Yin, S., Huang, J., Fan, M., Li, Z., et al. (2021). Anti-SARS-CoV-2 IgG levels in relation to disease severity of COVID-19. J Med Virol. 10.1002/jmv.27274.
Yao, X.H., He, Z.C., Li, T.Y., Zhang, H.R., Wang, Y., Mou, H., Guo, Q., Yu, S.C., Ding, Y., Liu, X., et al. (2020). Pathological evidence for residual SARS-CoV-2 in pulmonary tissues of a ready-for-discharge patient. Cell Res *30*, 541-543. 10.1038/s41422-020-0318-5.
Yao, X.H., Luo, T., Shi, Y., He, Z.C., Tang, R., Zhang, P.P., Cai, J., Zhou, X.D., Jiang, D.P., Fei, X.C., et al. (2021). A cohort autopsy study defines COVID-19 systemic pathogenesis. Cell Res *31*, 836-846. 10.1038/s41422-021-00523-8.
Yilmaz, A., Marklund, E., Andersson, M., Nilsson, S., Andersson, L.M., Lindh, M., and Gisslen, M. (2021). Upper Respiratory Tract Levels of Severe Acute Respiratory Syndrome Coronavirus 2 RNA and Duration of Viral RNA Shedding Do Not Differ Between Patients With Mild and Severe/Critical Coronavirus Disease 2019. J Infect Dis *223*, 15-18. 10.1093/infdis/jiaa632.
Youngblood, B., Oestreich, K.J., Ha, S.J., Duraiswamy, J., Akondy, R.S., West, E.E., Wei, Z., Lu, P., Austin, J.W., Riley, J.L., et al. (2011). Chronic virus infection enforces demethylation of the locus that encodes PD-1 in antigen-specific CD8(+) T cells. Immunity *35*, 400-412. 10.1016/j.immuni.2011.06.015.
Zeng, M., Smith, A.J., Wietgrefe, S.W., Southern, P.J., Schacker, T.W., Reilly, C.S., Estes, J.D., Burton, G.F., Silvestri, G., Lifson, J.D., et al. (2011). Cumulative mechanisms of lymphoid tissue fibrosis and T cell depletion in HIV-1 and SIV infections. J Clin Invest *121*, 998-1008.

10.1172/JCI45157.
Zevin, A.S., McKinnon, L., Burgener, A., and Klatt, N.R. (2016). Microbial translocation and microbiome dysbiosis in HIV-associated immune activation. Curr Opin HIV AIDS *11*, 182-190. 10.1097/COH.0000000000000234.
Zhang, D.K.Y., Cheung, A.S., and Mooney, D.J. (2020). Activation and expansion of human T cells using artificial antigen-presenting cell scaffolds. Nat Protoc *15*, 773-798. 10.1038/s41596-019-0249-0.
Zhang, N., and Bevan, M.J. (2011). CD8(+) T cells: foot soldiers of the immune system. Immunity *35*, 161-168. 10.1016/j.immuni.2011.07.010.
Zhang, Y., Chen, Y., Li, Y., Huang, F., Luo, B., Yuan, Y., Xia, B., Ma, X., Yang, T., Yu, F., et al. (2021). The ORF8 protein of SARS-CoV-2 mediates immune evasion through down-regulating MHC-Iota. Proc Natl Acad Sci U S A *118*. 10.1073/pnas.2024202118.
Zhen, A., Rezek, V., Youn, C., Lam, B., Chang, N., Rick, J., Carrillo, M., Martin, H., Kasparian, S., Syed, P., et al. (2017). Targeting type I interferon-mediated activation restores immune function in chronic HIV infection. J Clin Invest *127*, 260-268. 10.1172/JCI89488.
Zhou, R., To, K.K., Wong, Y.C., Liu, L., Zhou, B., Li, X., Huang, H., Mo, Y., Luk, T.Y., Lau, T.T., et al. (2020a). Acute SARS-CoV-2 Infection Impairs Dendritic Cell and T Cell Responses. Immunity *53*, 864-877 e865. 10.1016/j.immuni.2020.07.026.
Zhou, Z., Ren, L., Zhang, L., Zhong, J., Xiao, Y., Jia, Z., Guo, L., Yang, J., Wang, C., Jiang, S., et al. (2020b). Heightened Innate Immune Responses in the Respiratory Tract of COVID-19 Patients. Cell Host Microbe *27*, 883-890 e882. 10.1016/j.chom.2020.04.017.
Zohar, T., Loos, C., Fischinger, S., Atyeo, C., Wang, C., Slein, M.D., Burke, J., Yu, J., Feldman, J., Hauser, B.M., et al. (2020). Compromised Humoral Functional Evolution Tracks with SARS-CoV-2 Mortality. Cell *183*, 1508-1519 e1512. 10.1016/j.cell.2020.10.052.
Zuazo, M., Arasanz, H., Fernandez-Hinojal, G., Garcia-Granda, M.J., Gato, M., Bocanegra, A., Martinez, M., Hernandez, B., Teijeira, L., Morilla, I., et al. (2019). Functional systemic CD4 immunity is required for clinical responses to PD-L1/PD-1 blockade therapy. EMBO Mol Med *11*, e10293. 10.15252/emmm.201910293.
Zuo, Y., Yalavarthi, S., Shi, H., Gockman, K., Zuo, M., Madison, J.A., Blair, C., Weber, A., Barnes, B.J., Egeblad, M., et al. (2020). Neutrophil extracellular traps in COVID-19. JCI Insight *5*. 10.1172/jci.insight.138999.

Chapter 9 - Appendices

Appendix I : The candidate's contribution to addional manuscripts

Author's contribution to the first additional manuscript « Altered differentiation is central to HIV-specific CD4+ T cell dysfunction in progressive disease »

A.M. and D.E.K. designed the studies. A.M., E.B.-R., R.C., N.B., S.A., G.G.-L., L.Y. and

P.A.R. performed experiments. M.D. provided input on manuscript content and data representation. A.M., E.M., S.D. and F.L. performed bioinformatics analyses. K.N.-M., J.N., A.E.B., J.M.B., R.P.J., R.T.W., A.F. and D.C.D. provided technical expertise. C.T. and J.-P.R. obtained institutional review board approval and managed study participant recruitment. A.M. and D.E.K. interpreted the data and wrote the paper with all co-authors' assistance

Author's contribution to the second additional manuscript « Targeting Mitochondria to Revive Dysfunctional Regulatory T cells ».

Elsa Brunet-Ratnasingham performed the literature review and wrote the manuscript with input from Mathieu Dubé (who also did the figure) and Daniel E. Kaufmann.

Author's contribution to references not added in appendices

- Julia Niessl, Amy E. Baxter, Antigoni Morou, Elsa Brunet-Ratnasingham, Gérémy Sannier, Gabrielle Gendron-Lepage, Jonathan Richard, Gloria-Gabrielle Delgado, Nathalie Brassard, Isabelle Turcotte, Rémi Fromentin, Nicole F. Bernard, Nicolas Chomont, Jean-Pierre Routy, Mathieu Dubé, Andrés Finzi, Daniel E. Kaufmann. Persistent expansion and Th1-like skewing of HIV-specific circulating T follicular helper cells during antiretroviral therapy. EBioMedicine Volume 54,2020,102727,ISSN 2352-3964,https://doi.org/10.1016/j.ebiom.2020.102727.

Performed and analyzed experiments; scientific input.

- Zhou, S., Butler-Laporte, G., Nakanishi, T. et al. A Neanderthal OAS1 isoform protects individuals of European ancestry against COVID-19 susceptibility and severity. Nat Med 27, 659–667 (2021). https://doi.org/10.1038/s41591-021-01281-1

Clinical data compilation and curation.

- Bégin, P., Callum, J., Jamula, E. et al. Convalescent plasma for hospitalized patients with COVID-19: an open-label, randomized controlled trial. Nat Med 27, 2012–2024 (2021). https://doi.org/10.1038/s41591-021-01488-2

Clinical data compilation and curation.

- Anand, S. P., J. Prevost, M. Nayrac, G. Beaudoin-Bussieres, M. Benlarbi, R. Gasser, N. Brassard, A. Laumaea, S. Y. Gong, C. Bourassa, E. Brunet-Ratnasingham, H. Medjahed, G. Gendron-Lepage, G. Goyette, L. Gokool, C. Morrisseau, P. Begin, V. Martel-Laferriere, C. Tremblay, J. Richard, R. Bazin, R. Duerr, D. E. Kaufmann, and A. Finzi. 2021. 'Longitudinal analysis of humoral immunity against SARS-CoV-2 Spike in convalescent individuals up to 8 months post-symptom onset', Cell Rep Med, 2: 100290.

Clinical data compilation and curation.

- Nganou-Makamdop, K., A. Talla, A. A. Sharma, S. Darko, A. Ransier, F. Laboune, J. G. Chipman, G. J. Beilman, T. Hoskuldsson, S. Fourati, T. E. Schmidt, S. Arumugam, N. S. Lima, D. Moon, S. Callisto, J. Schoephoerster, J. Tomalka, P. Mugyenyi, F. Ssali, P. Muloma, P. Ssengendo, A. R. Leda, R. K. Cheu, J. K. Flynn, A. Morou, E. Brunet-Ratnasingham, B. Rodriguez, M. M. Lederman, D. E. Kaufmann, N. R. Klatt, C. Kityo, J. M. Brenchley, T. W. Schacker, R. P. Sekaly, and D. C. Douek. 2021. 'Translocated microbiome composition determines immunological outcome in treated HIV infection', Cell, 184: 3899-914 e16.

Performed and analyzed experiments.

- Sannier, G., M. Dube, C. Dufour, C. Richard, N. Brassard, G. G. Delgado, A. Pagliuzza, A. E. Baxter, J. Niessl, E. Brunet-Ratnasingham, R. Charlebois, B. Routy, J. P. Routy, R. Fromentin, N. Chomont, and D. E. Kaufmann. 2021. 'Combined single-cell transcriptional, translational, and genomic profiling reveals HIV-1 reservoir diversity', Cell Rep, 36: 109643.

Scientific input.

Appendix II : Additional manuscripts

Altered differentiation is central to HIV-specific CD4+ T cell dysfunction in progressive disease – *Nature Immunology 2019.*

Included with permissions allocated to authors of paper.

Targeting Mitochondria to Revive Dysfunctional Regulatory T cells – *Trends in Molecular Medicine 2019*

Included with permissions allocated to authors of paper.

nature immunology

ARTICLES

https://doi.org/10.1038/s41590-019-0418-x

Altered differentiation is central to HIV-specific CD4+ T cell dysfunction in progressive disease

Antigoni Morou[1,2], Elsa Brunet-Ratnasingham[1,2], Mathieu Dubé[1,3], Roxanne Charlebois[1], Eloi Mercier[4], Sam Darko[5], Nathalie Brassard[1], Krystelle Nganou-Makamdop[5], Sahaana Arumugam[5], Gabrielle Gendron-Lepage[1,2], Lifei Yang[6], Julia Niessl[1,2,3], Amy E. Baxter[1,2,3,9], James M. Billingsley[7], Premeela A. Rajakumar[7], François Lefebvre[4], R. Paul Johnson[7], Cécile Tremblay[1,2], Jean-Pierre Routy[8], Richard T. Wyatt[3,6], Andrés Finzi[1,2], Daniel C. Douek[5] and Daniel E. Kaufmann[1,2,3*]

Dysfunction of virus-specific CD4+ T cells in chronic human infections is poorly understood. We performed genome-wide transcriptional analyses and functional assays of CD4+ T cells specific for human immunodeficiency virus (HIV) from HIV-infected people before and after initiation of antiretroviral therapy (ART). A follicular helper T cell (T_{FH} cell)-like profile characterized HIV-specific CD4+ T cells in viremic infection. HIV-specific CD4+ T cells from people spontaneously controlling the virus (elite controllers) robustly expressed genes associated with the T_H1, T_H17 and T_H22 subsets of helper T cells. Viral suppression by ART resulted in a distinct transcriptional landscape, with a reduction in the expression of genes associated with T_{FH} cells, but persistently low expression of genes associated with T_H1, T_H17 and T_H22 cells compared to the elite controller profile. Thus, altered differentiation is central to the impairment of HIV-specific CD4+ T cells and involves both gain of function and loss of function.

CD4+ T cell responses are critical for durable control of viral replication in chronic infections[1,2]. Virus-specific CD4+ T cell immunity is of particular interest for HIV infection, which is characterized by functional impairment and destruction of CD4+ T cells. While classical models divided CD4+ T cells into distinct lineages, studies have demonstrated the importance of CD4+ T cell plasticity[3]. Persistent antigen and inflammatory signals cause impairment of antigen-specific responses, a state called immune exhaustion. Virus-specific CD8+ T cell exhaustion has been extensively investigated[4] and represents a bona fide cell differentiation program. These studies highlighted the relevance of genome-wide transcriptional studies to understand T cell impairment[5]. Compared with CD8+ T cells, less is known on CD4+ T cell dysfunction. Murine lymphocytic choriomeningitis virus (LCMV)-specific CD4+ T cells in chronic infection, while exhibiting some characteristics shared with CD8+ T cells, also present distinct features[6,7], including loss of a T_H1 signature[5] and skewing towards a T_{FH} phenotype[8,9].

Whether findings in mice can be extrapolated to HIV infection in humans is unclear. Some features of virus-specific CD4+ T cells are shared between both infections: upregulation of co-inhibitory receptors are found in HIV progressors with ongoing viremia (chronic progressors) and chronic LCMV infection[5,10]. Rare subjects who spontaneously suppress HIV (elite controllers) frequently exhibit robust virus-specific T_H1 responses[11] and strong proliferative capacity, similarly to mice infected with the acute strain of LCMV. However, HIV and LCMV are distinct viruses and there are notable differences between species in terms of T cell differentiation mechanisms, such as T_{FH} generation[12]. An issue of critical clinical relevance is the lack of restoration of effective anti-HIV immunity after suppressive ART: viral rebound is the rule after cessation of therapy. Whether persistent HIV-specific CD4+ T cell dysfunction on ART contributes to this failed response is an important, yet unresolved, question. The paucity of experimental tools capable of identifying highly heterogeneous antigen-specific CD4+ T cells has hampered the study of HIV-specific CD4+ T cell help. Intracellular cytokine staining (ICS) assays are of limited sensitivity for many non-T_H1 effector functions, and the use of HLA class II tetramers in humans is constrained by availability, requirement for pre-defined epitopes and genetic diversity.

To determine key pathways and molecules that link HIV-specific T cell help to viral control, we here performed genome-wide transcriptional analyses and functional assays of HIV-specific CD4+ T cells from HIV-infected humans with diverse viral loads before ART initiation and followed a subgroup of them longitudinally after viral suppression on therapy.

Results

Links between HIV-specific CD4+ transcriptome profiles and viremia. To define molecular features that discriminate HIV-specific CD4+ T cells in progressive versus controlled infection, we performed a cross-sectional study of 38 chronically infected people who were untreated at the time of sampling. These included 'elite controllers' (ECs, HIV plasma viral load <50 viral RNA (vRNA) copies ml^{-1}), 'viremic controllers' (VCs, viral load

[1]Research Centre of the Centre Hospitalier de l'Université de Montréal, Montreal, Quebec, Canada. [2]Université de Montréal, Montreal, Quebec, Canada. [3]Center for HIV/AIDS Vaccine Immunology and Immunogen Discovery, La Jolla, CA, USA. [4]Canadian Centre for Computational Genomics—Montréal Node, Montreal, Quebec, Canada. [5]Human Immunology Section, Vaccine Research Center, NIAID, NIH, Bethesda, MD, USA. [6]Department of Immunology and Microbiology, The Scripps Research Institute, La Jolla, CA, USA. [7]Yerkes National Primate Research Center and Emory University, Atlanta, GA, USA. [8]Chronic Viral Illnesses Service and Division of Hematology, McGill University Health Centre, Montreal, Quebec, Canada. [9]Present address: University of Pennsylvania, Perelman School of Medicine, Philadelphia, PA, USA. *e-mail: daniel.kaufmann@umontreal.ca

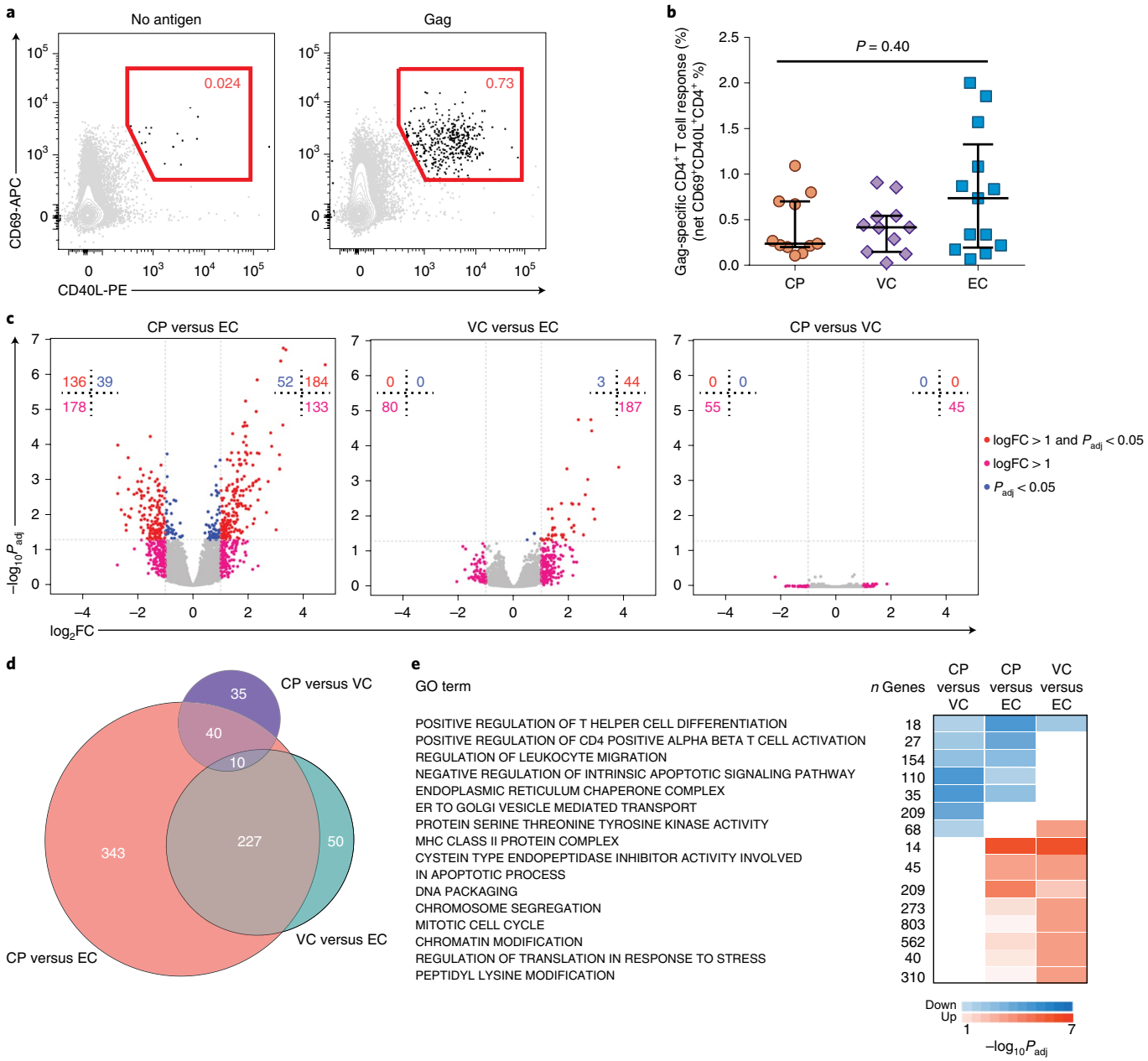

Fig. 1 | Deep coverage transcriptome analysis of HIV-specific CD4⁺ T cells from untreated HIV-infected people with distinct disease status. a, Representative flow cytometry plots from an EC of detection of HIV-specific CD4⁺ T cells by an AIM assay on the basis of co-upregulation of CD40L and CD69 9 h after stimulation with an HIV Gag peptide pool. **b**, Quantification of **a**. Comparison of net frequency (background of no antigen condition subtracted) of CD69⁺CD40L⁺ Gag-specific CD4⁺ T cells among the CP, VC and EC groups by Kruskal–Wallis test. Horizontal lines and bars represent median and ±interquartile range, respectively ($n = 11$ CPs, 11 VCs, 13 ECs). **c**, Paired volcano plot comparisons depicting DEGs as measured by microarray analysis of sorted HIV-specific CD4⁺ T cells in the three groups. Red, pink and blue dots represent DEG with $\log_2|\text{fold change (FC)}| > 1$ and $P_{adj} < 0.05$, $\log_2|\text{FC}| > 1$ or $P_{adj} < 0.05$, respectively. A two-sided moderated *t*-test followed by the Benjamini–Hochberg method correction was applied ($n = 11$ CPs, 9 VCs, 12 ECs). **d**, Euler diagrams of DEG between each pairwise comparison of the three groups of participants ($\log_2\text{FC} > 1$, $P < 0.05$); numbers represent DEGs. **e**, Top significant enriched gene ontology terms from the curated C5 MSigDB via two-sided CAMERA analysis. Blue, red and white color denote negative, positive or not significant (as defined by FDR < 0.05 by the Benjamini–Hochberg method), respectively.

between 50 and 5,000 copies ml^{-1}) and 'chronic progressors' (CPs, viral load ≥5,000 copies ml^{-1}) (for participant characteristics see Supplementary Table 1).

We utilized an activation-induced marker (AIM) assay to identify CD4⁺ T cells specific for the Gag protein (hereafter, termed HIV-specific CD4⁺ T cells). Ex vivo stimulated HIV-specific CD4⁺ T cells were identified by the co-upregulation of CD40L and CD69 on their surface after a 9-h stimulation with an HIV Gag peptide pool[13] (Fig. 1a and Supplementary Fig. 1a). Combining two markers enhanced detection of HIV-specific CD4⁺ T cells by reducing background compared to CD40L alone (Supplementary Fig. 1b,c). This AIM assay overcomes limitations of cytokine-based techniques for detection of virus-specific cells, allows live-cell sorting and captures a broader antigen-specific CD4⁺ T cell population (Supplementary Fig. 1d). There was no significant difference in the magnitude of HIV-specific CD4⁺ T cell responses among

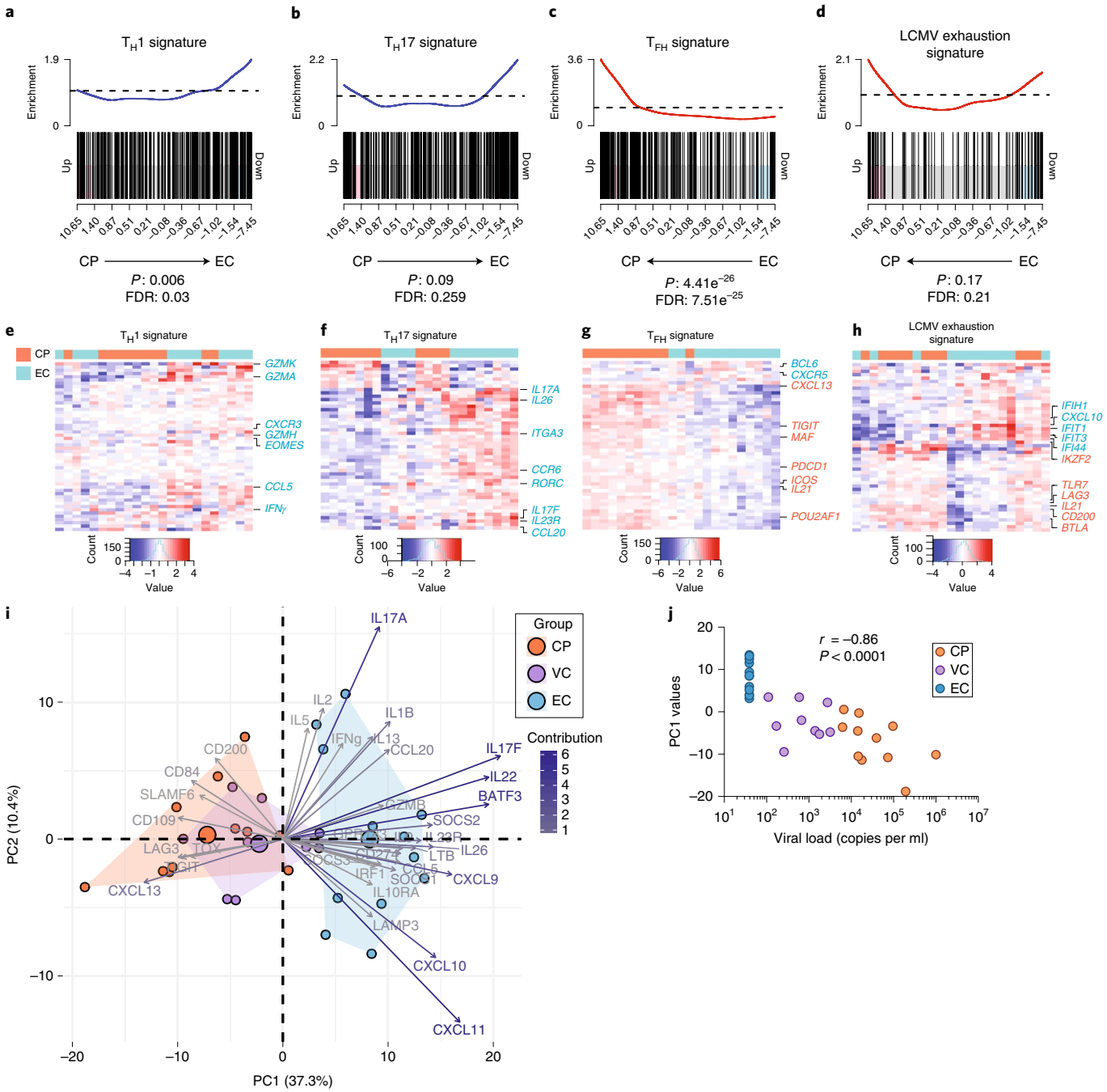

Fig. 2 | HIV-specific CD4⁺ T cell polarization is associated with level of viral control. a–d, Barcode plots of enriched helper T polarization and exhaustion gene sets by CAMERA in CP ($n=11$) versus EC ($n=12$) people. Red and blue lines denote positive and negative enrichment of CP genes versus EC, respectively. **a**, T_H1 signature: GSE59295 (T_H1 versus T_H2). **b**, T_H17 signature: GSE49703 (T_H17 versus T_H1). **c**, T_{FH} signature: GSE50391 ($CXCR5_{high}$ CD45RO versus $CXCR5_{neg}$ tonsil samples). **d**, LCMV exhaustion signature GSE41866 (LCMV Clone 13 D30 versus Armstrong D30-Exhausted versus Memory). Two-sided *P* value by CAMERA and FDR by Benjamini–Hochberg method. The arrows beneath the barcode plots depict the orientation of the enrichment between CP and EC. **e–h**, Heat maps of mRNA expression of the top 50 significant genes of each CD4⁺ T cell signature in CPs and ECs. Red and blue font of gene names denote upregulated and downregulated mRNA expression in CPs versus ECs, respectively. **i**, PCA representation of CPs ($n=11$), VCs ($n=9$) and ECs ($n=12$) on the basis of transcriptional expression of 90 genes associated with CD4⁺ T cell differentiation, effector functions and exhaustion. Transcriptional expression ($-\Delta Ct$ values) was evaluated by RT-qPCR (Fluidigm). The top 35 contributing genes are displayed and color-coded according to their contribution. Bigger dots represent the mean PC coordinates for each group. The numbers in parentheses stand for the percentage of variance that the PC accounts for. **j**, Correlation of PC1 values for each individual with viral load by two-tailed Spearman correlation ($n=11$ CPs, 9 VCs, 12 ECs).

cohorts or correlation with viremia or CD4 count (Fig. 1b and Supplementary Fig. 1e,f).

We reasoned that the AIM assay could reveal the transcriptome modulation in response to cognate antigen-mediated TCR signaling, reflecting the functional state of CD4⁺ T cells. We thus performed microarray analysis of sorted ex vivo stimulated HIV-specific CD4⁺ T cells. Pairwise comparisons between cohorts (Fig. 1c) revealed sets of differentially expressed genes (DEGs)

between all three cohorts, with extensive dissimilarities between CPs and ECs. Fewer transcriptional differences were detected between the VC and EC groups. The majority of DEGs between VCs and ECs were also observed in the CPs versus ECs comparison (Fig. 1d). CPs and VCs showed the fewest DEGs, suggesting that viremia strongly impacts the transcriptional landscape of HIV-specific CD4+ T cells.

We next used CAMERA (correlation adjusted mean rank gene set test)[14] enrichment analysis to investigate molecular mechanisms underlying HIV-specific T help alterations associated with disease status. We compared the identified DEGs to the Molecular Signatures Database (MSigDB) C5 collection of curated gene sets, which comprises the gene ontology (GO) terms associated with biological processes, molecular functions and cellular components (Fig. 1e). The 'Positive regulation of T helper cell differentiation' signature was negatively associated with viremia. Consistently, the 'Positive regulation of CD4+ αβ T cell activation' and 'Regulation of leukocyte migration' gene sets were significantly under-represented in CPs compared with both VCs and ECs, contrasting with upregulation of the MHC class II protein complex in CPs. Expression of genes associated with protein transport and/or processing was reduced in CPs. The pathways enriched with viremia included processes associated with chromatin modification, mitotic cell cycle, DNA packaging, chromosome segregation, response to stress and apoptosis.

This approach identifies potential pathways associated with HIV-specific CD4+ T cell dysfunction, and points to a central role for altered T cell differentiation, regulation and activation in this impairment.

HIV-specific CD4+ polarization is associated with disease status. Given the potential role for altered T cell differentiation in HIV-specific CD4+ T cell impairment, we determined features of CD4+ T cell differentiation associated with disease status. Using CAMERA we compared our sets of DEGs with human helper T polarization signatures from the C7 collection in the MSigDB and publicly available microarray datasets. While the different conditions used in the generation of these signatures (for example, activated versus unactivated cells) may complicate the interpretation of such associations, we observed notable differences among cohorts. Compared with CPs, ECs and VCs displayed enriched T_H1 and T_H17 signatures[15–17] (Fig. 2a,b,e,f, Supplementary Fig. 2a and Supplementary Tables 2–4). Cardinal genes associated with T_H17 cell differentiation and function were upregulated in ECs (Fig. 2f). In viremic people (CPs, VCs), we noted a striking enrichment of a T_{FH} signature[18] (Fig. 2c,g and Supplementary Fig. 2a) compared with ECs. There was congruent upregulation of several key T_{FH}-associated genes compared with ECs, with the notable exception of *BCL6*, which was instead upregulated in ECs (Fig. 2g and Supplementary Table 5). Although we did not observe a statistically significant enrichment of a LCMV-specific CD4+ T cell exhaustion signature[5] in CPs compared with ECs (Fig. 2d) (which might be due at least in part to the methodological differences), several of the DEGs enriched in CPs were well-known exhaustion-associated genes (Fig. 2h and Supplementary Table 6). Several interferon-stimulated genes upregulated in the LCMV model of exhaustion, such as *IFH1*, *IFIT3* and *IFI44*, were upregulated in ECs.

We next used real-time quantitative reverse transcription PCR (RT–qPCR) to further quantify levels of key DEGs identified by microarrays and selected additional CD4+ T cell genes. Principal component analysis (PCA) discriminated CPs from ECs, whereas there was more overlap between CPs and VCs (Fig. 2i). PC1 values significantly inversely correlated with viremia, showing that changes in the CD4+ T cell profile relate to antigen load (Fig. 2j). The RT–qPCR data were consistent with the microarray results (Supplementary Table 7). They confirmed that genes associated with T_{FH} functions and B cell help (*CXCL13*, *SLAMF6*, *CD84*) and exhaustion (*TIGIT*, *CD200*, *LAG3*, *TOX*) were enriched in CPs. This contrasted with genes related to T_H17 and T_H22 functions (*IL17F*, *IL22*) and the interferon-induced chemokines (*CXCL9*, *CXCL10*, *CXCL11*), which were enriched in ECs (Fig. 2i). Expression of selected transcription factors was consistent with these observations (Supplementary Fig. 2b): ECs expressed significantly more *TBX21* and *AHR* genes, respectively coding for T_H1 and T_H22 master transcription factors, and in ECs there was a trend for enhanced expression of *RORC*, a master transcription factor of T_H17 differentiation. The behavior of the master T_{FH} transcription factor *BCL6* contrasted to most T_{FH}-associated genes: *BCL6* was significantly upregulated in ECs compared to CPs in contrast to *MAF*, another transcription factor critical for T_{FH} differentiation, which was highly expressed in CPs. Helios (*IKZF2*), a transcription factor overexpressed in LCMV-specific CD4+ T cells in chronic infection, was also upregulated in CPs compared to ECs. Examining correlations between gene expression revealed positive and negative associations of genes, many not anticipated by classical dichotomic models of T_H differentiation. These results are consistent with a complex spectrum of differentiation and functional profiles of HIV-specific CD4+ T cells (Supplementary Fig. 2c,d).

These data show higher expression of a T_{FH}-like signature in HIV-specific CD4+ T cells in progressive infection, contrasting with enriched T_H1 and T_H17 signatures in subjects achieving spontaneous viral control.

Upregulation of classical T_{FH}-associated genes in $CXCR5_{neg}$ HIV-specific CD4+ of CPs. We next investigated whether the enrichment of the T_{FH} signature in HIV-specific CD4+ T cells of CPs compared to ECs was due to a higher fraction of HIV-specific circulating T_{FH} cells (cT_{FH}). We used the CD69/CD40L AIM assay to assess the percentages of HIV-specific $CXCR5^+CD45RA^-$ memory CD4+

Fig. 3 | An atypical T_{FH}-like transcriptional signature in $CXCR5_{neg}$ HIV-specific CD4+ T cells discriminates chronic progressors from elite controllers. **a**, Representative flow cytometry plots from a CP illustrating the enrichment of $CXCR5_{mem}$ ($CXCR5^+$ $CD45RA^-$) in $CD69^+CD40L^+$ Gag-specific CD4+ T cells versus total population in a CP subject, assessed 9 h after stimulation with a Gag peptide pool. **b**, Quantification from **a**. Comparison between CPs and ECs of the percentage of Gag-specific $CXCR5_{mem}$ assessed by flow cytometry (two-sided Mann–Whitney *U*-test) ($n = 10$ CPs and 10 ECs) (**b**) and the enrichment score of a T_{FH} tonsil signature (GSE50391) by ssGSEA (two-sided Mann–Whitney *U*-test) ($n = 11$ CPs and 12 ECs) (**c**). Bars represent the median ± interquartile range. **d**, Correlation of single-sample enrichment score for the T_{FH} tonsil signature with viral load by two-tailed Spearman test ($n = 11$ CPs, 9 VCs, 12 ECs). **e**, Volcano plots depicting differential gene expression between CP and EC among their live-sorted Gag-specific $CXCR5_{mem}$ or $CXCR5_{neg}$ subsets, by microarray analysis. Red and pink dots represent DEG with $\log_2|FC| > 1$ and $P_{adj} < 0.05$ or $\log_2|FC| > 1$, respectively, and the number of DEGs are displayed in the small tables. Two-sided moderated *t*-test followed by Benjamini–Hochberg correction method (P_{adj}) ($n = 5$ CPs and 3 ECs). **f**, CAMERA enrichment analysis of the tonsil T_{FH} signature of $CXCR5_{mem}$ or $CXCR5_{neg}$ Gag-specific CD4+ T cells of CPs compared to ECs ($n = 5$ CPs and 3 ECs). Two-sided *P* value by CAMERA and FDR by the Benjamini–Hochberg method. **g**, Comparison of expression of T_{FH} surface markers on $CXCR5_{mem}$ and $CXCR5_{neg}$ HIV-specific CD4+ T cells of CPs and ECs by flow cytometry ($n = 10$ CPs and 10 ECs). **h**,**i**, mRNA expression of T_{FH}-related surface markers (**h**) or transcription factors (**i**) by RT-qPCR (Fluidigm) ($n = 6$ CPs and 6 ECs) on sorted $CXCR5_{mem}$ and $CXCR5_{neg}$ HIV-specific CD4+ T cells of CPs and ECs. **g–i**, Two-tailed Mann–Whitney *U*-test or, for paired comparisons, by two-tailed Wilcoxon matched-pairs signed-ranked test were used to verify significance. Only $P < 0.05$ are displayed for clarity. Bars represent the median ± interquartile range.

T cells ($CXCR5_{mem}$) in both cohorts (Fig. 3a and Supplementary Fig. 3a,b). As PD-1 expression on HIV-specific $CD4^+$ T cells correlates with viremia[19], PD-1 was omitted as a T_{FH} marker to avoid bias towards CPs. We observed only a trend for higher fractions of HIV-specific $CXCR5_{mem}$ in CPs than in ECs, with considerable overlap between groups (Fig. 3b). In contrast, single-subject gene set enrichment analysis (ssGSEA) scores showed a significant enrichment of the T_{FH} signature in CPs compared with ECs (Fig. 3c), consistent with the cohort-based CAMERA analyses shown in Fig. 2c,g. The T_{FH} signature enrichment by ssGSEA correlated directly with viremia

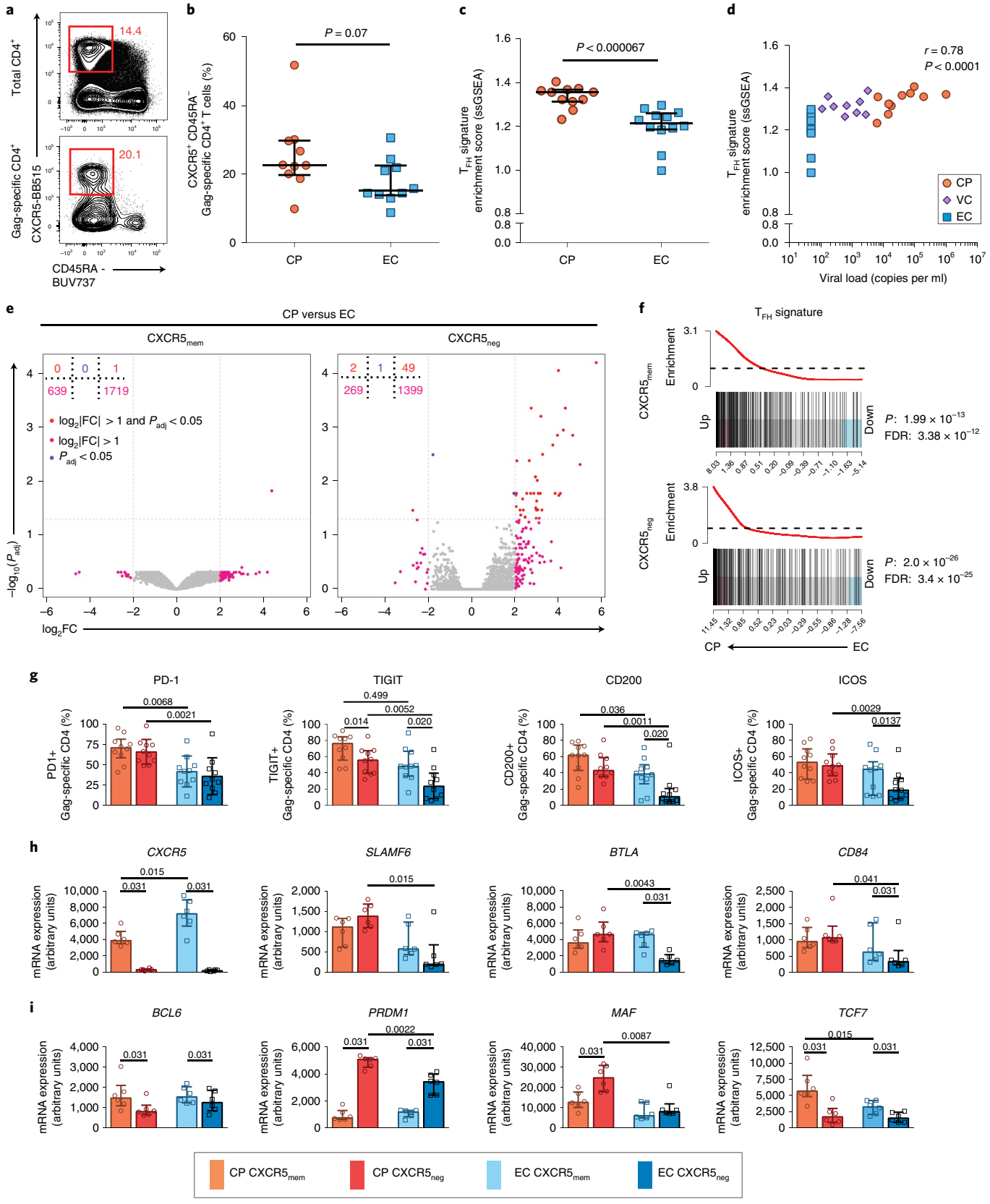

(Fig. 3d). These data suggest that differences in percentage of $CXCR5_{mem}$ alone are not sufficient to explain the markedly enriched T_{FH} signature observed in HIV-specific CD4+ T cells of CPs.

To define the cell subsets that contributed to the T_{FH} transcriptional signature observed in CPs, we applied microarray analysis to paired live-sorted subsets of $CXCR5_{mem}$ and $CXCR5_{neg}$ HIV-specific CD4+ T cells from CPs and ECs (Fig. 3e; gating strategy in Supplementary Fig. 3a). CXCR5 mRNA expression was consistent with protein expression (Fig. 3h). Differences in gene expression between CPs and ECs were more significant in the $CXCR5_{neg}$ than in the $CXCR5_{mem}$ subsets of HIV-specific CD4+ T cells (Fig. 3e). CPs displayed a marked enrichment of the T_{FH} signature not only in the $CXCR5_{mem}$ compartment, but also in the $CXCR5_{neg}$ HIV-specific CD4+ T cell subset (Fig. 3f). We confirmed expression of several markers classically associated with T_{FH} cells in $CXCR5_{mem}$ and $CXCR5_{neg}$ HIV-specific CD4+ T cells at the mRNA level by RT-qPCR or at the protein level by flow cytometry. Consistent with the microarray results, upregulation of the TCR co-receptors PD-1, TIGIT, CD200 and ICOS on $CXCR5_{neg}$ HIV-specific CD4+ T cells clearly differentiated CPs from ECs (Fig. 3g and Supplementary Fig. 3c). Surface markers *SLAMF6* and *CD84* (both associated with help to B cells) and *BTLA* (highly expressed in T_{FH} cells; Fig. 3h) were significantly higher in $CXCR5_{neg}$ CD4+ T cells of CPs compared with ECs, while the mRNA expression of *BCL6* and *TCF7* did not differ in $CXCR5_{neg}$ CD4+ T cells between the two groups. Transcriptional expression of *PRDM1* and *MAF* was significantly higher in $CXCR5_{neg}$ CD4+ T cells of CPs compared with ECs (Fig. 3i).

In contrast to ECs, CXCR5 expression in CPs did not clearly delineate cells with a T_{FH} transcriptional profile: *ICOS*, *SLAMF6*, *BTLA*, *CD84*, *TIGIT*, *CD200* and the T_{FH}-associated transcription factor *MAF* mRNA levels in $CXCR5_{neg}$ cells were equal or even superior to their $CXCR5_{mem}$ autologous counterparts (Fig. 3g–i and Supplementary Fig. 3c). These data demonstrate the atypical upregulation of the 'T_{FH}-like' signature in the $CXCR5_{neg}$ HIV-specific CD4+ T cells of CPs compared with ECs.

Robust expression of T_{FH} cytokines in $CXCR5_{neg}$ HIV-specific CD4+ of CPs. We next sought to elucidate if the enriched T_{FH} signature in $CXCR5_{mem}$ and $CXCR5_{neg}$ HIV-specific CD4+ T cells of CPs compared to ECs is congruent with the enhancement of some T_{FH} functions, and to determine the phenotype of these effector cells. We assessed mRNA expression of the T_{FH} cytokines CXCL13 and IL-21 at single-cell resolution using a sensitive flow cytometric RNA fluorescent in situ hybridization (RNA-flow-FISH) technique, as previously described[20,21]. This assay is superior to standard ICS for detection of IL-21-producing cells[20]. There were increased frequencies of *CXCL13* mRNA+ and *IL21* mRNA+ HIV-specific CD4+ T cells in CPs compared to ECs (Fig. 4a,b). This was a distinct feature of HIV-specific responses, as the expression after stimulation with the superantigen staphylococcal enterotoxin B (SEB) was similar in both cohorts (Fig. 4c) and cytomegalovirus (CMV) pp65-specific CD4+ T cells expressed less *CXCL13* and *IL21* than HIV-specific CD4+ T cells in paired comparisons within the same humans (Supplementary Fig. 4a). As CD40L is not expressed on all antigen-specific CD4+ T cells on activation, we confirmed that the differential expression of *CXCL13* and *IL21* between CPs and ECs holds true without combining the RNA-flow-FISH and AIM assays and without pre-gating on CD40L+ cells (Supplementary Fig. 4b–i). Largely distinct CD4+ T cell populations produced *CXCL13* and *IL21* mRNAs at the time point examined (Fig. 4d,e). We confirmed the increased CXCL13 production in CPs compared with ECs at the protein level by measuring CXCL13 concentration by ELISA in the supernatant of CD8-depleted peripheral blood mononuclear cells (PBMCs) after a 48-h stimulation with HIV Gag (Supplementary Fig. 5a). *CXCL13*+ and *IL21*+ cells expressed high levels of CXCR5 protein compared with total HIV-specific CD4+ T cells in ECs. In contrast, the levels of CXCR5 expression on *CXCL13*+ and *IL21*+ cell were comparable to the total population in CPs (Fig. 4f). This gain of T_{FH}-like functions by $CXCR5_{neg}$ HIV-specific CD4+ T cell in CPs was further apparent when we compared the ratios of *IL21*+ and *CXCL13*+ responses between the $CXCR5_{mem}$ and $CXCR5_{neg}$ subsets (Fig. 4g). As the inhibitory receptors PD-1 and TIGIT are markers of T_{FH} cells[12], and may also be associated with exhaustion, we examined their expression on *CXCL13* mRNA+ and *IL21* mRNA+ HIV-specific CD4+ T cells. The majority of these cytokine-expressing cells were PD-1+/TIGIT+, particularly in CPs (Fig. 4h,i and Supplementary Fig. 5b,c). Thus, the expression patterns of the inhibitory co-receptors PD-1 and TIGIT were consistent with T_{FH} skewing and may not imply exhaustion of these responses.

Finally, we explored possible links between HIV-specific CD4+ T cell help and antibody responses. We assessed plasma levels of p24-specific antibodies by ELISA and biolayer interferometry binding analysis. The results obtained by the two methods were highly correlated (Supplementary Fig. 5d). Although p24-specific antibody concentrations in the CP and EC groups were similar overall (Fig. 4j), we observed a significant correlation between the magnitude of HIV-specific CD4+ T cell responses and p24-specific

Fig. 4 | T_{FH} cytokine expression by $CXCR5_{neg}$ HIV-specific CD4+ T cells of chronic progressors. a, Representative RNA-flow-FISH plots from a CP of *CXCL13* and *IL21* mRNA in CD69+CD40L+ CD4+ T cells after a 15-h stimulation with a Gag peptide pool. Numbers represent the frequency of mRNA+ cells among (red) CD69+CD40L+ and (gray) total CD4+ T cells ($n=6$ CPs and 5 ECs). **b**,**c**, Quantification of **a**. Comparison of frequencies of *CXCL13* or *IL21* mRNA+ CD4+ T cells between CPs ($n=6$) and ECs ($n=5$) obtained as in **a** after Gag or SEB stimulation. Bars represent median frequencies ± interquartile range (two-tailed Mann–Whitney *U*-test). **d**,**e**, RNA-flow-FISH analysis of co-expression of *CXCL13* and *IL21* mRNA by Gag-specific CD4+ T cells with representative plots from CP and EC people (**d**) and related statistical analysis by permutation test (10,000 permutations) in SPICE ($n=6$ CPs and 5 ECs) (**e**). Pie slices represent median frequency of *CXCL13/IL21* mRNA+ subpopulations. **f**, Representative histograms from CP and EC people of CXCR5 expression on *CXCL13* or *IL21* mRNA+ HIV-specific CD4+ T cells overlaid on total HIV-specific CD4+ T cells (gray). Numbers represent the percentages of CXCR5+ cells within each cytokine+ population ($n=6$ CPs and 5 ECs). **g**, Statistical analysis on 6 CPs and 5 ECs of the ratios between the $CXCR5_{mem}$ to the $CXCR5_{neg}$ subsets of frequencies of cytokine or chemokine mRNA+ HIV-specific CD4+ T cells (*CXCL13*, *IL21*, *IL2* and *IFNγ*) as assessed by RNA flow cytometry. Bars represent median frequencies ± interquartile range (two-tailed Mann–Whitney *U*-test). **h**,**i**, Co-expression patterns of PD-1 and TIGIT (surface protein antibody labeling) on *CXCL13* mRNA+ or *IL21* mRNA+ Gag-specific CD4+ T cells identified by RNA-flow-FISH ($n=6$ CPs and 5 ECs). **h**, Representative examples of CP and EC people; cytokine/chemokine mRNA+ HIV-specific CD4+ T cells (red dots for CPs, blue dots for ECs) are overlaid on total HIV-specific CD4+ T cell subpopulations (gray dots). Numbers represent the percentages of *CXCL13* RNA+ or *IL21* mRNA+ HIV-specific CD4+ T cells located in each quadrant. **i**, SPICE analysis of PD-1 and TIGIT expression from **h** on *CXCL13* mRNA+ or *IL21* mRNA+ HIV-specific CD4+ T cells (permutation test, 10,000 permutations). Slices represent median frequency of PD-1 and TIGIT subpopulations. **j**, Comparison of p24-specific antibodies levels in plasma between CPs and ECs as assessed by ELISA. (two-tailed Mann–Whitney *U*-test ($n=12$ CPs and 13 ECs). Bars represent medians ± interquartile range. **k**–**m**, Correlation between p24-specific antibody levels measured by ELISA and frequencies of total HIV-specific CD4+ T cells (**k**); $CXCR5_{mem}$ HIV-specific CD4+ T cells (**l**) and $CXCR5_{neg}$ HIV-specific CD4+ T cells (**m**) assessed by the CD69/CD40L AIM assay after a 9-h stimulation with a Gag peptide pool (two-tailed Spearman test, $n=12$ CPs and 13 ECs).

antibodies, which was maintained when only the CP group was considered (Fig. 4k). There was no significant association between $CXCR5_{mem}$ responses and p24-specific antibodies (Fig. 4l). However, there was a significant correlation between $CXCR5_{neg}$ HIV-specific $CD4^+$ T cell frequencies and antibody responses in CPs, but not ECs (Fig. 4m), which might suggest that the $CXCR5_{neg}$ subset has helper T function to B cells in vivo.

These data demonstrate that dysregulated $CXCR5_{neg}$ HIV-specific $CD4^+$ T cells in progressive infection gain functions and phenotypic features classically attributed to T_{FH} cells.

Mucosal immunity-related cytokines in HIV-specific $CD4^+$ of ECs. As we observed an enriched T_H17 signature in HIV-specific $CD4^+$ T cells in ECs compared to CPs, we characterized the expression of

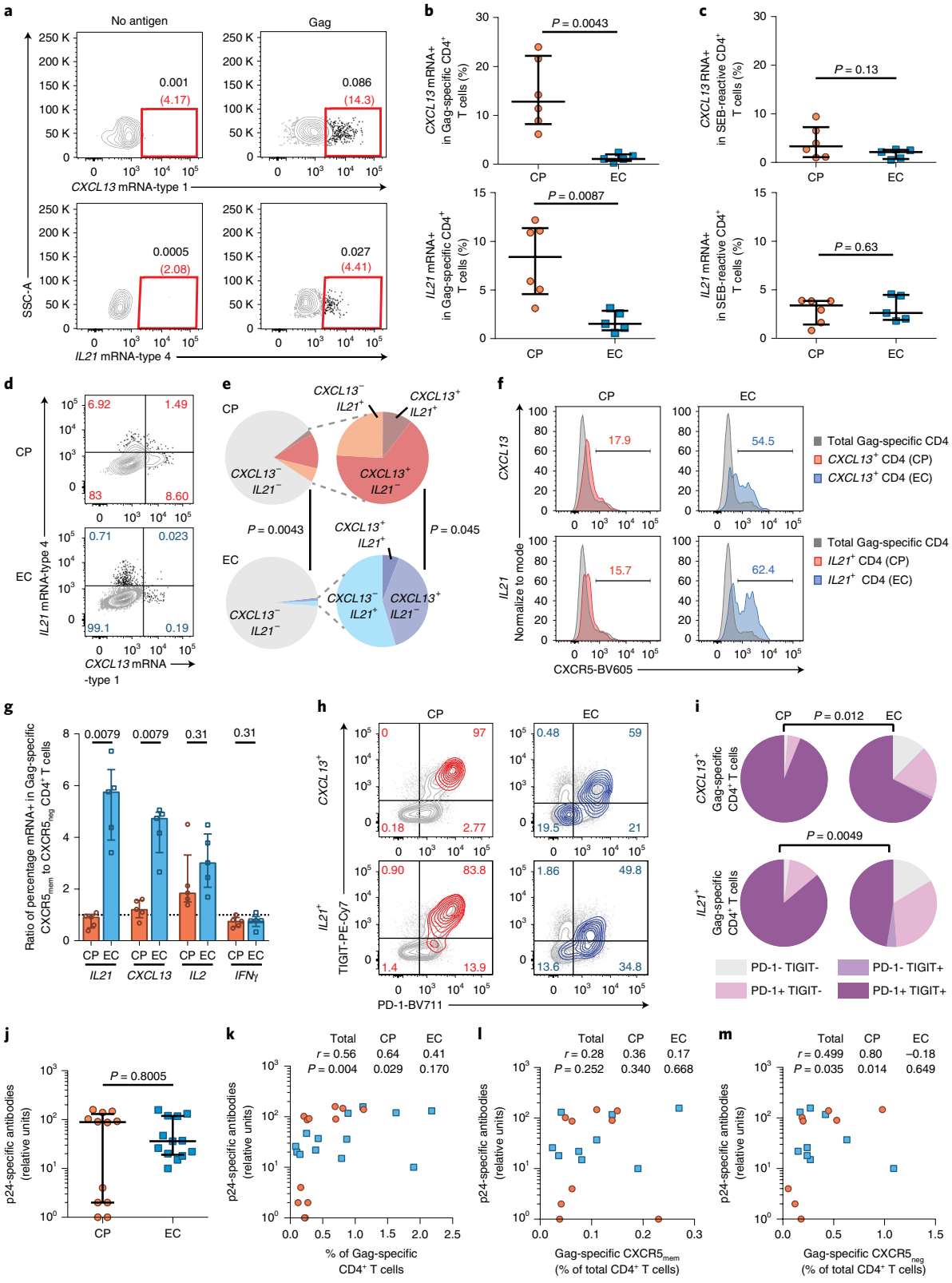

IL-17F and IL-22 at the single-cell level. RNA-flow-FISH enabled superior detection of these cytokines in HIV-specific CD4+ T cells compared with ICS (Fig. 5a,b). We observed more robust *IL17F* and *IL22* HIV-specific CD4+ T cell responses in ECs compared with CPs (Fig. 5c). In contrast, *IL17F* and *IL22* expression patterns in SEB- or CMV-activated CD4+ T cells did not differ between the groups (Fig. 5d and Supplementary Fig. 4a). We confirmed the strong IL-17F, IL-22 and IL-17A secretion by HIV-specific CD4+ T cells in ECs at the protein level, in contrast to low or undetectable production in CPs (Fig. 5e and Supplementary Fig. 5e–g).

The *IL17F* mRNA+ and *IL22* mRNA+ subsets constituted two partially overlapping, but mostly distinct, cell populations (Fig. 5f,g). In both CPs and ECs, these cells preferentially expressed CCR6, a chemokine receptor critical for recruitment of T_H17 and T_H22 cells to mucosal tissues (Fig. 5h). Expression of CXCR3, a marker of T_H1 cells also expressed on CD4+ T cells with mixed T_H1 and T_H17 properties that are expanded in some inflammatory diseases[17], was low on *IL17F* and *IL22* mRNA+ of both CPs and ECs (Fig. 5i and Supplementary Fig. 5h). Performing the RNA-flow-FISH without the AIM assay and CD40L+ pre-gating showed again contrasting patterns of *IL17F* and *IL22* expression between CPs and ECs (Supplementary Fig. 4b–i).

Systemic translocation of microbial products plays a critical role in immune activation related to HIV pathogenesis[22]. Loss of gut mucosal integrity and T_H17 cell depletion have been associated with immune activation and disease progression[23]. We thus investigated possible links between HIV-specific T_H17 and T_H22 responses and systemic immune activation. We observed an inverse correlation between *IL22* mRNA expression by HIV-specific CD4+ T cells and co-expression of the activation markers HLA-DR and CD38 on total CD4+ and CD8+ T cells (Fig. 5j and Supplementary Fig. 5i). We identified similar associations for *IL17F* (Fig. 5k and Supplementary Fig. 5j). We next investigated the relationship between preservation of *IL17*+ and/or *IL22*+ HIV-specific CD4+ T cells and microbial translocation by deep sequencing of cell-free RNA fragments in plasma—a reflection of the part of the body's microbiome that can access the circulation, the majority of which resides in the gut. The total levels of bacterial RNA reads in plasma did not significantly differ between the groups of CPs, ECs and uninfected control donors (UDs) (Fig. 5l). However, we observed a lower plasma bacterial RNA species diversity in CPs compared to the EC and UD groups (Fig. 5m). These observations may reflect low gut microbiome diversity, a state associated with systemic inflammation in several diseases[24] (Supplementary Fig. 5k, l). *IL22* and *IL17F* transcription in HIV-specific CD4+ T cells was significantly correlated with bacterial RNA species diversity (Fig. 5n,o). CPs and ECs qualitatively differed in the bacterial RNA profile, forming largely distinct clusters (Supplementary Fig. 5m). *IL22* and *IL17F* mRNA+ levels in HIV-specific CD4+ T cells inversely correlated with the prevalence of Proteobacteria, a phylum of Gram-negative bacteria that is increased in the gut microbiome in HIV-infected people[25] and has been proposed as a marker of dysbiosis[26] (Fig. 5p,q).

Thus, robust *IL22*+ and *IL17F*+ HIV-specific CD4+ T cells can be detected in the blood of ECs, while these responses are severely impaired in CPs. Associations of these deficiencies with systemic immune activation, reduced plasma bacterial RNA species diversity and a skewing towards greater Proteobacteria abundance, suggest that these findings in blood reflect perturbed gut homeostasis and a loss of protective mucosal immunity.

ART results in a distinct transcriptome of HIV-specific CD4+. Finally, we sought to determine whether the observed HIV-specific CD4+ T cell profiles were the consequences of ongoing viral antigen exposure, or the results of durable cell-fate decision programs that would persist after viral suppression on ART. We longitudinally followed a subgroup of eight CPs and analyzed a second sample obtained while on ART (for participant characteristics see Supplementary Table 8). Pairwise comparisons between the EC, CP pre-ART (CPpre) and CP post-ART (CPpost) cohorts (Fig. 6a,b) showed sets of DEGs between all three groups, with fewer differences in the CPpre versus CPpost and CPpost versus EC than the CPpre versus EC comparison, as might be expected. We next focused on selected GO terms and gene signatures that were identified as differentially expressed between CPs and ECs in Figs. 1 and 2. While initiation of ART in CPs modulated the activity of several pathways regulating apoptosis and gene expression towards the levels observed in EC, differences in the 'Positive regulation of T helper cell differentiation', 'Positive regulation of CD4+ αβ T cell activation' and 'Regulation of leukocyte migration' persisted (Fig. 6c). We therefore examined how ART affected helper T polarization signatures. Expression of the T_{FH} signature in HIV-specific CD4+ T cells was markedly reduced by ART, to levels similar to that found in ECs (Fig. 6d), while expression of the T_H1, T_H17 and LCMV exhaustion signatures was little affected by therapy: the differences clearly persisted between CPpost and EC (Fig. 6e,f and Supplementary Fig. 6a). Expression of selected individual genes of interest was also consistent with these findings when expression levels in EC were considered as references (Fig. 6g, Supplementary Fig. 6b and Supplementary Tables 9 and 10). While the results should be considered as trends, given the limited size

Fig. 5 | Increased expression of cytokines related to mucosal immunity in HIV-specific CD4+ T cells of elite controllers compared to chronic progressors. a,**b**, Representative flow cytometry plots depicting detection of *IL22* and *IL17F* in CD69+CD40L+ CD4+ T cells in one EC after stimulation with a Gag peptide pool by delayed ICS for cytokine protein and RNA-flow-FISH for cytokine mRNA, respectively. Numbers represent frequencies of mRNA+ HIV-specific CD4+ T cells among CD69+CD40L+ (blue) and total CD4+ T cells (gray) ($n=8$ CPs and 8 ECs). **c**,**d**, Statistical comparison from **a** of frequencies of cytokine mRNA+ CD4+ T cells between CPs and EC after a Gag peptide pool ($n=8$ CPs and 8 ECs) (**c**) or SEB stimulation ($n=6$ CPs and 8 ECs) (**d**). **e**, Statistical comparison of IL-22 and IL-17F protein levels detected by Luminex beads array in the supernatant of CD8-depleted PBMCs 48 h after stimulation with a Gag peptide pool ($n=8$ CPs and 8 ECs). Bars represent median ± interquartile range. *P* values by two-tailed Mann–Whitney *U*-test (**c**–**e**). **f**, Representative flow cytometry plots of co-expression patterns of *IL22* mRNA and *IL17F* mRNA in HIV-specific CD4+ T cells in CP and EC people ($n=6$ CPs and 6 ECs). **g**, Statistical analysis from **f** by SPICE (by permutation test, 10,000 permutations). Slices represent median frequency of *IL22*/*IL17F* mRNA+ subpopulations of HIV-specific CD4+ T cells ($n=6$ CPs and 6 ECs). **h**,**i**, Comparison of the frequencies of CCR6 and CXCR3 expression on *IL22* mRNA+ and *IL17F* mRNA+ HIV-specific CD4+ T cells compared to total HIV-specific CD4+ T cells in CPs ($n=6$) and ECs ($n=6$) by two-tailed Mann–Whitney *U*-test and by two-tailed Wilcoxon matched-pairs signed-ranked test. Only $P<0.05$ are displayed for clarity. Bars represent median with interquartile range. **j**,**k**, Correlation of *IL22* (**j**) and *IL-17F* (**k**) mRNA levels assessed by RT-qPCR on sorted HIV Gag-specific CD4+ T cells and ex vivo CD4+ T cell activation measured by HLA-DR and CD38 co-expression (two-tailed Spearman test; $n=10$ CPs, 6 VCs, 12 ECs). **l**,**m**, Statistical comparisons of microbial translocation in plasma of CP, EC and UD cohorts: quantitation of bacterial RNA reads in plasma (transcripts per million, TPM) (**l**); bacterial RNA species diversity (Shannon entropy score) (**m**) (Kruskal–Wallis test; $n=10$ CPs, 8 ECs and 6 UDs). Bars represent median ± interquartile range. **n**,**o**, Correlation between bacterial RNA species diversity in plasma and frequencies of HIV-specific *IL22*+ CD4+ T cells (**n**) and HIV-specific *IL17F*+ CD4+ T cells (**o**) (two-tailed Spearman test; $n=10$ CPs and 8 ECs). **p**,**q**, Correlation between abundance of Proteobacteria translocation and frequencies of HIV-specific *IL22*+ CD4+ T cells (**p**) and HIV-specific *IL17F*+ CD4+ T cells (**q**) (two-tailed Spearman test; $n=10$ CPs and 8 ECs).

of the cohorts, expression of some genes appeared corrected by ART (for example, *CXCL13*), whereas others are not restored (for example, *IL22*).

These data demonstrate that suppressive ART results in a transcriptional landscape of HIV-specific CD4+ T cells distinct from the profiles of both untreated CPs and ECs. We identified gene modules

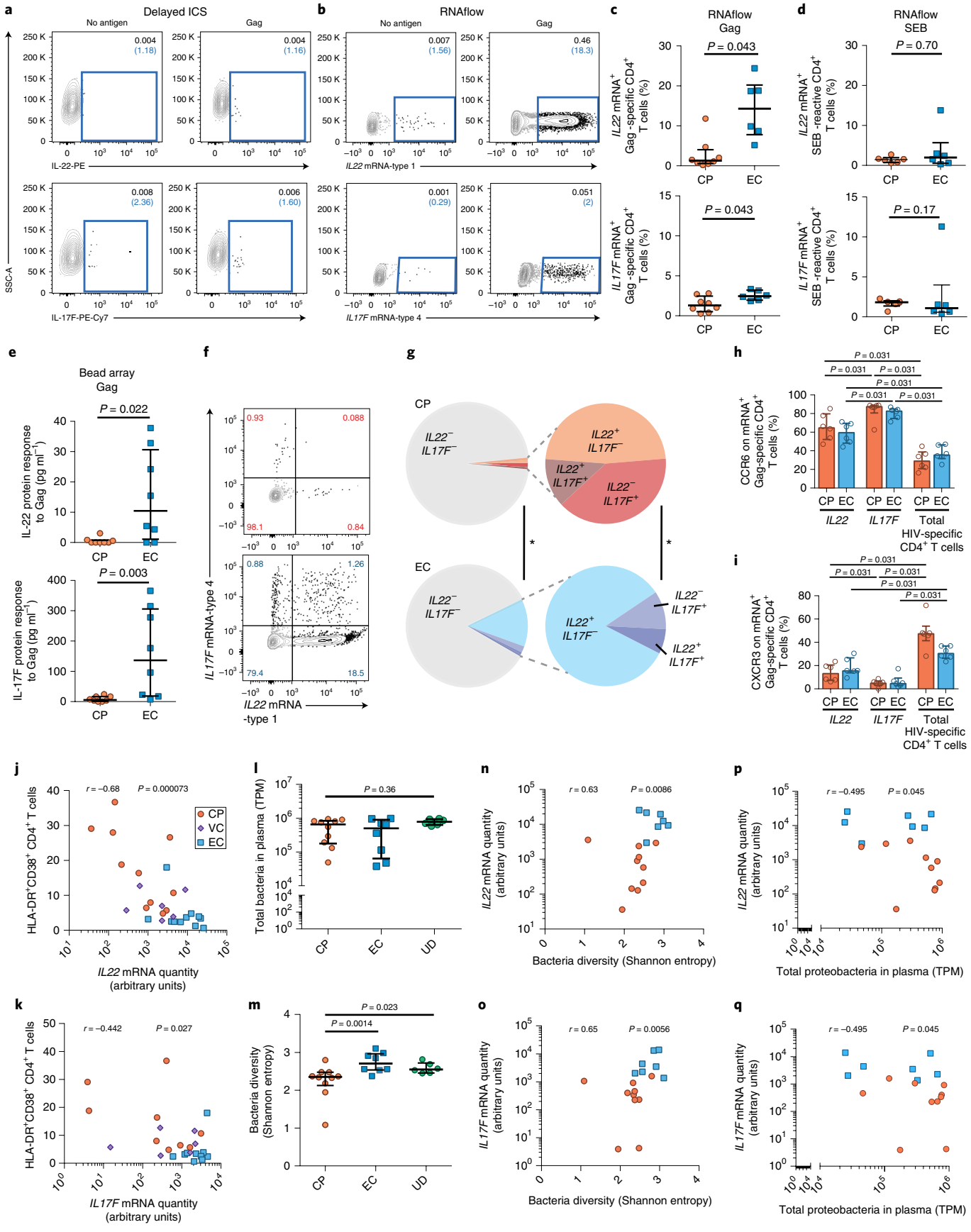

susceptible to manipulation of antigen load, while others were unresponsive to antiviral therapy alone.

Discussion

The molecular features of virus-specific CD4+ T cells associated with pathogen containment are poorly understood in chronic human infections. We used genome-wide transcriptional analyses following ex vivo stimulation with HIV antigen to uncover differences in HIV-specific CD4+ T cell differentiation and function in chronically infected humans with various viremia levels. An atypical enrichment of a T_{FH}-like signature in $CXCR5_{neg}$ HIV-specific CD4+ T cells characterized progressive infection. In contrast, elite control of viral replication was associated with robust HIV-specific T_H22 and T_H17 responses, which correlated negatively with immune activation and correlated positively with a greater diversity of bacterial RNA species in plasma and lower Proteobacteria abundance. None of these differences were detected in SEB or CMV pp65-reactive cells, revealing antigen-specific TCR signaling-driven processes. Suppressive ART in chronic progressors elicited a distinct HIV-specific CD4+ T cell transcriptome, revealing, in comparison to elite controllers, the presence of viremia-sensitive (for example, T_{FH} signature) and viremia-unresponsive (for example, T_H1, T_H17 and T_H22 signatures) gene modules. These data suggest that HIV-specific CD4+ T cell dysregulation does not represent a mere loss of helper T functions, as classically defined for immune exhaustion, but an adaptation to environmental cues combined with persistent changes, likely resulting from durable cell-fate decision programs.

At first sight, the marked T_{FH} signature[18] identified in CPs contrasts with the murine LCMV model, in which T_{FH} responses in chronic infection are critical for delayed viral control[8]. The extraordinary ability of HIV to generate escape mutations and elude autologous antibody neutralization likely contributes to these opposite associations between T_{FH} differentiation and disease outcome. A study showed that T_{FH} cells in chronic LCMV infection are capable of supporting generation of neutralizing antibody effective against the contemporaneous virus[9]. In contrast, the immune system lags behind the evolution of autologous HIV strains[27]. Kinetics of viral evolution in HIV infection may thus overcome the ability of adaptive T_{FH} skewing to contribute to delayed viral control. While technical limitations have so far hampered investigation of HIV-specific germinal center T_{FH} in lymph nodes, robust expansion of total germinal center T_{FH} populations was demonstrated in viremic HIV-infected people and simian immunodeficiency virus (SIV)-infected macaques, albeit with qualitative defects[28–31].

Genes classically associated with T_{FH} cells that are enriched in the $CXCR5_{neg}$ HIV-specific CD4+ T cells of CPs include *IL21* and *CXCL13*. HIV p24-specific antibody titers in plasma correlated with frequencies of $CXCR5_{neg}$ HIV-specific CD4+ T cells, suggesting that these responses may provide help to B cells in vivo. Studies in murine models have shown that $CXCR5^{-/-}$ CD4+ T cells are able to take over some helper B functions[32,33], resulting in the generation of low-affinity binding antibodies[9]. Acquisition of T_{FH}-like properties by $CXCR5_{neg}$ CD4+ T cells has also been reported in rheumatoid arthritis[34] and cancer[35] and combines B help function with migration to inflamed tissues. These analogies suggest shared pathways of CD4+ T cell differentiation between diverse diseases associated with chronic inflammation.

Damage to the gut mucosa with associated microbial translocation[22] and increased inflammatory properties of the enteric microbiota[36] are major drivers of HIV-associated chronic inflammation. We observed that HIV-specific T_H17 and T_H22 responses were abundant in ECs and rare in CPs. IL-17F and IL-17A are closely related cytokines recruiting neutrophils to sites of inflammation. IL-22 promotes intestinal barrier function[37] and supports complement-mediated elimination of pathobionts[38]. Lack of HIV-specific T_H17 and T_H22 responses was associated with CD4+ and CD8+ T cell activation and a reduced diversity of translocated bacterial RNA in plasma, with over-representation of Proteobacteria. These results are consistent with studies in SIV infection showing preferential translocation of Proteobacteria compared to other phylums from the gut lumen into tissues, resulting in enhanced immune activation[39]. Our data do not establish causal links between features of HIV-specific CD4+ T cells and microbial translocation. It is more likely that both the lack of HIV-specific T_H17/T_H22 responses and the altered translocated microbiome result from persistent insults to the gastrointestinal tract. The paucity of HIV-specific IL-17+ and IL-22+ CD4+ T cells observed in CPs may result from high susceptibility of T_H17 and T_H22 subsets to HIV infection[37,40] and/or alteration of CD4+ T cell differentiation[41]. Together with the analysis of bacterial RNA fragments in plasma, these CD4+ T cell data suggest that studies of peripheral blood can provide useful insight into the systemic consequences of perturbed gut homeostasis. Probiotic and IL-21 therapy in ART-treated SIV-infected macaques was associated with enhanced polyfunctional T_H17 expansion and reduced markers of microbial translocation and dysbiosis compared to ART alone[42]. It will be important to determine whether such interventions restore HIV-specific CD4+ T cell profiles.

This work raises questions that will need to be addressed in further studies. AIM assays require activation to enable cell identification. While we believe that analyzing the transcriptional profile modulated by TCR signaling is highly relevant for analysis of T cell responses, it will be important to investigate other populations of HIV-specific CD4+ T cells that do not co-upregulate CD69 and CD40L, for example, by other AIM markers or by tetramers. Experiments in animal models will be required to define the ontogeny of $CXCR5_{neg}$ CD4+ T cells with T_{FH}-like features and whether they transitioned through a bona fide T_{FH} stage during their development. Longitudinal studies from the time of acute infection may identify events in the genesis or persistence of HIV-specific CD4+ T cell dysregulation. Investigations of human gut and lymph node biopsies, while challenging, would define the relationships between features of HIV-specific CD4+ T cells in blood and other anatomical compartments.

In summary, this work identifies extensive alterations in HIV-specific CD4+ T cell transcriptional profiles and demonstrates that

Fig. 6 | Distinct transcriptional imprint with reduction in T_{FH}-associated gene expression but poor correction of T_H1, T_H17 and T_H22 gene levels after suppression of viremia by ART. a, Paired volcano plot comparisons depicting DEGs as measured by microarray analysis of sorted HIV-specific CD4+ T cells in 8 CPs before and after ART and 12 ECs. Red, pink and blue dots represent DEG with $\log_2|FC|>1$ and $P_{adj}<0.05$, $\log_2FC>1$ or $P_{adj}<0.05$, respectively. Moderated two-sided *t*-test followed by Benjamini–Hochberg method. **b**, Euler diagrams of DEG between each pairwise comparison of the three groups of participants ($\log_2|FC|>1$, $P<0.05$); numbers represent DEGs. **c**, Significant enriched gene ontology terms from the curated C5 MSigDB via CAMERA analysis. Blue, red and white color denote negative, positive or not significant (as defined by FDR < 0.05), respectively. Two-sided *P* value by CAMERA and FDR by Benjamini–Hochberg method. **d**–**f**, Barcode plots of enriched helper T polarization gene sets by CAMERA in paired comparisons between the three groups ($n=8$ CPpre, 8 CPpost and 12 EC). Red and blue lines denote positive and negative enrichment, respectively. T_H1 signature: GSE59295 (T_H1 versus T_H2), T_H17 signature: GSE49703 (T_H17 versus T_H1), T_{FH} signature: GSE50391 ($CXCR5_{high}$ CD45RO versus $CXCR5_{neg}$ tonsil samples). Two-sided *P* value by CAMERA and FDR by Benjamini–Hochberg method. **g**, Differential expression of genes associated with CD4+ T cell differentiation and function in HIV-specific CD4+ T cells of CPs before and after treatment compared to ECs. Red and purple denote logarithmic fold change for comparisons CPpre versus EC and CPpost versus EC, respectively, by microarray analysis in 8 CP before/after ART and 12 ECs.

skewed lineage differentiation is a key feature of altered CD4+ T cell help in the setting of high viral load, in which atypical gain of function is combined with classical exhaustion features. The data also reveal distinct features of HIV-specific CD4+ T cells after successful ART. The identified molecular features may therefore help direct selective interventions to improve immune function. Given the paucity of

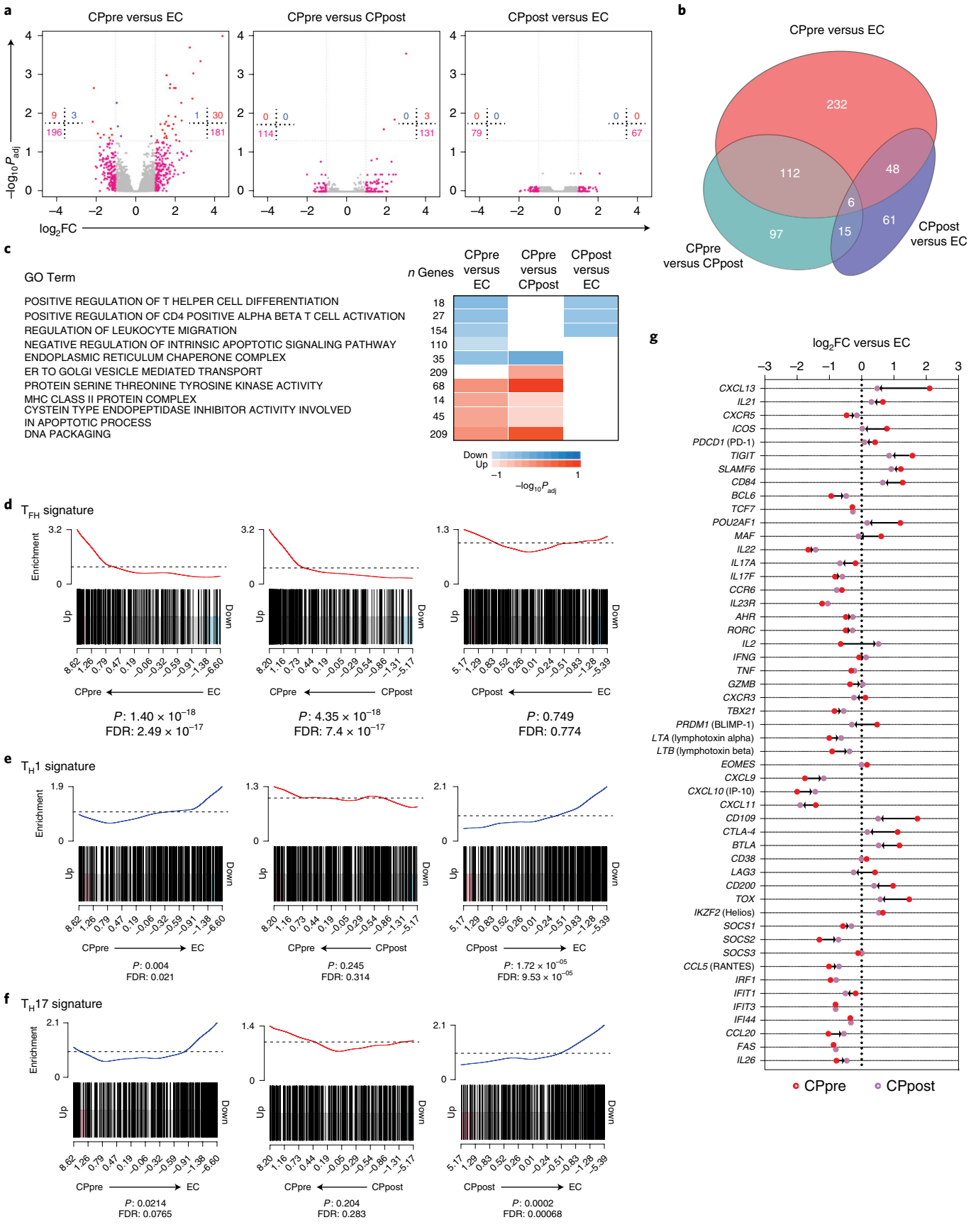

transcriptome datasets available on pathogen-specific CD4+ T cells in humans, our results will also provide useful benchmark comparisons for other infectious diseases and vaccine-induced responses.

Online content

Any methods, additional references, Nature Research reporting summaries, source data, statements of code and data availability and associated accession codes are available at https://doi.org/10.1038/s41590-019-0418-x.

Received: 7 August 2018; Accepted: 3 May 2019;
Published online: 15 July 2019

References

1. Laidlaw, B. J., Craft, J. E. & Kaech, S. M. The multifaceted role of CD4(+) T cells in CD8(+) T cell memory. *Nat. Rev. Immunol.* **16**, 102–111 (2016).
2. Swain, S. L., McKinstry, K. K. & Strutt, T. M. Expanding roles for CD4+ T cells in immunity to viruses. *Nat. Rev. Immunol.* **12**, 136–148 (2012).
3. O'Shea, J. J. & Paul, W. E. Mechanisms underlying lineage commitment and plasticity of helper CD4+ T cells. *Science* **327**, 1098–1102 (2010).
4. Wherry, E. J. & Kurachi, M. Molecular and cellular insights into T cell exhaustion. *Nat. Rev. Immunol.* **15**, 486–499 (2015).
5. Crawford, A. et al. Molecular and transcriptional basis of CD4+ T cell dysfunction during chronic infection. *Immunity* **40**, 289–302 (2014).
6. Morou, A., Palmer, B. E. & Kaufmann, D. E. Distinctive features of CD4+ T cell dysfunction in chronic viral infections. *Curr. Opin. HIV AIDS* **9**, 446–451 (2014).
7. Vella, L. A., Herati, R. S. & Wherry, E. J. CD4+ T cell differentiation in chronic viral infections: the Tfh perspective. *Trends Mol. Med.* **23**, 1072–1087 (2017).
8. Fahey, L. M. et al. Viral persistence redirects CD4 T cell differentiation toward T follicular helper cells. *J. Exp. Med.* **208**, 987–999 (2011).
9. Greczmiel, U. et al. Sustained T follicular helper cell response is essential for control of chronic viral infection. *Sci. Immunol.* **2**, eaam8686 (2017).
10. Kaufmann, D. E. et al. Upregulation of CTLA-4 by HIV-specific CD4+ T cells correlates with disease progression and defines a reversible immune dysfunction. *Nat. Immunol.* **8**, 1246–1254 (2007).
11. Ferre, A. L. et al. HIV controllers with HLA-DRB1*13 and HLA-DQB1*06 alleles have strong, polyfunctional mucosal CD4+ T-cell responses. *J. Virol.* **84**, 11020–11029 (2010).
12. Crotty, S. T follicular helper cell differentiation, function, and roles in disease. *Immunity* **41**, 529–542 (2014).
13. Reiss, S. et al. Comparative analysis of activation induced marker (AIM) assays for sensitive identification of antigen-specific CD4 T cells. *PLoS ONE* **12**, e0186998 (2017).
14. Wu, D. & Smyth, G. K. Camera: a competitive gene set test accounting for inter-gene correlation. *Nucleic Acids Res.* **40**, e133 (2012).
15. Ono, C. et al. Fluorescently activated cell sorting followed by microarray profiling of helper T cell subtypes from human peripheral blood. *PLoS ONE* **9**, e111405 (2014).
16. Zhang, W. et al. Effector CD4+ T cell expression signatures and immune-mediated disease associated genes. *PLoS ONE* **7**, e38510 (2012).
17. Ramesh, R. et al. Pro-inflammatory human Th17 cells selectively express P-glycoprotein and are refractory to glucocorticoids. *J. Exp. Med.* **211**, 89–104 (2014).
18. Locci, M. et al. Human circulating PD-1+CXCR3−CXCR5+ memory Tfh cells are highly functional and correlate with broadly neutralizing HIV antibody responses. *Immunity* **39**, 758–769 (2013).
19. Porichis, F. et al. Responsiveness of HIV-specific CD4 T cells to PD-1 blockade. *Blood* **118**, 965–974 (2011).
20. Porichis, F. et al. High-throughput detection of miRNAs and gene-specific mRNA at the single-cell level by flow cytometry. *Nat. Commun.* **5**, 5641 (2014).
21. Baxter, A. E. et al. Multiparametric characterization of rare HIV-infected cells using an RNA-flow FISH technique. *Nat. Protoc.* **12**, 2029–2049 (2017).
22. Brenchley, J. M. et al. Microbial translocation is a cause of systemic immune activation in chronic HIV infection. *Nat. Med.* **12**, 1365–1371 (2006).
23. Favre, D. et al. Critical loss of the balance between Th17 and T regulatory cell populations in pathogenic SIV infection. *PLoS Pathog.* **5**, e1000295 (2009).
24. Levy, M., Kolodziejczyk, A. A., Thaiss, C. A. & Elinav, E. Dysbiosis and the immune system. *Nat. Rev. Immunol.* **17**, 219–232 (2017).
25. Vujkovic-Cvijin, I. et al. Dysbiosis of the gut microbiota is associated with HIV disease progression and tryptophan catabolism. *Sci. Transl. Med.* **5**, 193ra191 (2013).
26. Shin, N. R., Whon, T. W. & Bae, J. W. Proteobacteria: microbial signature of dysbiosis in gut microbiota. *Trends Biotechnol.* **33**, 496–503 (2015).
27. Richman, D. D., Wrin, T., Little, S. J. & Petropoulos, C. J. Rapid evolution of the neutralizing antibody response to HIV type 1 infection. *Proc. Natl Acad. Sci. USA* **100**, 4144–4149 (2003).
28. Petrovas, C. et al. CD4 T follicular helper cell dynamics during SIV infection. *J. Clin. Invest.* **122**, 3281–3294 (2012).
29. Cubas, R. A. et al. Inadequate T follicular cell help impairs B cell immunity during HIV infection. *Nat. Med.* **19**, 494–499 (2013).
30. Lindqvist, M. et al. Expansion of HIV-specific T follicular helper cells in chronic HIV infection. *J. Clin. Invest.* **122**, 3271–3280 (2012).
31. Perreau, M. et al. Follicular helper T cells serve as the major CD4 T cell compartment for HIV-1 infection, replication, and production. *J. Exp. Med.* **210**, 143–156 (2013).
32. Miyauchi, K. et al. Protective neutralizing influenza antibody response in the absence of T follicular helper cells. *Nat. Immunol.* **17**, 1447–1458 (2016).
33. Kahan, S. M., . & Zajac, A. J. Late arising T follicular helper cells cultivate the B cell crop during chronic infections. *Sci. Immunol.* **2**, eaap9339 (2017).
34. Rao, D. A. et al. Pathologically expanded peripheral T helper cell subset drives B cells in rheumatoid arthritis. *Nature* **542**, 110–114 (2017).
35. Gu-Trantien, C. et al. CD4+ follicular helper T cell infiltration predicts breast cancer survival. *J. Clin. Invest.* **123**, 2873–2892 (2013).
36. Neff, C. P. et al. Fecal microbiota composition drives immune activation in HIV-infected Individuals. *EBioMedicine* **30**, 192–202 (2018).
37. Kim, C. J. et al. A role for mucosal IL-22 production and Th22 cells in HIV-associated mucosal immunopathogenesis. *Mucosal Immunol.* **5**, 670–680 (2012).
38. Hasegawa, M. et al. Interleukin-22 regulates the complement system to promote resistance against pathobionts after pathogen-induced intestinal damage. *Immunity* **41**, 620–632 (2014).
39. Klase, Z. et al. Dysbiotic bacteria translocate in progressive SIV infection. *Mucosal Immunol.* **8**, 1009–1020 (2015).
40. El Hed, A. et al. Susceptibility of human Th17 cells to human immunodeficiency virus and their perturbation during infection. *J. Infect. Dis.* **201**, 843–854 (2010).
41. Favre, D. et al. Tryptophan catabolism by indoleamine 2,3-dioxygenase 1 alters the balance of TH17 to regulatory T cells in HIV disease. *Sci. Transl. Med.* **2**, 32ra36 (2010).
42. Ortiz, A. M. et al. IL-21 and probiotic therapy improve Th17 frequencies, microbial translocation, and microbiome in ARV-treated, SIV-infected macaques. *Mucosal Immunol.* **9**, 458–467 (2016).

Acknowledgements

We thank J. Girouard, the clinical staff at the McGill University Health Centre in Montreal, the Ragon/MGH clinical and technical staff and all study participants for their invaluable role in this project; B. Walker for providing clinical samples; D. Gauchat and the CRCHUM Flow Cytometry Platform for technical assistance; N. Hamel and McGill University and Génome Québec Innovation Centre for microarray analysis; and J. Boss and S. Crotty for their input on this manuscript. The following reagent was obtained through the NIH AIDS Reagent Program, Division of AIDS, NIAID, NIH: HIV-1 IIIB p24 Recombinant Protein from ImmunoDX, LLC. This study was supported by the National Institutes of Health grants (no. HL092565 to D.E.K.; no. AI100663 CHAVI-ID to D.E.K. and R.T.W. (Consortium PI: D. Burton); nos. OD011103 and OD011132 to R.P.J.); the Canadian Institutes for Health Research grants (nos. 137694 and 152977 to D.E.K.; no. MOP-93770 to C.T.; and foundation no. 352417 to A.F.); the Canada Foundation for Innovation Program Leader grant (no. 31756 to D.E.K.); and the FRQS AIDS and Infectious Diseases Network. This work was funded in part by the Intramural Program of the National Institutes of Health (D.C.D., S.D.). D.E.K. and C.T. are supported by Senior Research Scholar Awards of the Quebec Health Research Fund (FRQS). J.-P.R. is the holder of the Louis Lowenstein Chair in Hematology & Oncology, McGill University. A.F. is a Canada Research Chair on Retroviral Entry.

Author contributions

A.M. and D.E.K. designed the studies. A.M., E.B.-R., R.C., N.B., S.A., G.G.-L., L.Y. and P.A.R. performed experiments. M.D. provided input on manuscript content and data representation. A.M., E.M., S.D. and F.L. performed bioinformatics analyses. K.N.-M., J.N., A.E.B., J.M.B., R.P.J., R.T.W., A.F. and D.C.D. provided technical expertise. C.T. and J.-P.R. obtained institutional review board approval and managed study participant recruitment. A.M. and D.E.K. interpreted the data and wrote the paper with all co-authors' assistance.

Competing interests

The authors declare no competing interests.

Additional information

Supplementary information is available for this paper at https://doi.org/10.1038/s41590-019-0418-x.

Reprints and permissions information is available at www.nature.com/reprints.

Correspondence and requests for materials should be addressed to D.E.K.

Publisher's note: Springer Nature remains neutral with regard to jurisdictional claims in published maps and institutional affiliations.

Methods

Participants and samples. Leukapheresis were obtained from study participants at the Montreal General Hospital, Montreal, Canada; at the Centre Hospitalier de l'Université de Montréal, Montreal, Canada; and at Massachusetts General Hospital, Boston, USA. The study was approved by the respective institutional review boards, written informed consent obtained from all participants before enrollment and PBMC samples obtained by leukapheresis. Samples were collected between 2013 and 2018. Subject characteristics are summarized in Supplementary Table 1. 'Chronic progressors' (CPs) were defined as people with a viral load of more than 5,000 vRNA copies per ml of plasma; 'viremic controllers' (VCs) were defined as people with more than 50 and less than 5,000 vRNA per ml plasma; and 'elite controllers' (ECs) were defined as subjects who spontaneously controlled viremia to below 50 RNA copies per ml plasma in the absence of therapy. CPs, VCs and ECs were either treatment naïve or untreated for at least 3 months. Eight CPs were followed longitudinally and a second sample was obtained at least 6 months after initiation of ART therapy and suppression of viral loads below 50 copies ml^{-1} (Supplementary Table 8). PBMCs were isolated by the Ficoll density gradient method and stored in liquid nitrogen.

Antibodies. For details of antibodies used, see Supplementary Tables 11–20 and descriptions of use below. In all cases, antibodies are monoclonal and raised in mice unless otherwise stated. All antibodies are commercially available, were validated by the suppliers and titrated using biological and/or isotype controls.

CD40L/CD69 AIM assay for live-cell sorting of HIV Gag-specific $CD4^+$ T cells. Cryopreserved PBMCs were thawed and rested at 37 °C for 3 h. Cells were aliquoted into wells of a 24-well plate, at a total of 15×10^6 cells per well in RPMI medium supplemented with 10% Human AB (HAB) serum and Pen-Strep. For each assay, we used a no exogenous stimulation (No Ag) condition as control and an HIV-specific stimulation with an overlapping peptide pool corresponding to HIV Gag (JPT, PM-HIV-Gag ULTRA) or HCMVA pp65 (JPT, PM-PP65) at a final concentration of 0.5 μg ml^{-1} per peptide. A CD40 blocking antibody (Miltenyi Biotec, clone HB14) was added to each well 15 min before stimulation at a final concentration of 0.5 μg ml^{-1}. Following a 9-h stimulation, the cells were stained for 30 min at 4 °C before live-cell sorting on a FACS Aria cell sorter (BD BioSciences) equipped for handling of biohazardous material. Two panels of antibodies were used to isolate live-cells subsets according to combinations of surface markers. In the first panel for isolation of total $CD69^+CD40L^+$ Gag-specific $CD4^+$ T cells, PBMCs were stained as indicated in Supplementary Table 11. The gating strategy for cell sorting is illustrated in Supplementary Fig. 1. In the second panel used for isolation of $CXCR5_{mem}$ and $CXCR5_{neg}$ subsets of $CD69^+CD40L^+$ Gag-specific $CD4^+$ T cells, PBMCs were stained as indicated in Supplementary Table 12. The gating strategy for cell sorting is illustrated in Supplementary Fig. 3. The FACS Aria was operated at 70 pounds per square inch with a 70-μm nozzle. For all populations, 5,000 cells were collected directly into RLT lysis buffer (Qiagen).

Phenotyping of Gag-specific $CD4^+$ T cells identified by the CD69/CD40L AIM assay. PBMCs were thawed and plated in 24-well plates at 10×10^6 cells ml^{-1} in RPMI + 10% HAB Serum (HAB) and rested for 3 h at 37 °C. Before stimulation, CD40 blocking antibody was added directly into culture at a final concentration of 0.5 μg ml^{-1}, as well as antibodies against CXCR5, CCR6 and CXCR3. Cells were incubated for 15 min, then left unstimulated or stimulated either with an overlapping peptide pool corresponding to HIV Gag (JPT, PM-HIV-Gag ULTRA), at a final concentration of 0.5 μg ml^{-1} per peptide, or with staphylococcal enterotoxin B (SEB) as a positive control (1 μg ml^{-1}). Cells were stimulated for 9 h, collected and stained for 30 min at 4 °C with the antibodies in Supplementary Table 13. Cells were washed, fixed for 20 min in 2% paraformaldehyde, washed and resuspended in 1% FCS/PBS for flow acquisition on a five-laser LSR II flow cytometer (BD BioSciences).

Phenotyping of immune activation markers. PBMCs were thawed and rested overnight at 37 °C. The next day, cells were washed and stained with viability dye (20 min at 4 °C) and surface markers (20 min at 4 °C) (Supplementary Table 14). Fluorescence minus one staining was used to define the cut-off for positivity. Cells were washed, fixed for 1 h in 2% paraformaldehyde, washed and resuspended in 1% FCS/PBS for flow acquisition on a five-laser LSR II flow cytometer (BD BioSciences).

Standard ICS for cytokine measurements. PBMCs were incubated for 6 h with an HIV Gag peptide pool at a concentration of 0.5 μg ml^{-1} per peptide in the presence of 2.5 μg ml^{-1} brefeldin A (BD GolgiPlug) and (0.3 μl ml^{-1}) monensin (BD GolgiStop). For delayed ICS assays, 2.5 μg ml^{-1} brefeldin A (BD GolgiPlug) and (0.3 μl ml^{-1}) monensin (BD GolgiStop) were added 9 h after stimulation with the Gag peptide pool, and cells were cultured for an additional 12 h. Unstimulated cells were used as negative control and SEB (0.5 μg ml^{-1}) as positive control. Cells were then stained with viability dye (20 min at 4 °C), surface markers (20 min at 4 °C), fixed with Fixation Solution (eBioscience) and stained for intracellular proteins in permeabilization 1× buffer (eBioscience) (30 min at 4 °C) as described in Supplementary Tables 15 and 16. Cells were acquired on an LSR II flow cytometer (BD Biosciences).

Gene expression analysis. *Whole-transcriptome analysis by microarrays.* Total RNA was purified using the RNeasy Plus Micro Kit (Qiagen). RNA integrity was assessed using a 2100 Bioanalyzer (Agilent Technologies). Sense-strand complementary DNA was synthesized from total RNA using a fixed volume of 3 μl. Fragmentation and labeling were performed to produce single strand DNA (ssDNA) with the Applied Biosystems GeneChip WT Pico Terminal Labeling Kit according to manufacturer's instructions (Applied Biosystems). After fragmentation and labeling, 5 μg DNA target was hybridized on GeneChip Clariom D, human (ThermoFisher Scientific) and incubated at 45 °C in the Genechip Hybridization oven 640 (Affymetrix) for 17 h at 60 r.p.m. GeneChips were then washed in a GeneChips Fluidics Station 450 (Affymetrix) using Applied Biosystems Hybridization Wash and Stain kit according to the manufacturer's instructions (Applied Biosystems). The microarrays were finally scanned on a GeneChip scanner 3000 (Affymetrix).

Validation of transcriptional expression by Fluidigm. Total RNA was purified using the RNeasy Plus Micro Kit (Qiagen). cDNA was synthesized using all RNA available (or 1–5 ng) with the High-Capacity Reverse Transcription Kit with RNase Inhibitor (Life Technologies) (25 °C for 10 min, 37 °C for 120 min, 85 °C for 5 min). cDNA equivalent to 1,000 sorted cells was subjected to gene-specific preamplification using TaqMan PreAmp MasterMix (Applied Biosystems) and 96 pooled TaqMan Assays (Applied Biosystems) (Supplementary Tables 21–23) diluted 1:5 (95 °C for 10 min, followed by 16 cycles of 95 °C for 15 s and 60 °C for 4 min). The preamplified cDNA was diluted fivefold in DNA suspension buffer (Teknova) and was mixed with TaqMan Universal PCR Master Mix (Life Technologies) and 20X GE sample loading reagent (Fluidigm). 20X TaqMan assays were diluted 1:1 with 2X assay loading buffer (Fluidigm). Taqman assay mixtures were loaded onto a primed 96.96 Dynamic Array chip (Fluidigm). The chip was loaded into the IFC Controller, where each sample was mixed with each assay in every possible combination. The chip was transferred in a Biomark (Fluidigm) for real-time PCR amplification and fluorescence acquisition using single probe (FAM-MGB, reference: ROX) settings and the default hot-start protocol with 40 cycles. Cycle thresholds (Ct) were calculated using the Fluidigm Biomark software v.1.4.2.

Combined cytokine/chemokine mRNA-flow-FISH and protein-staining assays. For experiments combining the AIM assay with mRNA-flow-FISH, PBMCs were either left unstimulated or were stimulated with an HIV Gag peptide pool (JPT) or SEB for 15 h. A CD40 blocking antibody (Miltenyi Biotec, clone HB14) was added 15 min prior to stimulation at a final concentration of 0.5 μg ml^{-1}. For experiments evaluating mRNA expression without CD40 blocking antibody, PBMCs were stimulated for 12 h. After stimulation, cells were stained with a viability dye (20 min, 4 °C, Fixable LiveDead, eBioscience) and then surface markers were labeled (30 min, 4 °C) with antibodies (see panels in Supplementary Tables 17–20). Samples were next subjected to the PrimeFlow RNA assay (Affymetrix/eBioscience/ThermoFisher) for specific mRNA detection as per manufacturer's instructions. All buffers and fixation reagents were provided with the kit, with the exception of flow cytometry staining buffer (2% FBS/PBS). After fixation and permeabilization, cytokine/chemokine mRNAs were labeled with sets of probe pairs, as listed in Supplementary Tables 17–20. The probes were diluted 1:5 in diluent and hybridized to the target mRNA for 2 h at 40 °C. Samples were washed to remove excess probes and stored overnight in the presence of RNAsin. Signal amplification was achieved as previously described[20] by sequential 1.5-h, 40 °C incubations with the preamplification and amplification mix. Amplified mRNA was labeled with fluorescently tagged probes for 1 h at 40 °C. A negative control probe and a positive control probe (against house-keeping gene *RPL13A*) were included in each experiment. Gates were set on the unstimulated control where appropriate or scrambled probes. Samples were acquired on an LSR II (BD Bioscience) or a BD LSRFortessa (experiments without CD40 blocking antibody). Analysis was performed using FlowJo (Treestar, v.10) and SPICE v.5.35 software.

Measurements of cytokine secretion by beads arrays and ELISA. One million CD8 T cell-depleted PBMCs (Dynabeads CD8, StemCell) were incubated with an HIV Gag peptide pool (1 μg ml^{-1} per peptide) or left unstimulated and incubated at 37 °C in RPMI supplemented with 10% HAB and Pen-Strep. Cytokine secretion in supernatants was measured 48 h after stimulation on a Luminex beads array platform, as previously described[19,20]. Measurements were performed in duplicates using the Human High Sensitivity Cytokine Premixed Kit B (R&D Systems) for IL-17A and IL-22 or for IL-17F on a Bio-plex 200 array system (Bio-Rad Laboratories) as per manufacturer's instructions. CXCL13 was measured separately with the Human CXCL13 Quantikine ELISA Kit (R&D Systems), as per manufacturer's instructions.

Measurement of p24-specific antibodies by ELISA. The anti-p24 ELISA was performed as follows: 96-well plates (Thermo Scientific Nunc, FluoroNunc/LumiNunc, MaxiSorp Surface) were coated with 0.1 μg ml^{-1} of recombinant p24 (NIH, catalog no. 12028) or BSA (Bioshop, catalog no. ALB001.100) in PBS

overnight at 4 °C. Plates were blocked for 90 min at room temperature (RT) with blocking buffer (TBS, Tween 0.1%, BSA 2%) and then washed four times with washing buffer (TBS, Tween 0.1%). Dilutions of human sera (1/1,000, 1/3,000, 1/6,000) or rabbit anti-HIV p24 antiserum (NIH, catalog no. 4250) in washing buffer containing 0.1% of BSA were incubated for 2 h at RT. Plates were washed four times with washing buffer before incubation for 90 min at RT with HRP-conjugated secondary antibodies: goat anti-human IgG HRP (Invitrogen, catalog no. 31413) or anti-IgG rabbit HRP (Invitrogen, catalog no. 31462). Plates were then washed four times with washing buffer before revealing with standard enhanced chemiluminescence reagent (Perkin Elmer, NEL105001EA) with a TriStar luminometer (LB 941, Berthold Technologies).

Plasma microbiome sequencing. Circulating total RNA and DNA were isolated from frozen plasma using RNAzolBD (MRCgene) according to the manufacturer's recommendations. After RNA fragmentation and reverse transcription using random hexamers, the obtained transcripts, as well as the isolated plasma DNA, were individually incorporated into barcoded cDNA libraries on the basis of the Illumina TruSeq platform. Libraries were validated by microelectrophoresis, quantified, pooled and clustered on Illumina patterned flow cells. Clustered flow cells were sequenced on an Illumina HiSeq 4000 in 75-base paired reads.

Gene expression data analysis. *Microarrays.* The preprocessing of the microarray data was done in R (v.3.3.3, ref. [43]) using the oligo package (v.1.38.0, ref. [44]). Specifically, the CEL files were loaded in R and the rma function was applied for background subtraction, normalization and summarization. Quality control was performed by inspecting various diagnostic plots of the intensity distribution and correlation structure of control and regular probes. After review of the QC plots, three outliers were removed. Combat (sva package v.3.30.1) has been applied for batch normalization of samples using four replicates as reference for the normalization. The normalized data were used for the subsequent subanalyses CPpre versus EC, CPpre versus CPpost and CPpost versus EC.

Differential expression. Differential analysis of gene expression was done by the R package limma[45]. Using the lmFit function, a linear model was fit to each gene separately. Moderated *t*-tests were performed between each group. *P* values were adjusted using the Benjamini–Hochberg method for multiple test correction.

CAMERA. T_H1 signature (GSE59295; T_H1 versus T_H2) was available in the C7 collection of MSigDB. The T_H17 signature (GSE49703; T_H17 versus T_H1), T_{FH} signature (GSE50391; CXCR5high CD45RO versus $CXCR5^-$ tonsil samples) and LCMV exhaustion signature (GSE41866; LCMV Clone 13 D30 versus Armstrong D30-Exhausted versus Memory) were created using the GEO2R online tool (https://www.ncbi.nlm.nih.gov/geo/geo2r/). For each signature, a gene-set test was performed using the camera function from the limma package, accounting for intergene correlation.

Venn diagrams were created using the online tool Eulerr.co (R package v.4.1.0, https://cran.r-project.org/package=eulerr)[46]. Unsupervised hierarchical clustering was performed using the in heatmap2 function in R[43] on relative signal intensity values applying the Euclidean distance metric and complete linkage clustering method. Barcode plots were generated with the barcodeplot function from the limma package.

RT–qPCR results. Analysis of the RT–qPCR data obtained on the microfluidic platform was carried out using GenEx software (MultiD Analyses: http://www.multid.se). Five endogenous control genes were included in the Fluidigm run and the stability of endogenous control genes across all experimental samples was evaluated applying the NormFinder algorithm[47] in GenEx. The mean expression of the most stable endogenous control genes was used for normalization and calculation of $-\Delta Ct$ values. PCA, biplots and correlograms were created using the prcomp, fviz_pca_biplot and corrplot functions, respectively, in R programming language.

Statistical analyses of flow cytometry, beads array and RT–qPCR results. Statistical analyses were performed using Prism v.6.0 (GraphPad) using non-parametric tests. Two-group comparisons were performed using the Mann–Whitney *U*-test and pairwise comparisons were performed using the Wilcoxon matched-pair test. For comparisons between three groups, Kruskal–Wallis or Friedman one-way analysis of variance with Dunn's post-test was used. Permutation test (10,000 permutations) was applied for pie-chart comparison using the SPICE software. For correlations, Spearman's *R* correlation coefficient was applied. Statistical tests were two-sided and $P < 0.05$ were considered significant.

Bioinformatic analysis of deep-sequencing results of cell-free RNA fragments in plasma. Raw, paired-end Illumina reads were first trimmed for low quality bases and adapter contamination with Trimmomatic[48]. As a first pass to remove host-derived sequences, trimmed reads were first aligned against the HG38 genome with Bowtie 2 (ref. [49]) and then aligned to HG38 transcriptome with the splice aware aligner, STAR[50]. Unaligned paired-end reads were then assembled into contigs using Trinity[51]. Trinity contigs were then aligned against HG38 again to further remove host-derived sequences with $BLAST^+$ (ref. [52]). Remaining contigs were then aligned against the NCBI nucleotide database[53] and quantified with Salmon[54]. Taxonomic information was assigned for each contig and TPM values were collapsed at the species level for each sample for downstream analysis. TPM values for each sample were collapsed on the genus taxonomic level and Morisita–Horn dissimilarity indexes were calculated on a pairwise basis using the R package vegan[55]. The pairwise dissimilarity matrix was then clustered and the heat map was produced with gplots[56].

Reporting Summary. Further information on research design is available in the Nature Research Reporting Summary linked to this article.

Data availability

Microarray data generated during the current study were deposited in the Gene Expression Omnibus public depository with the accession number GSE128297 for the SuperSeries, and the following accession numbers for the Subseries: GSE129872 (HIV-specific $CD4^+$ T cells samples from CPs, VCs and ECs), GSE128280 (CXCR5mem and CXCR5neg HIV-specific $CD4^+$ T cells from CPs and ECs), GSE128296 (HIV-specific $CD4^+$ T cells samples from CPs before/after ART and ECs). mRNA expression data by high-throughput RT–qPCR are available in the Supplementary Material. All the datasets that support the findings of this study are available from the corresponding author upon reasonable request.

References

43. R Core Team. *R: a language and environment for statistical computing* (R Foundation for Statistical Computing, 2014).
44. Carvalho, B. S. & Irizarry, R. A. A framework for oligonucleotide microarray preprocessing. *Bioinformatics* **26**, 2363–2367 (2010).
45. Ritchie, M. E. et al. limma powers differential expression analyses for RNA-sequencing and microarray studies. *Nucleic Acids Res.* **43**, e47 (2015).
46. Larsson, J. eulerr: area-proportional Euler and Venn diagrams with ellipses. R package version 4.1.0. (2018).
47. Andersen, C. L., Jensen, J. L. & Orntoft, T. F. Normalization of real-time quantitative reverse transcription-PCR data: a model-based variance estimation approach to identify genes suited for normalization, applied to bladder and colon cancer data sets. *Cancer Res.* **64**, 5245–5250 (2004).
48. Bolger, A. M., Lohse, M. & Usadel, B. Trimmomatic: a flexible trimmer for Illumina sequence data. *Bioinformatics* **30**, 2114–2120 (2014).
49. Langmead, B. & Salzberg, S. L. Fast gapped-read alignment with Bowtie 2. *Nat. Methods* **9**, 357–359 (2012).
50. Dobin, A. et al. STAR: ultrafast universal RNA-seq aligner. *Bioinformatics* **29**, 15–21 (2013).
51. Grabherr, M. G. et al. Full-length transcriptome assembly from RNA-Seq data without a reference genome. *Nat. Biotechnol.* **29**, 644–652 (2011).
52. Altschul, S. F., Gish, W., Miller, W., Myers, E. W. & Lipman, D. J. Basic local alignment search tool. *J. Mol. Biol.* **215**, 403–410 (1990).
53. O'Leary, N. A. et al. Reference sequence (RefSeq) database at NCBI: current status, taxonomic expansion, and functional annotation. *Nucleic Acids Res.* **44**, D733–D745 (2016).
54. Patro, R., Duggal, G., Love, M. I., Irizarry, R. A. & Kingsford, C. Salmon provides fast and bias-aware quantification of transcript expression. *Nat. Methods* **14**, 417–419 (2017).
55. Oksanen, J. et al. vegan: community ecology package. R package version 2.4-3 (2017).
56. Warnes, G. et al. gplots: various R programming tools for plotting data. R package version 3.0.3 (2005).

Trends in Molecular Medicine

CellPress REVIEWS

Spotlight

Targeting Mitochondria to Revive Dysfunctional Regulatory T Cells

Elsa Brunet-Ratnasingham,[1,2] Mathieu Dubé,[1] and Daniel E. Kaufmann[1,3,*]

Immunometabolism is important to T cell dysfunction in chronic infections. A recent publication in *The Journal of Clinical Investigation* (2018;128:5083–5094) [1] shows reduced mitochondrial fitness in regulatory CD4$^+$ T cells (Tregs) of patients with HIV and failed immune restoration on antiretroviral therapy (ART). This defect can be reversed by IL-15, revealing a new immunotherapy target for regulatory T cell restoration.

HIV-Mediated Immune Dysfunction Also Affects Regulatory CD4$^+$ T Cells

T helper CD4$^+$ T cells provide key signals to other immune cell types and, therefore, are strongly implicated in the orchestration of effective immunity. Whereas most CD4$^+$ T cell subsets have a stimulatory role, Tregs instead inhibit T cell activation and proliferation to limit immunopathology and mediate self-tolerance. Reduced Treg frequency or function is linked to immune dysfunction. Alternatively, aberrant ratios between other CD4$^+$ T cell subsets and Tregs can also result in immunopathology. A recent publication by Younes *et al.* [1] describes a dysfunctional state of Tregs that may have a role in the inability of some patients with HIV to normalize their CD4$^+$ T cell counts despite suppression of viremia on ART.

Immune Nonresponders Have Increased Cycling CD4$^+$ T cells, but Reduced Tregs

During HIV infection, CD4$^+$ T cell populations are depleted in various anatomic compartments, contributing to the increased susceptibility of infected individuals to opportunistic infections and non-AIDS-related comorbidities. By arresting viral replication, ART initiation allows the reconstitution of blood CD4$^+$ T cell counts in a biphasic fashion: a first quick increase in circulating CD4$^+$ T cells is thought to be the result of lymphocyte egress out of lymphoid tissues, where they were retained due to high inflammation; the second, slower increase is due to CD4$^+$ T cell homeostatic proliferation and thymic generation of new naive CD4$^+$ T cells. In most individuals, these mechanisms allow near-normalization of blood CD4$^+$ T cell counts. A fraction of patients, called immune nonresponders (INRs), fail to reconstitute CD4$^+$ T cell counts, a phenotype associated with increased non-AIDS-related comorbidities, such as cardiovascular disease, cancer, osteoporosis, and neurocognitive dysfunction [2]. Intriguingly, compared with immune responders (IR), INRs present an uncommonly high proportion of cycling CD4$^+$ T cells that do not appear to effectively replenish the CD4$^+$ T cell compartment [2].

The relationships between the increased systemic inflammation, high frequency of cycling CD4$^+$ T cells, and inability to normalize CD4$^+$ T cell counts in INR remain to be elucidated. To address this question, Younes *et al.* used a surrogate surface marker that allows sorting of unfixed cycling CD4$^+$ T cells (CD71) instead of the classical intracellular Ki67, a protein selectively expressed in the nuclei of proliferating cells, and compared their transcriptomic profile in IRs, INRs, and healthy controls (HC). Cells from INRs showed a reduced Treg signature, lower expression of FOXP3-upregulated genes and diminished production of TGF-β, all indicative of lower Treg activity. These findings were attributed to lower frequencies of Tregs in the cycling subset of CD4$^+$ T cells in INRs compared to IRs. Although it is known that Tregs expand following HIV infection both in number and relative frequency, their role remains controversial: Tregs may be beneficial in that they reduce systemic activation, yet detrimental if they reduce the effectiveness of the HIV-specific T cell response [3].

IL-15 Can Resolve Regulatory T Cell Mitochondrial Dysfunction and Apoptosis

Younes *et al.* observed that, as well as the reduced Treg signature, cycling CD4$^+$ T cells in INRs were characterized by the upregulation of apoptotic genes; *in vitro* experiments confirmed a profound loss of viability of these cells. The authors next turned to mitochondrial metabolism, given its role in cell survival. A series of elegant transcriptomic and flow cytometry analyses provided evidence that impairment of mitochondrial oxidative phosphorylation (OXPHOS; Box 1), a critical pathway for Treg development and maintenance [4,5], was a central component of this defect. Consistent with the observed apoptosis signature in cycling CD4$^+$ T cells, the inability of dysfunctional mitochondria to fuel proliferation may condemn Tregs or other cycling CD4$^+$ T cells to cell death, impeding further the reconstitution of CD4$^+$ T cell counts in INRs.

Finally, Younes *et al.* tested *in vitro* an intervention that has a therapeutic potential in humans: because IL-15 enforces the use of OXPHOS and fatty acid oxidation (FAO) in memory CD8$^+$ T cells [6], the authors assessed whether this cytokine could also restore mitochondrial fitness in the cycling Tregs from INRs. Incubation of Tregs from INRs with IL-15 corrected the mitochondrial mass, OXPHOS potential, and levels of PGC1a and TFAM, the latter two of which are mitochondria-related regulators of biogenesis and OXPHOS, respectively. These changes were associated with completion of the stalled cell cycling and sustained proliferation. Whether IL-15 exposure allows

Box 1. Different Metabolic Pathways Fuel CD4+ T Cell Subsets

The relative importance of metabolic pathways differs with the maintenance and functional differentiation of CD4+ T cell lineages [4,5] (Figure I). CD4+ T cell subsets with inflammatory functions (Th1, Th2, and Th17) require ATP and biosynthetic molecules to proliferate and perform effector functions. These effector CD4+ T cells primarily use glycolysis in the cytoplasm, where glucose is taken up and used for ATP, but, more importantly, to provide metabolites for the pentose phosphate pathway (PPP) (synthesis of growth molecules and control of oxidative stress) and fatty acid synthesis (FAS) (*de novo* lipid synthesis necessary for cell growth). Tregs are more flexible and can use fatty acid oxidation (FAO), where fatty acids are trafficked to the mitochondria for processing, then utilized in the tricarboxylic acid cycle (TCA). Derivatives from both these pathways are utilized by the electron transport chain (ETC) to generate ATP in a process called OXPHOS. Finally, amino acid metabolism (AAM) regroups anabolic and catabolic pathways of amino acids and is implicated in an array of survival, growth, activating, or inhibiting functions. Shared fuel substrates and metabolites result in a complex interplay between these different pathways.

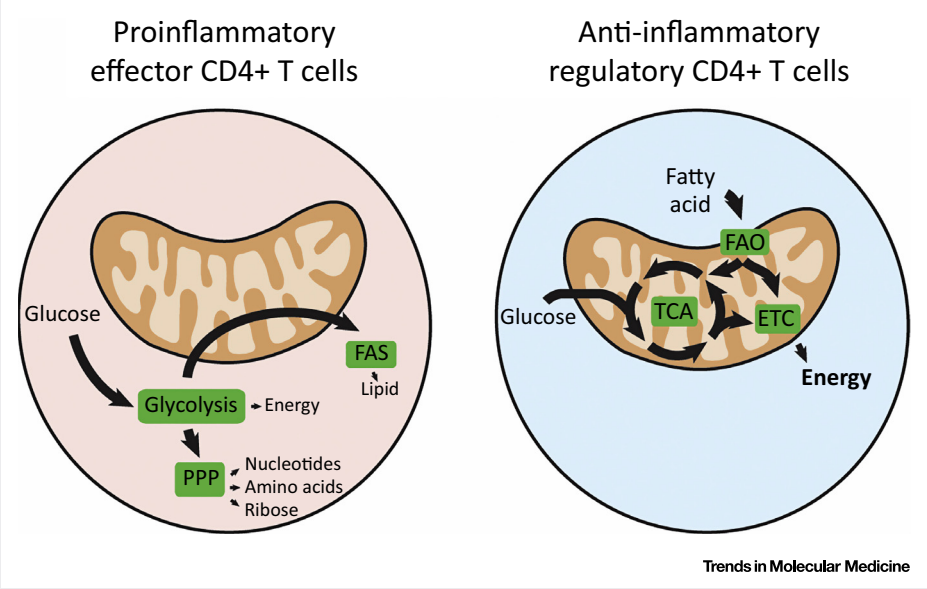

Figure I. The Metabolism of Regulatory T Cells (Tregs) Differs from That of Proinflammatory CD4+ T Cells. Proinflammatory CD4+ T cells tend to primarily use glycolysis to generate energy and metabolites. By contrast, Tregs are more flexible, and can use the more energetically efficient fatty acid oxidation (FAO) pathway. Abbreviations: ETC, electron transport chain; FAS, fatty acid synthesis; PPP, pentose phosphate pathway; TCA, tricarboxylic acid cycle.

restoration of other aspects of Treg dysfunction, for example TGF-β production, or impacts non-Treg cycling CD4+ T cells are interesting future directions for research. Indeed, stimulating IL-15 treatment in animal models of HIV infection resulted in the increased proliferation of CD4+ T cells [7], but whether this intervention leads to a lasting increase in CD4+ T cells and/or potential modulation of their phenotype remain to be addressed.

Concluding Remarks

The potential clinical relevance of this study is underlined by the current lack of satisfactory therapy for patients who are INRs, in whom no additional intervention has shown consistent benefit beyond ART alone. IL-15 and some of its powerful derivatives (e.g., IL-15 superagonists) are currently in clinical trials in both cancer and HIV infection. Besides increasing CD8+ T cell and natural killer (NK) cell responses, this pleiotropic cytokine acts as a latency-reversing agent for HIV [8] and SIV. IL-15 administration to macaques infected with a chimeric SHIV virus increased functional T cells in blood and mucosa, and resulted in higher infiltration of CD8+ T cells and reduced viral RNA in lymph nodes [7]. The findings of Younes *et al.* described here indicate that important additional parameters should be considered: does IL-15 affect the functional profile of CD4+ T cells? A preponderance of Tregs over Th17 cells in the gut mucosa was associated with faster disease progression in INRs, because functional Th17 cells have a key role in protecting the gut mucosa and preventing microbial translocation [9]. The effects of IL-15 on Th17 cells are context dependent and, given that only a few steps separate differentiation between Tregs and Th17, it will be important to determine whether IL-15 favors Tregs over Th17 cells in the gut in the context of HIV, with potential repercussions on gut mucosa integrity and systemic activation. Thus, this important article provides a new immunometabolic perspective on persistent immune dysfunction in HIV infection. The results raise hope that adjuvant interventions, involving either IL-15, agonists of the IL-15 pathway, or other drugs impacting mitochondrial function, could boost restoration of T-helper cells in a subpopulation of

patients with HIV who continue to be at higher risk of clinical complications in this era of highly effective ART.

Acknowledgement

D.E.K. is supported by a Senior Research Scholar Career Award of the Quebec Health Research Fund (FRQS #31035).

[1]Centre de Recherche du Centre Hospitalier de l'Université de Montréal (CRCHUM), Montréal, QC, Canada
[2]Department of Microbiology, Infectiology and Immunology, Université de Montréal, Montréal, QC, Canada
[3]Department of Medicine, Université de Montréal, Montréal, QC, Canada

*Correspondence:
daniel.kaufmann@umontreal.ca (D.E. Kaufmann).

https://doi.org/10.1016/j.molmed.2018.11.001

References

1. Younes, S.A. *et al.* (2018) Cycling CD4$^+$ T cells in HIV-infected immune nonresponders have mitochondrial dysfunction. *J. Clin. Invest.* 128, 5083–5094
2. Lederman, M.M. *et al.* (2013) Residual immune dysregulation syndrome in treated HIV infection. *Adv. Immunol.* 119, 51–83
3. Kleinman, A.J. *et al.* (2018) Regulatory T cells as potential targets for HIV cure research. *Front. Immunol.* 9, 734
4. Buck, M.D. *et al.* (2015) T cell metabolism drives immunity. *J. Exp. Med.* 212, 1345–1360
5. O'Neill, L.A. *et al.* (2016) A guide to immunometabolism for immunologists. *Nat. Rev. Immunol.* 16, 553–565
6. van der Windt, G.J. *et al.* (2012) Mitochondrial respiratory capacity is a critical regulator of CD8$^+$ T cell memory development. *Immunity* 36, 68–78
7. Watson, D.C. *et al.* (2018) Treatment with native heterodimeric IL-15 increases cytotoxic lymphocytes and reduces SHIV RNA in lymph nodes. *PLoS Pathog.* 14, e1006902
8. Jones, R.B. *et al.* (2016) A subset of latency-reversing agents expose HIV-infected resting CD4$^+$ T-cells to recognition by cytotoxic T-lymphocytes. *PLoS Pathog.* 12, e1005545
9. Pandiyan, P. *et al.* (2016) Mucosal regulatory T cells and T helper 17 cells in HIV-associated immune activation. *Front. Immunol.* 7, 228